Thermal Diffusivity of Hemp Concrete: Experimental and Numerical Studies

by

Ahmed Salem Bark Al-Tamimi

A thesis submitted in partial fulfillment of the requirements for the degree of

Doctor of Philosophy

in

STRUCTURAL ENGINEERING

Department of Civil and Environmental Engineering
University of Alberta

© Ahmed Salem Bark Al-Tamimi, 2023

ABSTRACT

The heat transfer from a hot to a cold medium occurs first in transient state before reaching a steady state. Hence, heat flux and surface temperatures fluctuate with changing times during the transient phase till they stabilizes after a period, and reach a steady phase. Heat conduction depends on thermal conductivity, specific heat capacity, and density (i.e., thermal diffusivity) during the transient state, while thermal conductivity dominates the steady state. In reality, the heat transfer occurs in the transient phase for building envelopes, while the steady state is used mainly for materials lab testing, such as the hot box technique. Therefore, materials for building envelopes must be assessed for thermal diffusivity and not just for thermal conductivity.

The first part of this study collates the thermal diffusivity of various types of concrete mixtures from literature, to explore the effect of mixture components and external factors on thermal properties. The outcome of that literature review indicates the significant effect of aggregate and binder properties on the overall thermal properties of the composite. Hemp concrete's reported thermal diffusivity values were at the bottom, showing low thermal conductivity and high specific heat capacity.

Hempcrete in the literature shows low thermal conductivity and high specific heat capacity, which are rarely reconciled, giving an advantage for building envelope application, to maximize energy storage and minimize thermal energy losses. There is a need to optimize the hempcrete mixture's components and balance thermal and mechanical properties with locally supplied materials to reduce the cost and make the hempcrete industry more available and affordable. Four groups of binders were

experimentally investigated for hempcrete's strength and thermal properties. The results showed that the presence of lime in the binder matrix of hempcrete is mandatory to enhance strength and overcome the negative impact of hemp to some extent due to pectin and hydrophilicity. Alkali-activated binders exhibit less impact with hemp hurds due to the alkaline solution that improves hemp surface and enhances the bond, which might not significantly be absorbed by hemp hurds. The thermal conductivity, diffusivity, and heat capacity are considerably higher due to the higher density and amorphous NASH. The maximum strength obtained in this study is alkali-activated metakaolin; thus, other mixtures might need optimizations to boost the strength. Increasing hemp content reduced density, strength, thermal conductivity, and volumetric heat capacity. Large hemp hurds disordered the arrangement of particles due to the flaky shape, while very fine hurds requires higher binder content and increase the possibility of interfacial failure under loading. The sizes of hemp hurds in the range of <3mm for width and <10mm for length achieved lower porosity and higher strength due to well gradation.

The second part of this work aims to enhance the compatibility and bonding between hemp hurds and binder matrix by conducting chemical treatments for hemp hurds. Such treatment aims to consume pectin and reduce the water absorption of hemp. Hemp hurds were treated with three chemical solutions: NaOH, $Ca(OH)_2$, and Na_2SiO_3. Sodium hydroxide treatment partially removed the amorphous components, roughening the surface and reducing particle size. Calcium hydroxide provides calcium ions that react with pectin and adhere to the hemp surface. Sodium silicate solution slightly roughened the surface, and silica bonded to enhance the interface zone. Hempcrete samples with

treated hemp showed a significant improvement in strength due to changes in the morphology of hemp and consuming pectin with slight changes in thermal properties.

The last part of this study is the evaluation of hempcrete mixtures produced in this study in a full-scale model for thermal performance in terms of thermal storing energy and losses. The evaluation has been done in two stages: First, literature thermal data for various concretes, including hempcrete mixtures, were assessed with the help of the ANSYS transient model. Second, the evaluation was conducted on the experimental data of hempcrete in this study. Hempcrete mixtures produced in this study showed a high potential due to their thermal performance with lower lost energy, between 12 and 24 %. In comparison, the literature on hempcrete describes losses between 19 and 60 %.

PREFACE

This thesis is an original work of Ahmed Salem Bark Al-Tamimi. The recognition and design of the research program were accomplished with the supervision of Dr. Vivek Bindiganavile at the University of Alberta and Dr. Naef Qasem at King Fahd University of Petroleum & Minerals. Seven journal papers related to this thesis have been published, submitted, or under preparation, as listed below.

1. Al-Tamimi, A., Bindiganavile, V. " Effect of mixture composition on thermal diffusivity of concrete for energy efficiency: a review." [Under preparation]
2. Al-Tamimi, A. and Bindiganavile, V. "Cement, lime and pozzolan binder compositions for optimizing hempcrete components for strength and thermal properties" [Under preparation]
3. Al-Tamimi, A. and Bindiganavile, V. " Exploring thermal performance and strength of hempcrete with alkali-activated binders " [Under preparation]
4. Al-Tamimi, A. and Bindiganavile, V. " Investigating hemp size and content effect on hempcrete strength thermal properties" Journal of Materials and Structures [Under preparation]
5. Al-Tamimi, A., Bindiganavile, V., Boluk, Y. " Effect of chemical treatments on hemp hurds and hempcrete thermal and strength properties." [Under preparation]
6. Qasem, N., Al-Tamimi, A., Bindiganavile, V. " Thermal energy storage and losses in various types of masonry concrete walls." Journal of Energy Storage [Published May 2023]
7. Al-Tamimi, A., Qasem, N., Bindiganavile, V. " Experimentally and numerically thermal performance evaluation of hempcrete masonry walls." Journal of Energy Storage [Under Review]

ACKNOWLEDGEMENTS

Pursuing graduate studies, especially a Ph.D., demands multiple kinds of support, guidance, and enormous patience along the academic journey for four to six years. My Ph.D. thesis is a sincere gratitude to everyone who loved, supported, and assisted me through almost the five years I spent towards my Ph.D. degree.

First, I would like to express my heartfelt gratitude to my supervisor, Dr. Vivek Bindiganavile, for his invaluable supervision, encouragement, guidance, and patience throughout my Ph.D. My gratitude extends to Dr. Naef Qasem for assistance and guidance while generating the thermal model. Further, I would like to express my appreciation to my committee members for their valuable comments and feedback, Dr. Yaman Boluk and Dr. Ying Hei Chui.

My late father had incredibly supported me to devote my effort and time towards education. I want to sincerely apologize for being far and not supportive, and no words could express my gratitude for everything. All the love and thanks to my mother, brothers, and sisters for their love, support, and advice. My lovely kids, sorry for the hard time, being busy with study and everything. Many thanks and love to my friends and colleagues around me during the hard times along the journey.

All my graduate studies won't be without the support of Shaikh Abdullah Bugshan for limitless support and encouragement. My thanks extend to the Hadhramout Foundation for providing the scholarship for my Ph.D.

TABLE OF CONTENTS

LIST OF TABLES

LIST OF FIGURES

1 CHAPTER 1: INTRODUCTION

1.1 Background

Building quality has improved significantly in recent decades with growing living standards and enhancing construction materials. Therefore, measures were initiated for buildings' excellence in indoor air quality and acoustic and thermal insulation. The thermally comfortable environment is mainly controlled by heating and cooling systems to maintain the desired indoor temperature. Thus, much energy is consumed to satisfy comfortable indoor conditions, which differ from country to country.

The building envelopes, including exterior walls, windows, cladding, exterior structural members, thermal bridges, etc., are the most critical elements affecting heat exchange between interiors and exteriors. Therefore, a comprehensive analysis is needed for building envelopes to identify the poor thermal behavior and, in accordance, improve design and construction decisions for sustainable buildings and saving energy. Buildings in the European Union consume about 40% of total power, in which space heating substituted about 60-80% of total power consumption of buildings [1], while that in Canada and the USA reaches 63% [2] and 42% [3], respectively. Consequently, massive energy could be saved if the building envelope's thermal properties (such as thermal conductivity, diffusivity, density, and specific heat capacity) are sufficiently improved. The masonry blocks as building envelopes are widely used for building exteriors worldwide. Concrete masonry units are widely used as a construction material for the masonry industry, with an annual production of about 4.3 billion units in the USA and Canada [4]. Further, governments established minimum requirements for energy and thermal performance of buildings and construction materials such as thermal insulation of building envelopes, including European Parliament [5], Canadian Standards Association (CSA) (A165 SERIES-14- R2019) [6], American Society for Testing and Materials (ASTM) [7].

The variation in exposure conditions for buildings throughout the day and night reflects changing the thermal behavior of building envelopes regarding the ability to store and lose thermal energy with time. Therefore, the heat transfer that simulates the practice is the transient phase. The heat transfer in transient conditions mainly depends on the medium's thermal diffusivity. Therefore, the most essential properties of building materials for thermal performance in natural conditions are

thermal conductivity, specific heat capacity, and density. Thermal diffusivity expresses the transient heat transfer and refers to the rate (How fast) of heat diffusion through materials (mm^2/s). In other words, thermal diffusivity is the thermal conduction of material relative to its thermal storing energy. Hence, the lower thermal diffusivity values mean extra time needed to reach the equilibrium with the environment and shallower penetration of heat [1]. From experimental measurements of thermal conductivity k, density ρ, and specific heat capacity C_p, thermal diffusivity could be calculated from Eq- 1.1, while Eq- 1.2 expresses the transient heat transfer using diffusion equation.

$$\alpha = \frac{k}{\rho C_p} = \frac{k}{C_v} \qquad \textbf{Eq- 1.1}$$

$$\frac{\partial^2 T}{\partial^2 x^2} = \frac{1}{\alpha}\frac{\partial T}{\partial t} \qquad \textbf{Eq- 1.2}$$

This study targeted concrete as a building envelope material for masonry blocks for its pricing and availability. However, surprisingly, most literature on thermal constants of cement-based systems is devoted to thermal conductivity, measurement, and test methods rather than thermal diffusivity, which is the dominant material property for transient heat transfer, as illustrated in Figure 1.1. Thus, this study is devoted to the thermal diffusivity of concrete for building envelopes, including thermal conductivity, specific heat capacity, and density.

As a summary of the above, the heat transfer in the building envelope is governed by the diffusion equation, which is dependent on thermal diffusivity; thus, materials for the building envelope must have low thermal diffusivity values to store higher thermal energy and minimal loss of thermal energy. From the literature, hempcrete showed low thermal conductivity with high heat capacity, which is rarely reconciled. Hempcrete is recently developed and requires more research to improve the composite due to its low strength and compatibility. This study targets enhancing the strength of hempcrete to reach the strength requirements for non-load-bearing blocks to be used as exterior building walls. Thus, the final goal of improving hempcrete is to reduce heat demand by minimizing heat loss and recycling the heat inside the building (i.e., storing heat in hempcrete, then releasing it back to warm up the interiors again).

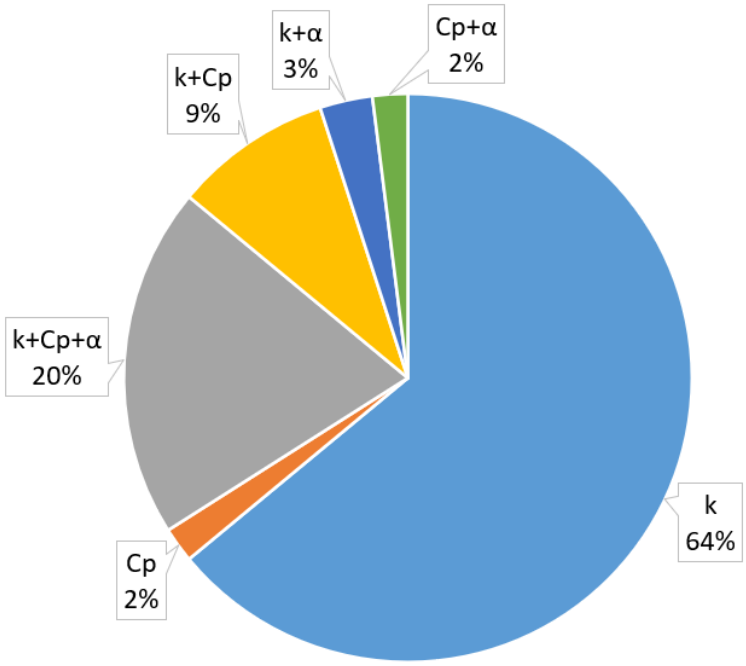

Figure 1.1: Percentage of measured thermal properties of cement-based materials [2]

The first step in this work is to conduct a literature review on the thermal diffusivity of all concrete types and affecting factors, as detailed in Chapter 2. It forms a vital prerequisite for optimizing the mixture to achieve suitable insulation and thermal comfort in a sustainable manner and energy efficiency. The thermal properties of concrete are found to be strongly affected by the binder, water content, and aggregate [1]. The aggregates occupy a considerable amount of concrete volume in the range of 60 – 80% of the total volume of concrete [21][3]. Such an amount affects the entire properties of the composite material. Hence, the used aggregate's properties greatly influenced the produced concrete's properties [21]. In other words, the thermal properties of aggregate will directly affect the thermal properties of concrete. Therefore, producing some concrete with thermal insulation and heat-storing ability needs an aggregate with the same properties. As highlighted in this review, hemp concrete shows a significantly low thermal conductivity and a higher specific heat capacity (i.e., lower thermal diffusivity) compared to all other concretes due to the superior properties of hemp hurds aggregate. Thus, another literature was conducted on hempcrete's thermal diffusivity and strength (in Chapters 3-5) and hemp treatment (Chapter 6) to optimize the mixture's components and improve the bond and compatibility. The targeted densities for applying hempcrete to produce masonry blocks are less than 1680kg/m^3 for lightweight units, according to

ASTM C90 and C129 for load-bearing and non-bearing masonry units [128]. Further, the targeted strength in this study might be sufficient for non-load-bearing masonry units, which is about 3.45 MPa for an individual masonry unit, according to ASTM C129 [128]. Such blocks could not be used for exterior walls exposed to freezing and thawing cycles without a protection layer or plastering [128]. According to the National Energy Code of Canada for Buildings, Edmonton falls under zone 7A, which stipulates U value requirements for wall assemblies within the range of 0.215 to 0.284 W/m² K. However, the results of this research exhibit different U values for exclusively hempcrete solid blocks (measuring 400 x 200 x 200 mm), ranging from 0.44 to 1.11 W/m² K. Regarding R-values, light, medium, and normal-weight masonry blocks demonstrated values between 0.2 and 0.99 m² K/W. In contrast, the solid hempcrete blocks produced in this study displayed notably elevated R-values, ranging from 0.90 to 2.25 m² K/W.

Chapter 3 presented a literature review of hempcrete thermal diffusivity, demonstrating the lack of research on hemp concrete with Canadian-sourced materials, including hemp hurds, proper binders, and additives. This raises the need for more studies to investigate and upgrade hemp composite in terms of mechanical, thermal, and acoustic properties, reducing hempcrete price and embodied energy (i.e., increasing the availability and affordability of hemp concrete around Canada). However, hemp concrete was non-structural concrete developed about 30 years ago and still needs to be investigated on thermal and strength properties. The technologies and spreading of hemp concrete have been increasing around Europe since 1990. On the contrary, the obstacles to getting a license to grow hemp in Canada due to its association with cannabis delay the implementation of hemp concrete around the country [8]. In 2012, hemp was approved as a construction material for residential buildings under the Ontario Building Code as an alternative solution [5]. Therefore, the hempcrete mixture's components must be optimized and balanced between thermal and strength properties. To understand the behavior of hemp concrete, an experimental program was conducted in this chapter to evaluate the impact of binders, hemp content, and hemp sizes on strength and thermal properties. Studies conducted elsewhere could serve as guidance for research, but findings could not be transferred to local standards of hempcrete with locally supplied materials [11].

The properties of hemp composite mainly depend on hemp hurd properties, binder matrix, and adhesion at the interface zone [1]. The hydrophilicity and chemical composition of hemp hurds are

critical problems for the incompatibility between binder and hemp aggregates, which leads to low interface strength. Therefore, many research projects were devoted to enhancing the compatibility between bio-aggregates (filler) and binder matrix, thus improving the interface zone strength and adhesion by chemical and physical treatment [1][2][3]. Hemp hurds reported to retarding and disturbing the hydration of cement due to sugar, pectin, and high water absorption [4][5][6][7][8][9]. Therefore, there is a need to explore an economic and ecological method for hemp hurd treatment to match the requirements of building material applications. The following section summarizes the chemical composition of hemp hurds and the negative impacts on binder performance to navigate individual problems and think of proper solutions for overcoming them. Chapter 4 showed the effect of hemp hurds on the binder matrix and the need for pre-treatment to improve hemp composite for strength and maintain superior thermal properties. Therefore, a literature review on chemical treatments on hemp hurds and fibers was recruited, and then three chemical treatments were selected, including NaOH, $Ca(OH)_2$, and Na_2SiO_3. Finally, hempcrete samples were prepared with treated hemp hurds to evaluate the treatment effect on strength and thermal properties.

Chapters 7 and 8 presented a transient thermal model using ANSYS Fluent to evaluate the thermal performance of various concrete types (from literature and hempcrete from chapter 3) for cold weather building envelopes in terms of thermal storage and losses over 24 hours. The study assesses the energy storage inside the wall and energy loss from walls to the ambient to suggest the best walls for energy saving in cold regions. Thus, materials for building envelopes are required to show high storage energy and thermal resistance. Materials with low thermal conductivity and high heat capacity (i.e., low thermal diffusivity) are expected to minimize energy loss to the exterior and store more energy. The combination of the thermal properties (ρ, Cp, and k) for transient heat flow on stored and lost energy is studied.

1.2 Problem Statement

In Canada, the energy consumption for residential and commercial space heating constitutes the largest sector, with about 55% of the total consumption ascribed to the harsh cold weather [97]. The corresponding CO_2 emission from the electricity and heating sector is about 42%, about double the CO_2 emitted from transportation [98]. However, the CO_2 emission from the building sector is the third-largest emitting sector in Canada, with about 12% [11]. In 2013, Canadians spent almost $195 billion on energy to heat and cool their homes and offices and to operate their appliances, cars, and industrial processes. This amount equals about 11% of the country's gross domestic product (GDP) [99]. However, the energy efficiency for residential and commercial sectors improved by 32, and 13%, respectively, between 2000 and 2019, saving about 8.5 and 3.2 billion [97]. Further, embodied carbon is a crucial global issue involving imposing regulations and limitations for building materials, such as using waste pozzolan materials [11]. Building performance certifications such as Leadership in Energy and Environmental Design (LEED) announce rewards for using low embodied carbon construction materials [11]. Moreover, all authorities in Canada will adopt the construction codes of buildings "net-zero energy ready" in 2030 [11]. Net zero energy-ready homes are buildings that produce as much clean energy as they consume [100]. According to Natural Resource Canada, NZER buildings are expected to be 80% more energy efficient than today's buildings; in Canada, less than 1% of buildings are NZER [100]. Buildings with high-performance envelope materials were considered net-zero energy buildings due to the importance of thermal insulation of building envelopes [11]. The efforts are continuous globally, focusing on improving the building envelopes to build greenhouses. This study targeted hempcrete for improvements to be used as building envelope material due to its promising thermal properties.

Hemp concrete has several distinct advantages such as high thermal insulation, high storing heat capacity, breathable material with high PH, high acoustic performance, fire resistance, fully recyclable, carbon-negative material, and locks considerably more atmospheric carbon dioxide than emits during building construction [11]. Although hempcrete is a superior, sustainable, and green composite, there are barriers preventing upgrading and investigation, such as a lack of local products, standards, and guidelines and the conservation of hemp concrete practitioners and companies due to commercial aspects. The literature on hemp concrete illustrated that the

properties of hemp composite depend on binder type, hemp content, and hemp size. Furthermore, the compaction and the amount of water directly affect density and porosity.

As illustrated in the literature, hemp concrete showed low thermal conductivity and high heat capacity among all concretes, which are rarely reconciled (i.e., low thermal diffusivity). Therefore, such material is a superior candidate for building envelopes to reduce heat loss and maximize heat storage, which leads to significant energy savings. However, hemp concrete was nonstructural concrete developed about 30 years ago and still needs to be investigated on thermal and strength properties. The technologies and spreading of hemp concrete have been increasing around Europe since 1990. On the contrary, the obstacles to getting a license to grow hemp in Canada due to its association with cannabis delay the implementation of hemp concrete around the country [8]. In 2012, hemp was approved as a construction material for residential buildings under the Ontario Building Code as an alternative solution [5]. Therefore, there is a lack of research on hemp concrete with Canadian-sourced materials, including hemp hurds, proper binders, and additives. This raises the need for more studies to investigate and upgrade the hemp composite's mechanical, thermal, and acoustic properties, reducing hempcrete price and embodied energy (i.e., increasing the availability and affordability of hemp concrete around Canada).

As noticed from the literature, limited studies are exploring the thermal diffusivity of hemp concrete, and all studies are European sources except one study from Canada (Manitoba, 2020 [24]). Therefore, there is a clear gap that could be summarized as follows:

1. Lack of database for hempcrete (1990s France, 2012 Canada)
2. Optimizing components of hemp concrete
3. Lack of standards and guidelines
4. Balancing between strength and thermal properties
5. Enhancing compatibility between hemp and binder matrix
6. Evaluation of hempcrete thermal performance in terms of storing and losing thermal energy for usage as a building envelope.

In order to understand the behavior of hemp concrete, a complete study should be conducted to evaluate all the parameters affecting the desired properties, such as binders, hemp content, and hemp sizes with locally supplied material. Studies conducted elsewhere could serve as guidance

for research, but findings could not be transferred to local standards of hempcrete with locally delivered materials [11].

1.3 Objectives and Scope

This research will deal with the above problem statement by planning an experimental program to improve the mechanical and thermal properties of hemp concrete to achieve the following:

1. Optimize components of hemp concrete

2. Optimize hemp particles to produce hempcrete

3. Enhancing compatibility between hemp and binder matrix

4. Conducting thermal model to evaluate hempcrete for storing and losing thermal energy

There is a lack of literature about hemp concrete, including the proper binders, hemp size, hemp content, and hemp treatment for optimizing hemp concrete components with the lowest thermal diffusivity and highest possible strength. Hemp concrete combines the two properties of high heat capacity and low thermal conductivity, which are challenging to integrate, leading to significantly lower thermal diffusivity (i.e., minimizing the rate of heat diffusion). The produced hempcrete was modeled in Ansys to build a wall to be evaluated for storing and losing thermal energy; hence, such materials could be reliable for building envelopes. Further, the limited studies conducted in Canada to produce hempcrete with locally supplied materials leads to the real need for more research on local materials to reduce the price and embodied energy. Hence, the industry of hempcrete has become more available and affordable.

More generally, this study aims to identify and quantify the components of hemp concrete that lead to the low thermal diffusivity and acceptable strength through an experimental program with four milestones:

1. Proposing four groups of binders

2. Using four different hemp sizes from Canadian and French harvests

3. Trying five various hemp content

4. Conducting three chemical treatments for hemp hurds

5. Performing a parametric study for hempcrete produced in this study and literature

1.4 Hypothesis

Thermal diffusivity expresses the transient heat transfer and refers to the rate (How fast) of heat diffusion through materials with time until it reaches a specific temperature (mm^2/s). Hence, the lower thermal diffusivity values mean extra time needed to get the equilibrium with the environment, as shown in Figure 1.2.

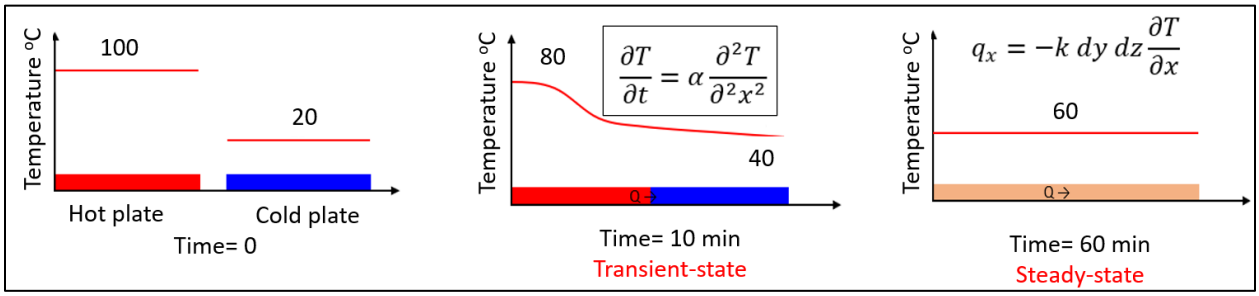

Figure 1.2: Temperature distribution throughout hot and cold plates with time

From Fourier's law, the general conduction equation for the transient state depends on thermal diffusivity (α). In contrast, the steady state depends on thermal conductivity (k), as equations [2] show.

$$\frac{\partial^2 T}{\partial^2 x^2} + \frac{\partial^2 T}{\partial^2 y^2} + \frac{\partial^2 T}{\partial^2 z^2} = \frac{1}{\alpha}\frac{\partial T}{\partial t} \quad \text{(Diffusion)}$$

$$\frac{\partial^2 T}{\partial^2 x^2} + \frac{\partial^2 T}{\partial^2 y^2} + \frac{\partial^2 T}{\partial^2 z^2} + \frac{q}{k} = 0 \quad \text{(Poisson)}$$

$$\alpha = \frac{k}{C_v} = \frac{k}{\rho C_p}$$

For one-dimensional heat conduction in the transient state with no heat generation, the thermal diffusivity equation, which means the rate of change of temperature depends on or is proportional to the temperature field/gradient.

$$\frac{\partial T}{\partial t} = \alpha \frac{\partial^2 T}{\partial^2 x^2}$$

As shown in Figure 1.3, buildings in cold weather environments need a heating system to warm the interior space and maintain a comfortable temperature ($T_{comfort}$). Thus, the heating system will be on until reaching $T_{comfort}$; during this time, some thermal energy will be stored inside the building envelopes Figure 1.3 (b). Then, the heating system will be off until the indoor temperature becomes less than $T_{comfort}$; during this period, some thermal energy will be released back from the envelopes into the interior space, maintaining the temperature at $T_{comfort}$ for a while. Therefore, the longer the time for the heating system to be off, the more energy saving and the more thermal efficient envelop.

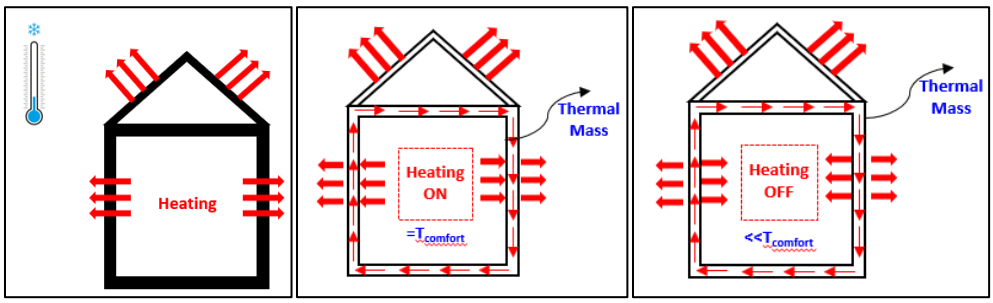

Figure 1.3: Significance of transient heat conduction throughout building envelopes in a cold environment

1.5 Methodology

The methodology followed in this research is illustrated in Figure 1.4, which comprises four main stages. The study followed the same sequence of stages, phases, and tasks in the flow chart (Figure 1.4). The lab tests are briefly mentioned at the bottom for all specimens produced in STAGE III.

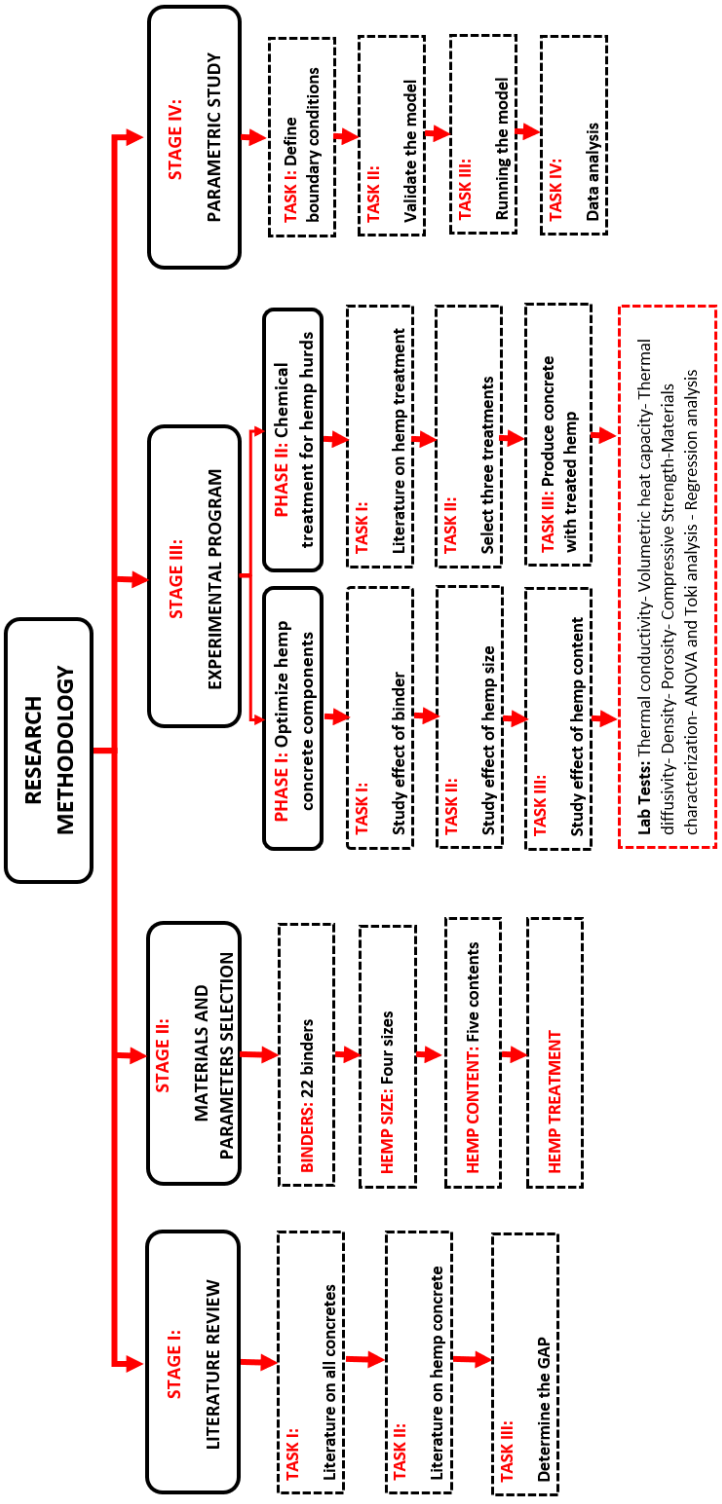

Figure 1.4: Flow chart for research methodology

1.6 Organization of Thesis

This research has been divided into two main parts, including experimental and analytical stages. The components of hempcrete were optimized for strength and thermal properties; then, hemp hurds were chemically treated before being used to produce treated hempcrete. The evaluation of such concrete for building envelope was assessed using the transient thermal model to obtain the capacity of storing and losing thermal energy. This thesis is organized into five chapters, as follows:

- **Chapter 1: Introduction –** Describes the principle of the research study and defines the target problem, hypothesis, and objectives.
- **Chapter 2: Literature review –** includes a comprehensive literature review of the thermal diffusivity of different types of concrete, the impact of concrete components, and the effect of external factors such as temperature and relative humidity.
- **Chapter 3: Optimizing hempcrete components –** Presents the experimental program, particularly for the factors affecting the thermal diffusivity of hemp concrete, including binder type (four groups), hemp size (four sizes), and hemp content (five dosages). Further, the lab tests included hemp characterization, thermal diffusivity, heat capacity, thermal conductivity, density, compressive strength, and porosity.
- **Chapter 4: Chemical treatments for hemp hurds –** Presents a review of treatments for hemp hurds and fibers, then proposes three chemical treatments for this study. Finally, hempcrete samples were prepared with the treated hemp hurds and tested for strength and thermal properties.
- **Chapter 5**: **Parametric study –** Presents the generation of the transient thermal model using ANSYS, model validation, and conducting a parametric study for different concretes from literature, then another parametric study for hempcrete data from previous chapters and comparing with literature hempcrete.
- **Chapter 6: Conclusions and recommendations –** summarizes the key results from the preceding chapters and suggestions for future research.

2 CHAPTER 2: LITERATURE REVIEW

Effect of Binder and Aggregates on Thermal Diffusivity of Concrete

Abstract

Cooling and heating building interiors consume excessive energy to ensure human comfort. The construction materials could supply a thermal mass designed to act as a heat sink during the daytime, storing thermal energy released later at night. Cementitious composites can be optimized for minimum thermal diffusivity by suitably designing their composition and morphology. This review describes the thermal diffusivity of concrete as affected by individual components and mixture design. Specifically, it explains how the binder composition, aggregates, chemical admixtures, fiber reinforcement, temperature, and moisture content contribute to thermal diffusivity. External factors might affect the diffusivity of concrete, including environmental temperature and relative humidity, which are both included in different studies from the literature. This study aims to understand the behavior of thermal diffusivity with internal components of composite and external variation; thus, the next stage is to construct concrete with low thermal diffusivity to be used as construction material, achieving a superior energy save. Finally, the thermal diffusivity results for hempcrete were promising, showing low thermal conductivity with high heat capacity relative to other concretes. This led to targeted literature on hempcrete, as conducted in Chapter 3, to explore profoundly such composite for thermal purposes.

Keywords: Thermal diffusivity, heat capacity, storing energy, thermal properties, thermal mass, insulation concrete

Nomenclature

Ag	Agrex
BA	Bagasse ash
BFS	Blast furnace slag
BFS	Blast furnace slag aggregate
BOFSS	Basic Oxygen Furnace Steel Slag
BP	Brick powder
Bx	Bauxite
C	Cement
CA	Coarse aggregate
KL	Kaolin
Latex	La
Le	Leca
Li	Lime
LWA	Lightweight aggregate
LWAC	Light weight aggregate concrete
Ly	Lytag
MA	Mineral additions
Me	Methylcellulose
MK	Metakaolin

CCA	Corn cob ash	*NA*	Natural aggregate
CCF	Coconut coir fiber	*OPS*	Oil palm shell
CF	Carbon fiber	*PF*	Plastic fiber
CH	Portlandite	*PPF*	Polypropylene fiber
CoA	Cork Aggregates	*PSB*	Polystyrene beads
Cp	Specific heat capacity (J/g K)	*Pu*	Pumice
CRu	Crumb rubber	*RH*	Relative humidity
CSH	Calcium silicate hydrate	*RHA*	Rice husk ash
Cv	Volumetric heat capacity (J/m^3K)	*RiH*	Rice husk ash
CW	Coffee waste	*RLA*	River lite Aggregate
CWM	Crushed waste marble	*S*	Sand
DPF	Date palm fiber	*SD*	Saw dust
ECA	Expanded clay aggregate	*SF*	Silica fume
EPL	Expanded perlite	*Si*	Silane
ESA	Expanded shale aggregate	*SS*	Steel slag
FA	Fine aggregate	*St*	Stalite
FA	Fly ash	*StF*	Steel fiber
FAC	Fly ash cenospheres	*Vc*	Vermiculite
G	Gravel	*WA*	Wood ash
GF	Glass fiber	*WRA*	Water reducing agent
Gy	Gypsum	*WS*	Wood shavings
HS	Hemp shives	*WW*	Wood wool
k	Thermal conductivity (W/m K)	*α*	Thermal diffusivity (g/cm^3)

2.1 Introduction

Energy consumption for cooling and heating, especially in residential and commercial buildings, has become a crucial issue worldwide. Therefore, many studies have been initiated to minimize exhaustion usage by improving the thermal insulation properties of concrete because concrete constitutes most of the exterior parts of buildings [1]. Building materials' most important thermal properties are thermal conductivity, specific heat capacity, and density (i.e., thermal diffusivity) because losing thermal energy mainly depends on these properties. In particular, high specific heat capacity and low thermal conductivity (i.e., low thermal diffusivity) are desirable due to the capability to retain heat and provide thermal insulation. Thermal diffusivity expresses the transient

heat transfer and refers to the rate (How fast) of heat diffusion through materials (mm^2/s). In other words, thermal diffusivity is the thermal conduction of material relative to its thermal storing energy. Hence, the lower thermal diffusivity values mean extra time needed to reach the equilibrium with the environment and shallower penetration of heat [1]. From experimental measurements of thermal conductivity k, density ρ, and specific heat capacity C_p, thermal diffusivity could be calculated from Eq- 2.1, while Eq- 2.2 expresses the transient heat transfer using diffusion equation.

$$\alpha = \frac{k}{\rho C_p} = \frac{k}{C_v} \qquad \textbf{Eq- 2.1}$$

$$\frac{\partial^2 T}{\partial^2 x^2} = \frac{1}{\alpha}\frac{\partial T}{\partial t} \qquad \textbf{Eq- 2.2}$$

The thermal properties of concrete are strongly affected by binder type, water content, and aggregates [2]. As illustrated in Figure 2.1, most of the literature on thermal constants for cement-based systems is devoted to thermal conductivity, its measurement, and test methods. There is a lack of studies on how the mixture components affect the three thermal properties simultaneously (thermal conductivity, specific heat capacity, and thermal diffusivity). In what follows, the available data on the effect of individual components upon the thermal diffusivity of cementitious systems is reviewed. It forms a vital prerequisite for optimizing the mixture to achieve suitable insulation and thermal comfort in a sustainable manner and energy efficiency. This review targeted the internal and external factors affecting the diffusivity, including components of cementitious composite and environmental impact, as illustrated in Figure 2.2.

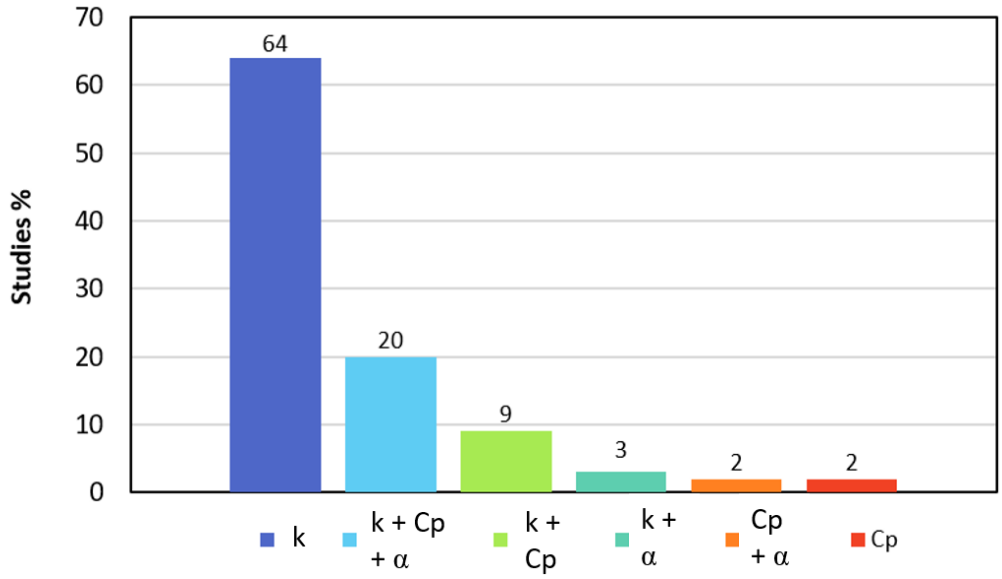

Figure 2.1: Percentage of studies that measured the thermal properties of cement-based materials [3]

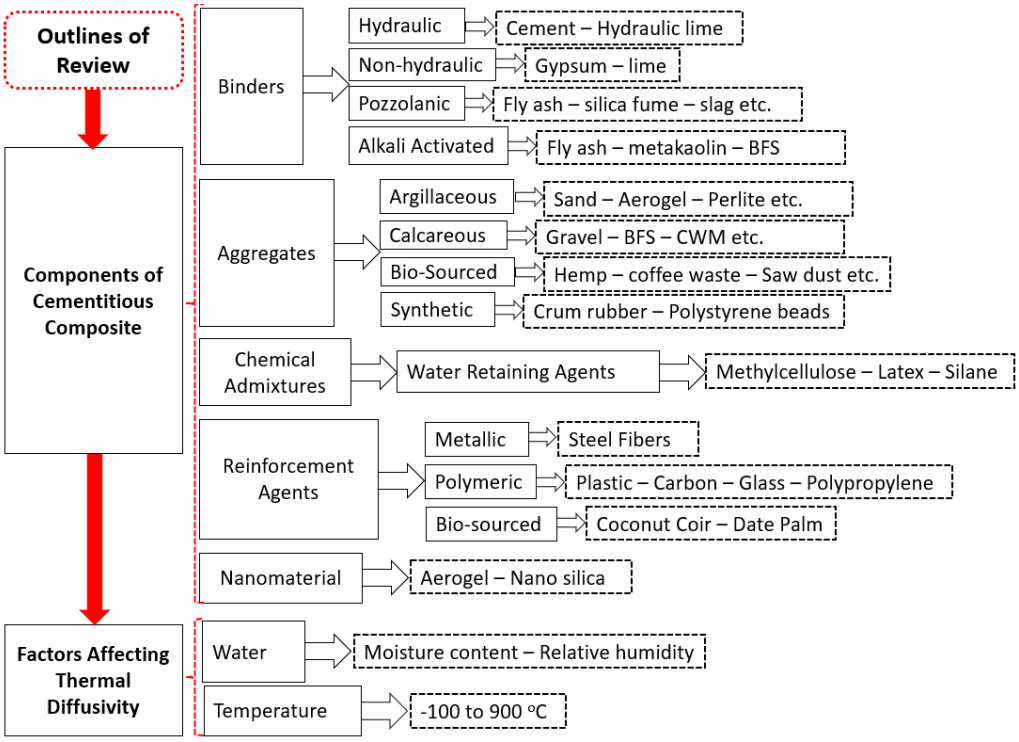

Figure 2.2: Flowchart showing the outlines of this review

2.2 Components of Cementitious Composite

2.2.1 Binders

The binders used in cementitious composites may be classified into four categories: hydraulic, pozzolanic, non-hydraulic, and alkali-activated. The hydraulic binders are composed of lime and aluminosilicate, such as cement and hydraulic lime. At the same time, the pozzolanic admixtures are mainly rich in silica (SiO_2) and alumina (Al_2O_3), such as fly ash, silica fume, and slag. The products of the hydration process of binders affect the thermal properties of the composite significantly. The formation of crystalline products such as calcium hydroxide (CH) tends to increase porosity; hence, the conductivity and heat capacity decrease. On the other hand, the production of amorphous structures like calcium silicate hydrate (CSH) will decrease the porosity and, in turn, raise the density of thermal conductivity and might down the heat capacity.

2.2.1.1 Hydraulic Binders

Hydraulic binders are powder materials reacting with water (i.e., hydration process), forming a uniform mixture setting with time at room temperature, such as cement and hydraulic lime [4]. The main components of hydraulic binders are silica (SiO_2), alumina (Al_2O_3), and lime (CaO), which affect the reaction with water (hydration products), hardening, and thermal properties. The hydration products of hydraulic binders are amorphous CSH and crystalline CH due to the higher amount of C_3S and C_2S [4]. Therefore, increasing hydraulic content decreases the air pores by filling them with hydrates, leading to an increment in density and thermal conductivity (i.e., decrement in heat capacity).

2.2.1.2 Pozzolanic Binders:

The addition of pozzolanic with cement decreases the density of the mixture because the density of pozzolan is lower than cement (3.15 g/cm^3). On the contrary, the porosity decreased due to filling the pores with the formation of new CSH and Ettringite [5]. The thermal conductivity and specific heat capacity depend on the pozzolanic material's density, structure (Amorphous or crystalline), and surface area (Particle size). Thus, thermal diffusivity would be mostly reduced. The density of pozzolanic admixtures is lower than cement, thereby reducing the density of the mixture. The higher crystallinity of pozzolanic disturbs the production of CSH, thus increasing the porosity. On the other hand, the amorphous structure enhances the formation of CSH and reduces

porosity. The larger particle sizes disturb the hydration and the production of CSH, thus increasing porosity and vice versa.

2.2.1.3 Non-hydraulic Binders:

Binders start hardening in the presence of air, such as gypsum and lime, during calcination and carbonation processes.

2.2.1.3.1 Gypsum (Gy):

Gypsum is calcium sulfate dihydrate ($CaSO_4 \cdot 2H_2O$) with a chemical composition of 95% CaO [6]. Then calcined gypsum (Partially dehydrated) ($CaSO_4 \cdot 1/2H_2O$) produced at temperatures (110-150 ºC), which is soluble in water, hence crystalline gypsum forms again according to equation [7][8]:

$$CaSO_4 \cdot 2H_2O \xleftrightarrow{110-150\ C^o} CaSO_4 \cdot \frac{1}{2}H_2O + H_2O$$

The thermal conductivity of gypsum is in the range of 0.2-0.3 W/m K, and the specific heat capacity is 0.7-1.10 J/g K [8][9]. For gypsum wood boards, the density and thermal conductivity decreased with increasing the content of wood shavings (i.e., less gypsum) by 22% and 61%, respectively [9] due to increasing air voids (Air filling the voids is lower 5-time than wood in terms of thermal conductivity) and lower thermal conductivity of wood shives [9]. In the same trend, the specific heat capacity decreased by about 44% due to the decrement of gypsum content, which has higher Cp 0.7-1.02 J/g K (The authors of this article have an opposite opinion due to the high Cp values of wood and more heat stored in pores). Thus, the thermal diffusivity has a remarkable increment of about 19% [9] and 32% for [10], depending on the mix components. There is an agreement that the thermal conductivity is reduced by reducing the gypsum content [11][10]. As a comparison between pastes of cement and gypsum as binders for insulation materials (Table 2.1), gypsum reduced the density and thermal conductivity by 14 and 56%, respectively, because gypsum is a lighter and more insulator than cement [11]. Further, the heat capacity of gypsum paste is much higher than cement (33%). Thus, the diffusivity is much lower by about 50% [12][10].

2.2.1.3.2 Non-hydraulic Lime (Li):

Binders composed mainly of calcium oxide (CaO) and low silica and alumina content, with a typical density of around 1.40 g/cm^3 and thermal conductivity of about 0.70 W/m K, are used in lime-based systems [13]. As shown in the following Equations, the two-stage reactions of quick lime depend upon the ambient temperature and carbon dioxide content, the presence of water, and relative humidity [14][15][16]:

$$CaO\ (Quick\ Lime) + H_2O \rightarrow Ca(OH)_2\ (Portlandite, CH), (Hydrated\ or\ slaked\ lime)$$

$$Ca(OH)_2 + CO_2 \rightarrow CaCO_3\ (Calcite) + H_2O$$

As shown in Table 2.1, mass substitution of Portland cement with 25% hydrated lime decreased the density and thermal conductivity by 13 and 28%, respectively [17]. This drop is due to a 20% rise in the porosity and the lower density of lime compared to cement. Additionally, the hydration products CH and CSH found in purely Portland cement systems are now accompanied by the formation of calcite monolayers [14]. Note that the specific heat capacity remains the same. The above study records a 20% drop in thermal diffusivity. Similar results were obtained by Monika for slaked lime (CL90) plaster [18]. On the other hand, the replacement of cement by lime showed a slight improvement in thermophysical properties as resulted in references for slaked lime CL90 [19], lime mud (CaO >40%) [20], Lime mud (CaO>50%) [21], lime mud (CaO>40%) [22]. The addition of metakaolin with hydrated lime (CL90) (same content as MK) reduced the diffusivity by about 35% [23] due to an increment of 25% in porosity (ascribed to the porous structure of metakaolin which unreacted) and a decrement of 40% in thermal conductivity [23].

2.2.1.4 Alkali Activated Binders (Geopolymer):

The alkali-activated binder is a green construction material due to its low cost (waste materials), low production energy, and low CO_2 emission. The thermal conductivity, specific heat capacity, and thermal diffusivity depend on the porosity of the alkali-activated [24]. Goncalves et al. [25] tested the thermal conductivity and heat capacity of alkali-activated paste of fly ash with sodium silicate (Na_2SiO_3) and sodium hydroxide (NaOH) (1.0:0.30). The calculated thermal diffusivity was found 0.237 mm^2/s with bulk density of 1.14 gm/cm^3 (i.e. there is a reduction of 35% as compared to paste with normal cement [26]). XRD analysis showed crystalline aluminosilicate

phases and a hump, indicating the amorphous phases [25]. Therefore, alkali-activated adhesives have a high potential for reducing thermal diffusivity significantly. Jittabut produced an alkali-activated cement paste (Aluminosilicate materials: fly ash, bagasse ash, and rice husk ash + Alkaline activating agents: Na_2SiO_3 and NaOH (2.0:1.0)) with a thermal diffusivity in the range of 0.6-0.9 mm^2/s [27]. Further, alkali-activated were prepared by activating metakaolin (with Na_2SiO_3 and NaOH (0.40-1.20)), resulting in a thermal diffusivity between 0.22-0.44 mm^2/s [28]. The density increased with increasing the ratio of activating agents due to expanding the content of Na_2SiO_3, which has a higher density than NaOH [28]. Therefore, the porosity decreased due to the higher silica content, resulting in a new formation of aluminosilicate [28]. The porosity decreased with increasing the ratio of activators until the optimum value was 1.0, then the porosity increased due to retarding the alkali activatedisation process with the excessive content of alkali [28]. Caicedo et al. activated metakaolin with potassium hydroxide (mixed with rice husk ash and silica fume SiO_2:K_2O = 2:1), resulting in lower values of thermal diffusivity (0.16-0.27 mm^2/s) [24].

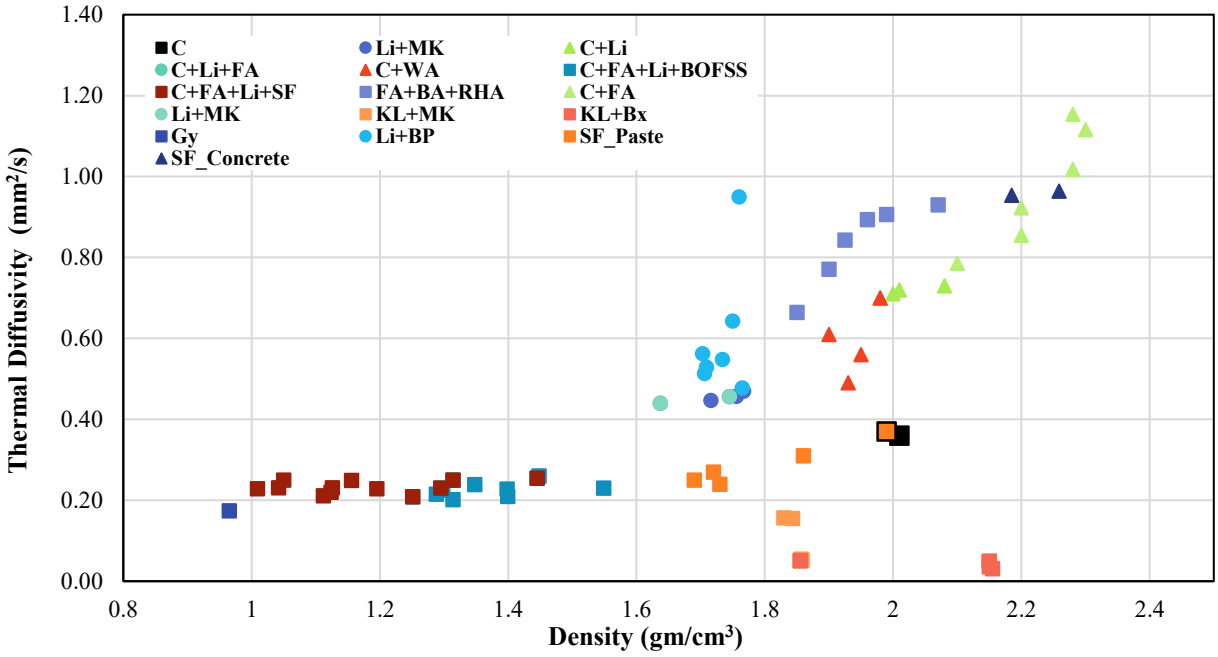

Figure 2.3: Effect of binder type on thermal diffusivity

Table 2.1: Effect of binders on thermal properties of paste, mortar, and concrete

Mix Type	Binder Type and Content	ρ (g/cm^3)	K (W/m K)	Cp (J/g K)	α (mm^2/s)	Porosity (%)	W/B	Ref	Remarks
Paste	C	1.990-2.010	0.520-0.530	0.703-0.736	0.370-0.360	-	0.45-0.35	[26], [12]	Increasing cement content increased density, conductivity, and heat capacity, slightly reducing diffusivity (3%).
Paste (With **Li**)	C + FA + (12-25%) Li	1.445-1.251	0.350-0.251	0.950-0.960	0.255-0.209	47.10-57.49	-	[17]	The addition of lime decreases the density and conductivity while increasing Cp (i.e., reduced diffusivity by 18%)
Paste (With **BOFSS**)	C + FA + Li	1.445	0.350	0.950	0.255	47.10	-	[17]	The addition of BOFSS increased porosity, but the density negligibly increased. However, the k and Cp values decreased. Hence, the diffusivity was reduced (10%).
	C + FA + Li + (10-20%) BOFSS	1.448-1.549	0.32-0.285	0.850-0.800	0.260-0.230	52.98			
Paste (With **SF + WRA**)	C	1.99	0.52	0.703	0.37	2.32	0.45	[26]	The addition of SF decreases density and conductivity while increasing Cp due to the amorphous structure of SF and the production of the extra amount of amorphous CSH from hydration (i.e., higher porosity). Thus, the diffusivity decreased significantly (30%).
	C + 15% SF	1.72	0.36	0.765	0.27	3.14	0.35		
Paste (with **SF + WRA+0.4% Me**)	C	1.86	0.42	0.732	0.31	2.12	0.32		
	C + 15% SF	1.69	0.33	0.771	0.25	2.97	0.35		

Paste (With **RHA**)	FA + BA	2.070	1.735	0.958	0.930	-	0.60	[27]	The conductivity and heat capacity have a considerable reduction. The diffusivity was reduced by about 29%, ascribed to the high amorphous silica content and porosity.
	FA + BA + (2-10%) RHA	1.990-1.850	1.672-1.117	0.981-0.909	0.906-0.664	-			
Paste (With **KL** + **MK**)	KL	1.855	0.44	3.235	0.051	18	-	[29]	The diffusivity of refractory mortar with KL is super low. However, adding metakaolin increased the diffusivity due to the dramatic drop in Cp.
	KL + (10-40%) MK	1.858-1.830	0.42-0.36	3.122-0.874	0.052-0.157	22.3-25.5			
Paste (With **KL** and **Bx**)	KL	1.855	0.440	3.235	0.051	18.0	-	[29]	The addition of Bx increased the density of refractory mortar. Further, the conductivity and heat capacity increased significantly (i.e., the thermal diffusivity reduced).
	KL + (10-40%) Bx	2.150-2.155	0.450-0.502	3.395-4.640	0.050-0.031	17.90-17.45			
Paste (With **Gy**)	Gy	0.965	0.185	1.102	0.174	-	-	[10]	Gypsum reduced the density and conductivity and increased Cp (i.e., diffusivity decreased).
		1.162	0.486	-	-	-	0.45	[9]	
Mortar (With **BP**)	Li	1.760	1.35	0.807	0.950	32.10	-	[18]	Adding BP considerably reduces conductivity and diffusivity (50%) with a slight increment in Cp (due to the amorphous silica).
	Li + (8-80%) BP	1.750-1.765	0.920-0.710	0.817-0.841	0.643-0.478	32.90-33.20	-		
Mortar (With **MK**)	Li	1.745	0.650	0.817	0.456	38.5	0.266	[19]	The reaction of lime with MK produces CSH and reduces the porosity. The thermal conductivity and Cp slightly increased, while the density and diffusivity slightly decreased.
	Li + 20% MK	1.637	0.664	0.922	0.440	33.9	0.278		

Concrete (With **WA**)	C	1.98	1.12	0.808	0.70	20	0.4	[20]	The addition of WA reduces density and conductivity, and the Cp increased (i.e., diffusivity decreased significantly), which ascribed the crystalline structure of WA (i.e., Retarding formation of CSH, thus porosity increased).
	C + (5-20%) WA	1.90-1.93	0.98-0.91	0.847-0.964	0.61-0.49	22-25			
Concrete (With **FA**)	C	2.70	1.37	0.77	0.66	-	-	[30]	Adding FA decreased density and conductivity while increasing heat capacity (diffusivity reduced by 30%), which may be ascribed to the amorphous structure and lower density of FA.
	C + (20-30%)FA	2.73-2.57	1.31-1.21	0.80-1.0	0.60-0.47				

Figure 2.3 shows the change in thermal diffusivity with density for different binder compositions and types. The square, circle, and triangle markers indicate paste, mortar, and concrete composites. As shown in Figure 2.3, the thermal diffusivity values increased with increasing the density from 0.03 to 1.2 mm^2/s, ascribed to decreasing porosity (i.e., increasing rate of heat diffusion). The lowest diffusivity values for pastes, while concrete values are the highest (mortars are in between) due to the higher thermal diffusivity of fine and coarse aggregates (0.9-1.4 mm^2/s). However, density, conductivity, heat capacity, and porosity mainly affect the diffusivity results. Furthermore, the crystalline and amorphous phases of the hydration products are significantly affecting thermal diffusivity. As a recommendation for future studies, some binders showed high potential for minimizing thermal diffusivity (i.e., decreasing conductivity and increasing heat capacity), including kaolin, bauxite, gypsum, and lime-based binders, mainly lime with metakaolin (with higher content of MK).

2.2.2 Aggregates:

The aggregates occupy a considerable amount of concrete volume in the range of 60 – 80% of the total volume of concrete [31][3]. Such an amount affects the entire properties of the composite material. Hence, the used aggregate's properties greatly influenced the produced concrete's properties [31]. In other words, the thermal properties of total will directly affect the thermal properties of concrete. Therefore, producing some concrete with thermal insulation and heat-storing ability needs an aggregate with the same properties. The aggregates' thermal properties depend on their mineralogical compositions (degree of crystallinity), porosity, and moisture content [31]. Most aggregates contain a high content of silica, 60-73% hence their thermal diffusivity (thermal conductivity and heat capacity) mainly depending on the degree of crystallinity [31]. The type of aggregate directly affects the heat capacity and thermal conductivity of concrete. The specific heat is inversely proportional to the density (of LWA and LWAC), while thermal conductivity is directly balanced [3]. The amorphous structure generally has low thermal conductivity, density, and high specific heat capacity, attributed to the high porosity and long (staggered) paths compared to the crystalline structure. Therefore, thermal diffusivity has a high potential for reducing and revealing better thermal behavior for transient (unsteady) conditions. The water absorption of the aggregate affects the thermal properties significantly because the thermal conductivity of free water is 0.6 W/m K, and the specific heat capacity of free water is

4.19 J/g K. In comparison, bound water is 2.2 J/g K. Whereas the thermal conductivity of air at the pores is 0.02 W/m K [32][33].

The structural lightweight aggregates (SLWA) are typically expanded clay, expanded shale, or pumice [34]. Using structural lightweight aggregate improved the thermal properties of concrete. The thermal conductivity and specific heat capacity of lightweight concrete are mainly dictated by the volume fraction of SLWA and concrete density [31]. The porosity of SLWA affects all thermal properties due to the very low k-value of air in concrete voids (0.02 W/m K) [32]. Thereby, the thermal conductivity of the produced concrete could be in the range of 0.92 – 1.21 W/m K, the specific heat capacity of 0.932 – 1.002 J/g K, and thermal diffusivity of 0.62 – 0.73 mm^2/s [35]. Generally, the results indicated that the thermal conductivity was reduced by 39 – 53% and the density also reduced in the range of 19 – 31%, while the specific heat capacity increased by 26 – 35%; hence, the thermal diffusivity reduced by 38 – 47%, as compared to concrete with average weight aggregate [35]. The low thermal conductivity and high heat capacity of lightweight aggregate were attributed to the air trapped in the porous structure of LWA that resists/absorbs the heat flow. Further, the slippage at the interface between LWA and cement paste increased due to the higher surface area of LWA (i.e., more energy absorbed) [12]. However, the mineralogical composition of SLWA and their degree of crystallinity significantly affect the thermal properties of concrete [31]. Generally, the SLWA proved a high potential for thermal insulation in both a steady state (with low thermal conductivity) and a transient state (with low thermal diffusivity) [31]. Furthermore, the SLWA is very sensitive to relative humidity, which may modify liquid water in concrete by condensing vapor water in the pores. Thus, thermal conductivity and heat capacity will increase dramatically [36].

As seen in the literature, there are many equations to predict the thermal conductivity of concrete [37], while the specific heat capacity is rarely indicated. Based on the density, the thermal conductivity of heat could be calculated using the following Equations.

$k_{LWCC}\left(\frac{W}{mK}\right) = 0.00143\rho\ (\frac{kg}{m^3})$ – 1.405 (By Zhou) [31]

$k_{LWCC} = 0.072 * e^{0.00125\rho}$ (ACI 122) [38]

Further, the heat capacity (ρCp) for lightweight cementitious composite (LWCC) could be predicted using the Equation [31].

$$Cv_{LWCC}\left(\frac{kJ}{m^3K}\right) = 0.897\rho\ \left(\frac{kg}{m^3}\right) + 32.58 \text{ (By Zhou) [31]}$$

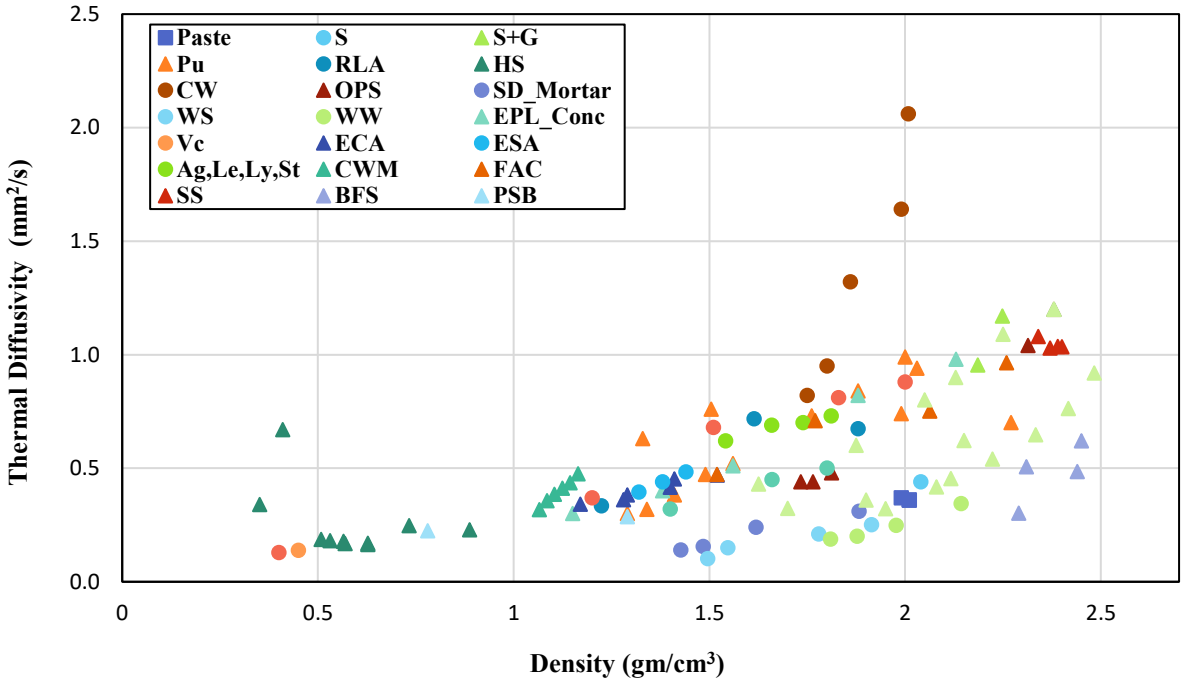

Figure 2.4: Effect of Aggregate type on thermal diffusivity

Table 2.2: Effect of aggregates on thermal properties of paste, mortar, and concrete

Mix Type	Aggregate Type	ρ (g/cm^3)	K (W/m K)	Cp (J/g K)	α (mm^2/s)	Porosity (%)	W/B	Ref	Remarks
Mortar (With **C**)	**S** (C:S=1:1)	2.04	0.58	0.642	0.44	-	0.35	[39]	The addition of sand reduces the heat capacity and increases the conductivity. Thus, the diffusivity increased (18%).
Mortar (With **C**)	**SD** (2-10%)	2.143-1.427	0.42-0.26	0.576-1.301	0.340-0.140	20.54-56.77	0.4	[40]	Adding SD and WS reduced conductivity and diffusivity (54%) significantly. Cp increased considerably due to the high porosity and high specific heat of sawdust and the interaction between cement and saw matrix.
	WS (2-10%)	1.914-1.495	0.34-0.24	0.708-1.574	0.251-0.102	24.22-55.01			
Mortar (With **C**)	**WW** (35-58%)	2.143-1.809	0.420-0.283	0.570-0.837	0.344-0.187	-	0.6	[41]	The density and conductivity reduced significantly, and heat capacity increased considerably due to porosity and high Cp of WW. Hence, the diffusivity decreased significantly (46%).
Mortar (With **C**)	**EPL** (25-100%)	2.0-1.20	1.44-0.18	0.794-0.642	0.88-0.37	-	-	[42]	The density and conductivity were reduced significantly, while heat capacity increased due to the porous and amorphous structure of EPL (i.e., diffusivity decreased substantially by 75%).
Concrete with (**C+SF**)	S+ G + **EPL** (10-50%)	2.38-1.15	1.98-0.38	0.710-0.960	1.20-0.30	10-28	0.48	[43]	

Mortar (With **C**)	**Vc**	0.450	0.11	1.800	0.139	-	1.82	[44]	The addition of Vc improves all thermal properties. Hence, the diffusivity was reduced by 60% compared to cement paste.
Concrete (With **C**)	**S + G**	2.185-2.030	1.817-1.600	0.871-0.837	0.954-0.940	-	0.35-0.45	[31], [45]	Adding gravel increased all thermal properties of concrete due to the high values of gravel's thermal properties compared to sand.
Concrete (With **Gy**)	**WS_C** (20%)	1.162-0.993	0.486-0.241	1.051	0.171	-	0.45	[9]	Adding WS decreased density, conductivity, and diffusivity due to the high porosity generated from the loose interaction between Gy and WS, leading to very low diffusivity.
	WS_F (20%)	1.162-1.052	0.486-0251	1.042	0.242	-			
Concrete (With **C**)	**S + G + SD** (5-20%)	1.98-1.40	1.12-0.55	0.808-1.229	0.70-0.32	20-47	0.4	[20]	The conductivity and diffusivity were reduced significantly. The specific heat increased considerably due to the high porosity and high specific heat of sawdust.
Concrete with (**Lime based**)	**HS** (B: H=2)	0.627-0.508	0.138-0.117	1.34-1.24	0.164-0.186	-	1.55-1.65	[46]	Lime-based binders were the most used with hemp, which exerts a thermal diffusivity of 0.1-0.2 mm^2/s because of lime's low thermal conductivity and high heat capacity.
Concrete with (**C+SF**)	NA + (10-50%) **Pu**	2.38-1.29	1.98-0.40	0.710-0.995	1.20-0.30	10-27.50	0.48	[43]	The density decreased due to increasing the porosity enormously. Hence, the conductivity is significantly reduced. The CP increased considerably. The diffusivity decreased (75%).

Concrete (With **C**)	S + G + **CRu** (10-30%)	2.15-1.70	1.30-0.75	0.970-1.38	0.622-0.323	-	0.55	[47]	Adding CRu decreased the density and conductivity significantly, while the heat capacity increased due to rubber properties and trapped air on the surface of rubber aggregates. Thus, the diffusivity decreased (64%).
Mortar (With **C**)	**PSB** (2-11%)	1.290-0.780	0.39-0.22	1.050-1.260	0.286-0.224	-	0.67-0.48	[44]	The porous structure and low k-value of EPS reduced density and conductivity. The Cp increased appreciably due to the porosity and high heat capacity of PS. The diffusivity decreased by about 50%.

Figure 2.4 shows the effect of fine and coarse aggregates on the thermal diffusivity of mortars and concretes for different types of binders. Circles and triangle markers indicate mortars and concrete, respectively. As shown in Figure 2.4, the density is directly proportional to thermal diffusivity (similar to thermal conductivity) due to porosity (Obviously, porosity is directly proportional to density). At the same time, the specific heat capacity is reversely proportional to density (i.e., lower porosity means lower stored energy). Some specimens showed unexpected behavior, such as mortars with WW, WS, and SD (bio aggregates). The density varied between 1.4-2.2 gm/cm^3 (high because of sand) but still achieved low values of thermal conductivity (0.2-0.4 W/m K), which ascribed to the low thermal conductivity of bio aggregates (<0.1 W/m K). For hempcrete (excluding sand), the density and conductivity values are shallow, which credits hemp aggregates to be used as insulation materials for construction (Similarly, perlite and vermiculite due to their porous and amorphous structure). The hemp, perlite, and vermiculite aggregates group showed the highest specific heat capacity values due to their porous structure, moisture content (high water absorption), and high heat capacity (0.8- 1.6 J/g K). Therefore, the same group showed the least values for thermal diffusivity due to the low values of thermal conductivity and high values of heat capacity, as shown in Figure 2.4. Mortars with CW have high diffusivity values due to the high conductivity and low heat capacity (Figure 2.4).

For future studies, reducing the content of sand and gravel is essential to minimize thermal diffusivity and use hemp, perlite, vermiculite, and pumice aggregates, which showed promising behavior in terms of diffusivity. Hemp aggregates may need chemical treatment to enhance bonding with a binder, reduce hygienic behavior, and maximize heat capacity. Thus, thermal diffusivity results would be optimistic.

The thermal conductivity of hemp shives is very low, about 0.071 – 0.076 W/m K [48], the density is 0.127 g/cm^3 [49], and the specific heat capacity reaches 1.60 J/g K [50]. The properties of hemp vary based on growing, harvesting, and storing conditions [46]. The water content of hemp shives depends on the relative humidity, and the moisture content significantly affects the properties of the concrete [46]. Due to the negative impact of extremely high water absorption of hemp particles (325% of its weight), water retainers (modified hydroxypropyl methylcellulose) were used to minimize the loss of mixing water, hence enhancing the physical and durability of concrete [46].

Lime-based binders were used with hemp, which exerts a thermal diffusivity of 0.1-0.2 mm^2/s [46] because of lime's low thermal conductivity and high heat capacity [13].

Adding hemp stems has promising results in terms of the thermal properties of concrete. As shown in Table 2.2, the thermal diffusivity of hemp concrete is in the range of 0.10-0.30 mm^2/s due to the variation in density, thermal conductivity, and heat capacity. It's evident that the thermal conductivity is affected directly by the density and porosity, which means the conductivity decreases with decreasing density due to high hemp content (has a low density and thermal conductivity) and high porosity percentage [49]. However, the porosity increased with increasing particle size of hemp stems and reducing compaction stress [51]. The presence of fiber with hemp has no advantage in terms of thermal diffusivity because it reduces the porosity (i.e., the diffusivity slightly increased by 11%) [52]. The specific heat capacity increased from 0.50-1.60 J/g K, while the value for concrete with normal aggregate is 0.741 J/g K with an enhancement reaching 54%. The heat capacity of hemp concrete is mainly affected by hemp stems (type and content), binders (type and content), and moisture content and porosity. As shown in the summary, the higher content of bio aggregates increased appreciably the heat capacity due to its high energy absorption. Binders with hydraulic additions have slightly higher heat capacity than pozzolan additions (lime, slag, and Metakaolin). Further, water retainer such as Methylcellulose increased heat capacity slightly because the heat capacity of water (retained) is considerably high, and the use of methyl cellulose produces a higher amount of hydrates (i.e., a more elevated amount of amorphous CSH) in the resulting product [13].

2.3 Conclusions

The mass of buildings could be used as a thermal storage medium, which absorbs and stores the heat during daytime for night heating and vice versa to minimize energy consumption. Such concrete must have high heat capacity and low thermal conductivity (i.e., low thermal diffusivity) to store much energy and prevent losing that energy as noticed in literature that the factors affecting the thermal diffusivity of concrete are binders, aggregates, chemical admixtures, reinforcement agents, water content and temperature. The conclusions of this review could be drawn as follows:

1. The hydration products of binders contribute significantly to thermal properties, in which amorphous structures insulate and absorb energy more than crystalline ones. The grain size and crystallinity of binder particles affect the hydration process and the amount of hydrates and porosity.
2. Aggregates are the most effective component of thermal diffusivity due to their high content. The porosity and moisture, as well as the mineralogical structure, may identify the ability of concrete to reduce heat diffusion.
3. Hemp aggregates showed promising results with shallow thermal diffusivity values relative to other sums obtained from low thermal conductivity values and high heat capacity. This leads to the increased potential of using g such aggregate for thermal insulation, as undertaken in the following chapters.

3 CHAPTER 3: OPTIMIZING HEMPCRETE COMPONENTS (PART I)

Journal paper #2

Optimizing Strength and Thermal Properties of Hempcrete Components Using Cement, Lime, and Pozzolan Binder Compositions

Ahmed S. Al-Tamimi[a], Vivek Bindiganavile[a]

Abstract

Hemp concrete is a sustainable and green concrete produced with binder and hemp hurds as aggregates, which developed in France in the early 1990s and was recently approved in Canada in 2012. Hempcrete is non-structural concrete with superior thermal performance (low thermal conductivity and high specific heat capacity), assisting the utilization of such concrete as building envelope material. Due to the need for more literature on the thermal data of hempcrete and the promising reported thermal behavior, this study is devoted to optimizing hempcrete components to enhance thermal and strength properties. Further, the incompatibility between organic aggregate and inorganic binder matrix, which is already recognized in scientific studies such as high-water absorption, pectin, and sugar effect, this study proposed various binder compositions depending on lime, cement, and pozzolan to enhance integration between hemp and binder matrix. Thus, proper binder composition needs to be with lower hydraulicity to reduce competing about water with hemp hurds, consuming pectin that blocks calcium ions to form CSH, reducing glucose effect on delaying hardening of the binder with alumina and activating carbonation process with the advantage of the porous structure of hempcrete that facilitate the diffusion of CO_2 into the composite. Therefore, this study explored experimentally the integration of cement, lime, and pozzolan binder compositions with hempcrete for thermal and strength properties. Seventeen binders were used to produce hempcrete samples in three groups, including cement, lime, and cement-lime group binders, to assist the marriage with hemp aggregates. Cement-lime group binders (Group III) showed a higher hydraulicity and stiffness matrix relative to cement and lime group binders (reaching 50%) due to strengthening the interface zone with the formation of hydrates with the availability of calcium ions for pectin consumption, CSH, and calcite formation.

This substitution of cement with lime and pozzolan will significantly reduce the carbon footprint due to cement production. However, the optimization for curing conditions for lime binder compositions is required due to the high moisture content after the curing period. Cement group binders showed low strength and thermal properties with highly porous structures ascribed to the minor water/binder ratio that produced a less workable mixture.

Keywords: Hempcrete, thermal diffusivity, thermal conductivity, heat capacity, compressive strength, porosity

Nomenclature

Abbreviations

b/h	Binder to hemp ratio
C	Cement
Ca	Calcium
CB	Crushed bricks
CSH	Calcium silicate hydrate
EDX	Energy dispersive X-ray
FA	Fly ash
G	Gravel
GGBS	Ground granulated blast furnace slag
Gy	Gypsum
HDM	Hot Disk Method
HS	Hemp shives
LEED	Leadership in Energy and Environmental Design
Li	Hydrated lime
Me	Methylcellulose
MIP	Mercury intrusion porosimetry
MK	Metakaolin
n	Amount of gas (moles)
NHL	Natural Hydraulic lime

NZER	Net-zero energy ready
r	Radius of the probe
R	Gas constant
S	Sand
S4-FR	Size 4- French hemp harvest
SD	Sawdust
SEM	Scanning electron microscope
SF	Silica fume
SG	Specific gravity
t	Total measurement time
TPS	Transient plane source
w/b	Water to binder ratio
w/c	Water to cement ratio
WS	Wood shives
XRD	X-ray diffraction

Symbols

Cp	Specific heat capacity (J/kg K)
Cv	Volumetric heat capacity (MJ/m^3 K)
D(τ)	Dimensionless specific time function
P_{gas}	Pressure of gas
P_o	Output power from the probe
t_c	Time correction
$T_{comfort}$	Indoor comfortable temperature
T_{gas}	Temperature of gas
V_a	Added volume
V_c	Empty sample cell volume
V_{CA+FA}	Volume of coarse and fine aggregates (m^3)
V_{gas}	Volume of gas

$\Delta T_s(\tau)$ Temperature increase of the sample surface

Greek letters

α Thermal diffusivity (mm^2/s)

ρ Density (kg/m^3)

σ_c Compressive strength (MPa)

3.1 Introduction

Energy consumption for cooling and heating, especially in residential and commercial buildings, has become a crucial issue worldwide. Therefore, many studies have been initiated to minimize exhaustion usage by improving the thermal insulation properties of concrete because concrete constitutes most of the exterior parts of buildings [1]. Building materials' most important thermal properties are thermal conductivity, specific heat capacity, and thermal diffusivity because losing thermal energy mainly depends on these properties. In particular, the high specific heat capacity and low thermal conductivity (i.e., low thermal diffusivity) are desirable properties due to the ability to retain heat and provide thermal insulation. Thermal diffusivity could be calculated from experimentally measured thermal conductivity k, density ρ, and specific heat capacity Cp ($\alpha = k/ \rho Cp$). As illustrated in Figure 3.1, most literature on thermal constants of cement-based systems is devoted to thermal conductivity, its measurement, and test methods. Thus, there is a lack of information on how the mixture components simultaneously affect the three thermal properties (thermal conductivity, specific heat capacity, and thermal diffusivity).

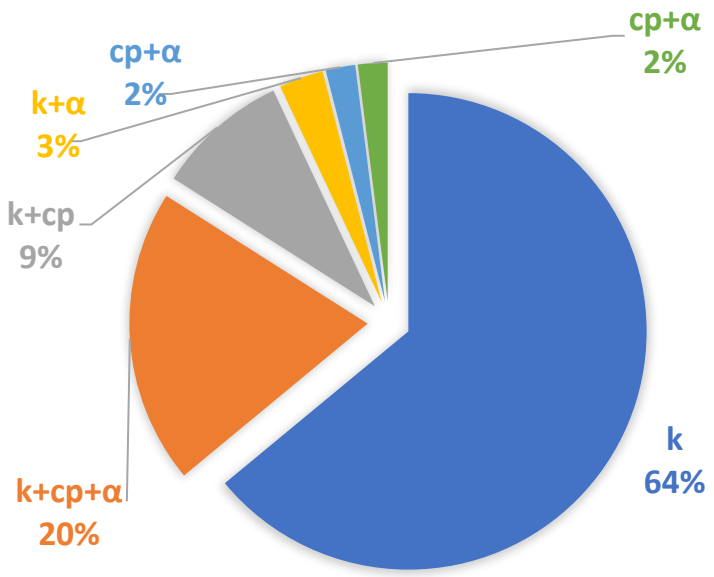

Figure 3.1: Percentage of measured thermal properties of cement-based materials in literature [2]

To explain the importance of thermal diffusivity in the building envelope, Figure 1.2 shows an example of heat transfer through two plates with different temperature gradients. The heat is transferred throughout a material when subjected to a temperature gradient from hot to cold governed by the Diffusion Equation (based on thermal diffusivity) until it reaches a steady state, which is governed by the Poisson Equation (based only on thermal conductivity), as shown in Figure 1.2. Thermal diffusivity expresses the transient heat transfer and refers to the rate of heat diffusion through materials with time until reaching a specific temperature. Hence, the lower thermal diffusivity values mean extra time needed to get the equilibrium with the environment, as illustrated in Figure 1.2. Thus, it could be noticed that the actual case scenarios, such as heat transfer through building envelopes, are transient conditions. At the same time, the steady state is observed chiefly in lab experimental tests such as the hot box or hot plate methods [3].

To explain the importance of thermal diffusivity in the building envelope, Figure 3.2 shows an example of heat transfer through two plates with different temperature gradients. The heat is transferred throughout a material when subjected to a temperature gradient from hot to cold governed by the Diffusion Equation (based on thermal diffusivity) until it reaches a steady state,

which is governed by the Poisson Equation (based only on thermal conductivity), as shown in Figure 3.2. Thermal diffusivity expresses the transient heat transfer and refers to the rate of heat diffusion through materials with time until reaching a specific temperature. Hence, the lower thermal diffusivity values mean extra time needed to get the equilibrium with the environment, as illustrated in Figure 3.2. Thus, it could be noticed that the actual case scenarios, such as heat transfer through building envelopes, are transient conditions. At the same time, the steady state is observed chiefly in lab experimental tests such as hot box or hot plate methods [3].

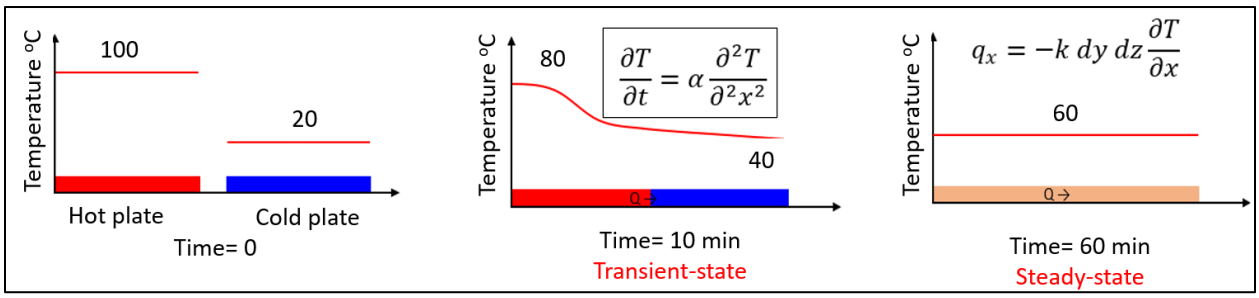

Figure 3.2: Temperature distribution throughout hot and cold plates with time

The significance of transient heat transfer in building heating systems can be illustrated in Figure 3.3, in which buildings in cold weather environments need a heating system to warm the interior space and maintain an indoor comfortable temperature ($T_{comfort}$). Thus, the heating system will be on until reaching $T_{comfort}$; during this time, some thermal energy will be stored inside the building envelopes. Then, the heating system will be off until the indoor temperature becomes less than $T_{comfort}$; during this period, some thermal energy will be released back from the envelopes into the interior space, maintaining the temperature at $T_{comfort}$ for a while. Therefore, the longer the time for the heating system to be off, the more energy saving and the more thermal efficient envelop.

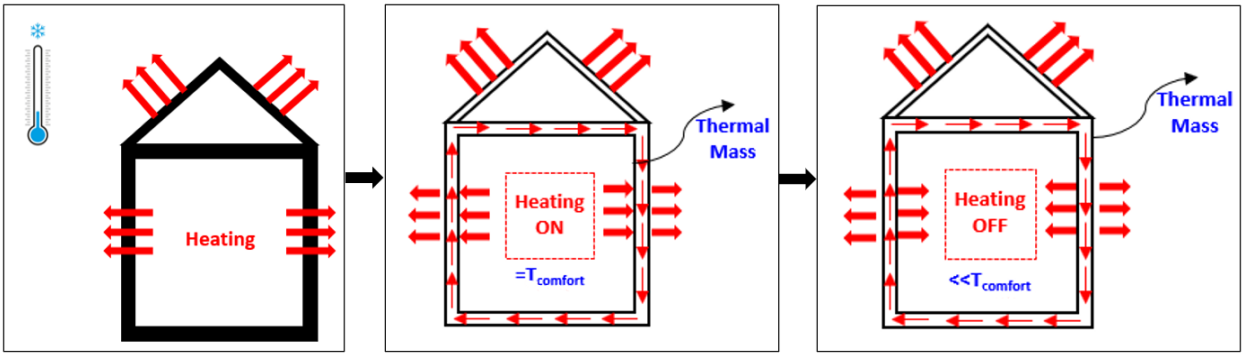

Figure 3.3: Significance of transient heat conduction throughout building envelopes in a cold environment

The first step to implementing this concept in the cementitious composite is to conduct a comprehensive review of the thermal properties of all concretes to identify the factors affecting thermal diffusivity. As highlighted in this review, hemp concrete shows a significantly low thermal conductivity and a higher specific heat capacity (i.e., lower thermal diffusivity) than all other concretes (Figure 3.4). Thus, another literature (as presented in Table 3.1) was conducted on the thermal diffusivity of hemp concrete as a second step toward optimizing components for strength and thermal properties.

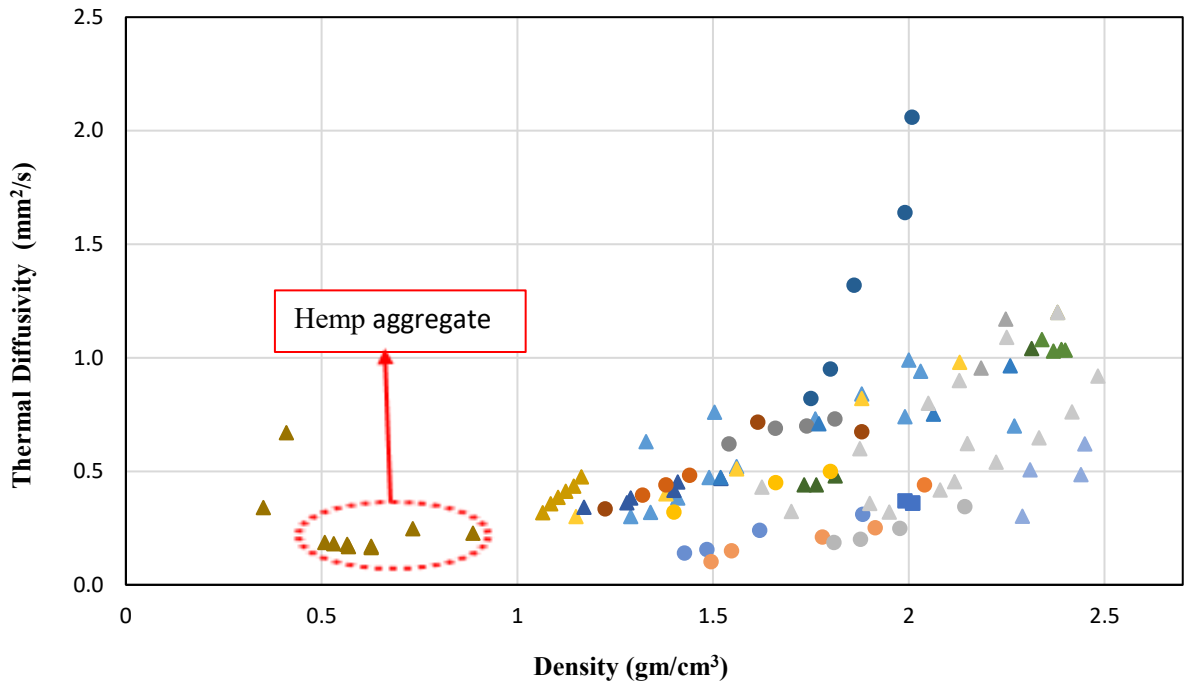

Figure 3.4: Effect of various aggregate types on density and thermal diffusivity of cementitious composites from literature

Hemp concrete is a sustainable, green concrete produced with binder and hemp stems/shives as aggregates. Hemp concrete, called hempcrete or hemp composite, is mainly used with lime as a binder. Hempcrete was developed in France in the early 1990s and spread around Europe. Unluckily, it was approved in Canada as a construction material in 2012 [4][5]. This material could be used for many applications, such as walls, roofs, and floors, which could be implemented by casting, pre-casting, or spraying [4][6]. Hundreds of hemp buildings were constructed around Europe, such as the multi-story French Environment Ministry [6][4][7]. Hempcrete is nonstructural concrete with super thermal and acoustic insulation properties, which could be used within structural frames and still not used for building structural members. Hence, such concrete requires more research to improve the mechanical and physical properties to serve as structural members or masonry. Due to hempcrete's porous and permeable structure, the coating is required, at least for the exterior surface, to prevent hemp hurds' degradation and hygrothermal behavior [8]. Hempcrete exhibits superior fire resistance compared to wood, primarily due to the presence of

binders that exhibit exceptional resistance to flames and high temperatures. In contrast, being entirely organic, wood is susceptible to combustion at elevated temperatures, necessitating the application of fire-resistant coatings.

The following literature focused on hemp concrete's thermal properties and strength to find the gaps and approaches to improve such concrete for thermal insulation. Table 3.1 shows a literature review of hemp concretes with different binders, hemp sizes, and hemp contents, including their thermal and strength properties. This literature is devoted to the thermal diffusivity of hemp concrete; surprisingly, few research were found measuring the thermal diffusivity of hemp concrete, mostly all studies shown in Table 3.1. Therefore, there is a demand for more research on the thermal diffusivity and strength of hemp concrete, including the effect of different binders, hemp sizes, and contents to balance between insulation and strength properties. However, this study will explore the validity of using three groups of binders with cement, hydrated lime, and pozzolan.

As shown in Table 3.1, hemp concretes were produced using lime or cement binders, binder/ hemp ratios (2.0, 1.0, and 6.6), and different graded hemp particles. Thermal properties, including thermal conductivity, specific heat capacity, and thermal diffusivity, were measured for wet and oven-dry samples. The bulk density of hemp particles is 70 to 127 kg/m^3, and the water absorption reached 325% after 24 hours. The thermal diffusivity values varied between 0.156-0.450 mm^2/s for hempcrete with different binders, hemp sizes, and hemp contents, while the thermal conductivity values were within the range of 0.063-0.214 W/m K. However, the thermal conductivity of hemp hurds is about 0.055-0.062 W/m K [9], heat capacity is 1600 J/kg K [10], and water absorption reached nearly 400% by wt. after 24hrs [9].

Lime-based binders are the most common for hemp concrete, as shown in Table 3.1. Walker et al. 2014 [11] used hydrated lime (Li) and hydrated lime blended with cement (C), metakaolin (MK), and ground granulated blast-furnace slag (GGBS) (similar binder composition by [12][13][14]). Hydrated lime ($Ca(OH)_2$), or called slaked lime, is set by carbonation (i.e., Consuming CO_2 to produce calcite ($CaCO_3$)). Therefore, cement and pozzolanic were blended with hydrated lime to accelerate setting and hardening due to their high reactivity and fast setting by hydration and

carbonation [11]. The amorphous silica and alumina react with lime ($Ca(OH)_2$) to produce calcium silicate hydrate (CSH) calcium aluminosilicate hydrates. The authors concluded that increasing hydraulic binder tends to increase the hydrates filling the air pores and increasing thermal conductivity, but there is no significant effect on specific heat capacity. Lime is considered the compatible binder for hemp concrete production due to its breathability, high water vapor permeability, mold resistance, pest obstructive, and low embodied energy compared to cement [7][14]. Natural hydraulic and slaked lime was mixed with fly ash to increase the hydraulicity of hydrated lime (70%) to fasten setting and hardening [15] (similar usage of NHL with slaked lime [14]). Gourlay used Pure cement with hemp to investigate water content on the thermal properties of hempcrete [16]. Thus, there's a need to discover the compatibility of different binder compositions with hemp concrete, including lime, cement, and pozzolans, which will be investigated in this study.

Table 3.1: Literature review on thermal and strength properties of hemp concrete (C: cement, Li: hydrated lime, NHL: natural hydrated lime, GGBS: ground granulated blast furnace slag, MK: metakaolin, FA: fly ash, Me: methylcellulose, CB: crushed blocks, ρ: bulk density, k, thermal conductivity, Cp: specific heat capacity, Cv volumetric heat capacity, α: thermal diffusivity, σc: compressive strength)

Binder type	Binder/ hemp By wt.	ρ (kg/m^3)	k (W/m K)	Cp (J/kg K)	Cv (MJ/m^3 K)	α (mm^2/s)	Porosity (%)	σ_c MPa	Wet/ dry	Ref.
C	2.0	340-415	0.102-0.115	600-770	0.211-0.316	0.37-0.45	-	-	Oven-dried	[16]
70% C + 20% Li + 10% NHL	2.0	627	0.138	1340	0.840	0.164	-	0.12	Oven-dried	[11] [7]
Commercial		627	0.138	1300	0.815	0.169	-	0.21		
70% Li + 30% GGBS		565	0.126	1250	0.706	0.178		0.14		
80% Li + 20% MK		508	0.117	1240	0.630	0.186	-	0.10		
75% Li +15% NHL + 10% FA	1.10-1.80	298-395	0.094-0.105	333-385	0.099-0.152	0.282-0.274	-	-	Wet	[15]
Li+ Mineral Addition	6.67	733-887	0.179-0.214	996-1009	0.730-0.895	0.247-0.228	72-66	-	Wet	[17]
70% Li +30% GGBS + 0.5% Me	2.0	508	0.129	1627	0.827	0.156	-	-	Oven-dried	[12]
80% Li + 20% MK + 0.5% Me	2.0	377-382	0.099-0.105	1601-1575	0.604-0.602	0.164-0.174	81.7-82.2	0.24-0.29	Oven dried	[13]
Li + 10-20% CB	1.0	325-326	0.096-0.094	1504-1398	0.489-0.456	0.197-0.207	-	0.32-0.19	Wet	[14]
		309-311	0.092-0.090	1350-1250	0.417-0.389	0.221-0.232	-		Dry	
Li +10-20% MK	1.0	336-328	0.101-0.098	1536-1530	0.516-0.502	0.195-0.195	-	0.36-0.21	Wet	
		321-312	0.096-0.094	1397-1385	0.448-0.432	0.214-0.217	-		Dry	
Li + 50-70% NHL	1.0	304-323	0.091-0.095	1520-1557	0.462-0.503	0.196-0.189	-	0.26-0.30	Wet	
		291-309	0.087-0.091	1383-1421	0.402-0.439	0.216-0.208	-		Dry	
Wheat starch	0.10-1.25	126-143	0.063-0.074	1264-1288		0.351-0.430	88.5-89.3	0.57-0.63	Dry	[18]

The thermal properties of all concrete types are strongly affected by many factors, including binder, water content, aggregate type and content, and compaction degree [1]. The binders are the bonding component of hemp concrete that creates a connective matrix between hemp particles and prevents biological corrosion of the organic aggregate [19]. Therefore, the binder properties directly affect hemp composite's strength and thermal properties [20]. Unfortunately, hemp hurds have high water absorption capacity, which elongates the hydration surrounding the hemp particles, prevents setting, and weakens the bond at the interface between binder and hemp (i.e., reducing the strength of the hempcrete) [6][20]. Thus, the compatibility between binder matrix and hemp aggregates is necessary to exhibit acceptable mechanical performance [6]. The literature review shows that various binders, such as lime, cement, and pozzolan, could be mixed with hemp to produce a compatible hemp composite with acceptable strength properties [19][6]. Also, commercial binders were explicitly developed for producing hemp concrete, mainly composed of lime, cement, pozzolan, and mineral admixtures such as Tradical® [20]. However, the composition of proprietary binders was not accurately known due to commercial considerations [6]. Many independent practitioners successfully used mixed binders with different proportions to produce hemp concrete, which raises a caution about the reliability of such binders, as stated by Sutton et al. (2011) and Bevan and Woolley (2008) [6]. However, selecting a proper binder for hemp concrete depends on sustainability, environmental, and economic impacts [19]. Pure cement is not favorable for hempcrete production for the following aspects:

- High water demand for hydraulic binders leads to high competition about the available water and remains mainly hemp-surrounded binder uncured, causing fatal effects for the transition zone.
- Setting and hardening delays due to sugar and pectin.
- Impermeability of hydraulic binders could trap the moisture inside hemp particles, causing fungal attack, and the release of water could result in microcracks weakening the system.
- The higher stiffness of hydraulic binder relative to hemp hurds increased incompatibility due to weakening the interface zone.
- High embodied energy and CO_2 emissions (1 ton of cement emitted 1 ton of CO_2 [21])

Many researchers highlighted that lime-based binders were favorable and more compatible and appropriate with hemp concrete due to the following reasons [6][20][7][14][13]:

1. Availability and low harmful emissions during manufacture.
2. Low embodied energy as compared to cement.
3. Environmentally friend due to CO_2 absorption for carbonation
4. Breathability and high-water permeability, less rigidity that is more compatible with hemp hygroscopicity, moisture disappears without damaging the structure [22]
5. High PH that prevents biological deterioration of hemp
6. Relatively low thermal conductivity and density
7. Carbonation of lime requires less water than hydration of hydraulic binders, which minimizes the competition for water between hemp and lime.
8. Due to hemp hygroscopicity (absorb and release moisture), moisture might be supplied back from hemp for the continuity of the carbonation process since a smaller amount of water is needed for ions diffusion relative to hydration ([6][23]).

   $$\text{Available}(OH)_2\ (\text{solid}) + CO_2\ (\text{gas}) \rightarrow CaCO_3\ (\text{Calcite})\ (\text{solid}) + H_2O\ (\text{aqueous}) + 74\ \text{kJ/mol}$$
9. Adding aggregate generally increases porosity and facilitates the transfer of carbon dioxide gas, which is reserved into the highly porous hemp structure [24], and external diffusion through connected pores or from wood alkaline degradation [24] to facilitate carbonation.
10. This is particularly important in lime-pozzolan binders because the pozzolanic reaction starts early but is slow; therefore, water is required for an extended period [24].

Pozzolan is a fine powder with amorphous silicate and alumina (at least 25%) that reacts with portlandite to form hydrates like cement hydration and accelerate the hardening of lime by producing hydrates [24]. Pozzolan materials were added with lime to increase strength and reduce setting time due to the formation of hydration products, which minimize permeability and enhance durability [6]. The smaller particle size of pozzolan (i.e., higher surface area) facilitates the rapid reaction of pozzolan [6]. This is particularly important in lime-pozzolan binders because the pozzolanic response starts early but is slow; therefore, water is required for an extended period

[24]. The addition of approximately 20-30% of pozzolans improves early age properties of lime (such as setting and drying) and strength due to their reaction with lime and the formation of hydration products [6][13][7][25][26]. Further, using 30% hydraulic content with 70% lime is highly recommended by lime-hempcrete practitioners [6], which is similarly found in the literature review of hempcrete, as summarized in Table 3.1. The reaction of lime with pozzolan produces hydration products similar to the hydration of cement, with the difference in the amount rather than the nature of hydrates. However, soluble constituents of hemp proved to delay the setting and hardening of lime pozzolan paste, which is evident at the interface zone with few hydrates [24].

The transition zone between the binder matrix and aggregate is essential because the quality of such region is governed by the mechanical performance of concrete, which is considered the weakest part of composite materials [27]. SEM images showed a severe problem at the interface area, which worsens with increased hemp content due to lapping through the gap area [27]. Elfordy found that the hemp particles' surface was covered with calcium, proofing the failure at the lime binder, not at the interface [28]. On the contrary, Nozahic observed the presence of calcium on hemp hurds and non-solidified product halo around the particles hypothesized to either unreacted binder or interface cavity [27]. The unreacted binder-surrounded hemp particles could be ascribed to the competition on the available water between binder and hemp, which mostly succeeded by hemp since strength was reduced. Thus, the failure depends on the propagation and merging of microcracks, which turns to a large extent on the performance of the interface transition zone between coarse aggregates and mortar [29]. Hemp fiber could cause a flow effect due to high water absorption, leading to higher porosity at the interface area and portlandite crystals due to the high mobility of calcium ions [30].

Walker et al. [24] found few hydrates on hemp particles despite abundant hydrates in the paste for hempcrete with lime-pozzolan. Then, the hemp shives were washed to remove water-soluble constituents such as pectin and sugar. However, the SEM image showed slightly more hydrates on hemp (less than paste). This concluded that water-soluble constituent is not the only disruptive factor of hydration. Many studies mention that the main reason is the high-water suction of hemp, reducing the available water for hydration. As we know, the pozzolan reaction starts early but

slowly; thus, the water should be available longer for the pozzolanic response [24]. Furthermore, the presence of calcite at the interface zone is produced with the availability of CO_2, which is stored in the porous structure of hemp, diffused through connected pores, or from wood degradation [24].

Hemp hurds have a thermal insulation advantage over hempcrete; on the other hand, there are vital effects on binder matrix reducing bond, strength, and compatibility between hemp hurds and binder. The sugar in the binder matrix is a retarder for hydration [4] and carbonation [31], thus delaying setting and hardening. However, the retardation depends on the polysaccharide's binder composition and chemical structure. The effect of polysaccharide on retardation is reduced with higher content of alumina (i.e., high alumina content leading to lower retardation) because alumina and its hydration products consume a higher amount of glucose, maintaining the continuity of hydration and growth of CSH [32][4][33]. The presence of pectin on hemp blocks calcium ions and forms a 3-dimensional gel network (insoluble salt residue in the solution), hence shortening the supply of ions for hydration and lowering the production of CSH gel (i.e., strength reduction) [6]. Therefore, binders with a high content of lime are more proper for hempcrete or conducting a chemical treatment for hemp using calcium hydroxide. However, the effect of pectin is higher on hemp fiber due to the higher content reaching 18% [34][20]. Hemp hurds absorb incredibly high water, getting 500% by wt. after 24 hours of soaking. Therefore, hemp hurds competes with the binder to consume the available water, disturb the hydration process, and reduce hydration and strength [6][35]. However, the excessive water content may cause hemp swelling [36], increased shrinkage [37], and spongy aggregate behavior [38], which all lead to the initiation of microcracks. On the other hand, the lack of water could lead to unreactive and non-solidified products surrounding hemp particles, weakening the interface zone between hemp and binder [27].

As noticed from the literature, there needs to be more studies that explore the thermal diffusivity of hemp concrete. Therefore, a clear gap could be summarized as a need for more data, standards, and optimizing components of hempcrete. This research will deal with the above problem statement by planning an experimental program to improve the mechanical and thermal properties

of hemp concrete with three groups of cement and lime binders to overcome the effect of hemp on binders and reduce carbon footprint by reducing or eliminating cement usage.

3.2 Materials and Sample Preparation

This study prepared hempcrete with three components: binder, water, and hemp hurd aggregate. Four groups of binders were mixed with hemp and tap water: cement, lime, cement-lime, and alkali-activated binders. Further, four sizes of hemp hurds were explored with hempcrete production from Canadian and French harvests.

3.2.1 Cementitious materials

Most cementitious materials were supplied by LAFARGE, including general-use cement (C), dry-density silica fume-SF 100 (SF), fly ash type F (FA), and ground granulated blast furnace slag (GGBS). High calcium-hydrated lime type N (Li) was provided by GRAYMOUNT in Canada. BASAF provided Metakaolin with a highly reactive (glassy) structure. The specific gravity for all cementitious materials is summarized in Table 3.2.

Table 3.2: Specific gravity of cementitious materials in this study

Cementitious material	Cement (C)	lime (Li)	Silica fume (SF)	Fly ash (FA)	Metakaolin (MK)	GGBS
Specific gravity	3.15	2.3-2.4	2.2	2.50	2.50	2.90

Fly ash type F was used due to the higher content of pozzolan materials (silica and alumina) as compared to type C [39][26]. GGBS was not used to produce alkali-activated binders due to the high content of lime. XRD was conducted for all cementitious materials to examine the reactivity (crystalline and amorphous structure), as shown in Figure 3.5. Peaks of the XRD pattern reflect the crystalline structure, while hump patterns show the amorphous phase, as observed for all pozzolanic admixtures (i.e., representing the reactive components). For the alkali-activated binders, two activators were used, including sodium hydroxide (NaOH) and sodium metasilicate

(Na_2SiO_3), which were supplied by BASAF with pellets and solution forms, respectively. The specific gravity of NaOH pellets and Na_2SiO_3 are 2.13 and 1.40, respectively. Further, the PH value of sodium silicate solution is 11.2, and the molar ratio of water glass is >3.2 with 40% sodium silicate and 60% water.

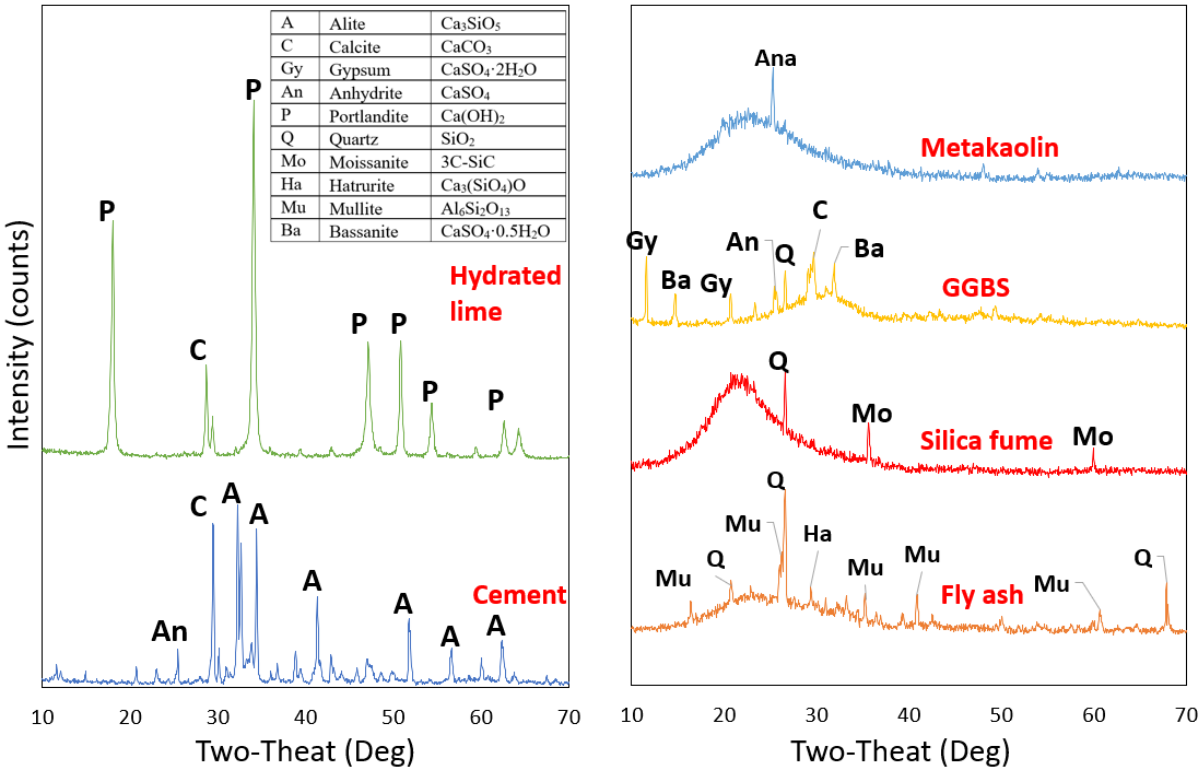

Figure 3.5: XRD pattern for cement, hydrated lime, and pozzolanic admixtures

3.2.2 Hemp hurds

The hemp hurds in Figure 3.6 were supplied from LCDA in France, which meet all technical standards of French hemp building professional rules. Bulk density and water absorption after 24 hours of S4-FR are 164 kg/m^3 and 350%, respectively.

Figure 3.6: Hemp size used in this study (S4-FR).

3.3 Mix Design

Twenty-two batches of hemp concrete with a volume of 0.0024-0.0029 m^3/mix, containing four groups of binders and the same binder-to-hemp ratio, as shown in Table 3.3. The total No. Of samples for each mixture is 12 specimens, including six 50mm cubes and six 75mm dia. discs (i.e., the total samples= 264). The hempcrete mixtures were designed according to the absolute volume method (ACI 211) [40], which mainly depends on the absolute volume of concrete ingredients.

Table 3.3: Mix proportions of hemp concrete with four groups of binders

Binder Type	Binder composition (% by wt.)	W/B	Hemp abs. (%)	w/b (Including abs.)	b/h (By wt.)
Cement based binders	100% C 70% C+ 30% SF 70% C+ 30% FA 70% C+ 30% MK 70% C+ 30% GGBS 70% C+ 30% Li	0.35	200	1.15	2.50
Lime based binders	100% Li 70% Li+ 30% SF 70% Li+ 30% FA 70% Li+ 30% MK 70% Li+ 30% GGBS 70% Li+ 30% C	0.90	200	1.70	2.50
Cement -Lime based binders	50% C+ 50% Li 35% C+ 35% Li+ 30% SF 35% C+ 35% Li+ 30% FA 35% C+ 35% Li+ 30% MK 35% C+ 35% Li+ 30% GGBS	0.625	200	1.42	2.50

3.4 Mixing, Casting, and Curing

In this study, trials have been conducted to determine the amount of absorbed water by hemp during the mixing process, which is about 150%. Water is adjusted until the mixtures become homogeneous and consistent. The following procedures were followed during the mixing process for all hemp concrete mixtures produced in this work, which are similarly followed by Gourlay and Taoukil [16][41]:

- Mixing hemp hurds for 1 min to separate hemp particles agglomerates.
- Add 1/3 of the total water amount and mix for 2 min to wet the hemp.
- Addition of binder, and mix for 2 min.
- Adjust the water and mix for 2 min until it becomes homogeneous.

  The components were mixed in a rotating pan mixer (EIRICH RV02E) with 8-10 Liter capacity, rotating pan, and rotor for 7 min/ mix, as shown in Figure 3.7.

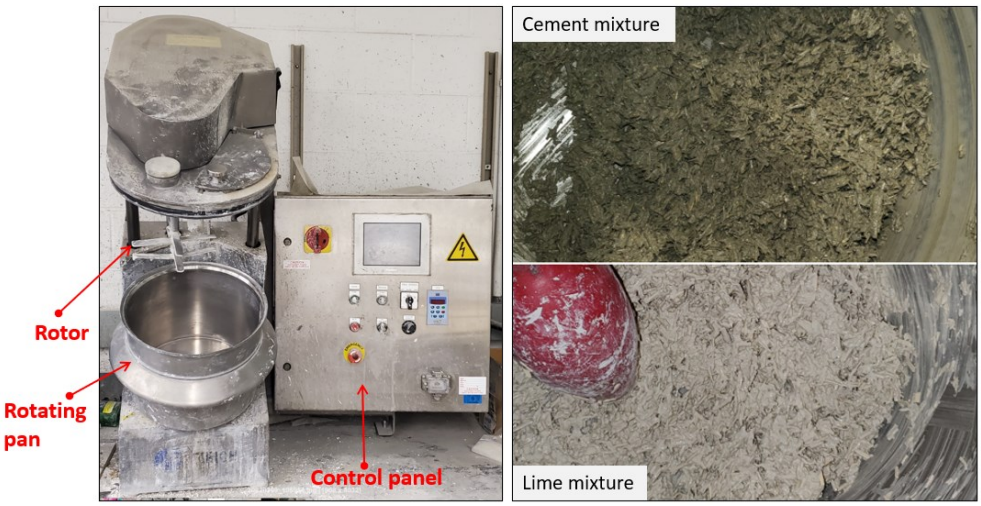

Figure 3.7: (a) Rotating pan mixer (EIRICH RV02E); (b) Homogeneity of mixture for lime and cement binders.

For each batch of hemp concrete, six 50mm cubes were for strength and density, and six 75 mm dia. discs were for thermal properties, as shown in Figure 3.8. Molds were filled with the mixture in three layers, and each layer was hand-tamped by a 16mm rod to ensure compaction (Similarly done by Reilly [12]). However, some techniques are used in literature to enhance the homogeneity of compaction due to the variation of manual compaction [15][16]. Steel manual device was used for compaction of hempcrete as described [42], unified compaction stress of 0.05MPa using a compression test machine [43], and compaction device with piston [27].

Figure 3.8: A typical freshly cast hemp concrete for lime and cement

The specimens were demolded after 24 hrs. and arrowed into a covered container with plastic sheets and rubber bands to minimize loss and gain moisture, as shown in Figure 3.9 (Similarly done by Gourlay [16] and Sonebi [44]). Then, containers were kept in a humidity room at a temperature and relative humidity of 15 and 70%, respectively, according to the following protocol:

1. 7 days of curing: tested for thermal properties on their wet condition, then returned to curing.
2. 28 days of curing: Samples tested for thermal properties and strength on their wet condition, representing the current moisture content in hempcrete samples after the curing period. Then, it was kept inside the oven for 24 hrs. and weighed regularly until there was negligible change in weight.
3. On day 29, Samples were tested for thermal properties and strength in oven-dry conditions.

Pure lime is cured in the lab because lime hardening depends on carbonation, as recommended by Sonebi [44], at a temperature and relative humidity of 24 30%, respectively.

Figure 3.9: Samples prepared for curing after demolding

3.5 Testing/ Experiments

3.5.1 Compressive strength

Three 50mm/mix cubes were prepared and tested for compressive strength. Wet and oven-dry conditions were considered for each mixture. Due to the lack of standards for hempcrete, the ASTM D4832 was followed, in which the load was applied continuously without shock for 4-6 min/sample [45]. Similar studies followed the same standard for hempcrete compressive strength with different load ratings, such as 5 mm/min [13][14][43] and 50N/s (20kPa/s for 50mm cubes) [7]. In this study, the load rating of the available compressive strength machine could be adjusted as (kPa/s). Thus, the rate of loading was adjusted to ensure the failure of each sample was at least 2 minutes (as ASTM D4832), as the selected load rating was 50kPa/s.

3.5.2 Porosity

Hemp concrete is characterized as a highly porous microstructure, which has an open porosity (connected pores) ranging from 60 to 90% [16][8][12]. The interconnected pores (i.e., large pores open on smaller ones) are multiscale and distributed as follows [16][46][47][15][8][12][43]:

- Macropores (>1mm could reach 1cm) due to the arrangement between the hemp particles.
- Mesopores (0.1-1.0 mm) within hemp shiv and binder due to trapped air.

- Micropores (<0.01 µm) between binder hydrates.

The open porosity of hempcrete was measured using different techniques such as mercury intrusion porosimetry (MIP) technique [6][48], air porosimeter [16], and water displacement pycnometer [12]. Further, a helium pycnometer measured the density of solid parts or skeleton of hempcrete samples, as investigated at [47][35][49].

3.5.2.1 Helium pycnometer

Helium pycnometer is designed to measure the skeletal or apparent volume (V_s+V_{CP}) of solid materials based on Archimedes' principle of fluid and Boyle's law ($P_1V_1=P_2V_2$) and ideal gas law ($PV= RnT$), where P_{gas}: pressure of gas, V_{gas}: volume of gas, T_{gas}: temperature of gas, n: amount of gas (moles), R: gas constant. Helium is used as a displacing fluid to penetrate the finest open pores ($<10^{-4}$ µm) due to its small atomic size and chemical inertness towards many materials at normal temperatures [50][51].

Hemp concrete has different types of pores, including closed, open, and external pores, as shown in Figure 3.10. In this study, two samples of hemp concrete were tested for each mix using a helium pycnometer to measure the apparent volume and open porosity. However, the tested samples were the same samples tested for thermal properties after cutting and adjusting the dimensions to fit into the sample chamber (about 50 x 38 x 25 mm).

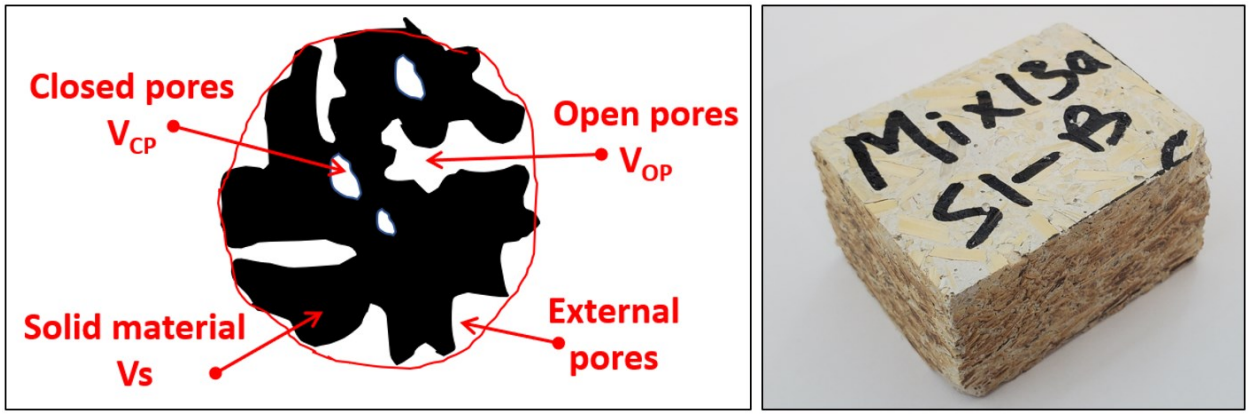

(a) (b)

Figure 3.10: (a) Grain and pores structure; (b) Hemp concrete sample

In this study, the apparent volume was determined by helium pycnometer technique using PENTAPYC 5200e- True Volume and Density Analyzer, as shown in Figure 3.11. The flow diagram in Figure 3.11 shows the typical components of a helium pycnometer, including two chambers of known volume (sample chamber V_c and added volume chamber V_a), a pressure transducer, and a helium gas source. The two chambers are connected in series to the gas source and external vent valve [52][53].

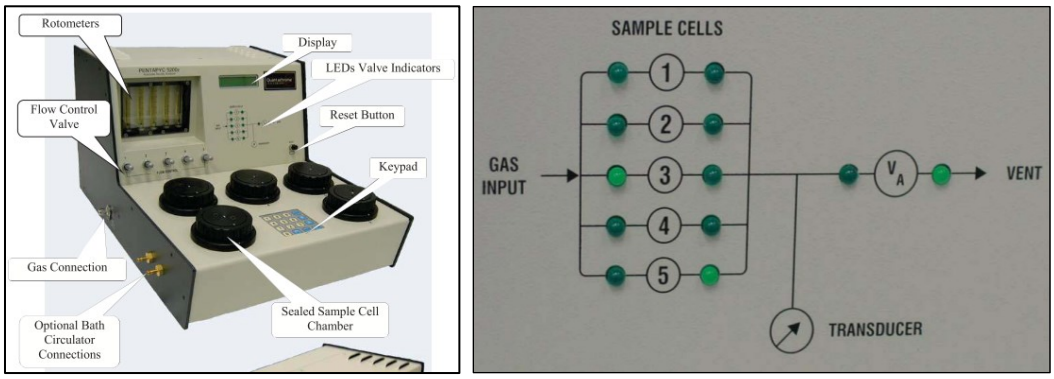

(a) (b)

Figure 3.11: Pentapyc 5200e instrument; (b) Flow diagram of the Helium Pycnometer

3.5.2.2 Water displacement method

Open porosity for hempcrete could be measured using the water displacement method used by Walker et al. [6][51]. Hempcrete samples were soaked in water for two weeks and weighed regularly. Walker was able to measure the weight of hempcrete samples underwater. However, hempcrete samples in this study are floating on water. Thus, the weight placed on the sample to be kept soaking, as shown in Figure 3.12. Then, vacuuming of 100mm Hg (Torr) was applied (same as for soil-specific gravity measurement ASTM D845 [10]) for 15 minutes to ensure the accessibility of water to the open pores.

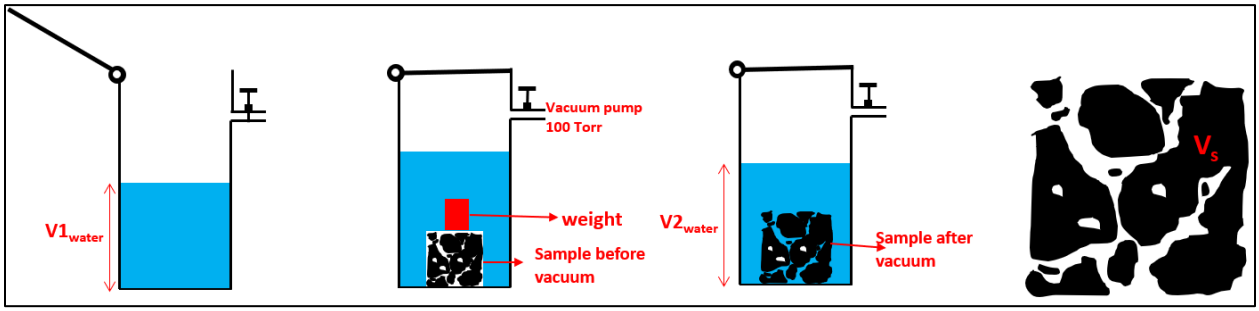

Figure 3.12: Porosity measurement procedures using water displacement method

Hence, the apparent volume could be found with the known V1water and V2water according to Eq- 3.1 and Eq- 3.2:

$$V_s \text{ or } V_{apparent} = V2_{water} - V1_{water} \qquad \textbf{Eq- 3.1}$$

$$V2_{water} > V1_{water}$$

$$Porosity_{Open}\ \% = \left(1 - \frac{V_{apparent}}{V_{bulk}}\right) * 100 \qquad \textbf{Eq- 3.2}$$

As shown in Figure 3.13, a specific water volume is added to the beaker ($V1_{water}$= 350ml), then an oven-dry hempcrete cube is placed on water (sample floating due to low density). A beaker was inserted into a vacuuming cell under 100Torr for 15 minutes to remove air and accelerate water accessibility to the sample pores. Cube samples are sinking into the water after vacuuming, assuring the saturation of pores with water, and the water volume is recorded as $V2_{water}$. The apparent volume could be counted as the difference between the two water volumes.

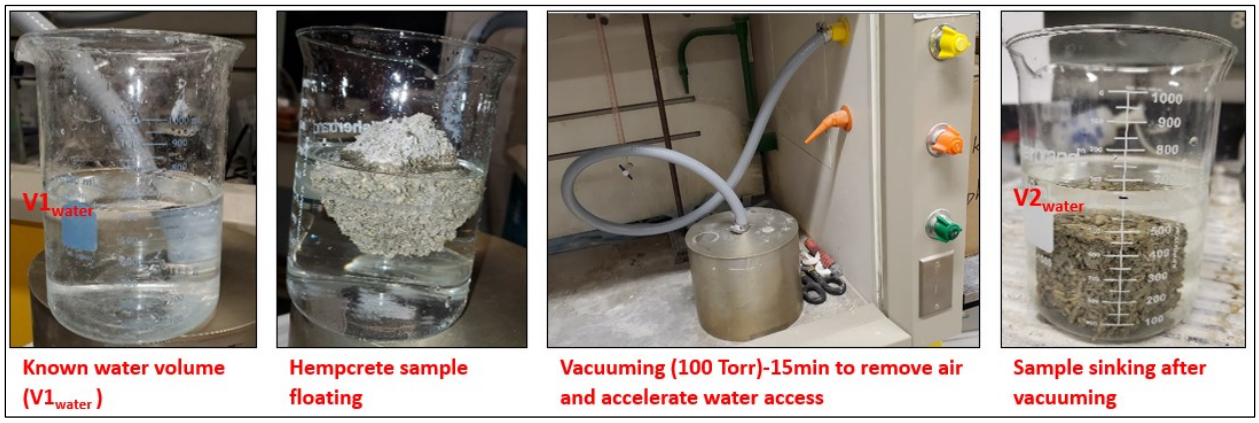

Figure 3.13: Measuring porosity of hempcrete cubes using the water displacement method with vacuuming.

3.5.2.3 BSEM for porosity analysis

Samples were cut from hempcrete cubes using a fine saw, mounted, and soaked with epoxy to stabilize the system. The transparent epoxy system with a dimension of 45x25x10 mm was used for testing under SEM, as shown in Figure 3.14.

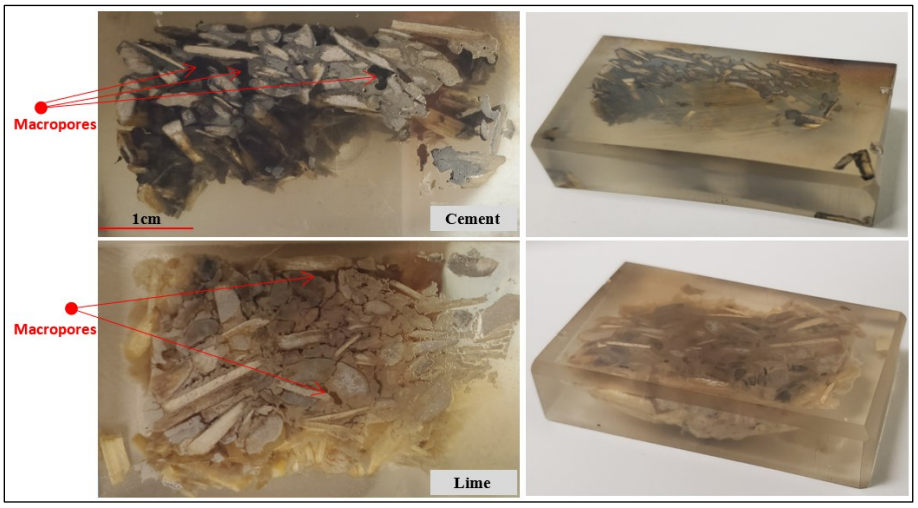

Figure 3.14: Hempcrete samples molded with epoxy.

Backscatter SEM (BSEM) images were captured with a magnification of 50x and an accelerating voltage of 15kV. A series of images were assembled to have a larger image of the hempcrete microstructure. Two samples were prepared, including cement and lime hemp composite, and showing macro, meso, and micropores, as depicted in Figure 3.15. Four types of pores could be noticed in the hempcrete microstructure, including binder, hemp, interface, and connected pores, as presented in Figure 3.15.

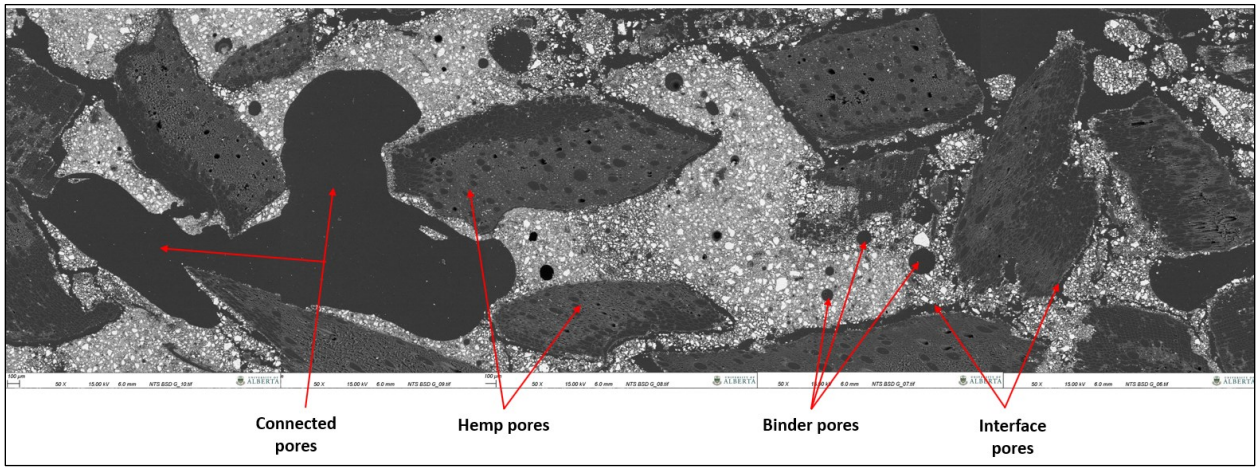

(a)

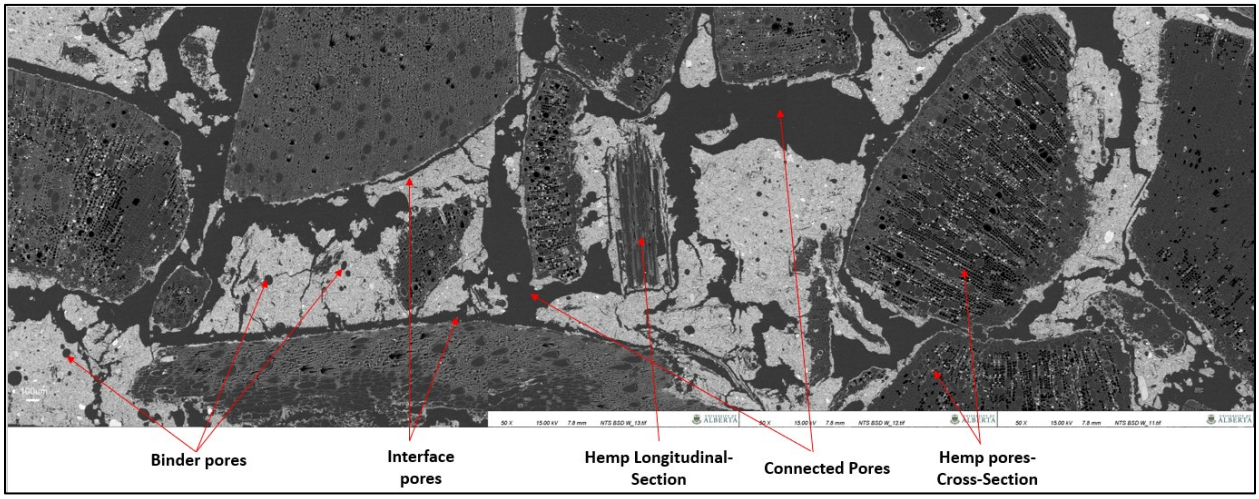

(b)

Figure 3.15: Series of assembled BSEM images showing the microstructure of hempcrete with (a) Cement, (b) Lime

As summarized in Table 3.4, the largest pores in hempcrete composite were the macropores with various sizes (1-10mm), connected pores generated between hemp particles. Mesopores are three types: hemp, interface, and biner air-entrapped pores with sizes ranging from 10-200µm.

Table 3.4: Types of pores and sizes of hempcrete

Macropores > 1mm		**Mesopores (10-200)µm**		
1-2mm (Figure 3.15)	2-10mm (Figure 3.14)	Hemp pores < 60µm	Interface pores (20-100)µm	Spherical air-entrapped pores (20-200)µm

3.5.3 X-ray diffraction (XRD)

XRD is a characterization technique widely used to detect hydration products of cementitious materials [54]. The peaks of XRD patterns reflect the formation of crystalline phases, while the amorphous components could be identified by the presence of humps in the patterns [55]. This study used the XRD (Bruker XRD) as a qualitative analysis to compare the peaks of different binder compositions with hempcrete. Hence, the binder composition performance with hemp could be evaluated.

3.5.4 Thermal properties

The thermal diffusivity and conductivity were assessed for wet and dry conditions using the transient plane source (TPS) measurement technique called Hot Disk Method (HDM) [56], which was developed by Gustaffson in 1990 to measure the thermal properties of solid materials [57]. In this study, Hot Disk TPS 1500 (Thermal Constants Analyzer) was used to measure the thermal constants of the prepared samples of hemp concrete with an accuracy better than 5% according to ISO 22007-2 [56]. As shown in Figure 3.16, the setup mainly contains TPS-1500, PC, and hot disc probe (a thin electrically conducting nickel double spiral inserted between two insulating layers made of Kapton), which is embedded horizontally between two halves of the tested specimen. In this study, a Kapton-insulated probe with a radius of 14.60 mm (Recommended by the

manufacturer for sample size of this study) was used for low temperatures (-196 to 300°C) [55][58]. However, the hot disk acts as a heat source and resistance thermometer to raise the sample temperature and record time-dependent temperature increases.

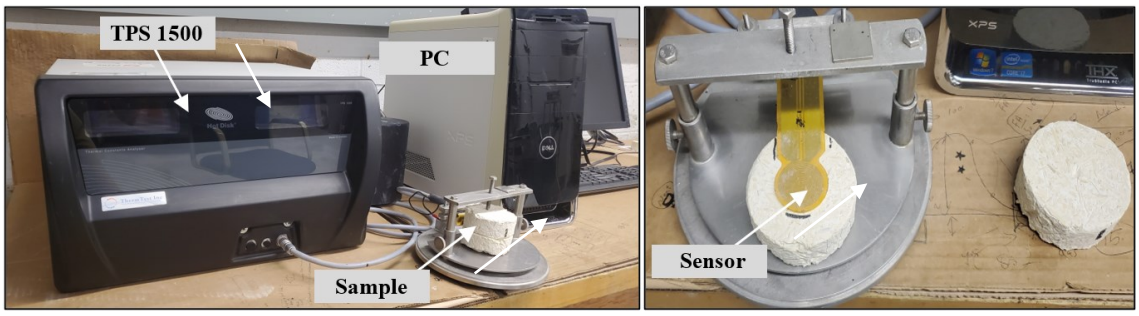

Figure 3.16: Setup for thermal diffusivity test: (a) TPS 1500- Thermal Constant Analyzer; (b) Hot disc probe

The principle of the Hot Disk Method is to produce a heat pulse for a defined period (by electrical current) in the form of a stepwise function through a hot disk sensor to generate a dynamic temperature field within the specimen's two halves [56]. The increase in the average temperature of the hot disk probe is measured as a function of time by monitoring the electrical resistance of the probe (sensor or adaptor) [56][59].

As shown in Eq- 3.3, the overall temperature increase ($\Delta T(t)$) consists of two parts, including the temperature increase over the probe ($\Delta T_p(t)$) and the surface temperature increase of the sample ($\Delta T_s(t)$) during the transient time (t).

$$Increment\Delta T(t) = \Delta T_p(t) + \Delta T_s(t) \qquad \textbf{Eq- 3.3}$$

The solution of the thermal conductivity equation is given by Eq- 3.4 and Eq- 3.5:

$$\Delta T_s(\tau) = \frac{P_o}{\pi^{1.5}\, rk} D(\tau) \qquad \textbf{Eq- 3.4}$$

$$\tau = \sqrt{\frac{\alpha(t - t_c)}{r^2}} \qquad \textbf{Eq- 3.5}$$

Where, $\Delta T_s(\tau)$ is the temperature increase of the sample surface, P_o is the output power from the probe, r is the radius of the probe, k is the thermal conductivity of the sample, $D(\tau)$ is a dimensionless specific time function [56], α is thermal diffusivity of sample, t is the total measurement time, t_c is time correction less than 0.5% of the total time because the development of full output power is not coincide exactly with t=0

To solve equation (Eq- 3.4), an iteration procedure with diffusivity (α) and time correction (t_c) is established, and a linear relationship between $\Delta T_s(t)$ and $D(\tau)$ is created. The values of α and t_c were obtained from the last step of iteration. Finally, thermal conductivity is the slope of the generated line.

The iteration (guessing values for α and t_c) continued until the temperature increase (ΔT) difference between the two constitutive points was less than 0.01°C, as shown in Figure 3.17. The values of the last iteration are the corresponding material results of α and t_c. To calculate the k value, the values of $\Delta T(\tau)$ and $D(\tau)$ corresponding to the last iteration α and t_c were picked up and implemented into Eq- 3.4. Further, the slope of the generated chart between $\Delta T(\tau)$ and $D(\tau)$ reflects the thermal conductivity value.

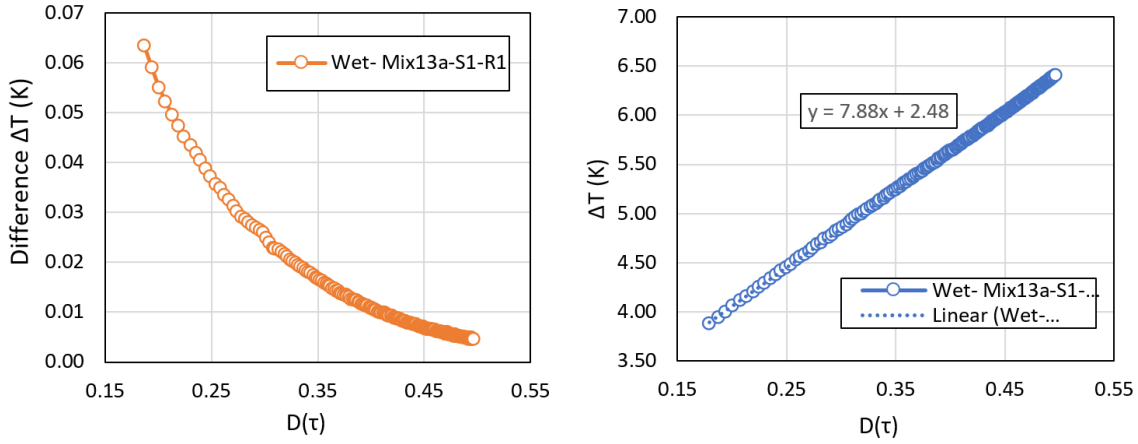

Figure 3.17: Temperature increase $\Delta T(\tau)$, and difference of temperature increase versus $D(\tau)$- TPS1500 typical results

Finally, the volumetric heat capacity (C_v) could be obtained by dividing thermal conductivity by thermal diffusivity.

$$C_v = \frac{k}{\alpha}$$

If the bulk density of samples is available, the specific heat capacity (C_p) could be calculated.

$$C_p = \frac{C_v}{\rho}$$

The probing depth is the penetration depth of the heat wave into the sample in the direction of heat flow during the time window and can be calculated as follows.

$$\Delta p_p = \beta\sqrt{\alpha . t_{max}}$$

Where β is a constant depending on the sensitivity of temperature recordings, t_{max} is the maximum time of the time window for transient. However, the sample thickness must always exceed the probing depth.

3.5.4.1 Sample preparation

1. The specimen's shape can be circular, square, or rectangular. However, in this study, discs were prepared with 75mm diameter and 30mm thickness.
2. As advised by the manufacturer, the diameter of the samples shall not be less than twice the prob diameter, and the thickness of the sample shall not be less than the radius of the sensor to ensure measuring the sample's outer surfaces. Therefore, sensor design 4922 probe (double spiral nickel foil encased in Kapton layer) was used in this study with a radius of 14.60 mm.
3. The two surfaces of the two halves of the sample, which clamped the hot disk probe, shall be flat and smooth. Therefore, samples were sanded using a grinding machine to minimize the wall effect and loss of thermal energy at the contact area, as shown in Figure 3.18. Then, the average thickness of the flattened sample was measured using a caliber.

Figure 3.18: Smoothening and flattening samples with grinding machine.

4. For dry samples, due to the hygroscopicity of hemp, the samples were placed inside a container with silica xerogel to absorb moisture and prevent moisture gain.

3.5.4.2 Test procedures and parameters:

1. The probe is placed between a pair of specimens with flat and smooth surfaces, and each has a thickness of (25-30mm), as shown in Figure 3.19.
2. The specimen's two halves were clapped with the embedded sensor to improve the contact. Then, the base holding the probe and sample was covered with a cap to minimize the external disturbance (Figure 3.19).

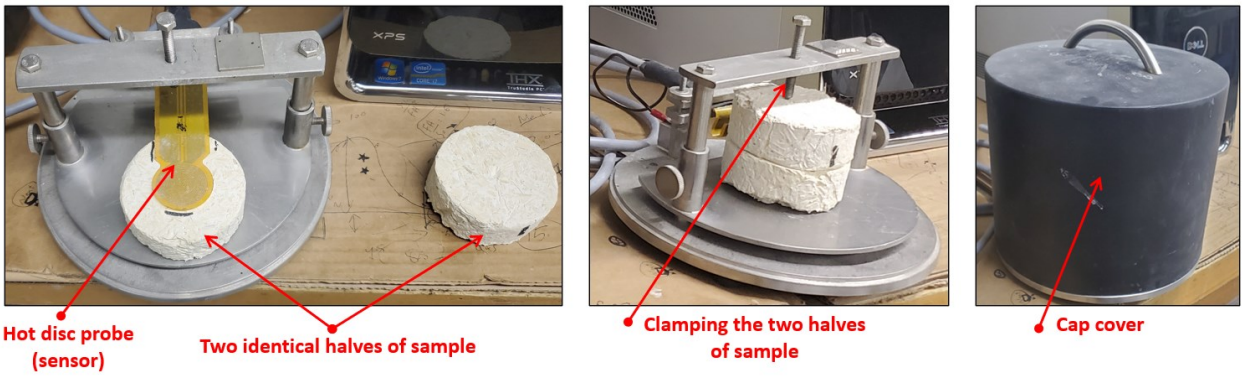

Figure 3.19: Placing the two identical halves of the sample into the test cell.

3. Inputting the parameters, as illustrated in Table 3.5.

Table 3.5: Test parameters, sample dimensions, sensor specifications

Parameters	Value
Sample dia. (mm)	75
Sample thickness (mm)	25-30
Sensor type	Kapton-insulated probe
Sensor dia. (mm)	29.20
Applied heat power (mW)- Wet	250
Applied heat power (mW)- Dry	150
Testing time (s)	640
Testing temperature (°C)	21
Precision of α (%)	5-10
Precision of k (%)	2-5

4. The thermal diffusivity was measured for three samples from each mixture and three readings for each sample. Thus, the diffusivity averages nine readings (3 readings/sample).
5. The heat power was adjusted for wet and dry samples, ensuring the probing depth was less than the sample thickness. The wet samples needed higher heating power than dry ones for the same transient time (640s).
6. The output power and measuring time were adjusted based on the parameters wizard tool in the software (Hot Disk Thermal Constants Analyzer 7.2.1), and the test outcomes fell within all the acceptable ranges recommended by the manufacturer, as shown in Table 3.6.

Table 3.6: Experimental results ranges recommended by the manufacturer.

Parameters	Value
Temp. increase	3-10°C
Prob depth	<sample thickness
Testing time/ characteristic time (r^2/α)	(0.33-1.0) => green flag (0.20-2.0) => yellow flag
The mean deviation of points from the fitting line	< 0.003 K
t_c	< 3.20s (0.50% * testing time)

It's helpful to know that the hot disk sensor functions as a resistance thermometer, which is directly affected by heating power and current through the sensor. As recommended by Wizard, wet samples required a high output power and measuring time (250mW and 640s) relative to dry samples (150mW and 640s). In other words, wet samples have a high thermal conductivity and need a higher output power, leading to a higher current (i.e., precise reading for resistance increase). Hence, the temperature increase could be less than dry samples, as shown in Figure 3.20.

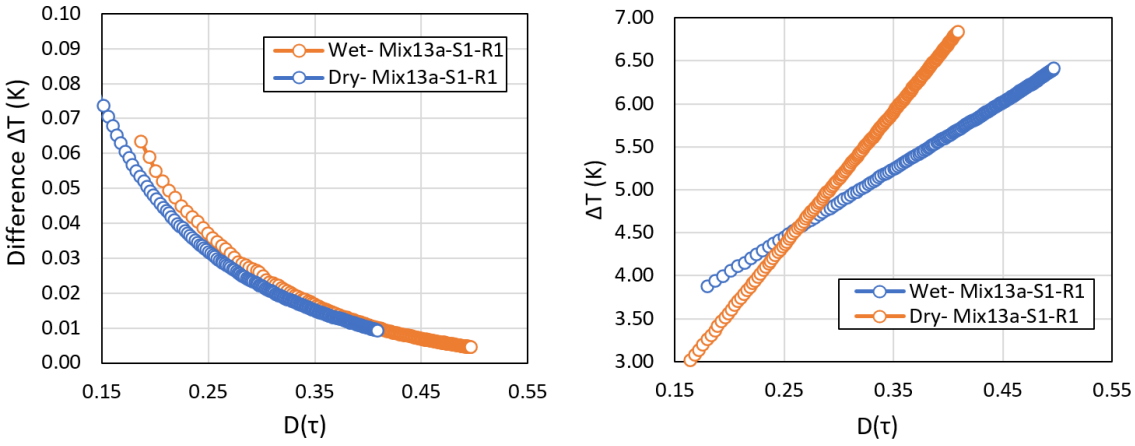

Figure 3.20: Temperature increase and difference of temperature increase versus D(τ)- TPS1500 results.

3.6 Results and Discussions

The components of hempcrete need to be optimized and more compatible; hence, this study is dedicated to evaluating binder compositions with cement, lime, and pozzolan for strength and thermal properties. Seventeen mixes were prepared for hemp concrete with different binders, the same hemp content (40% by wt.% or b/h= 2.5), and the same hemp size (S4-FR). The samples were evaluated as wet at 28 days; then, samples were oven-dried at 60^{o}C for 24 hours and assessed for thermal strength and porosity at dry conditions. Thus, this task studied the effect of binder type and moisture on hemp concrete's thermal and strength properties.

3.6.1 Cement-based binders

The wet densities of hempcrete cubes with cement and pozzolans varied between 886-956 kg/m^3, while the oven-dry ones are in the range of 500-541 kg/m^3 with a difference of about 7%, as shown in Figure 3.21. Thus, adding 30% pozzolans does not significantly affect the bulk density of hemp composite (<7%). However, the moisture content varies between 41-47%, which assures the amount of water consumed by each binder and the significant increment of wet densities (43-46% relative to oven-dry ones). The mixture with higher moisture content indicates that the binder was relatively slower reactive. The compressive strength for moist samples is 0.53-1.07 MPa, while the oven-dry ones are 0.48-0.89 MPa. The presence of water increased the strength by 4-31%, attributed to capillary pressure [60] and dry shrinkage [37]. In contrast, the strength was reduced for the dried samples due to the propagation of microcracks and debonding with hemp contraction [60]. Interestingly, microcracks and debonding are the dominant factors for the failure of dry samples, potentially ascribed to the group I binders' lower stiffness since cracks are initiated easily after drying. However, the stiffness of cement binders was strongly affected by hemp due to the shortage of calcium ions since pectin significantly consumed the available ions, resulting in lower production of CSH and ettringite and lower binder stiffness. Further, the lack of water due to hemp absorption and the incomplete hydration (since there is high water content, reaching 47% at testing time) are valid reasons for the lower strength. The average porosity of cubes using the water displacement method varies between 54 and 61% (about 11% difference). The difference is ascribed to the uncontrolled variation in compaction, hemp particle distribution, and accessibility

of water into pores (i.e., Closed pores are not counted). The least porosity mixture achieved the highest strength (cement with lime), while the highest porosity mix (cement with fly ash) was not the weakest composite (Pure cement mixture showed the least strength). Therefore, other factors, such as the amount of hydrates and bonding, might affect the strength significantly.

The addition of lime shows the fastest rate of reaction since it shows the least water content, which might be ascribed to the extra content of Ca^{+2} reacting with pectin; hence, hydration is not disturbed (i.e., available Ca ions for the formation of CSH and ettringite [6][24]). Furthermore, the results of porosity and strength confirmed the same trend for lime since it showed the least porosity (55%) and the highest strength (0.89-1.07 MPa) due to the formation of CSH and ettringite filling the pores and enhancing the bond [6][24]. Also, carbonation of lime takes place with the availability of CO_2 either from air trapping during mixing or diffusion through the porous structure of hempcrete and from the degradation of hemp due to high alkalinity (Hypothesis mentioned by [24]), as calcite peaks are clearly shown in XRD results for all group I binders Figure 3.24. The slag dries faster than metakaolin (Similarly found by [61]), which might be due to the presence of lime. However, metakaolin showed a higher strength relative to slag by about 13, and 29% for wet and dry samples, respectively, which might be due to the formation of more CSH and CASH (due to the presence of high amorphous aluminosilicate materials in metakaolin), and high alumina content leading to reduce sugar effect. The mixture with fly ash showed the highest moisture content (about 47%) and the highest porosity (about 61%), which reveals a slower pozzolan reaction and reduces the water demand due to the bearing effect of fly ash [62]. Nevertheless, the strength was still relatively high, with about 0.91 and 0.64 MPa for wet and dry samples of silica fume, respectively, which ascribed to two reasons: improved interface area and competition to have water due to the high fineness ratio [63][62]. Silica fume increased the strength of hempcrete due to high amorphous silica content relative to metakaolin, as found for concrete and mortar [25][26]. The highest hydraulicity of pure cement mixture showed the minor strength (0.48-0.53 MPa), which could be ascribed to the shortage of demanded water (as similarly found by Nguyen [6]), the absence of the pozzolan effect and the impact of hemp (pectin and sugar). However, the interior binder of cube samples was found to be powder due to the unavailability of water and un-

reactivity, which was proved by XRD data in Figure 3.24, showing many peaks of Hatrurite (similar findings by Evrard [64]).

In conclusion, the substitution of pozzolans with cement for hempcrete increased the strength significantly by 18-50% for wet samples and 6-46% for oven-dry samples. However, the density of wet and dry samples was moderately affected. The most compatible binder composition from cement-based binders in this study is cement with lime (70% C + 30% Li), which showed the fastest reaction and achieved the highest strength in this group due to the higher availability of lime-consuming pectin; the occurrence of carbonation (i.e., formation of calcite), higher production of CSH and ettringite filling pores and enhancing bond.

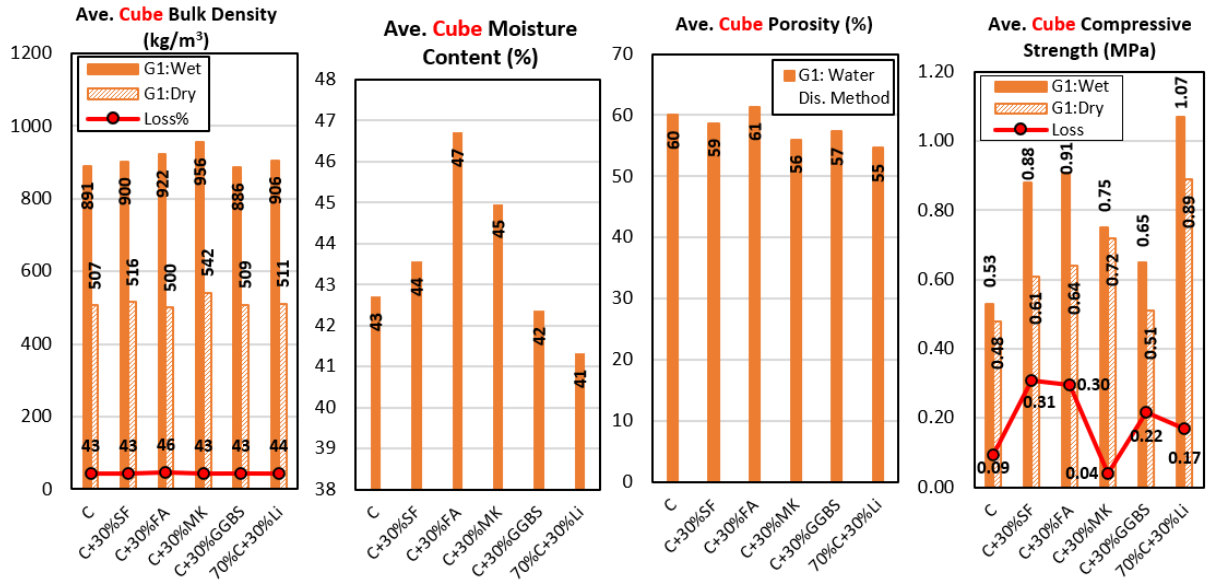

Figure 3.21: Physical and strength properties of hemp concrete cubes with cement-based binders at 28 days (Loss%= Loss*100)

Hempcrete has a ductile (high deformability) behavior under compression due to the high compressibility of hemp hurds and the highly porous structure of hempcrete. The hempcrete samples compressed with loading closing the pores, and hemp with binder deforms simultaneously, as shown in Figure 3.22. Hemp can withstand higher strain than the binder. Thus, failure should occur at the binder matrix, not the hemp particle. However, the failure occurs at the

interface zone, neither binder nor hemp, which is ascribed to the poor cohesion between the two components, as depicted in Figure 3.23 (Similar findings [6][64][65][28]).

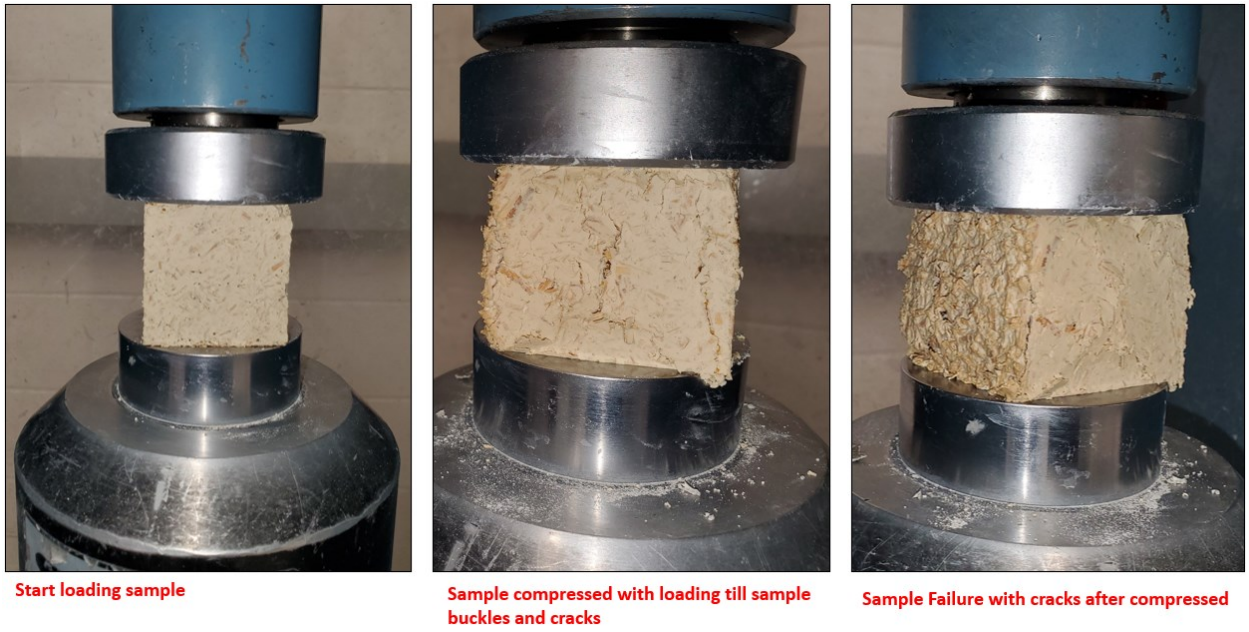

Figure 3.22: Compression test for a typical hempcrete sample showing failure mode (buckles and cracks)

The presence of non-solidified products (as powder) after crushing hempcrete cubes (at oven dry condition) refers to the unreactive binder due to the lack of water for hydration, which is absorbed by hemp particles around the binder matrix (similar findings [83]), as shown in Figure 3.23. However, the powdered binder was not observed after crushing hempcrete cubes in wet conditions due to the presence of water and continuity of hydration, as shown in Figure 3.23. As a summary of the behavior of hempcrete cubes under compression, the following notes could be drawn:

- Hemp hurds could be compressed or bent during load application of hempcrete sample, but failure first occurs at the interface zone and is never noticed in hemp particles.

- Some traces of binder were noticed on hemp hurds after crushing (Figure 3.23), meaning that the reaction was started at the hemp surface at early curing time with high availability of water, then the response was disturbed surrounding hemp particles because hemp absorbed the water from the surrounded binder matrix, and fatally affected the contact zone.
- Hemp hurds with a flaky shape are distributed in the binder matrix randomly in all directions, and debonding occurs in all directions, even for the particles perpendicular to the load direction (Figure 3.23).

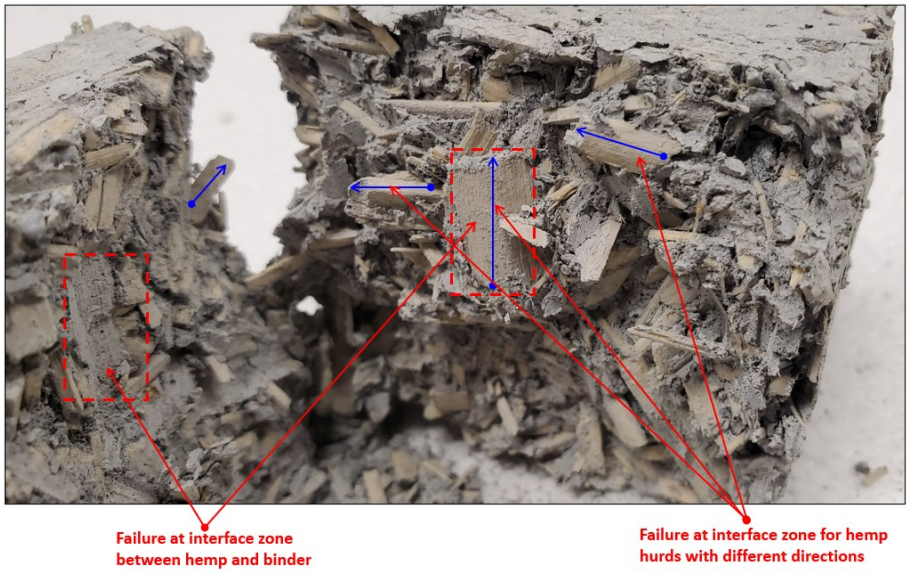

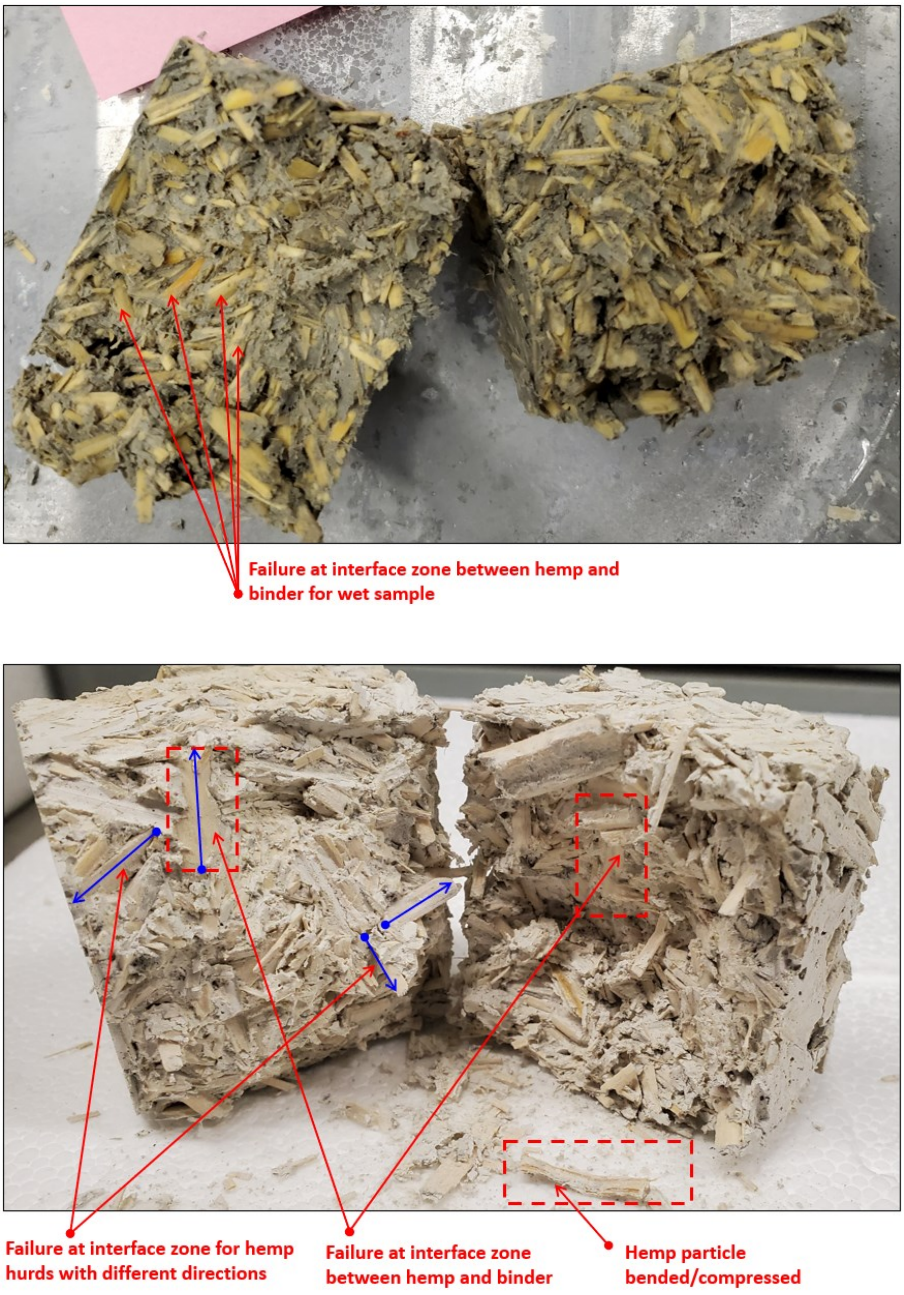

Figure 3.23: Failure of hempcrete 50mm cubes of typical samples with different binder compositions and the same binder/ hemp ratio

Figure 3.24 shows the peaks of crystalline products of group I binders. Calcite and Aragonite crystals appear in all the XRD patterns, which proves the occurrence of carbonation, which is

facilitated by the availability of CO_2, either trapped or diffused through the porous structure of hempcrete. Furthermore, most peaks represent Hatrurite (Ha) in all XRD patterns, a mineral substituted C_3S or Alite (See cement XRD Figure 3.5). That proved the water consumption of hemp hurds disturbed the hydration and prevented the reactions of C_3S due to the lack of water. Thus, the higher hydraulicity of cement-based binders used with hemp in this study demonstrated the un-reactivity of C3S due to the lack of water (i.e., reducing binder hydraulicity (by increasing lime content) for the usage with hemp aggregates is beneficial to enhance mechanical properties). Also, Portlandite peaks in fly ash, slag, and lime mixtures appeared due to the presence of CaO. Small peaks of Ettringite (Et) (reaction between sulfate and calcium aluminate at an early stage - first few hours- to prevent flash setting) appeared in samples with silica fume, metakaolin, slag, and lime due to the high presence of C3A in MK and GGBS (i.e., high C3A to calcium sulfate leading to early formation of ettringite). However, SF and lime probably prohibited the negative impact of hemp on the formation of ettringite by providing sufficient calcium ions.

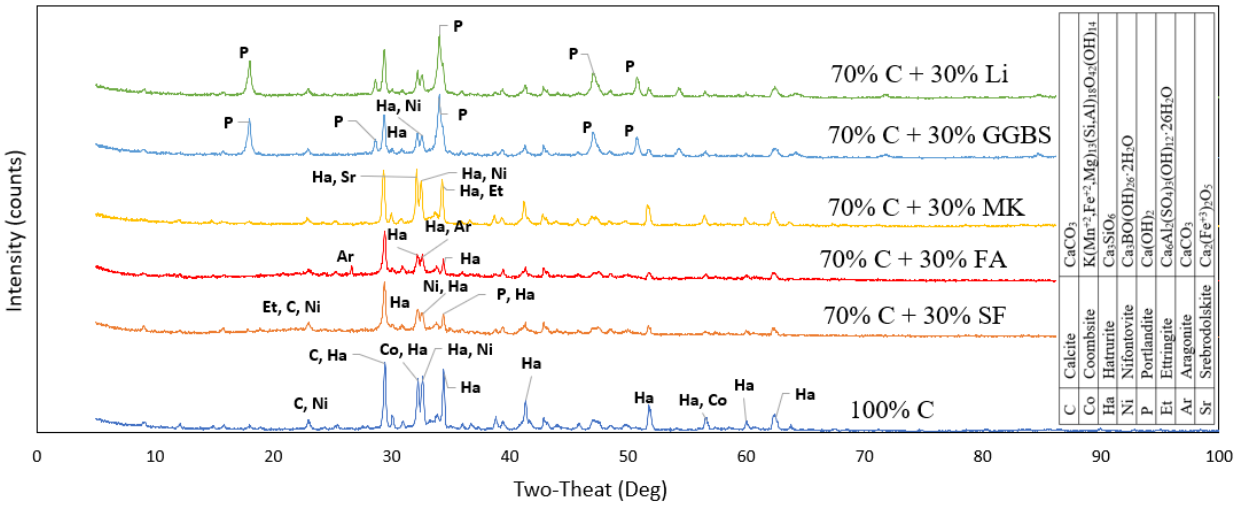

Figure 3.24: XRD patterns for cement-based mixtures

The density of wet disc samples is between 655-817 kg/m^3 (about 20% difference due to moisture content, which varies between 31-40 %), while the oven dry one is 507-549 kg/m^3 (about 7% due

to porosity variation of 69-71%), as shown in Figure 3.25. Density and moisture content divergence between disc and cube samples could be ascribed to the compaction degree and hemp hurds arrangement into different mold sizes. The porosity for disc samples was measured using a helium pycnometer, which afforded higher values relative to the water displacement method for cube samples. However, disc porosity values are similar and do not significantly differ (67-72%).

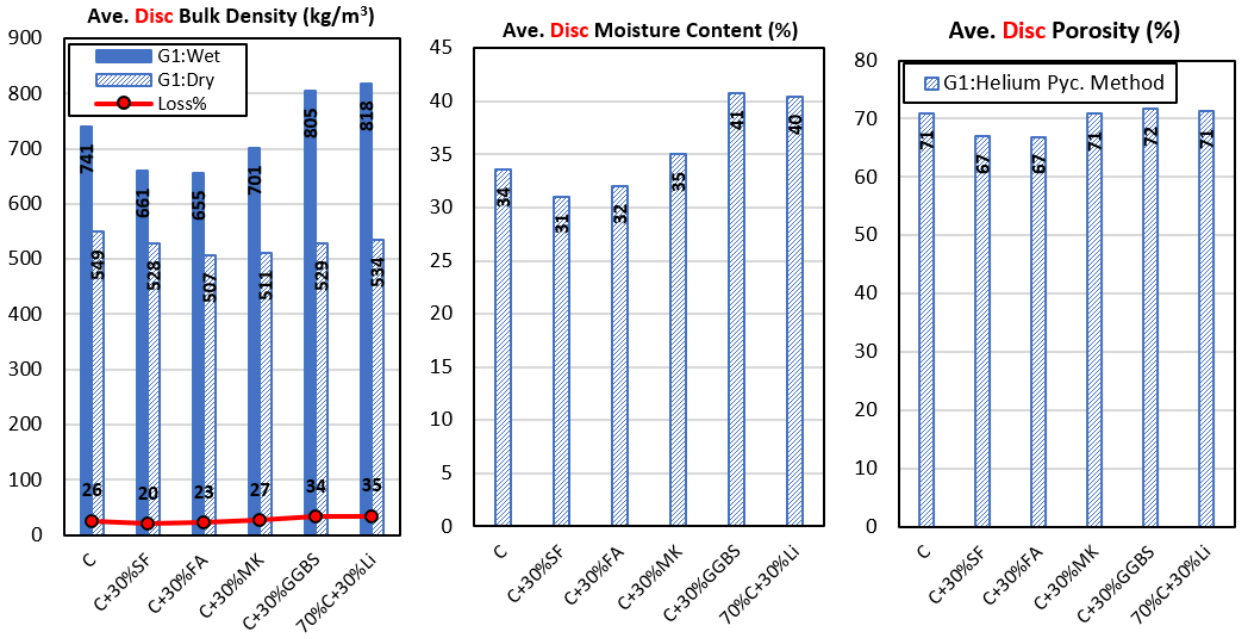

Figure 3.25: Physical properties of disc hemp concrete with cement-based binders at 28 days

As shown in Figure 3.26, the thermal conductivity of cement-based binders varies between 0.277-0.450 W/m K for moist samples with a difference of 38% ascribed to the porosity and moisture content (31-40%) since the thermal conductivity of water (0.60W/m K) is much higher than air (0.03 W/ m K) [66][14]. Thus, the difference in thermal conductivity between wet and dry samples varies between 66-74%, as shown in Figure 3.26. The oven-dry samples are in the range of 0.089-0.115 W/m K with a variation of 23% attributed to the porosity (67-72%) and binder properties (Amount of hemp hurds assumed to be same for all samples). The conductivity of dry samples falls within the literature results, as shown in Table 3.1. In contrast, the moist samples seem to be

higher due to the high moisture content of disc samples (31-41%) (similar findings found by Taoukil [66]). It's good to recall the effect of varying moisture content on thermal properties, but this study focuses on measuring thermal properties at the existing moisture content after the curing period. Another reason for having higher k values for wet samples is that wet samples' rough surface forms air voids and loses energy at the interface, increasing resistance. The least thermal conductivity for dry samples is 0.089 W/m K for fly ash. In comparison, the highest one is 0.115 W/m K for lime, which is ascribed to the higher mixture density and higher conductivity of lime (around 0.70 W/m K [12]) relative to fly ash (around 0.119 W/m K).

The thermal diffusivity of moist samples is 0.281-0.405 mm^2/s (i.e., about 30% difference), while for dry ones is 0.103-0.125 mm^2/s (with about 18% difference), comparable with the literature data in Table 3.1. The thermal diffusivity of moist samples is significantly higher than oven-dry samples (about 59-74%), ascribed to the effect of moisture content on thermal diffusivity. As explained earlier, the impact of moisture content on concrete's thermal diffusivity is unclear and varies with each moisture content. Therefore, for such moisture content (31-41%), the thermal diffusivity of wet samples is hugely higher than that of dry ones as the diffusivity values varied with the change of moisture content for the same sample (i.e., α might increase or decrease with changing moisture content). The thermal conductivity of the material defines the diffusivity to its volumetric heat capacity; thus, the higher diffusivity of wet samples reveals that their thermal conductivity increased faster than the heat capacity at the existing moisture content as explained by Taoukil [41], and Bruijn [15]. The diffusivity change with varying water content is not yet apparent and is not targeted in this study. This behavior (high diffusivity of moist samples relative to dry ones) is assured to be ascribed to the higher thermal energy (P_0) required for wet samples for testing (Eq- 3.4) due to the higher conductivity of water relative to air. From the definition of diffusivity ($\alpha=k/C_v$), the conductivity is directly proportional to diffusivity. Thus, the diffusivity will increase with water's presence relative to dry ones.

Generally, the replacement of pozzolan with cement showed a noticeable difference in thermal conductivity and diffusivity (<23% for dry and <38 for wet) but may not only ascribed to the

pozzolan effect since hemp particle distribution, compaction degree, and moisture content are indirect influencers towards physical and thermal properties.

The values of volumetric heat capacity in Figure 3.26 were calculated from the previous values of thermal conductivity and diffusivity. As shown in Figure 3.26, C_v values of dry samples vary between 0.825-1.102 MJ/m^3 K (with a difference of 25%), while the moist samples have values of 0.846-1.15 MJ/m^3 K (with a difference of 26%). The C_v values are comparable with the literature summarized in Table 3.1. The increment in conductivity and diffusivity will affect the volumetric heat capacity un-monotonous because their increments differ. For example, heat capacity (C_v=k/α) will increase more if the increment of k is much higher than α, and vice versa. The wet C_v showed similar or higher values than dry ones, which might be explained similarly to Taoukil [41], as conductivity increased faster than diffusivity, leading to higher C_v and vice versa. Since the moisture content is different for all mixtures (31-41%), the diffusivity and conductivity will be varied. In other words, the thermal properties of wet samples were measured for the existing moisture content, which is not the same in all samples. Further, the thermal properties will be varied for the same sample with varying moisture content. Therefore, it's hard to ascribe the difference to the effect of pozzolan or moisture. However, the dry samples' porosity is varied, to which the difference in thermal data might be ascribed, as well as the pozzolan effects.

The specific heat capacity (C_p= C_v/ρ) for dry samples was 1114-1748 J/kg K (i.e., a difference of 36%), while the values for the moist samples was 1578-2061 J/kg K (i.e., a difference of 23%). Again, here, the dry values seem to be higher than the moist ones (8-32%), ascribed to the effect of higher wet densities (C_p= C_v/ρ). Hemp concrete is known to have a high heat capacity relative to regular concretes, as can be seen in Table 3.1. The C_p values reached 1627 J/kg K [12], more than 1500 J/kg K [14], and could reach up to 2900 J/kg K [67]. However, the conventional concretes showed a thermal capacity of 800-1200 J/kg K [68][17].

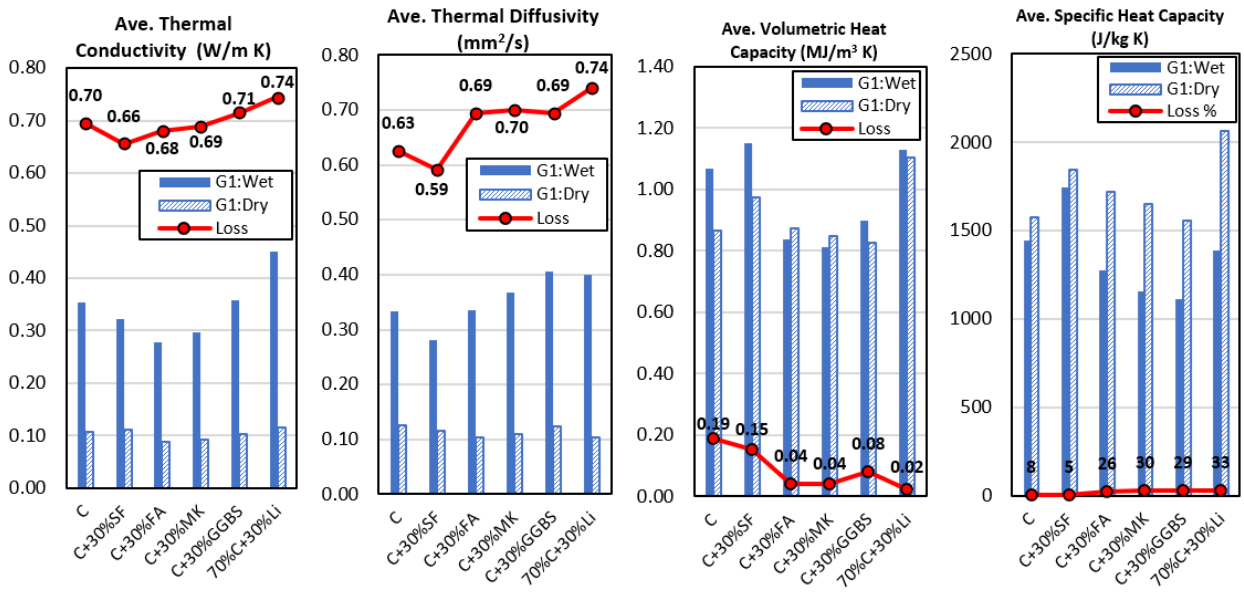

Figure 3.26: Thermal properties of hemp concrete with cement-based binders at 28 days (Loss%= Loss*100)

3.6.2 Lime-based binders

Pure lime mixture (Li) was cured in a lab atmosphere with temperature and relative humidity of 24ºC and 30%, respectively, because only carbonation is needed for setting and hardening the composite. However, all the pore water evaporated during the curing period, as there is no difference between wet and oven-dry densities (Figure 3.27). Therefore, such relative humidity (30%) is not a suitable environment for the continuity of the carbonation process (Similar findings for hydraulic and air/slaked lime binders [43]). Other mixtures with hydrated lime with 30% pozzolans seem to have a high moisture content even after 28days of curing in a humidity room (RH= 70%, Temp= 15ºC) inside containers covered with a plastic sheet, which might be ascribed to:

1. Relative humidity is too high, sharply slowing down the setting (hydration and carbonation). Arnaud et al. found that RH of 75-98% dramatically reduced the setting and hardening of hemp concrete with hydraulic and slaked lime [43].

2. This group has 70% slaked lime (hydrated lime) and CaO from pozzolans; thus, carbonation governed the setting and hardening of the composite rather than hydration. Due to the saturation of pores, the diffusion of CO_2 from air is hindered [43]. Therefore, water remains internally and minimally consumed for hydration after 28 days.

Arnaud and Gourlay (2012) observed that the optimum curing condition for binders with hydraulic and slaked lime for strength evolution at 28 days is 20°C and 50% RH [43]. Further, the temperature affected the setting and hardening of hydraulic lime after constructing a wall [6].

As shown in Figure 3.27, the density of moist samples is in the range of 907-1053 kg/m^3 with a difference of 14%, while the values for dry samples are in the range of 447-507 kg/m^3 (with a variation of 12%). The wet density is mainly affected by moisture content (44-56%), which increased with increasing water content due to the higher porosity (46-60%) and water-to-binder ratio (water content increased for lime-based binders relative to cement binders). The reaction of pozzolan with lime depends on the reactivity and composition of the pozzolan. The moisture content shows the reactivity of pozzolan, in which the higher reactivity consumes high water for hydration. The oven dry density increased with decreasing the porosity due to the formation of hydration products (Lower peaks of portlandite as shown in XRD for the addition of cement and slag- Figure 3.28) and carbonation products (as the presence of many calcite peaks in Figure 3.28). Adding SF, FA, and MK decreased the density minimally, while adding cement and slag increased the density slightly due to the higher hydraulicity. The increment is ascribed to the higher concentration of Ca^{+2} reacting with pectin and preventing the blocking of Ca ions from hydration; hence, the available ions would participate in hydration and improve density and strength.

The compressive strength of lime-based binders is in the range of 0.30-1.19 MPa (74% difference) and 0.29-0.69 MPa (58% difference) for wet and dry samples, respectively, which shows a higher strength for wet samples relative to oven dry ones, as shown in Figure 3.27. The higher strength of wet samples (3-42%) might be ascribed to capillary pressure and dry shrinkage as group I binders (cement-based binders). However, the dry samples showed lower strength due to the lower binder stiffness, which is ascribed to lower binders hydraulicity (because the moisture content of samples is the highest since the carbonation phase in the dominant, as many calcite peaks shown

in XRD patterns in Figure 3.28, not the hydration due to higher lime content 70%). The highest strength is achieved with the addition of 30% cement for wet and dry samples, while the lowest strength is with the addition of silica fume because the hydration of the silica phase is significantly delayed and inhibited by wood particles [33]. Similar trends were found by Abdellatef et al., where the strength increases with increasing water content for lime hempcrete with metakaolin and crushed bricks because of the suction ability of hemp disturbing the binder hydration [14]. The addition of pozzolan with lime does not show an improvement in strength, which is due to the curing condition inhibiting the carbonation, and such a pozzolan percentage might not be enough for higher strength development by hydration, as Arnaud found out a binder with 75% air lime, 15% hydraulic lime, and 10% pozzolan achieved the highest strength with a relative humidity of 30% and 50% with strength 0.30-0.33 MPa. Also, the higher relative humidity disrupts the setting and strength of the hemp concrete (0.16-0.20 MPa) at day 28 [43]. In this study, hydrated lime with 30% pozzolan achieved a strength of 0.29-0.69 MPa for oven-dry samples, which cured in an RH of 70%. The strength of GGBS is slightly higher than metakaolin by about 10, and 23% for dry and wet samples, respectively, which is explained by the existence of extra lime in slag-consuming pectin (Similar findings by Walker due to the change in the morphology of hydration products [7]). The strength increased significantly with the addition of cement by about 33-29% for wet and dry samples, respectively, relative to pure lime (similar findings [69]) because strength developed from both carbonation and hydration due to cement hydraulicity (formation of hydrated products). Similar strength improvement for commercial binders mainly composed of CL 90 with hydraulic components relative to pure CL90 produced by Murphy et al., and the rate of strength gain increased with increasing hydraulicity, while pure lime relied solely on carbonation for strength development [70]. Furthermore, the high relative humidity disturbs hemp concrete's setting and strength development with hydraulic-based binders [43], which might have similarly occurred in this study. This attitude could be ascribed to the physio-chemical interaction between hemp and binder at high RH, as described by Arnaud [43].

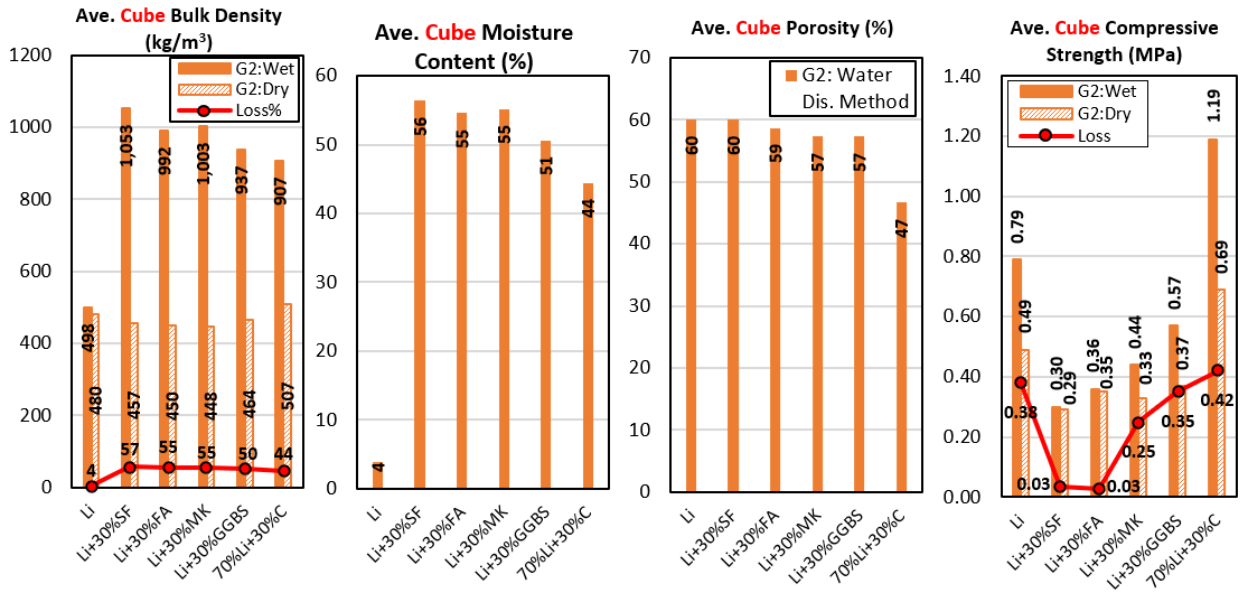

Figure 3.27: Physical and strength properties of hemp concrete cubes with lime-based binders at 28 days (Loss%= Loss*100)

Referring to XRD patterns in Figure 3.28, lower peaks of portlandite indicate higher formation of hydration products because portlandite is consumed to produce CSH gel. The portlandite peaks with the addition of lime, cement, and slag are relatively lower than other pozzolans, which is ascribed to the extra amount of lime reacting with pectin and preserving hydration continuity. Further, high alumina, as in MK and FA, reduces the hemp sugar retardation because the alumina hydration products consume the retarders (sugar), which interprets the noticeable increase in density and strength. However, the hydration of the silica phase is significantly delayed and inhibited by wood particles [33], which is noted with the addition of silica fume and clearly shown in XRD patterns in Figure 3.28. It's noticeable that many peaks of calcite are shown in the XRD for all mixtures, proving the occurrence of carbonation due to high lime content (70%), which accidentally accelerated due to the porous structure of hempcrete, facilitating the diffusion of CO_2 gas into the water pores.

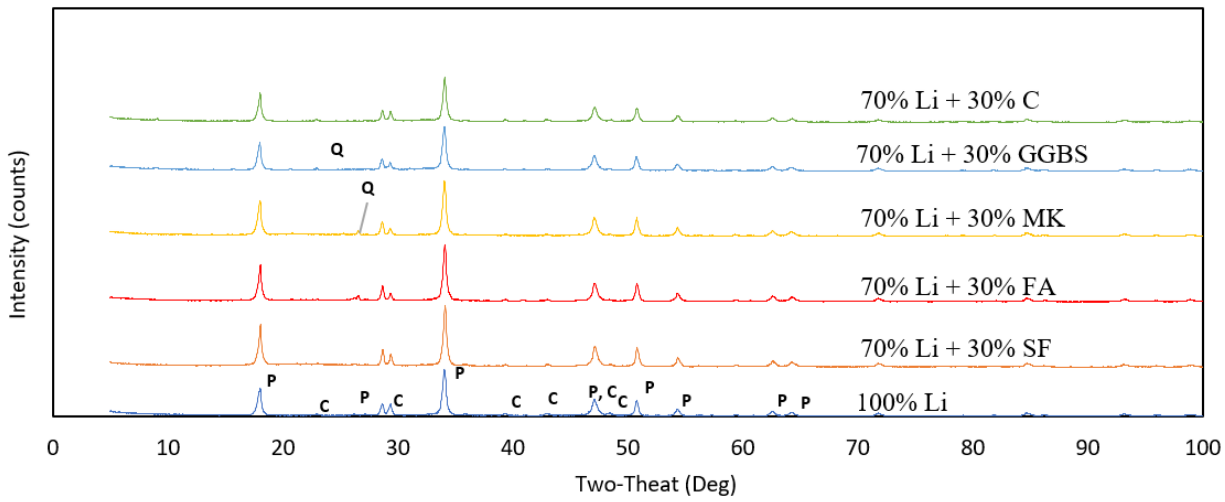

Figure 3.28: XRD patterns for lime-based mixtures

As shown in Figure 3.29, the moist density of disc samples varied between 857-1013 kg/m^3 (15 % difference), while the dry one is 445-543 kg/m^3 (18% difference). Again, there is minimal difference for a pure lime mixture between wet and dry samples because samples were exposed to the atmosphere in the lab for carbonation. The other mixtures were cured in a humidity room with high RH. Hence, the moisture content for disc samples is high, 43-61%, similar to cube moisture content. The open porosity was measured using a Helium pycnometer for disc samples showing values of 69-80% with a difference reaching 14%, which could be ascribed to the lower stiffness of such binders (i.e., high porous structure).

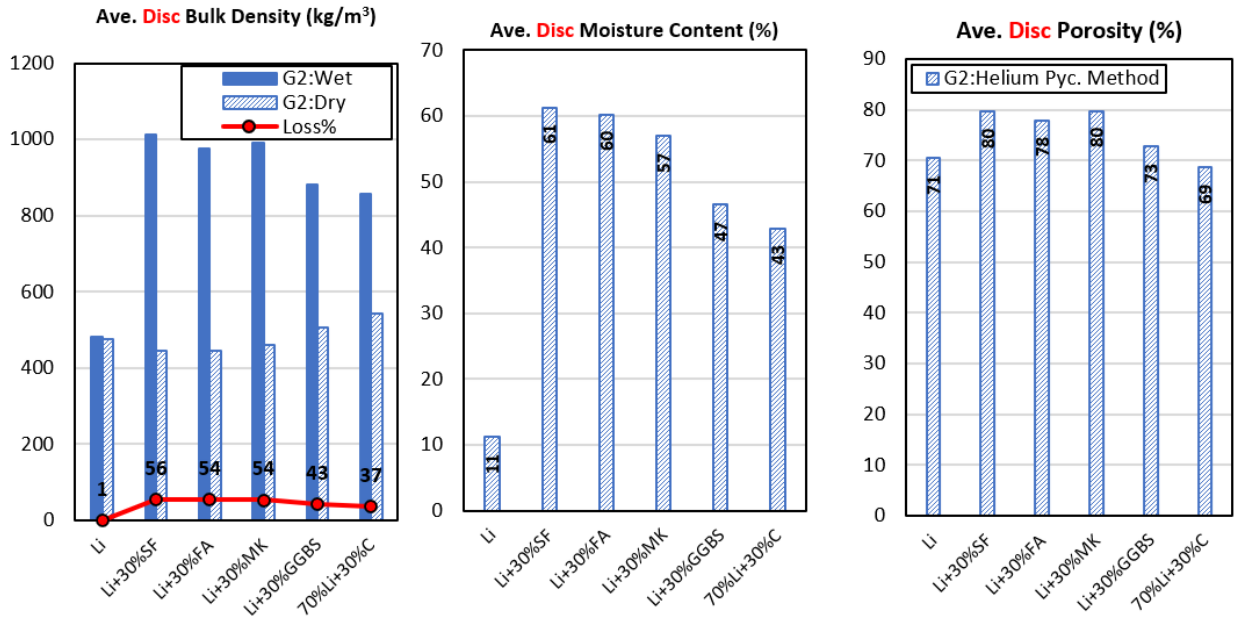

Figure 3.29: Physical and strength properties of hemp concrete with Lime-based binders at 28 days

Again, the thermal conductivity of wet samples is higher than dry ones (29-84%) due to the presence of water [14][66]. As shown in Figure 3.30, values of conductivity of wet samples fall in the range of 0.461-0.573 W/m K (excluding pure lime with k= 0.144 W/m K) with a difference reaching 20%, while the oven-dried samples showed a conductivity between 0.089-0.176 W/m K (difference reaching 50%). It's demonstrated that the conductivity of moist samples increased with increasing moisture content with a percentage of 29-84% relative to dry ones, while the k values for dry samples increased with decreasing porosity (porosity range 69-80%). Furthermore, the conductivity increased with increasing density for wet and dry samples. Silica fume, fly ash, and metakaolin showed a similar thermal conductivity for dry samples. At the same time, slag and cement increased the conductivity significantly, as compared to other pozzolans, due to the higher density and lower porosity (similar findings found for metakaolin [14] slag, cement [11][7], and fly ash [15]).

The thermal diffusivity values are between 0.169-0.330 mm^2/s (difference reaching 48%) and 0.110-0.185 mm^2/s (difference going 40%) for wet and dry samples, respectively, as shown in Figure 3.30. These values fall within the literature data summarized in Table 3.1. The reason for having higher diffusivity values for moist samples relative to dry ones has already been explained under the Group I binder section. Silica fume, fly ash, and metakaolin showed high conductivity and high volumetric heat capacity for wet samples due to higher moisture content (Also low k and low C_v for dry samples); hence, the diffusivity is relatively lower than the replacement with slag and cement (<24%). On the other hand, the conductivity of slag and cement increased faster than $C_{v,}$ leading to considerably higher diffusivity (<24%).

The volumetric heat capacity (calculated from k and α) varies from 0.858-2.203 MJ/m^3 K for wet samples, while the oven-dry ones are 0.649-1.099 MJ/m^3 K, as shown in Figure 3.30. The moist samples showed a significantly higher C_v than dry ones (3-70%) due to the higher moisture content. The wet values of C_v decreased with decreasing moisture content (behavior of C_v with different moisture content is varied and not targeted in this study). In contrast, the dry ones increased with decreasing porosity (i.e., more hemp particles compacted together). It's evident that at high moisture content (43-61%), C_v values are much higher than dry ones, as heat capacity changes with the moisture content for the same sample. This finding proved that the effect of moisture on C_v becomes more visible on high content rather than smaller percentages, as found in the literature. The Cv values are not a trend (increase or decrease) at a slight moisture content. Rather than continuously changing and unpredictable, in other words, at a specific moisture content, a higher volumetric heat capacity ($C_v = k/\alpha$) will be observed once the conductivity increases faster than the diffusivity, and vice versa.

The specific heat capacity ranges between 1619 and 2257 J/kg K for wet samples, while the dry one varies from 1457 to 2025 J/kg K. The specific heat capacity is directly proportional to C_v and adversely to density (i.e., $C_p = C_v/\rho$). Therefore, at a high moisture content of 57-61% for FA, SF, and MK, the C_p is much higher for wet samples than dry ones, ascribed to the extra increment in C_v relative to density. At lower moisture content with slag and cement, C_v increased relatively lower to density. Hence, the values of C_p decreased considerably.

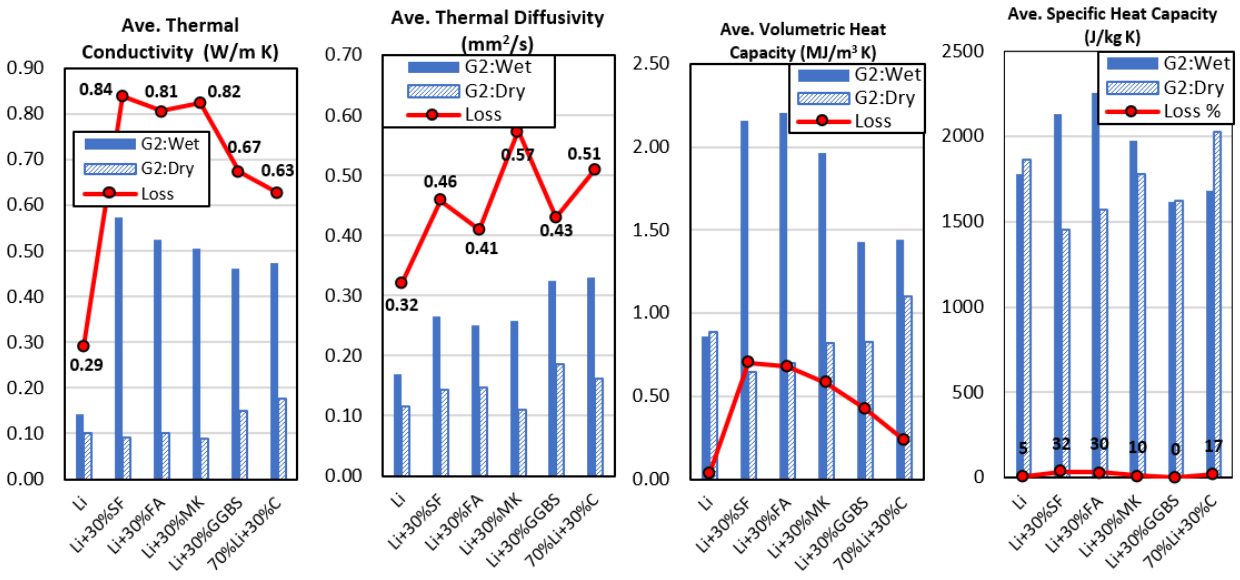

Figure 3.30: Thermal properties of hemp concrete with lime-based binders at 28 days (Loss%= Loss*100)

3.6.3 Cement-lime-based binders

The densities of group III binders are slightly different (986-1007 kg/m^3 for wet samples and 527-559 kg/m^3 for dry samples) with a variation of 44-48% between damp and dry samples, as shown in Figure 3.31. The remaining moisture at day 28 is 43-48%, indicating a relatively faster reaction of slag and metakaolin due to lime and alumina. Fly ash and silica fume showed a similar moisture content somewhat higher to other pozzolans, which might be due to the delaying and inhibiting of the silica phase by hemp, as noticed by Govin et al. [33]). However, the replacement of cement and lime with pozzolan admixtures showed a negligible difference (<5%) in terms of dry and wet densities, as shown in Figure 3.31, which might ascribed to the higher water-to-binder ratio (w/b= 0.625), higher workable mixture, easier compaction, denser structure, and higher content of available water. The water displacement porosity for cubes decreased with the addition of pozzolan from 53 to 32% (difference <40%), while the helium pycnometer did not show a significant difference (<10%). This difference between the two techniques (22-52%) might be due to the

difficult accessibility of water into the pores in cube samples relative to the accessibility of helium into disc samples. Also, the pore size distribution and connectivity of pores varied between cube and disc samples, possibly due to the sample size. The exterior surface of most cubes is not highly porous due to the higher workability and compaction degree, which hinders the accessibility of water with vacuuming (i.e., lower porosity results).

The compressive strength of oven-dry samples varies between 1.25-2.11 MPa (with a difference <41%), while the moist samples showed lower values between 0.73-1.01 MPa (with a difference <28%), as shown in Figure 3.31. The compressive strength of dry samples is significantly higher than the wet samples, with 41-52% percentages, unlikely to groups I and II. That means contraction of hemp and debonding after drying does not affect the strength because the interface zone becomes relatively more robust, and the binder-hemp composite is more compliable because hydrates formed on the hemp surface, filling the transition zone enhancing the bond as well as into binder matrix. Further, such binders showed a higher stiffness and needed more energy to initiate and extend microcracks than saturated samples (as similarly found for paste [29]). However, wet samples were defeated earlier than dry ones due to the spongy behavior of hemp hurds after reaching the compressibility limit, and then pieces started buckling (Similar observations [38][65]). As seen in this binder group, the capillary suction enhances the strength but to a lower limit than the dry sample carrying capacity. In addition, Neville mentions that the presence of water in wet samples lets the cement gel absorb water. Thus, the water gel is dilated, reducing the adhesion between the solid particles (i.e., reducing strength for wet samples) [37]. On the other hand, the microcracks into saturated paste grow easier because water reduces the surface free energy of the solid phase (surface tension of water), resulting in lower strength [29].

As shrinkage decreases with increasing binder hydraulicity [70], the advantage of the presence of lime enhanced binder hydraulicity in two ways: first, providing Ca ions for pectin, hence hydration is not significantly disturbed (i.e., more production of CSH and ettringite). Second: high water demand of lime providing backup water for hydration, constituting some of the absorbed moisture by hemp. In the results, the composition of (50% cement + 50% lime) seems to be the least affected by shrinkage and microcracks due to the higher stiffness, thus achieving the highest dry strength.

Silica fume, metakaolin, and slag replacements showed a slightly lower strength, possibly due to the slow pozzolan reaction delaying strength gain. However, adding fly ash significantly reduced the strength by 28% and 41% for wet and dry samples, respectively. This might be ascribed to the relatively high peaks of portlandite shown in XRD (Figure 3.32). Fly ash type F has high silica content (about 60%), but the particle size is much bigger relative to silica fume, which may be the reason for slow reactivity.

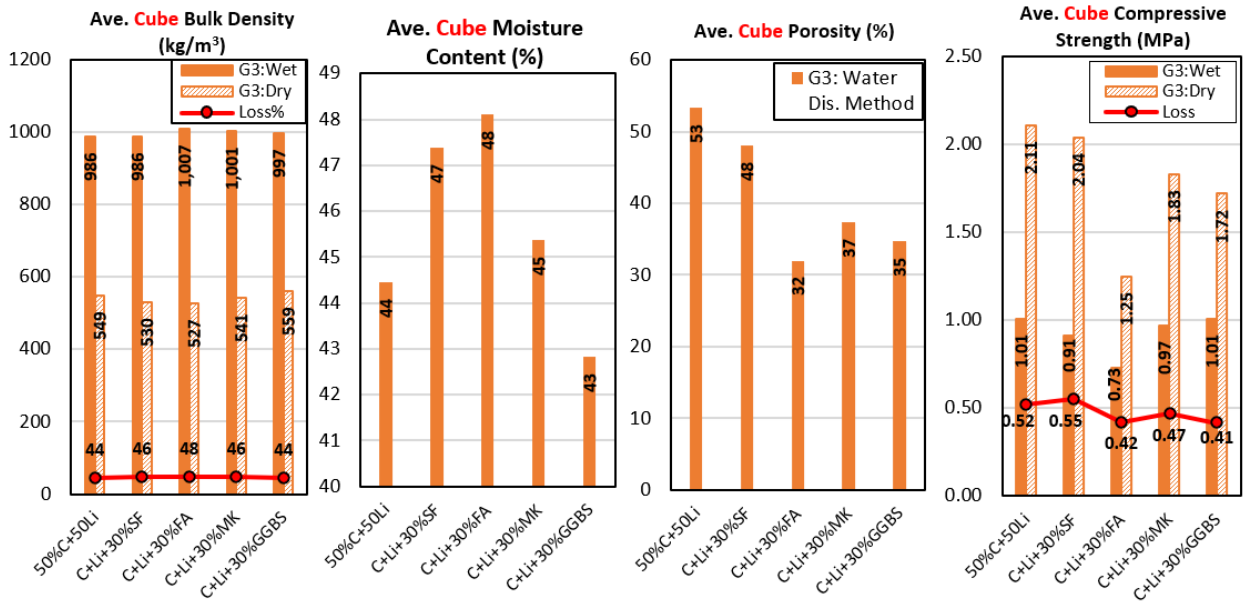

Figure 3.31: Physical and strength properties of hemp concrete cubes with cement-lime based binders at 28 days (Loss%= Loss*100)

XRD patterns of group III binders showed multiple peaks of portlandite and calcite for all binder compositions, as shown in Figure 3.32. Many peaks of calcite appeared, confirming the occurrence of carbonation due to the excess amount of portlandite and the presence of CO_2 (appreciable lime content facilitates carbonation validation). The higher peaks of portlandite might be due to the higher range of lime (i.e., more production of portlandite such as C+Li) or the slow reaction of portlandite with silica and alumina to form hydrates and calcite (due to pozzolan reaction such as fly ash).

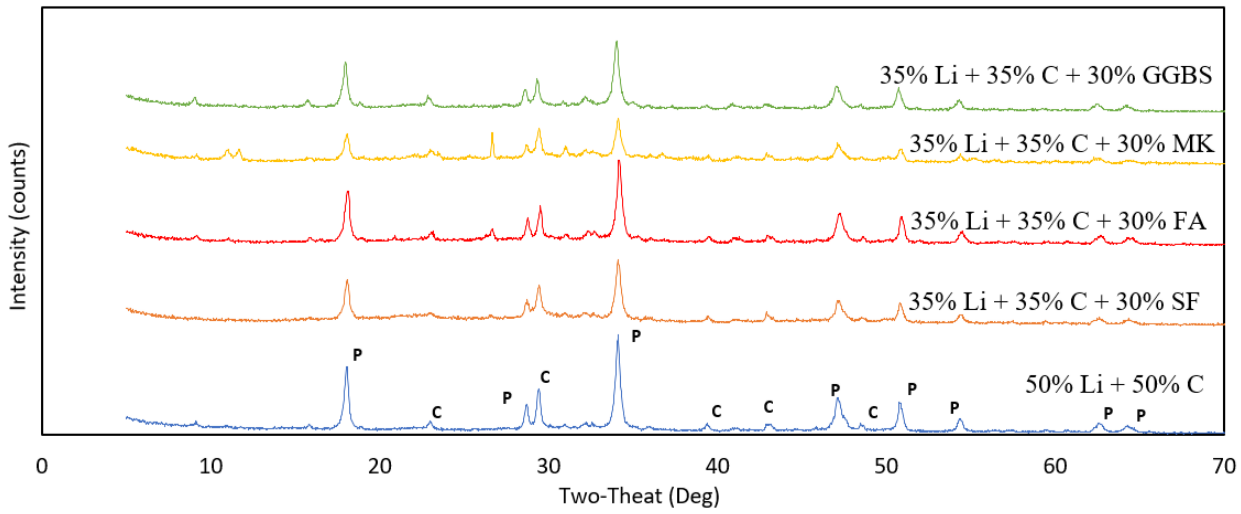

Figure 3.32: XRD patterns for cement-lime mixtures

The disc density of wet samples varies between 834-912 kg/m^3 (difference <8%), while the oven-dry ones are between 527-618 kg/m^3 (contrast <15%), as shown in Figure 3.33. The moisture content varies between 37-45%, and the open porosity for dry samples is 62-69%. It's noticed that the differences among this group of binders are insignificant, which might be ascribed to the similar reaction of the composition of the mixed cementitious materials.

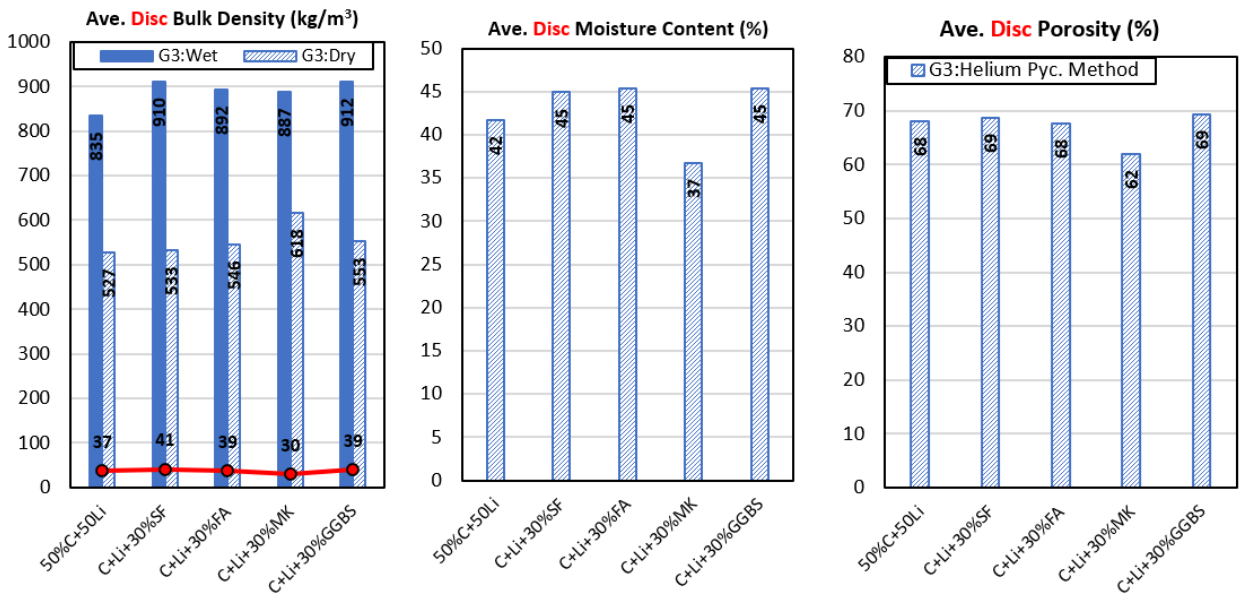

Figure 3.33: Physical and strength properties of hemp concrete with Group III binders at 28 days

The thermal conductivity of wet samples ranges between 0.412-0.494 W/m K (difference <16%), while the oven-dry samples showed a conductivity of 0.103-0.185 W/m K (difference <44%). The thermal conductivity of moist samples was significantly higher than oven-dry samples, with a difference of 55-77% ascribed to the high moisture content (37-45%). The conductivity values of this group are comparable with summarized data from the literature in Table 3.1 and similar to findings found by Taoukil [66]. The moisture content significantly affects wet samples' conductivity, while the dry ones are affected by density and porosity. Metakaolin shows the highest conductivity for oven-dry samples due to the highest density and most minor porosity. The least conductivity was achieved by silica fume for dry samples (with a difference of <44%) due to the low density and the highest porosity. However, the difference among binders within this group is less than 16% for wet conditions because the reserved water dominates the thermal conductivity. While for dry conditions, the porosity and glassy/crystalline structure of binders are the dominant factors. This study does not evaluate the amount of crystalline and amorphous binder matrix. Generally, the replacement of pozzolan affected the conductivity significantly, ascribed to porosity, the reactivity of pozzolan, and the effect of hemp on the binder.

The thermal diffusivity varied between 0.428-0.331 mm^2/s (difference <23%) and 0.106-0.168 mm^2/s (difference <37%) for wet and oven-dry samples, respectively, as shown in Figure 3.34. Similarly, wet samples' diffusivity is significantly higher than dry samples, with a 50- 62% percentage due to the high moisture content, 37-45%. The difference in thermal diffusivity among wet samples is less than 23%, while the difference is higher for dry conditions reaching 37%. Metakaolin showed the most increased diffusivity for dry pieces (due to high k and high C_v), while silica fume showed the lowest value (due to low k and high C_v). However, other pozzolans were noticed to be similar in terms of thermal diffusivity.

The volumetric heat capacity ranges from 1.058-1.386 MJ/m^3 K and 0.803-1.109 MJ/m^3 K for wet and dry samples, respectively, comparable with the literature data. Wet samples showed higher heat capacity than dry samples, with a 7-33% percentage, attributed to each sample's thermal conductivity and diffusivity behavior at the existing moisture content. Lower C_v values ($C_v = k/\alpha$) were achieved with higher conductivity and lower diffusivity values, which indicated faster thermal conduction than diffusion at a specific moisture content. Since the thermal behavior significantly changes with changing moisture content. The highest C_v values were observed for metakaolin, which might be attributed to the highest density and amorphous components.

The specific heat capacity is within the range of 1186-1526 J/kg K (difference <22%) and 1525-1863 J/kg K (difference <18%) for wet and dry samples, respectively. Interestingly, the dry samples showed higher heat capacity than the wet samples (with about 9-34%) due to the high values of wet density at the existing moisture content ($C_p = C_v/\rho$). The wet Cp values might show a different trend at various moisture contents. In other words, the higher value of dry C_p is ascribed to the lower diffusivity relative to conductivity for the same density ($C_p = k/\alpha\rho$). The highest Cp values for SF, FA, and Mk may be ascribed to the high porosity and amorphous content.

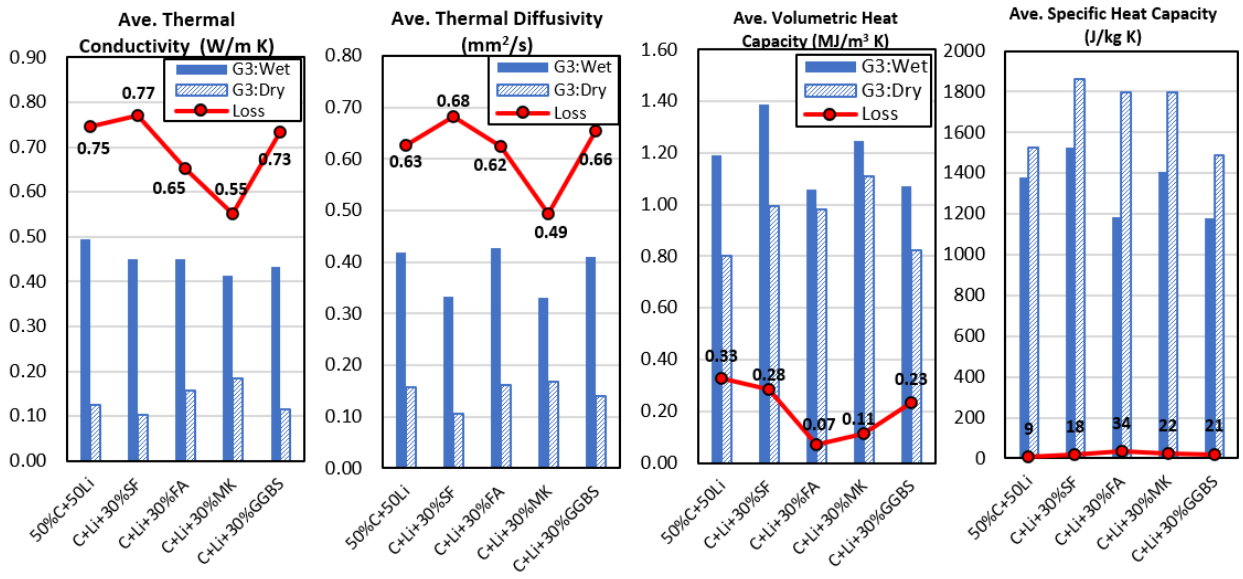

Figure 3.34: Thermal properties of hemp concrete with cement-lime based binders at 28 days (Loss%= Loss*100)

3.6.4 Linear regression analysis

Linear regression analysis was conducted using IBM SPSS for about 200 test readings of the thermal properties of hempcrete samples to generate linear equations for predicting thermal properties without conducting a real test. Eq- 3.6 and Eq- 3.7 showed the regression equations for thermal conductivity for dry and moist samples, respectively, regarding dry and damp densities with a considerable R2 value (0.70-0.82). On the other hand, the prediction equations for C_p show very low R2 values, indicating k as a significant factor and density as an insignificant one (Eq- 3.8 and Eq- 3.9). Thermal diffusivity showed linear equations with the highest R^2 values (0.97-0.95) for dry and wet conditions, respectively, showing k, C_p, and ρ as significant factors (Eq- 3.10 and Eq- 3.11). Finally, porosity could be used to predict the density of dry samples using Eq- 3.12 with a considerable R2 value (0.79).

Table 3.7: Linear regression analysis for thermal properties of hempcrete experimental data (dry and wet conditions)

Dependent Variable	Independent Variable	P-value	Significance	R^2	Regression Equations	Eq No.
k @ dry (W/ m K)	ρ (kg/m^3)	0.000	Yes	0.70	**k @dry**= 0.000326 **ρ** – 0.052	**Eq-3.6**
k @ wet (W/ m K)	ρ (kg/m^3)	0.000	Yes	0.82	**k @wet**= 0.001 **ρ** – 0.085	**Eq-3.7**
Cp @ dry (J/kg K)	k (W/m K)	0.002	Yes	0.21	$\mathbf{C_p}$ **@dry**= 3067.51 **k** – 0.456 **ρ** + 1587.51	**Eq-3.8**
	ρ (kg/m^3)	0.232	No			
Cp @ wet (J/kg K)	k (W/m K)	0.013	Yes	0.10	$\mathbf{C_p}$ **@wet**= 2020.14 **k** – 1.036 **ρ** + 1530.62	**Eq-3.9**
	ρ (kg/m^3)	0.057	No			
α @ dry (mm^2/s)	k (W/m K)	0.000	Yes	0.97	**α @dry**= 1.007 **k** – 0.000251 **ρ** – 0.000083 $\mathbf{C_p}$ + 0.287	**Eq-3.10**
	Cp (J/kg K)	0.000	Yes			
	ρ (kg/m^3)	0.000	Yes			
α @ wet (mm^2/s)	k (W/m K)	0.000	Yes	0.95	**α @wet**= 0.80 **k** – 0.000364 **ρ** – 0.000204 $\mathbf{C_p}$ + 0.617	**Eq-3.11**
	Cp (J/kg K)	0.000	Yes			
	ρ (kg/m^3)	0.000	Yes			
ρ @ dry (kg/m^3)	Ψ (%)	0.000	Yes	0.79	**ρ @dry**= -13.31 **ψ** + 1477.03	**Eq-3.12**

w%: water content

As shown in Figure 3.35 and Figure 3.36, the linear regression equations for thermal diffusivity for dry and wet samples are drawn. As depicted in the ternary phase diagram, the three factors, including k, Cp, and ρ, were normalized to assess their effect on diffusivity. Interestingly, the three

factors are affecting the diffusivity of hempcrete almost equally, as points accumulated at the middle of the triangle (k: 24-39%, ρ: 28-41%, Cp: 27-43%), (k: 17-42%, ρ: 25-38%, Cp: 23-57%) for dry and wet conditions, respectively.

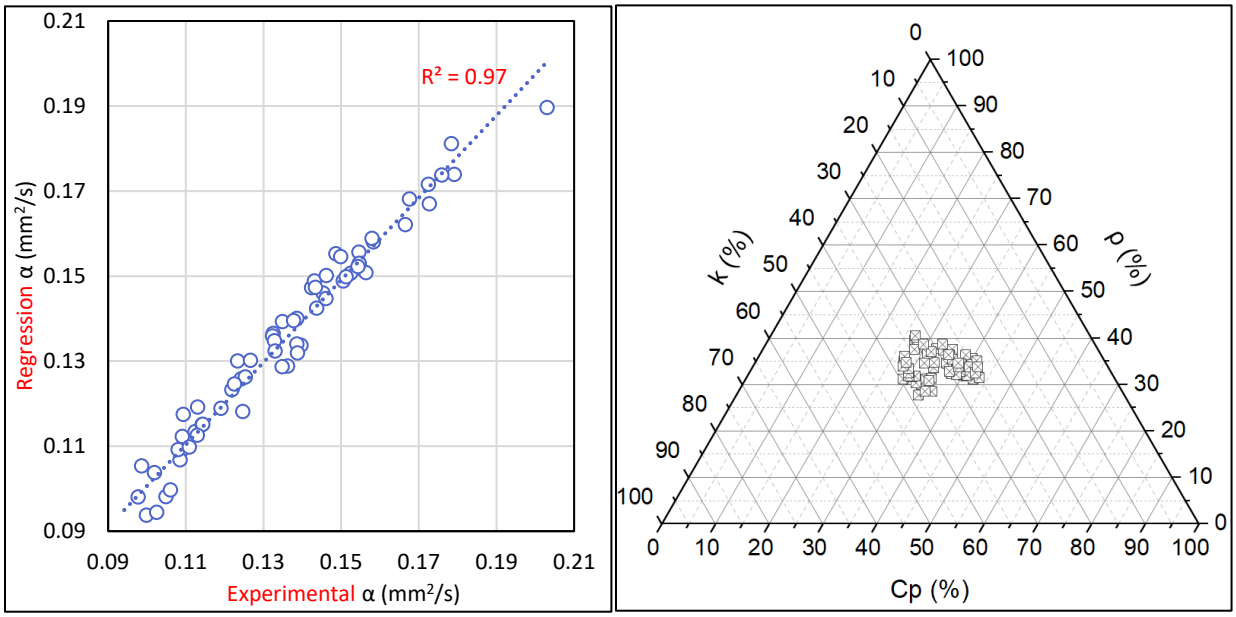

(a) (b)

Figure 3.35: Linear regression analysis for dry samples thermal diffusivity: (a) Experimental and regression α; (b) Normalized factors affecting α.

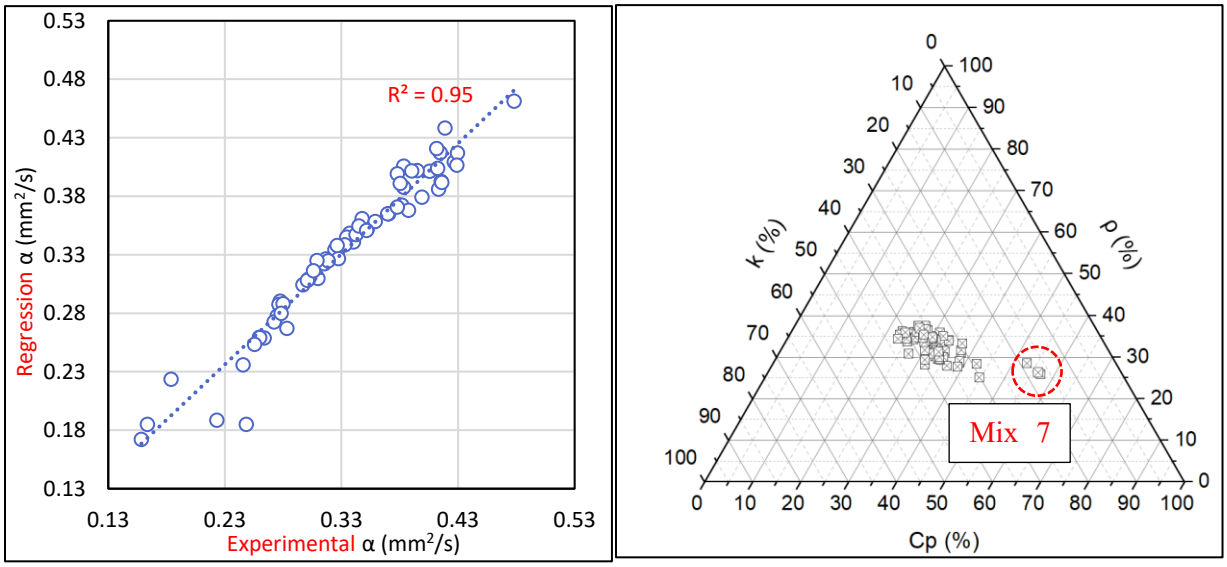

Figure 3.36: Linear regression analysis for wet samples thermal diffusivity: (a) Experimental and regression α; (b) Normalized factors affecting α

3.7 Conclusions

This study aimed to optimize binder compositions for more compatible hemp composite, including three compositions of binders. Cement, lime, and cement-lime binder compositions with pozzolana were used for hemp concrete with different contents to evaluate the marriage of such binders with hemp hurds due to the impact of biomaterials such as pectin and sugar effect. The hempcrete samples were tested for thermal and strength properties to optimize the components of hemp composite. The following conclusions could be drawn:

- Cement binders showed relatively lower strength and thermal properties due to lower w/b ratio and workability, leading to a more porous structure. The higher peaks of C3S of XRD analysis of the cement binders group proved the disturbance of hemp hurds for the hydration process by consuming higher water. Hence, adding lime is recommended for the dependence on carbonation and to reduce the negative impact of hemp. The replacement with lime (70% C + 30% Li) showed the highest strength within this group (with increments of 100 and 85% for wet and dry conditions) due to the higher availability of lime (consumed pectin), the

occurrence of carbonation (i.e., formation of calcite), and reduced the hydraulicity and water competition (i.e., higher production of CSH and ettringite filling pores and enhancing bond). The strength of wet samples is significantly higher than dry ones, with about 4-31% ascribed to capillary pressure and dry shrinkage for moist samples and debonding at the interface zone due to the initiation of microcracks for dry samples.

- Lime binders require optimization for curing conditions to improve the hempcrete mixture's setting hardening and strength. The substitution of cement with lime showed appreciable strength increment with about 34 and 29% for wet and dry conditions. For dry samples, the replacement of lime with pozzolan (silica fume, fly ash, and metakaolin) showed similar thermal conductivity. In contrast, replacing hydraulic binders (slag and cement) increased the conductivity by about 33-44%, compared to pozzolans due to the higher density and lower porosity for the same curing conditions.
- Cement-lime binders improved the strength of hempcrete and considerably increased the thermal properties. Calcite formation was confirmed from XRD results, which occurred with easy accessibility of CO_2 through the porous structure of hempcrete. The addition of pozzolan showed slightly lower strength, which might be ascribed to the slow reaction of pozzolan. The compressive strength of dry samples is significantly higher than the wet samples, with 41-52% percentages, unlikely to groups I and II. That means contraction of hemp and debonding after drying does not affect the strength because the interface zone becomes relatively more robust, and the binder-hemp composite is more compliable. Further, such binders showed a higher stiffness, needing more energy to initiate and extend microcracks than saturated samples. Finally, reducing the amount of cement in binder composition will lead to more environmental benefits due to the high embodied energy of cement and CO_2 emissions.

This study concluded that cement-lime-based binder compositions showed more compatible hempcrete samples relative to other binder compositions in terms of strength due to the effect of lime on hemp hurds, the hydraulic of cement, and the occurrence of carbonation with sufficient lime.

4 CHAPTER 4: OPTIMIZING HEMPCRETE COMPONENTS (PART II)

Journal paper #3

Exploring Thermal Performance and Strength of Hempcrete with Alkali-Activated Binders

Ahmed S. Al-Tamimi[a], Vivek Bindiganavile[a]

Abstract

Using hemp hurds in concrete as aggregates show incompatibility due to high water absorption and pectin effect on the binder matrix. Therefore, many studies have been initiated to evaluate the composite with various existing binders such as lime, cement, and pozzolan. This study is devoted to integrating the alkali-activated binder with hemp hurds and assessing such composite's strength and thermal properties, which have not been seen in the literature for thermal diffusivity. Therefore, two aluminosilicate materials were investigated for alkalization with hemp hurds, including fly ash type F and metakaolin with sodium hydroxide and silicates as activators. The results showed a significant increase in density due to the higher production of NASH and CSH, which led to a rise in thermal conductivity and diffusivity compared to cement and lime binders. Alkali-activated binders showed a promising jump in hempcrete strength (reached 3.80MPa) with an increment of 50% relative to cement-lime binders in a previous study. However, mixture components require more optimization to enhance such properties. Hence, this study highlighted the alkali-activated binders as superior candidates for hempcrete with higher strength and better thermal properties due to maintaining the high content of hemp hurds.

Keywords: alkali-activated, Hempcrete, thermal diffusivity, thermal conductivity, heat capacity, compressive strength

Nomenclature

Abbreviations

AA-FA	Alkali activated fly ash

AA-MK	Alkali activated metakaolin
b/h	Binder to hemp ratio
Cp	Specific heat capacity
CSH	Calcium silicate hydrate
Cv	Volumetric heat capacity
FA	Fly ash
k	Thermal conductivity
MK	Metakaolin
NASH	Sodium aluminosilicate hydrate
w/b	Water to binder ratio
α	Thermal diffusivity

4.1 Introduction

A new type of cementitious binders produced by a chemical reaction (Alkali activatedisation Reactions) between amorphous aluminosilicate materials and alkaline activating agents to form aluminosilicate gel (Alkali started) with binders properties of setting and hardening to be used as a promising binder alternate for constructions [1]. Pozzolanas such as fly ash, metakaolin, and blast furnace slag were considered aluminosilicate materials (rich in reactive/ amorphous alumina Al_2O_3, and silica SiO_2, low CaO), thus could be used for alkali activatedisation reaction [1][2]. The alkaline activating agents commonly include sodium hydroxide and sodium silicate, while sodium carbonate and potassium hydroxide were rarely used [1]. The process of producing an alkali-activated binder needs the following steps [1]:

1. Amorphous/reactive aluminosilicate material with more than 80% content by wt.
2. Aluminosilicate material dissolved into a high alkalinity solution to produce aluminosilicate monomers.
3. Aluminosilicate monomers bond together (Oligomerization) to form a chain of [-O-Si-O-Al-Si-O-]
4. Aluminosilicate chains condense to a stable polymer network (Polycondensation/ Setting reaction).
5. Forming a three-dimensional framework of polymeric chains with ring structures such as hydrated sodium aluminosilicate [N-A-S-H].

6. For example, activating fly ash with NaOH produces an alkali-activated, which mainly depends on the ratios of oxides (SiO_2/Al_2O_3), (Na_2O/Al_2O_3), (H_2O/Na_2O), and (CaO/Na_2O).
7. In case of the presence of CaO in aluminosilicate material (such as fly ash), alkali activatedization and hydration will take place to form (NASH+ CSH+ CASH, etc.). At the same time, MK has (hydrated sodium aluminosilicate) NASH [2].

The alkali-activated binder is a green construction material due to its low cost (waste materials), low production energy, and low CO_2 emission. The thermal conductivity, specific heat capacity, and thermal diffusivity depend on chemical composition, porosity, interconnectivity of pores, gel phase, and crystalline and amorphous phases [3][4]. The alkali-activated binders could be classified into two categories: a high calcium system, such as GGBS, produces majorly CSH gel from hydration, while a low calcium system mainly generates 3D NASH gel due to the polymerization process [5].

Goncalves et al. [6] tested the thermal conductivity and heat capacity of alkali-activated paste of fly ash with sodium silicate (Na_2SiO_3) and sodium hydroxide (NaOH) (1.0:0.30); thus, the calculated thermal diffusivity was found 0.24 mm^2/s with bulk density of 1.14 gm/cm^3 (i.e., there is a reduction of 35% as compared to paste with ordinary cement [7]). XRD analysis showed crystalline aluminosilicate phases and a hump, indicating the amorphous phases [6]. Therefore, alkali-activated adhesives have a high potential for reducing thermal diffusivity significantly. Jittabut produced an alkali-activated cement paste (Aluminosilicate materials: fly ash, bagasse ash, and rice husk ash + Alkaline activating agents: Na_2SiO_3 and NaOH (2.0:1.0)) with a thermal diffusivity in the range of 0.6-0.9 mm^2/s [8]. Further, alkali-activated were prepared by activating metakaolin (with Na_2SiO_3 and NaOH (0.40-1.20)), resulting in a thermal diffusivity between 0.22-0.44 mm^2/s [9]. The density increased with increasing the ratio of activating agents due to increasing the content of Na_2SiO_3, which has a higher density than NaOH [9]. Therefore, the porosity decreased due to the higher silica content, resulting in a new formation of aluminosilicate [9]. The porosity decreased with increasing the ratio of activators until the optimum value was 1.0, then the porosity increased due to retarding the alkali activatedisation process with the excessive content of alkali [9]. Caicedo et al. activated metakaolin with potassium hydroxide (mixed with

rice husk ash and silica fume SiO_2:K_2O = 2:1), resulting in lower values of thermal diffusivity (0.16-0.27 mm^2/s) [3].

The curing condition of alkali-activated is different from hydration, which requires a specific temperature and relative humidity (typically 20ºC and 70%). However, temperature affected the polymerization process significantly, as the reaction dramatically accelerated at high temperatures. The strength increased from about 5 to 38MPa for curing temperatures of 20 and 80ºC, respectively, which represents an increment of about 87% [10]. Similarly, the strength of alkali-activated fly ash concrete increased with increasing curing temperature from 30-90ºC (about 70% increment) [11]. Interestingly, Joseph and Mathew found that the strength of fly ash alkali activated increased with increasing temperature from 20-100ºC by about 72%. The strength reduced with higher temperatures due to drying and cracks [11] (Similar findings [5]). In summary, the curing temperature of alkali-activated should be higher than the hydration temperature. It should be optimized for individual alkali activated because the optimum curing temperature is affected by the individual components of alkali-activated, including activator concentration, type, and binder type and content.

This study used two aluminosilicate materials, including fly ash and metakaolin. Fly ash type F contains a high alumina and silica content and a slight lime content. Metakaolin is mainly composed of glassy structure of silica (53%) and alumina (43%). However, fly ash type C and GGBS were not used to produce the alkali-activated due to the high content of lime. The raw components used in alkali-activated binders, such as sodium hydroxide and sodium silicate, possess toxicity and can cause significant harm to the human body. Adhering to appropriate safety protocols can effectively manage the preparation process. Once solidified, the resulting product, Sodium aluminosilicate hydrate (NASH), is not considered hazardous, similar to conventional concrete. Alkali-activated binders are generally regarded as safe mixtures; nonetheless, if there is skin or eye contact, promptly rinse the affected area with copious amounts of water.

Effect of oxide compositions on properties of the alkali-activated system:

4.1.1 Alkali Activated fly ash

Fly ash is activated by sodium hydroxide and sodium silicate (or both) to produce the alkali-activated. The concentration of NaOH solution (molarity), Na_2SiO_3/NaOH, amorphous aluminosilicate content, solution/fly ash, and SiO_2/Na_2O are the critical factors for alkali-activated production [5][12]. Based on the literature, these ratios need to be optimized, and guidelines should be drawn for an alkali-activated with better thermal and mechanical properties [13]. The higher concentration of NaOH solution increased the strength of the alkali-activated because high PH increases the breakage of the amorphous surface of fly ash and accelerates the reaction. However, the exceptionally high concentration hindered the response because the excess hydroxyl ions disturbed the condensation of silica [5], and the excess sodium ions led to the form of solidate (silicate mineral), reducing the strength [14]. On the other hand, low concentration of solution (i.e., low Na content) leads to reduced PH and rate of reaction. The mass ratio of sodium hydroxide and sodium silicate significantly affects alkali-activated properties. Hence, proportions should be optimized for higher strength alkali activated as conducted by Ding (NaOH concertation 8-16 M, Na_2SiO_3/NaOH= 1.5-3.5) [5].

As shown in Table 4.1, literature was collected on alkali-activated fly ash to identify the types and contents of activators and their percentages to obtain an alkali-activated with higher strength. The activators used with fly ash are sodium hydroxide (4-16 M) and sodium silicate (>3.2 M). The summarized parameters are the ratios of solution/fly ash (0.25-1.80), Na_2SiO_3/ NaOH (1.5-3.33), and SiO_2/Na_2O (0.04-2.38). The high molarity of the solution showed a higher strength; however, other parameters needed to be optimized for higher strength. The ratio of SiO_2/Na_2O depends on the solution to binder ratio; as solution/fly ash = 0.40, the SiO_2/Na_2O= 0.12 showed the highest strength, while higher and lower ratios of SiO_2/Na_2O fall mechanical strength [12]. At high concertation of NaOH, the water demand of lightweight aggregate reduces and strength increases [13]. Thermal conductivity of AA-FA paste varied between 0.18-0.48, and diffusivity of 0.27-0.34 mm^2/s depending on the density of alkali-activated [6]. For this study, trials were conducted

in the lab to choose the suitable ratios to produce fly ash alkali-activated with higher strength with the help of the literature in Table 4.1.

Table 4.1: Literature on the production of alkali-activated fly ash with NaOH and Na_2SiO_3

Mixture	Aluminosilicate	Activator	Sol. Molarity (M)	Na_2SiO_3/ NaOH	SiO_2/ Na_2O	Sol/ FA	Notice	Ref.
Paste	Fly ash-type F	NaOH + Na_2SiO_3	16 >3.2	3.33	2.38	0.61	-	[6]
Mortar	Fly ash-type F	NaOH	-	-	-	0.35	Higher molarity shows higher strength 32-70 MPa	[12]
		NaOH + Na_2SiO_3	-	-	1.23-0.04	0.35-0.40	Highest strength with SiO_2/Na_2O= 0.12, Sol/Binder= 0.40	
Paste	Fly ash-type F	NaOH	12	-	-	0.25-0.30	Oven cured-35-40 MPa	[15]
		NaOH + Na_2SiO_3	-	-	1.23	0.25-0.30	Oven cured-Reached 90 MPa	
Paste	Fly ash-type F	NaOH	10 12 14	-	-	1, 1.2, 1.4, 1.6, 1.8	Higher molarity shows higher strength	[16]
Concrete	Fly ash-type F	NaOH + Na_2SiO_3	4, 6, 8	1.5	-	0.25	Higher molarity shows higher density and strength	[13]

4.1.2 Alkali-activated metakaolin

Metakaolin is a pozzolanic admixture mainly composed of silica and alumina, produced by calcinating kaolin [17] and satisfying the ASTM C618 standards [18]. All parameters affecting fly ash alkali activated are affecting alkali-activated metakaolin with an advantage to SiO_2/Al_2O_3 ratio (higher silica content increases gel phase) [19][4]. Thus, the activation using both Na_2SiO_3 and NaOH produces an alkali-activated with higher mechanical properties relative to activation only by NaOH because sodium silicate suppresses crystallization [14][2][20]. In other words, the produced amorphous NASH gel with only NaOH activation showed a chemical composition as zeolitic with extensive crystalline structure compared to the activation with sodium silicate [2]. Further, Na_2SiO_3 provides more silicate to be assembled with aluminate from metakaolin to form an amorphous product (this condensation process is slow) [20]. As summarized in Table 4.2, metakaolin alkali activated produced various ratios and parameters. The higher concentrations of NaOH enhanced the properties of the alkali-activated, similar to fly ash. Two ratios were calculated to monitor the sodium ions to prevent excess/ lack of Na+, including Na_2O/ SiO_2 and H_2O/ Na_2O.

Table 4.2: Literature on the production of alkali-activated metakaolin with NaOH and Na_2SiO_3

Mixture	Alumino silicate	Activator	Sol. Molarity (M)	Na_2SiO_3/ NaOH	Na_2O/ SiO_2	H_2O/ Na_2O	SiO_2/ Al_2O_3	Sol/ MK	Notes	Ref
Paste	MK	KOH + K_2SiO_3	-	-	0.28	-	2.5	0.40	ρ=1415-1338 kg/m^3 porosity = 33-35% k= 0.16-0.35 W/mK	[4]
Paste	MK	NaOH	12, 15, 18	-	-	-	-	-	Reaction increases with increasing concentration.	[21]
Paste	MK	NaOH + Na_2SiO_3	-	-	0.11-0.44	5.49-15.57	2.88-3.66	-	High Si, low water=> less porosity	[14]
Paste	MK	NaOH	-	-	2-0.67	14.5-4.83	1	1.28	High concentration NaOH=> crystallization rate increased	[20]
Paste	MK	NaOH+ Na_2SiO_3	-	2.22-1.67	0.80-1.0	5.60-4.90	1.35	1.62	Suppresses crystallization	[20]

4.2 Materials

BASF provided Metakaolin with a highly reactive (glassy) structure (SG= 2.50). LAFARGE supplied fly ash type F (FA) with a specific gravity of 2.50. Two activators were used, including sodium hydroxide (NaOH) and sodium metasilicate (Na_2SiO_3), supplied by BASAF with pellets and solution forms. The specific gravity of NaOH pellets and Na_2SiO_3 are 2.13 and 1.40, respectively. Further, the PH value of sodium silicate solution is 11.2, and the molar ratio of water

glass is >3.2 with 40% sodium silicate and 60% water. Hemp hurds were provided by LCDA in France with a bulk density of 164 kg/m^3 and water absorption of about 350% after 24 hours. Hemp sizes were analyzed, showing about 80% of hurds <3 mm in width and <10 mm in length, and an aspect ratio of 3.84.

4.3 Mix Design

Mixing components of alkali-activated hempcrete followed the preparing binder slurry and wetting the hurds before mixing as observed in these references [22][23][24][25] with the following detailed steps:

1. Prepare a solution and leave it for one day to cool down.
2. Next day, mix the solution in a Hobert mixer for 1 min.
3. Add FA or MK gradually and mix for 2 min, then the slurry is ready.
4. Pre-wetting hemp with 200% by wt. with water before mixing.
5. Add wet hemp gradually into the slurry and mix for 2 min.

With the help of literature mix designs in Table 4.1, two mixes were prepared by the activation of fly ash with NaOH and Na_2SiO_3 by adjusting solution molarity and ratios of Na_2SiO_3/NaOH, SiO_2/Na_2O, and Sol/FA. For NaOH activation, the morality of 16M showed an alkali-activated with acceptable workability and strength. Similarly for the activation by both NaOH and Na_2SiO_3 with ratios Na_2SiO_3/NaOH (2.33), SiO_2/Na_2O (4.06), and Sol/FA (0.80) showing good workability and strength properties, as shown in Table 4.3.

Table 4.3: Trials to produce an alkali-activated with fly ash

Aluminosilicates	Activator	Solution Molarity (M)	Na_2SiO_3/ NaOH	SiO_2/ Na_2O	Sol/FA	Notes
Fly ash- type F	**NaOH**	**16**	**-**	**-**	**0.67**	**Good mix**
Fly ash- type F	NaOH + Na_2SiO_3	16 >3.20	3.33	6.58	0.67	Low workability Weak strength
Fly ash-type F	NaOH + Na_2SiO_3	6.14 >3.20	3.33	6.58	0.85	Good workability Weak strength
Fly ash- type F	NaOH + Na_2SiO_3	16 >3.20	2.33	3.44	1.0	High sol. Vol. Segregation
Fly ash- type F	**NaOH + Na_2SiO_3**	**16** **>3.20**	**2.33**	**4.06**	**0.80**	**Good workability** **Good strength**

As shown in Table 4.4, trials have been conducted in the lab to produce metakaolin alkali-activated. The ratios of Na_2SiO_3/NaOH, Na_2O/SiO_2, H_2O/Na_2O, SiO_2/Al_2O_3, and Sol/MK were selected within literature values (Table 4.2) to obtain mixtures with proper mechanical properties. This study aims to investigate alkali-activated compatibility with hemp rather than optimizing the parameters for improved alkali-activated. The final mix was prepared with metakaolin and fly ash alkali-activated with the previous two combinations of FA and MK and the two activators, as shown in Table 4.4.

Table 4.4: Trials to produce an alkali-activated with metakaolin

Aluminosilicate	Activator	Na_2SiO_3/ NaOH	Na_2O/ SiO_2	H_2O/ Na_2O	SiO_2/ Al_2O_3	Sol/ MK	Notes
MK	NaOH	-	0.42	10.47	2.1	1.0	Dry mix
MK	**NaOH**	**-**	**0.48**	**12.0**	**2.1**	**1.26**	**Good mix**
MK	**NaOH+ Na_2SiO_3**	**5.90**	**0.26**	**11.0**	**3.40**	**1.38**	**Good mix**
FA+MK	**NaOH+ Na_2SiO_3**	**3.94**	**0.26**	**10.12**	**4.37**	**1.09**	**Good mix**

In this task, five batches of hemp concrete with a volume of 0.0024-0.0029 m^3/mix containing alkali-activated binders and the same binder-to-hemp ratio, as shown in Table 4.5. The total No. of samples for each mixture is 12 specimens, including six 50mm cubes and six 75mm dia. discs.

For this assignment, five sets of hemp concrete mixture were prepared. Each group had a volume ranging from 0.0024 to 0.0029 cubic meters per mixture. These mixtures incorporated alkali-activated binders and maintained a consistent binder-to-hemp ratio, as specified in Table 4.5. To thoroughly evaluate each mixture, a total of 12 samples were collected. This consisted of six 50mm cubes for strength and six discs with a diameter of 75mm for thermal testing.

Table 4.5: Mix proportions of hemp concrete with alkali-activated binders

Binder Type	Binder composition (% by wt.)	w/b	Hemp abs. (%)	b/h (By wt.)
Alkali activated binders	AAFA- NaOH	0.67	200	2.50
	AAMK- NaOH	1.26		
	AAFA- (NaOH+ Na_2SiO_3)	0.80		
	AAMK-(NaOH+ Na_2SiO_3)	1.38		
	(AAFA+AAMK)- (NaOH+ Na_2SiO_3)	1.09		

4.4 Testing

For each mixture, two samples were prepared for testing, including three 50mm cubes for compressive strength and six 75 mm dia. For thermal properties. By the guidelines outlined in ASTM D4832, a load rating of 50 kPa/s was chosen for this particular purpose [26]. Figure 4.1 shows that thermal properties were evaluated using TPS 1500 based on the Hot Disk Method according to ISO 22007-2 standards [27]. As shown in Figure 4.2, the porosity of hempcrete samples was examined using two different techniques, including Helium Pycnometer and water displacement method [28][29][30].

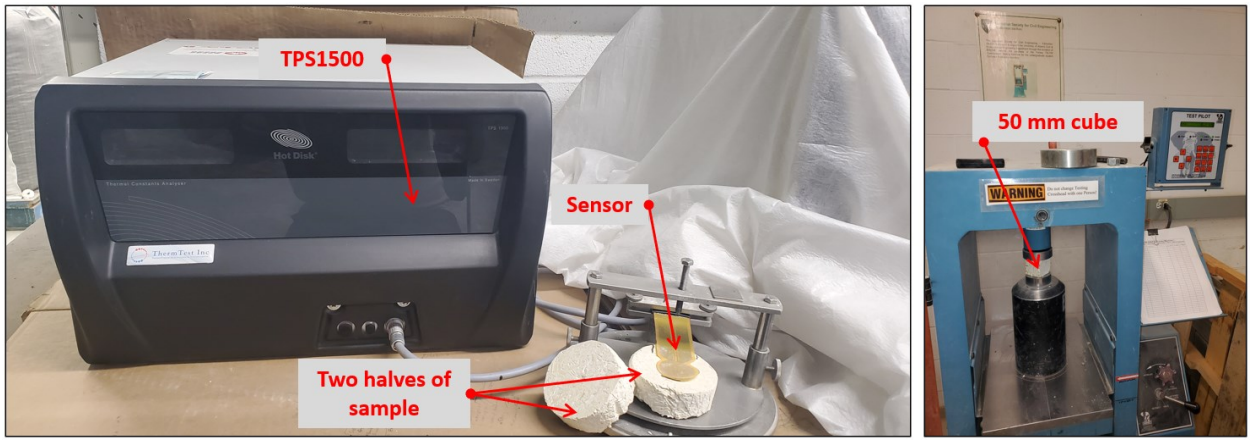

Figure 4.1: Thermal test setup and compression test machine

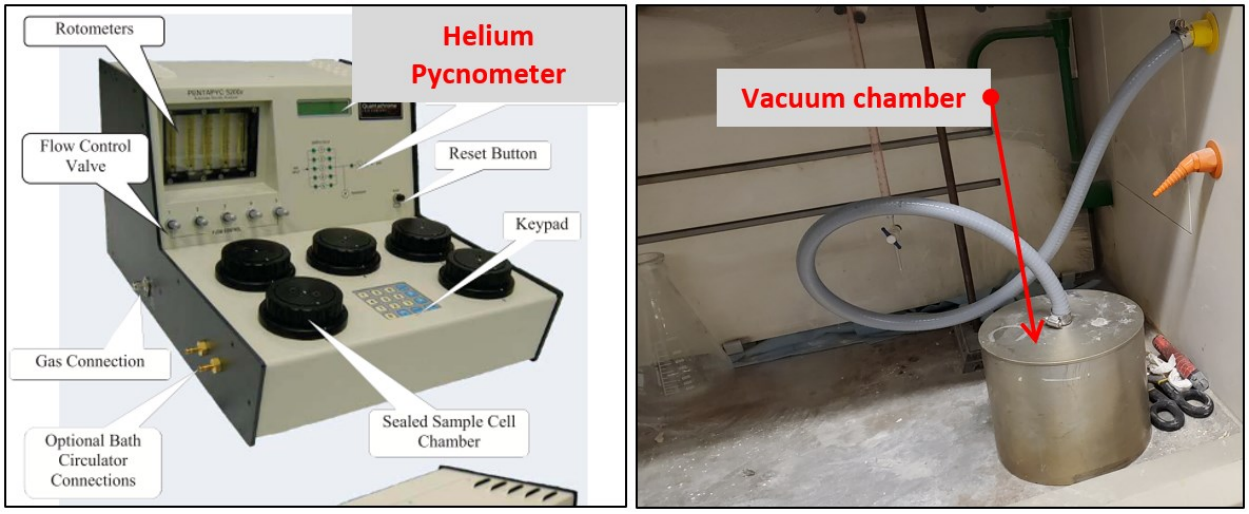

Figure 4.2: Porosity measurements techniques: (a) Helium Pycnometer; (b) Water displacement

4.5 Results and Discussion

The densities of hempcrete with alkali-activated binders varied between 1061-1321 kg/m^3 and 623-1054 kg/m^3 for wet and oven dry samples, respectively. However, such binders increased hempcrete's density significantly for the same binder-to-hemp ratio compared to hempcrete in literature. The increment in density could be ascribed to the higher formation of amorphous products, including NASH (density= 2400 kg/m^3 [31]) and CSH (density 2600 kg/m^3 [31]) that is seen in XRD hump patterns in Figure 4.4. Probably, hemp hurds are not absorbing the solution of sodium silicate and hydroxide (Similar findings with lightweight aggregate [13]). Hence, the polymerization process is not interrupted due to water absorption of the pectin effect, which makes alkali-activated binders the proper candidates for hempcrete. The moisture content of this group of mixtures falls between 32-44% due to hemp absorption, while the open porosity (using water displacement) for hempcrete cubes differed between 39-62%. The average compressive strength was noticed between 0.36-1.72 MPa (with a difference reaching 79%) and 0.49-3.84 MPa (with a difference going 87%) for wet and oven-dry samples, respectively, as shown in Figure 4.3. Fly ash activated with sodium hydroxide shows a higher strength than the activation with sodium silicate,

with about 63% and 24% for wet and dry samples, respectively. However, using sodium silicate should improve the strength [2][20], but that happens only with the optimum dosage. Therefore, better mixes could be achieved by optimizing the ratios of Na_2O/SiO_2 and SiO_2/Al_2O_3 because the excess amount of Na^+ leads to the formation of sodalite (silicate mineral that reduces the strength) [14]. At the same time, the lower content of Na_2O lowers the PH of the solution and negatively affects the reaction rate [12]. For metakaolin, the sodium hydroxide activator does not increase the strength of hempcrete, which might be due to the need for optimizing the ratios. Surprisingly, the average strength jumped significantly with activating metakaolin with sodium silicate to 3.84 MPa after drying at 60ºC for 24hrs, which greatly accelerated the strength gain attributed to the formation of NASH, as shown in XRD hump patterns in Figure 4.4 (as alkali-activated strength gain accelerated at elevated temperature curing 30-100ºC [5][10]). Further, the aluminosilicate structure is more resistant than calcium silicate to shrinkage at elevated temperatures, preventing the formation of cracks and debonding. Thus, the stiffness of the dried alkali activated is significantly higher than that of the wet one cured for the same period due to accelerating curing with elevated temperature. Further, the spongy behavior of hemp hurds was diminished due to water evaporation. Hence, the sample compressibility reduced significantly with the higher binder stiffness. According to ASTM C129, the minimum strength for non-load bearing blocks is 3.45 MPa, which is satisfied by metakaolin activated with ($NaOH+Na_2SiO_3$). Thus, hempcrete blocks could be produced with such binders as exterior blocks for building envelopes [32].

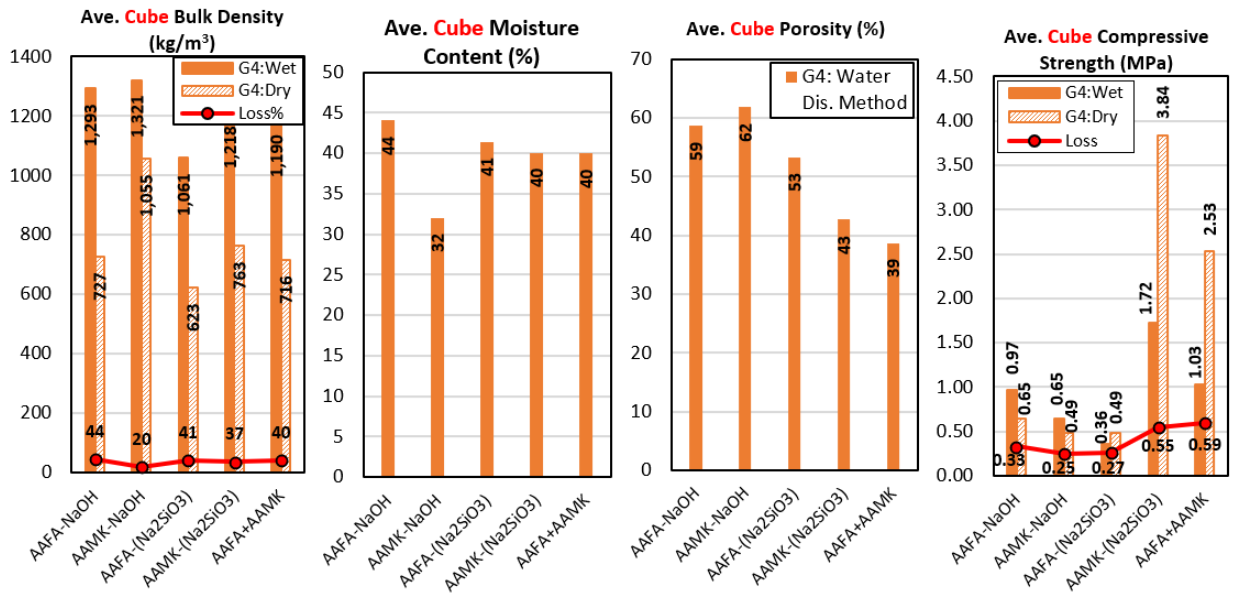

Figure 4.3: Physical and strength properties of hemp concrete cubes with alkali-activated binders at 28 days

The XRD patterns for alkali-activated binders show some peaks and noticeable humps, as shown in Figure 4.4. The peaks represent the crystalline products such as mullite, calcite, and portlandite, while humps indicate the amorphous phases such as CSH gel and NASH. Alkali-activated fly ash with NaOH showed many peaks for calcite, enstatite, and nifontovite, with a slight hump representing the formation of amorphous NASH and CSH. Interestingly, the activated fly ash with sodium silicate showed similar peaks of quartz and mullite due to un-reactivity, which may be ascribed to the ratios of the NaOH and $Na_2(SiO_3)$ (i.e., ratios need to be optimized), and the presence of crystalline products in fly ash. However, metakaolin shows a higher hump of amorphous products because of the amorphous (reactive) metakaolin. Using sodium silicate enhances the reaction to produce a more amorphous phase for metakaolin, as seen in XRD patterns. Finally, using fly ash with metakaolin showed some peaks of quartz and mullite from fly ash and a hump representing the glassy structure of CSH and NASH.

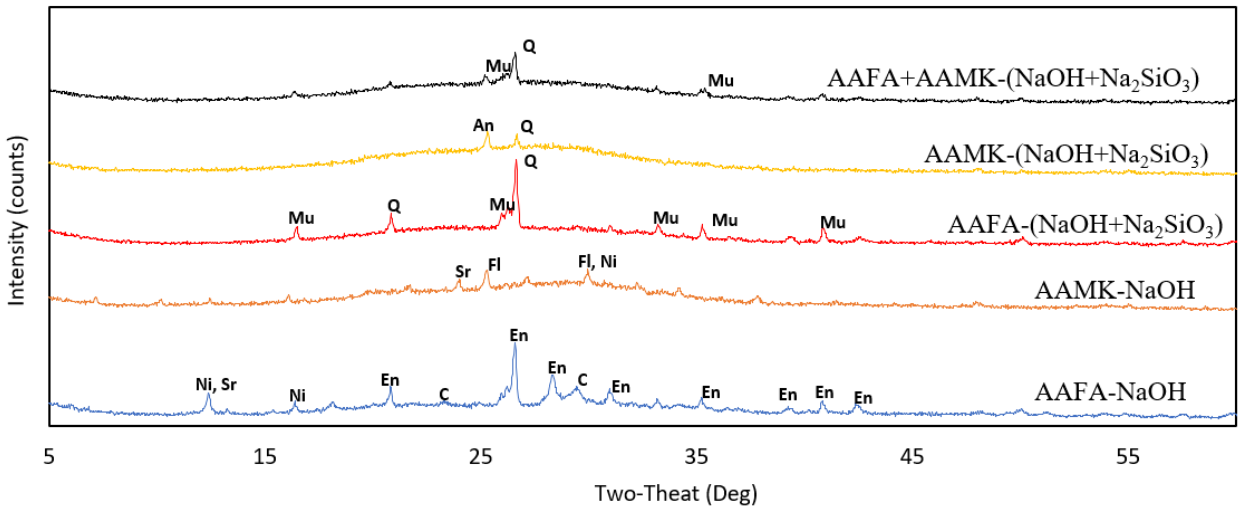

Figure 4.4: XRD patterns for alkali-activated mixtures

For disc samples, the density varied between 984-1177 kg/m^3 and 719-837 kg/m^3 for wet and dry samples, respectively. The moisture content is 27-39%, and the open porosity using a helium pycnometer for disc dry samples varied between 50-67%, as shown in Figure 4.5.

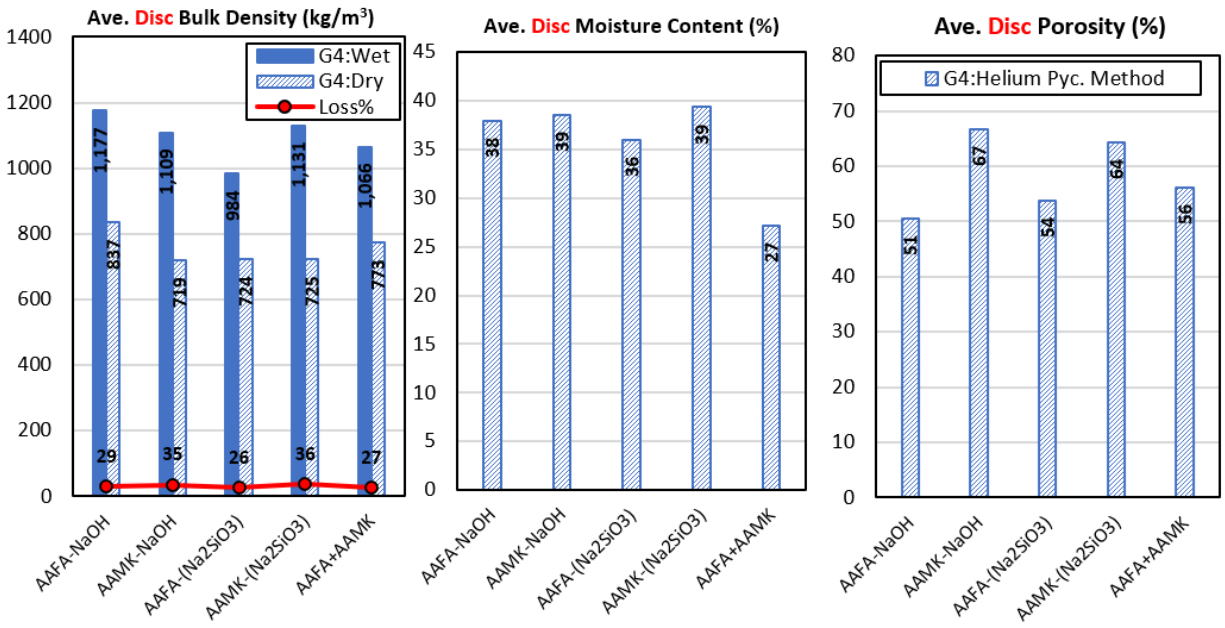

Figure 4.5: Physical and strength properties of hemp concrete with alkali-activated binders at 28 days

As shown in Figure 4.6, the thermal conductivity varied between 0.461-0.604 W/m K and 0.143-0.221 W/m K for wet and dry samples, respectively. The wet samples were mainly affected by moisture content, which significantly increased thermal conductivity by 55-75%. However, the conductivity of dry samples was affected by porosity (i.e., the conductivity decreased with increasing porosity). The difference in conductivity of wet samples for hempcrete with alkali-activated is less than 23% (affected by existing moisture content). The dry samples showed a less than 32% difference ascribed to the porosity and binder structure (glassy and crystalline). It could be noticed that the alkali-activated metakaolin showed a lower thermal conductivity, which may be ascribed to the amorphous alkali activated that has been observed in XRD patterns (Figure 4.4). On the other hand, the highest conductivity was achieved by AAFA-NaOH, which is ascribed to the multiple crystalline phases as observed in XRD. Generally, the properties of alkali-activated, the effect of hemp alkali-activated, and compaction degree are considered the most critical factors affecting thermal conductivity due to the direct impact on density, porosity, and crystalline products.

Similarly, the thermal diffusivity varied between 0.280-0.404 mm^2/s and 0.133-0.171 mm^2/s for wet and dry samples, respectively, as shown in Figure 4.6. As noticed, the rate of heat diffusion

through wet samples is significantly higher than dry samples within 52-67% due to the presence of water. The difference between alkali-activated hempcrete is less than 8% and 31 for dry and wet samples, respectively. The thermal diffusivity of dry samples is affected by many factors, including porosity, hemp content, degree of compaction, properties of alkali-activated, and amount of crystalline and amorphous products.

The volumetric heat capacity ranged between 1.396-1.857 MJ/m^3 K and 1.078-1.658 MJ/m^3 K for wet and dry samples, respectively, as shown in Figure 4.6. The wet samples showed higher values than dry ones because conductivity increased faster than the diffusivity (C_v=k/α) at the existing moisture content (as the thermal properties varied with varying moisture content for the same sample). There is a significant difference among the produced alkali-activated hemp for wet and dry mixtures, less than 25 and 57%, respectively, ascribed to the corresponding thermal conductivity and diffusivity behavior.

The specific heat capacity (C_p) is varied between 1330-1577 J/kg K and 1512-1990 J/kg K for wet and dry samples, respectively, as shown in Figure 4.6. However, the dry samples showed considerably higher values than the wet samples, ascribed to the damp and dry densities (C_p= C_v/ρ). The formation of glassy structure is more in metakaolin with sodium silicate activation than only sodium hydroxide, hence showing higher heat capacity values. Further, the AAFA+AAMK showed values between the individual activated fly ash and metakaolin. Again, the difference in Cp values among the alkali-activated binders is less than 24 and 16% for dry and wet samples, respectively.

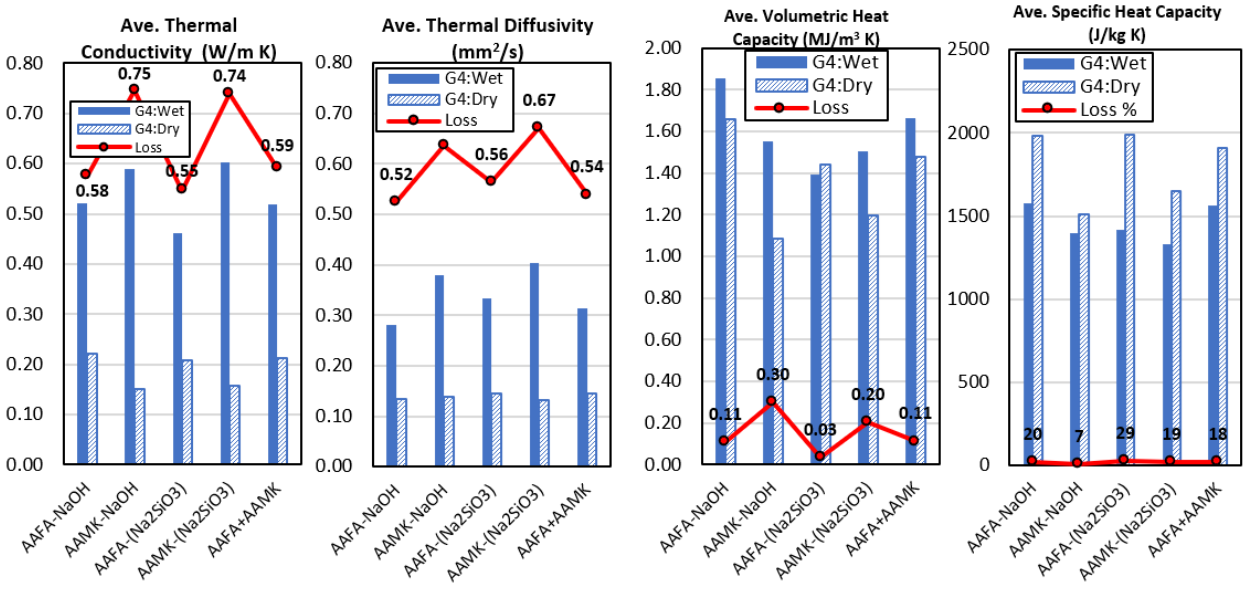

Figure 4.6: Thermal properties of hemp concrete with **alkali-activated binders** at 28 days (**Loss%= Loss*100**)

Figure 4.7 summarizes experimental hempcrete thermal properties, including thermal conductivity, resistivity, and transmittance of 0.20m thick hempcrete walls. The lowest k value is 0.089 W/m K for mixtures (C+30%FA) representing a resistivity of 2.25 m^2K/W, and a U value of 0.44 W/m^2K (Similar R values of 2.24 m^2K/W obtained by Li+30% MK). However, the cement and lime groups showed the highest thermal resistivity (1.14-2.25 m^2K/W), while the alkali-activated group binder showed the least ones (0.90-1.34 m^2K/W). However, cement-lime-based binders showed a considerable R-value in the 1.08-1.95 m2K/W range.

Based on the National Energy Code of Canada Buildings, Edmonton is in zone 7A, requiring U values for wall assembly of 0.215 – 0.284 W/m^2 K. However, this study achieved U values for solely hempcrete solid block (400 x 200 x 200 mm) between 0.44 – 1.11 W/m^2 K. The R-values of light, medium, and normal weight masonry blocks were in the range of 0.2 – 0.99 m^2K/W, while solid blocks of hempcrete produced in this showed significantly higher R-values between 0.90 – 2.25 m^2K/W.

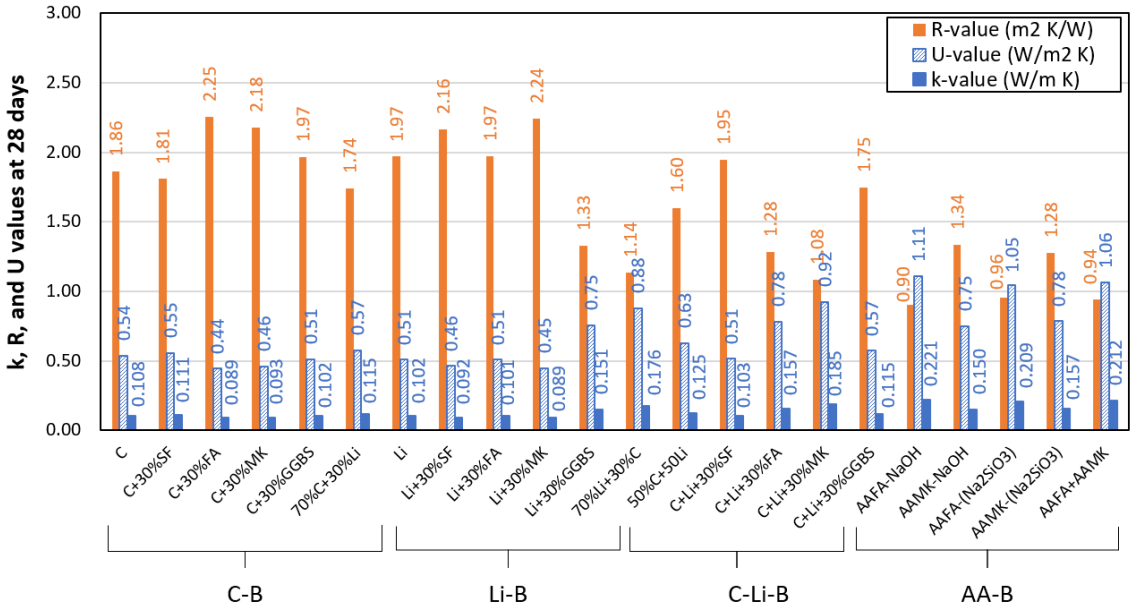

C: cement, B: binder, Li: Lime, AA: Alkali Activated

Figure 4.7: Thermal properties of hempcrete with four groups of binders

4.6 Conclusions

This study explored the effect of alkali-activated binders on hempcrete's strength and thermal properties. Two aluminosilicate materials, including fly ash (type F) and metakaolin, produced the alkali-activated hempcrete with sodium hydroxide and sodium silicates as activators. Compressive strength, thermal conductivity, heat capacity, and porosity were experimentally measured for the evaluation of such binder on hemp composite, and the following conclusions could be drawn:

- The density of hempcrete was significantly increased when using alkali-activated binders compared to other binders with the same binder-to-hemp ratio. This enhancement can be attributed to the more excellent production of NASH and CSH compounds.
- Alkali-activated binders are considered suitable for hempcrete because it is likely that hemp hurds do not absorb the sodium silicate and hydroxide solution, resulting in minimal disruption to the polymerization process.

- The highest strength achieved under dry conditions is 3.84 MPa due to the accelerated strength gain of alkali-activated during high-temperature curing. As a result, further optimizations may be necessary to achieve greater strength when utilizing alkali-activated binders and addressing bonding challenges with hemp.
- The presence of a substantial amount of water in wet samples results in a significant increase in thermal conductivity and diffusivity. Specifically, there is an approximately 55-75% increase in thermal conductivity and a 52-67% increase in thermal diffusivity.
- Several factors affect the properties of dry samples, including porosity, hemp content, degree of compaction, alkali-activated properties, and the amount of crystalline and amorphous products present.
- The wet samples exhibited higher values than the dry samples due to the faster increase in conductivity compared to diffusivity ($Cv = k/\alpha$) at the moisture content present. This variation in thermal properties with changing moisture content occurs within the same sample.

5 CHAPTER 5: OPTIMIZING HEMPCRETE COMPONENTS (PART III)

Journal paper #4

Investigating hemp size and content effect on hempcrete strength thermal properties

Ahmed S. Al-Tamimi[a], Vivek Bindiganavile[a]

Abstract

Hempcrete is green and sustainable concrete with superior thermal insulation properties. This concrete was developed in France in the 1990s and recently approved in Canada as construction materials. This study aimed to optimize components of hempcrete by exploring the effect of different hemp sizes and contents to raise recommendations about the size and dosage of hemp hurds. Four hemp sizes were examined for strength and thermal properties, including three from the Canadian harvest and one from the French crop. Based on the findings, it was observed that the optimal range for hemp hurd sizes is below 3mm in width and 10mm in length, as S4-FR. This selection resulted in a well-graded hemp hurd composition with reduced porosity, thereby enhancing the overall strength of the composite. However, it should be noted that excessively fine particles (like S3-CA) necessitate higher binder content and increase the risk of interfacial failure under load, compromising the compatibility of the composite. Additionally, longer hemp hurds (as S1 and S2-CA) tend to disrupt the arrangement due to their flaky shape, leading to a highly porous composite. Coarse hemp particles exhibited higher thermal conductivity values primarily due to increased porosity. On the other hand, fine particles demonstrated higher conductivity compared to coarse ones. The use of well-graded hemp hurds resulted in the formation of a denser composite, leading to higher conductivity values, as seen in the case of S4-FR. Fine hemp particles hamper heat diffusion due to slippage at the interface zones. Conversely, coarse particles can achieve similar outcomes because of their higher porosity. However, using well-graded particles, such as S4-FR, may lead to higher heat diffusion values; as the hemp content increases, the composite's strength, density, thermal conductivity, and heat capacity decrease due to porosity. However, thermal diffusivity is primarily influenced by the conductivity and heat capacity behavior in

tandem. Therefore, the optimal hemp content recommendation depends on the desired strength of the composite.

Keywords: Hemp size, Hemp content, thermal diffusivity, thermal conductivity, heat capacity, Strength

Nomenclature

Abbreviations

ANOVA	Analysis of variance
b/h	Binder to hemp ratio
C	Cement
EDX	Energy dispersive X-ray
HDM	Hot Disk Method
HS	Hemp shives
Li	Hydrated lime
MIP	Mercury intrusion porosimetry
NHL	Natural hydraulic lime
R-value	Thermal resistivity (m^2 K/W)
S1-CA	Size 1- Canadian hemp harvest
S2-CA	Size 2- Canadian hemp harvest
S3-CA	Size 3- Canadian hemp harvest
S4-FR	Size 4- French hemp harvest
SEM	Scanning electron microscope
U-value	Thermal transmittance (W/m^2 K)
w/b	Water to binder ratio
w/c	Water to cement ratio

Symbols

Cp	Specific heat capacity (J/kg K)
Cv	Volumetric heat capacity (MJ/m^3 K)
V_A	Added volume
$V_{apparent}$	Apparent volume of sample
V_{bulk}	Bulk volume of sample
V_c	Empty sample cell volume
$\rho_{apparent}$	Apparent density of sample
ρ_{bulk}	Bulk density of samples

Greek letters

α	Thermal diffusivity (mm^2/s)
ρ	Density (kg/m^3)
σ_c	Compressive strength (MPa)

5.1 Introduction

Hempcrete, or hemp composite or hempcrete, is an environmentally friendly form of concrete that combines a cementitious binder with hemp hurds (also known as shives) as coarse aggregates. Lime is predominantly used as the binder in this sustainable construction material. Originating in France during the early 1990s, hempcrete gained popularity across Europe and was approved as a construction material in Canada in 2012 [1][2]. Hempcrete exhibits notably reduced thermal conductivity and increased specific heat capacity, resulting in lower thermal diffusivity compared to other types of concrete [3][4][5]. Hence, this thermal behavior promoted hempcrete for building envelope materials. The composition of the hempcrete mixture, including the binder components, water content, and aggregate, significantly impacts the thermal properties [6]. Therefore, this research paper focuses on exploring how the size and scope of hemp hurds affect hemp concrete's strength and thermal properties.

Hemp hurds are obtained from the inner woody part of the hemp plant stem (cannabis sativa). As shown in Figure 5.1, the hemp stem has a hollow cross-section with four primary layers, which, from the exterior towards the open interior, are Epidermis/ bark, phloem, cambium, and xylem[7][8][9]. The bast fibers are extracted primarily from the phloem and secondarily from the cambium and xylem layers. The hemp hurds (or shives), on the other hand, which are used as aggregates in hempcrete, are obtained by removing the epidermis and phloem layers and then mechanically cutting hemp stem into chips with different sizes [8]. Hemp stem consists of approximately 20–40 wt.% of bast fibers and 60–80 wt.% of hurds, which are primarily composed of cellulose and secondary of non-cellulose, including hemicellulose, lignin, and pectin [10][4]. The hemp hurds consist mainly of 40–48% cellulose, 18–24% hemicellulose, and 21–24% lignin, and these components depend on the stage of growth, plant maturity, and plant variety [11][10][8]. However, the bast fibers contain higher amounts of cellulose (57–77%), while the hemicellulose

(9–14%) and lignin (5–9%) are lower, as compared to hemp hurds [10][8]. Further, pectin (with some impurities such as wax and oil) exists on the surfaces, ranging from 18 to 4% in the fibers and hurds, respectively [7][8].

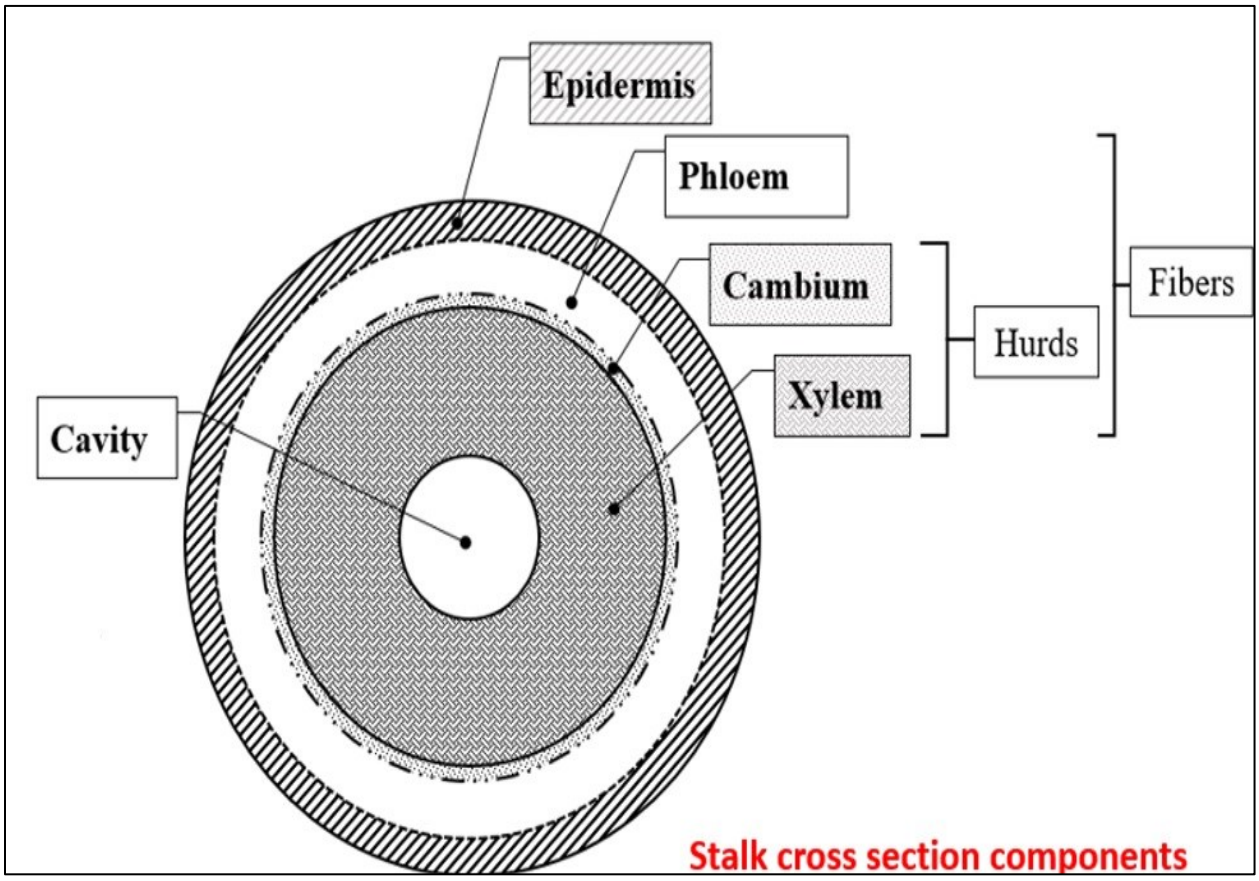

Figure 5.1: Hemp hurds and fibers from Cannabis stalks

As shown in Table 5.1, hemp concretes were produced using lime or cement binders, binder/ hemp ratios (2.0, 1.0, and 6.6), and different graded hemp particles. Thermal properties were measured, including thermal conductivity, specific heat capacity, and thermal diffusivity. The bulk density of hemp particles is in the range of 70 to 127 kg/m^3 [3][5], and the water absorption reached 325% after 24hrs [3][4]. The thermal diffusivity values varied between 0.156-0.450 mm^2/s for hempcrete with different binders, hemp sizes, and hemp contents, while the thermal conductivity values were

within the range of 0.063-0.214 W/m K. However, the thermal conductivity of hemp hurds is about 0.055-0.062 W/m K [12], heat capacity is 1600 J/kg K [13], and water absorption reached nearly 400% by wt. after 24hrs [12].

Table 5.1: A literature review on the strength and thermal properties of hempcrete

Binder type	Hemp content b/h	Hemp size (mm)	ρ (kg/m^3)	k (W/m K)	Cp (J/kg K)	α (mm^2/s)	w/b	σc MPa	Ref
Cement	2.0	Coarse S1<10	351-415	0.105-0.110	600-700	0.38-0.45	1.3	-	[3]
	2.0	Fine S2<10 S1>S2	340-410	0.102-0.115	750-770	0.37-0.40		-	
70C+20Li+10NHL	2.0	As received	627	0.138	1340	0.164	1.55	0.12	[4] [14]
Commercial			627	0.138	1300	0.169	1.45	0.21	
70Li+30GGBS			565	0.126	1250	0.178	1.55	0.14	
80Li+20MK			508	0.117	1240	0.186	1.65	0.10	
75% Li+15% NHL+ 10% FA	1.80	Graded <32	395	0.105	385	0.274	2.3	-	[5]
	1.10	Graded <32	298	0.094	333	0.282	2.7	-	
Li+ Mineral Addition	6.67	Fine <4	887	0.214	1009	0.228	-	-	[15]
	6.67	Coarse <11	733	0.179	996	0.247		-	
70% Li + 30% GGBS	2.0	Graded <8	508	0.129	1627	0.156	1.55	-	[16]
80% Li + 20% MK+	2.0	Fine <12	382	0.105	1575	0.174	1.72	0.29	[17]
	2.0	Coarse <50	377	0.099	1601	0.164	1.63	0.24	
Li + 10-20% CB	1.0	Fine <6.3	325-326	0.096-0.094	1504-1398	0.197-0.207	2.50	0.32-0.19	[18]

As the literature noticed, hemp concrete's compressive strength is affected by hemp content, water content, binder type, hemp sizes, and compaction degree [6]. The binder-to-hemp ratio of 1:1 with a density of 220-336 kg/m^3 showed a compressive strength between 0.05-0.36 MPa [14][15]. Doubling the amount of binder (2:1) increases the power of hemp concrete from 0.22 to 0.85 with a density of 291-481 kg/m^3 [16][15][17][18] (i.e., Strength increasing with increasing density of hempcrete). Similarly, the binder to hemp ratio of 3:1 and 4:1 could increase the strength of hemp concrete to 0.80-1.15 MPa [15]. Further, the strength reduced with increasing length of hemp hurds, reaching 30-50% due to decreasing the density, as indicated by [19][20].

5.1.1 Hemp particle size

The sizes of hemp hurds directly affect their arrangement into the composite and the compaction degree. Arnaud and Gourlay found that the larger the hemp particles achieved lower density relative to finer hurds because of their higher porosity and lower mechanical properties after 28 days. However, the strength of hempcrete with finer hurds progressed slowly. It increased significantly after four months, ascribed to the lower porosity, thus lower diffusion of CO_2 and slowing down the hardening kinetics [21]. Therefore, it's expected to have lower thermal properties than hempcrete with larger hemp hurds. Brzyski et al. produced lime hempcrete with fine and coarse hemp sizes and found that the coarse particles reduced the density and thermal conductivity. However, the finer hurds demonstrated higher strength (about 20%), which might be due to the lower porosity [16]. On the contrary, Nguyen et al. observed that the largest hemp size exhibited the highest strength at 28 days, attributed to a lower surface area coated with binder than finer hurds [9]. Further, the presence of fibers with hurds was observed to reduce the strength [9], while Bruijn et al. showed a negligible difference [22].

Gourlay et al. 2017 [3] used fibered coarse (<10mm) and un-fibered fine hemp particles with a binder-to-hemp ratio of 2.0 and cement to produce hemp concrete. The density and thermal conductivity of concrete with fine hemp shives slightly (around 3%) reduced, as compared to the coarse one, which may ascribed to the fibers filling the pores reducing the porosity (Similar findings [19][20]). The specific heat capacity noticeably increased (about 20%) for fine hemp particle concrete, which seems to be due to the porosity. Thus, the thermal diffusivity decreased by roughly 10-15% compared to coarse hemp. Further, the effect of hemp concrete's varying water content on thermal diffusivity and specific heat capacity is still unclear, but the thermal conductivity increased with increasing moisture content. Brzyski et al. 2020 [16] produced hemp concrete with the same binder-to-hemp ratio but with lime-metakaolin binder. Non-fibered fine and coarse hemp particles were used with a fraction of 0-12 mm and 0-50 mm, respectively. The authors found that fine hemp has similar density and porosity to coarse particles. At the same time, the thermal conductivity and diffusivity of coarse shives were slightly lower (about 6%) relative to the fine ones. However, the specific heat capacity is almost the same. Further, the strength of

fine hemp concrete exerts a higher strength than the coarse shives by roughly 17%, which may be ascribed to the arrangement of shives during compaction. Mazhoud et al. 2016 [23] produced a hemp plaster with a higher binder-to-hemp ratio (6.67) and fine and coarse hemp particles. The plaster with fine hurds showed a higher density (16%), thermal conductivity (16%), and specific heat capacity (12%) as compared to the coarse ones. In contrast, fine hemp plaster's thermal diffusivity and porosity were lower by about 8%. In conclusion, the higher content of fine hemp fractions tends to increase the bulk density of the composite, leading to higher strength thermal conductivity due to the lower porosity (similar findings [24][25]). Therefore, higher specific heat capacity and lower thermal diffusivity values could be observed in such hemp concrete, depending on hemp particle arrangement and degree of compaction [4].

5.1.2 Hemp content

Increasing the content of hemp hurds decreases the density due to increasing porosity and light components. The arrangement of hemp hurds with binder matrix forms a messy net structure due to the flaky shape of hemp hurds, increasing the content of hurds, leading to accumulation and more porosity. Thus, the strength dramatically decreases with the higher content of hemp hurds, even with higher hydraulicity of the binder. However, the composite becomes more brittle than the lower hemp content, which showed higher strength and relatively ductile behavior [26][27]. Bruijn and Johansson found that increasing the content of hemp hurds decreases the density (roughly 25%) and thermal conductivity (about 10%) due to increasing porosity and light components [5]. In comparison, the specific heat capacity decreased by 15% (might be due to air voids) [5]. However, the thermal diffusivity was minorly increased. Madrid et al. 2017 [28] showed a reduction in density and thermal conductivity with increasing the content of sawdust in concrete due to the presence of voids and light materials. At the same time, the specific heat capacity increased due to the same reason and wood's high thermal storage function. Hence, the thermal diffusivity decreased significantly (about 36%) [28] (Similar findings for wood shives [29]).

It's evident that hemp size and content affect the properties of hempcrete, and there is a lack of details about proper hemp size and content for better thermal and strength properties; thus, this study aimed to explore various hemp sizes and contents to verify and recommend hemp sizes and contents for better hemp composite. The recent approval for such material in Canada raised the responsibility to address the locally supplied materials to produce such composite with competitive properties as in Europe, for example. Further, hitting the net zero energy-ready code is a pushing factor that will be adopted by 2023 in Canada [30].

5.2 Materials

This study prepared hempcrete with three components: binder, water, and hemp hurd aggregate. The previous research selected the cement-lime-based composition as a binder to mix with four different sizes of hemp hurds. LAFARGE supplied General Use Cement (C), while high calcium hydrated lime type N (Li) was provided by GRAYMOUNT in Canada. In this work, four sizes of hemp hurds were used, as shown in Figure 5.2. Three were supplied locally by Canadian Harvest (AWE Solution Inc.) and one by LCDA in France.

Figure 5.2: Four hemp sizes used in this study.

As shown in Figure 5.3, the bulk density of the four-hemp size varied between 97 – 164 kg/m^{3,} and moisture content was in the range of 4.44-8.74%.

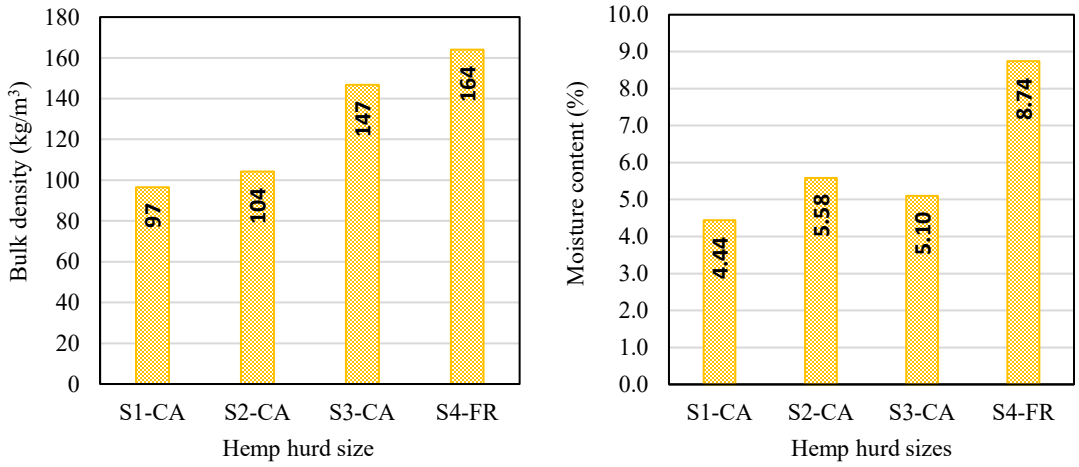

Figure 5.3: Bulk density and moisture content of hemp hurds

5.2.1 Grading analysis

The methods of showing the particle size distribution of hemp hurds were varied based on literature in three ways, including grading curve [14][5][3][23][28][31], width to length particle sizes [21], average particle dimension and aspect ratio [32][16]. Sieving analysis was conducted for a sample of 100 gm of each hemp size for about 20 minutes; then, grading curves were drawn, as shown in

Figure 5.4 (similarly done by [5][14]). The sieve mesh sizes were 16, 12.5, 5.0, 2.5, and 1.25 mm. Most hemp hurds were retained on 5mm sizes with 76, 51, 5, and 44% percentages for S1, S2, S3, and S4, respectively. However, S4 is the finest particle in this study, with about 40% passed through the sieve 1.25mm.

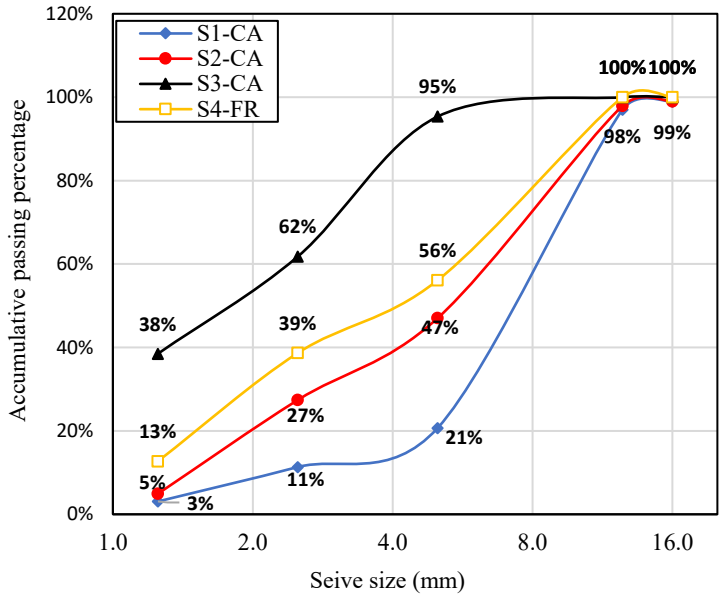

Figure 5.4: Grading curve of hemp hurds used in this study

The second method was identifying the individual particle dimensions using image analysis software (ImageJ), including the length and width of each hemp piece for a sample of about 5gm, as shown in Figure 5.5 (b). Then, a chart could be drawn with length and width imaging data for each hemp particle, as shown in Figure 5.5 (a). S1 showed fine hemp particles with length <10mm and width <2mm, while S4 showed a similar length and larger width of about 3mm. S1 and S2 showed a similar particle size with different contents.

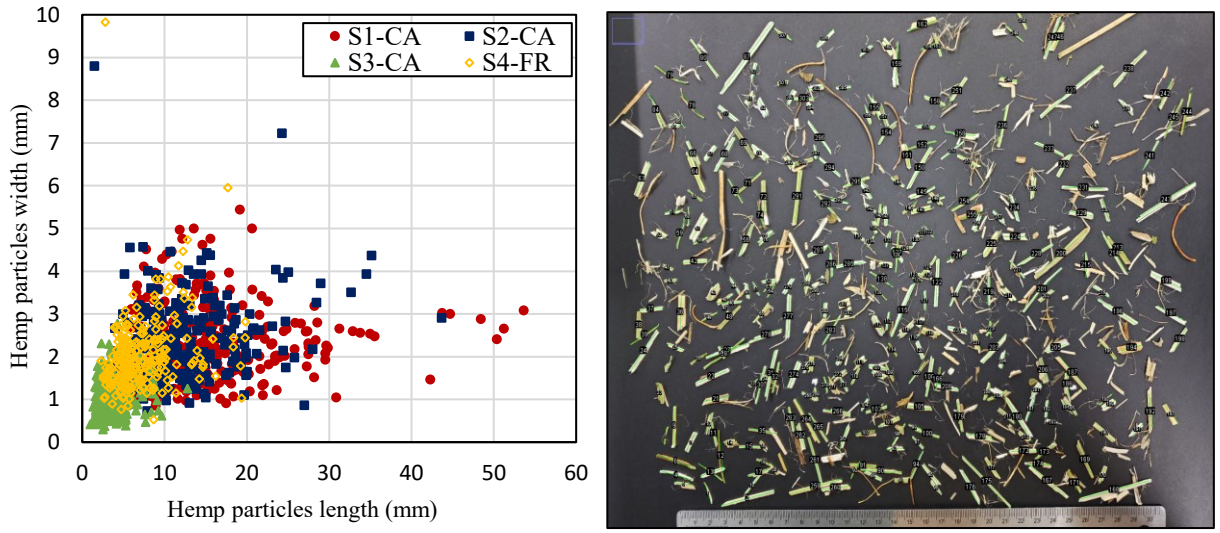

(a) **(b)**

Figure 5.5: (a) Length and width of hemp particle sizes in this study, (b) Imaging analysis for hemp sample

Imaging data were summarized in Table 5.2 with the maximum, minimum, average, and aspect ratio of hemp particles for each size. The average width of S1 and S2 is almost the same, but the average length of S1 is greater than S2 by about 3 mm (18%) (i.e., the aspect ratio of S1 is higher than S2). The smallest particles used are S3 with average length and width of 3.65 and 1.04 mm, respectively (i.e., aspect ratio 3.93). European hemp (S4-FR) size is in the middle, with an average width and length of 2.05 and 7.24 mm, respectively, and an aspect ratio of 3.84, similar to the aspect ratio of S3.

Table 5.2: Summary of data imaging of hemp particles used in this research

Hemp Size	Min width (mm)	Max width (mm)	**Ave. width (mm)**	Min length (mm)	Max length (mm)	**Ave. length (mm)**	Ave. aspect ratio (Length/width)	About 80% of particles	
								Width < (mm)	Length < (mm)
S1-CA	0.85	5.44	**2.33**	3.72	53.65	**15.05**	7.23	5	20
S2-CA	0.73	8.80	**2.32**	1.46	43.65	**12.36**	5.90	4	18
S3-CA	0.30	2.78	**1.04**	0.96	12.80	**3.65**	3.93	2	4.80
S4-FR	0.53	9.83	**2.05**	2.29	19.82	**7.24**	3.84	3	10

5.2.2 EDX analysis

Energy Dispersive X-ray (EDX) analysis was undertaken using a Zeiss Sigma FESEM machine to identify the elemental composition of hemp hurds. Table 5.3, Figure 5.6, and 5.7 show the elemental composition and EDX spectrum of hemp hurds with their relative concentrations. The hemp sample was tested as received from the supplier without washing or treatment. As received from suppliers, the analysis showed a similar elemental composition between Canadian and French hemp hurds.

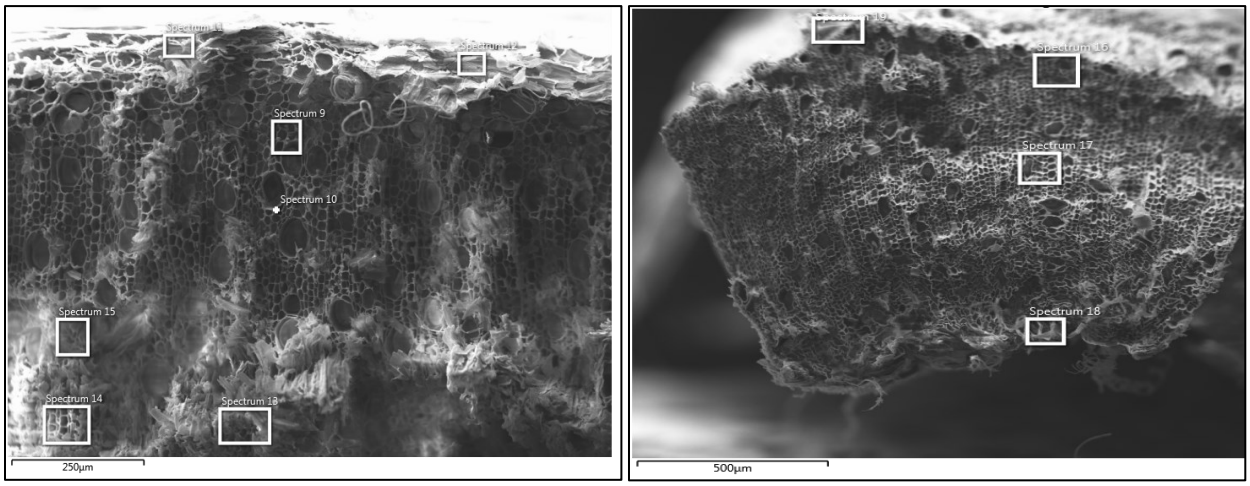

(a) **(b)**

Figure 5.6: EDX spectrums of cross-sectional: (a) CA hemp; (b) French hemp

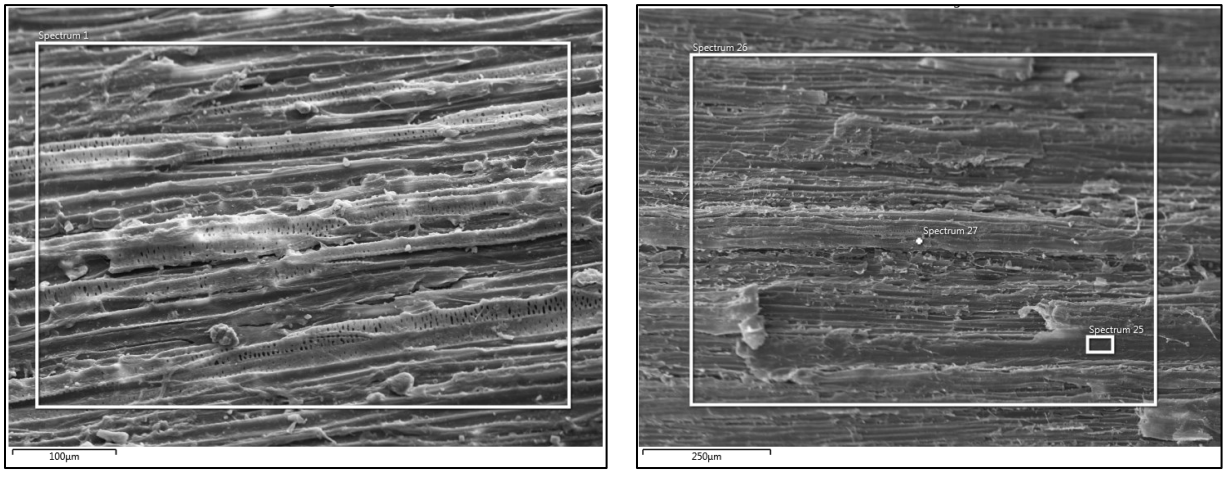

(a) **(b)**

Figure 5.7: EDX spectrums of surface: (a) CA hemp; (b) FR hemp

Table 5.3: Elemental composition of CA and FR hemp hurds using EDX analysis

Position	Element	C	O	Mg	Al	Si	P	S	Cl	K	Ca	Mo
Cross section	**S1-CA**	59.34	31.25	0.23	0.11	0.23	0.29	0.28	0.88	4.18	1.27	0.71
	S4-FR	58.34	37.46	0.32	2.40	0.21	0.21	-	-	1.23	1.10	0.59
Surface	**S1-CA**	56.71	39.61	0.25	0.29	0.57	-	-	0.32	0.88	0.84	-
	S4-FR	53.09	39.99	-	-	-	-	-	-	2.86	4.06	-

5.2.3 SEM micrographs

Scanning Electron Microscopy (SEM) images were taken using Zeiss Sigma FESEM w/ EDX & EBSD with an in-lens secondary electron (SE) detector and a backscatter detector (BSD). The hurds were coated with a 20-nm layer of gold to improve their conductivity and avoid charging to obtain more explicit images. The images were taken at a slow scanning speed, at different magnifications ranging from 30 to 1000x, and at an acceleration voltage speed of 20kV. The SEM images (micrographs) were used to study morphology (texture) of the hurd surface and the porosity analysis [33][34][1]. The SEM images were taken for the cross-section and both surfaces (inner and outer) of hemp hurds. The SEM images of a cross-section of hemp show the porous structure of hurds, which is surrounded by a light solid layer (cambium), as shown in Figure 5.8 (Similar structure shown [35]).

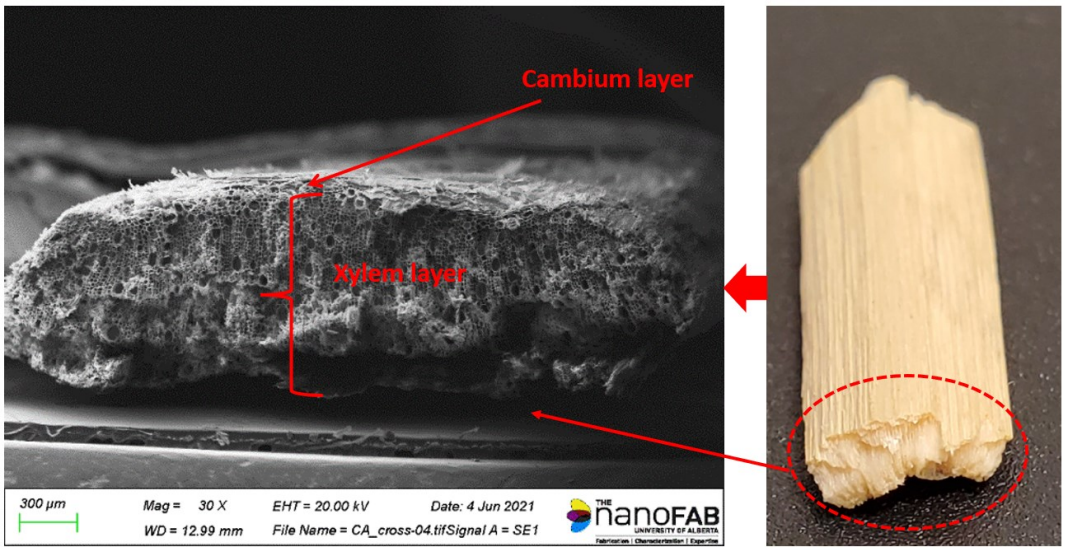

Figure 5.8: Micro-image of hemp hurds cross-section

SEM images were produced for hemp hurds to illustrate the porous microstructure, including cross-section, longitudinal section, and exterior surfaces, as shown in Figure 5.9.

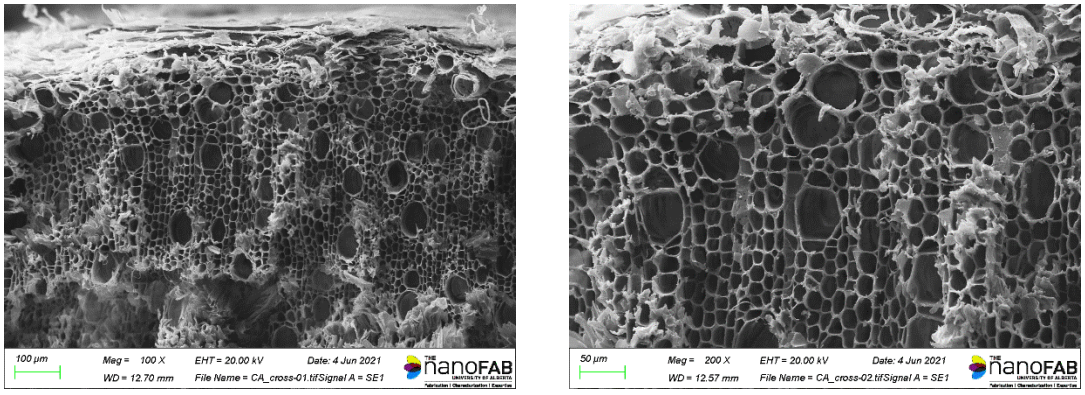

(a)

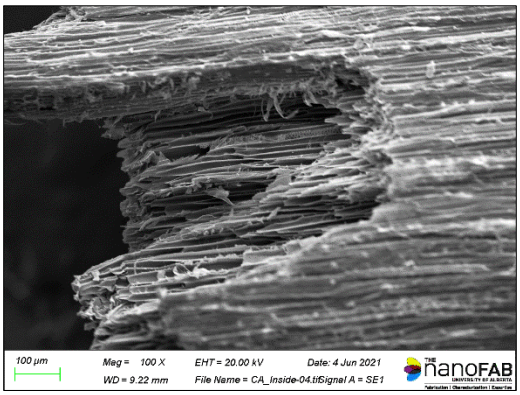

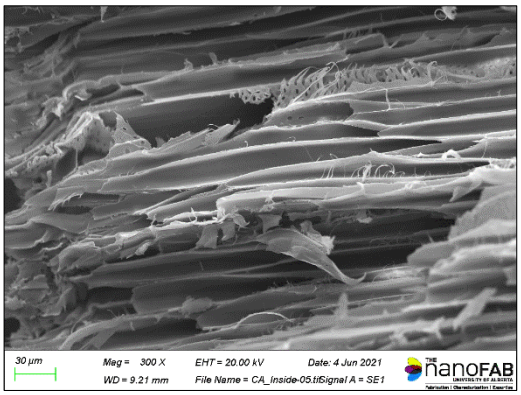

(b)

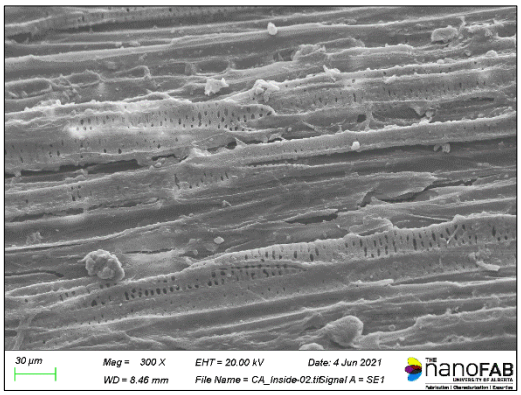

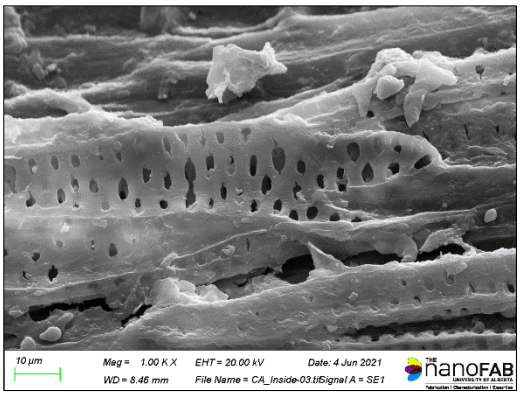

(c)

Figure 5.9: SEM images for CA hemp: (a) Cross section; (c): Longitudinal section; (b): Exterior surfaces

5.2.4 Porosity

SEM micrographs for the cross section (perpendicularly to the plane of growing direction) showed two different sizes of pores, the smaller was called xylem and the giant vessel, with average diameters of 3-30µm and 40-60µm, respectively, as shown in Figure 5.10 and Figure 5.11 for Canadian and French hemp harvests (Similar findings [1]). Vessel pores have the form of an ellipse, which results from the vascular bundles; the length of the longer ellipse axis is an average of 55µm, and the shorter ellipse axis is 30µm. Xylem ray pores are of various forms (polygonal or round) with an average diameter of 15µm, which derives from the ground tissues and continuously distribute like a honeycomb around the large pores (Similar findings [36][1][37][35]).

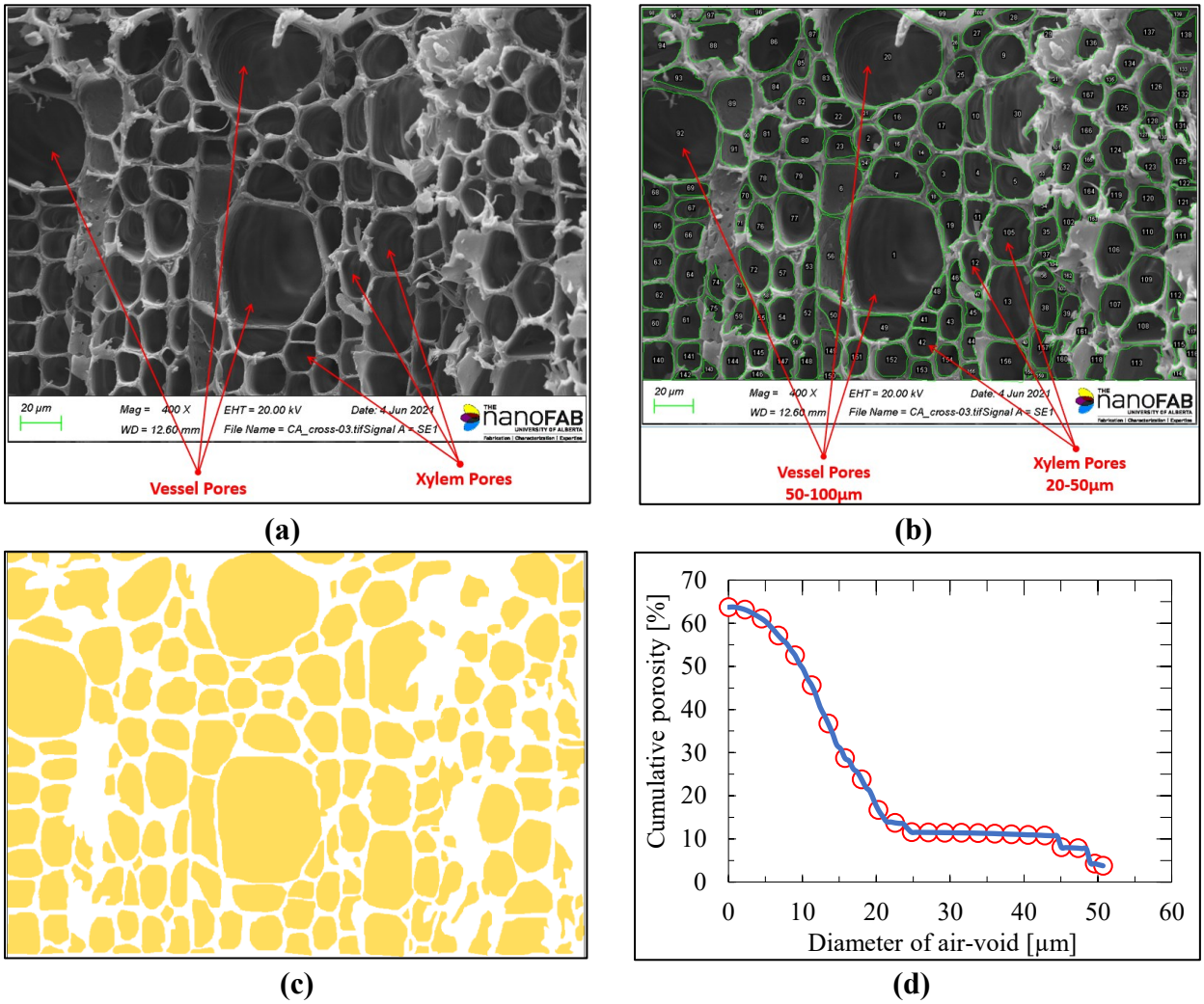

Figure 5.10: SEM for Canadian harvest hemp: (a) SEM Image (Cross-section); (b) Air void outlined; (c) Air void extracted; (d) Void size distribution

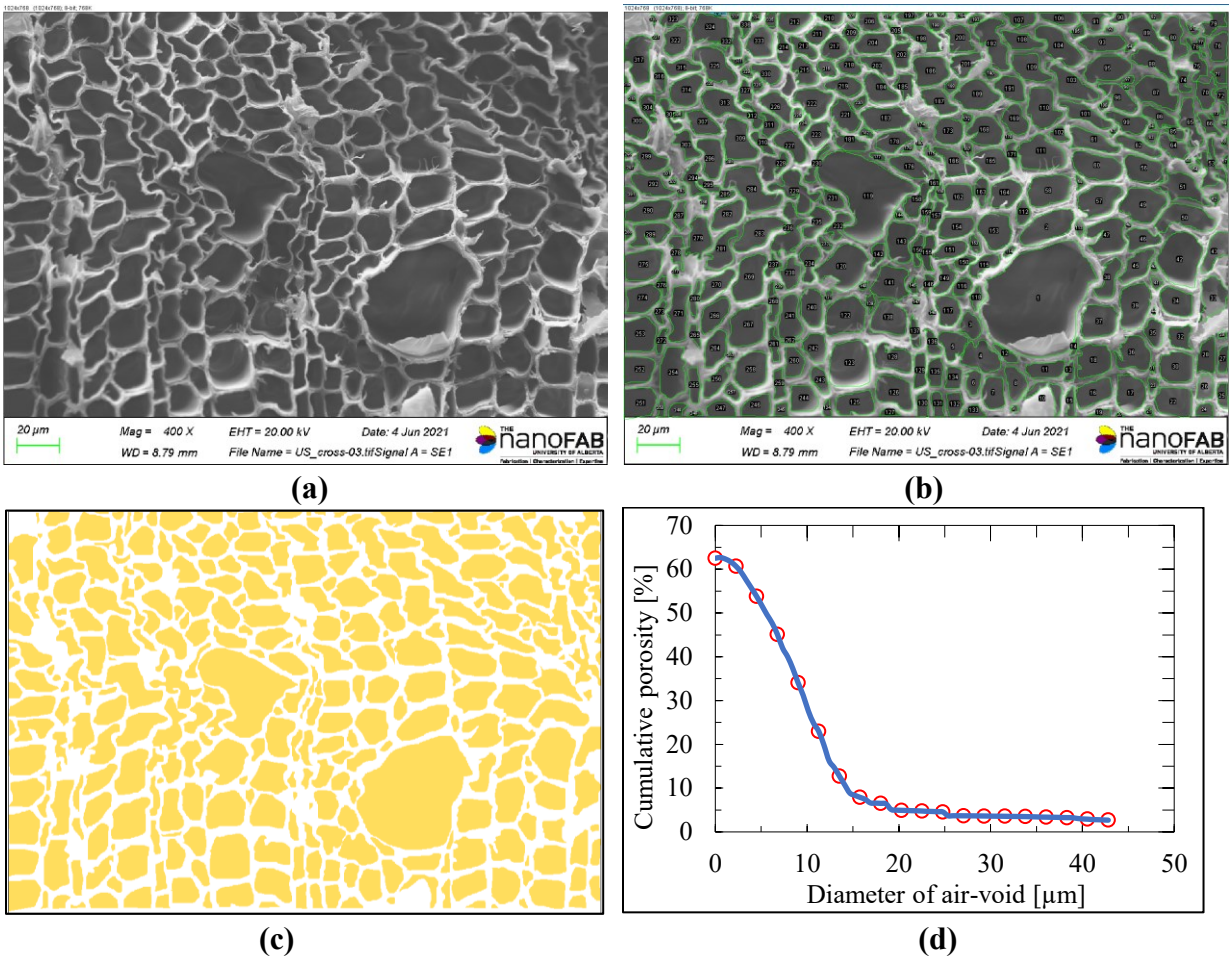

Figure 5.11: SEM for French harvest hemp: (a) SEM Image (Cross-section); (b) Air void outlined; (c) Air void extracted; (d) Void size distribution

The data of pores were summarized from (ImageJ) in Table 5.4 for Canadian and French hemp, which show a similar pore size. The shape of pores in French hemp was affected by how it cut; pores look wavy and compressed.

Table 5.4: Comparison between Canadian and French hemp pores size

	Canadian Harvest Hemp	French Harvest Hemp
Porosity (%)	64	63
Max void diameter	59 µm	52.5 µm
Min void diameter	3.4 µm	0.3 µm
Median void diameter	14.2 µm	9.6 µm

5.3 Mix Design of Hempcrete

5.3.1 Hemp size

The hempcrete compositions were formulated utilizing the absolute volume technique (ACI 211) [38]. Each hemp size has a different water absorption; hence, the initial water absorption was assumed to be 150% for all hemp sizes, and then water was adjusted until the mixtures became homogeneous and consistent. Thus, the water absorption was varied for all hemp sizes, as shown in Table 5.5. However, the binder-to-hemp ratio is fixed for all mixtures. The total No. of samples in this task is 48 (i.e., 12 samples/ mix).

Table 5.5: Mix proportions of hemp concrete with different hemp sizes for Task II

Binder Type	Mix composition (% by wt.)	w/b	Hemp abs. (%)	w/b (Including abs.)	B/H (By wt.)
Cement-Lime based binders	50% C+ 50% Li+ S4-FR	0.625	200	1.42	2.50
	50% C+ 50% Li+ S1-CA		200	1.42	
	50% C+ 50% Li+ S2-CA		270	1.71	
	50% C+ 50% Li+ S3-CA		300	1.82	

5.3.2 Hemp content

In this task, hemp hurds' content varied from 20-100% by wt. of binder, as shown in Table 5.6. However, it could be noticed that the w/b ratio increases with increasing hemp content. Again, the total No. of prepared specimens is 48 (i.e., 12 sample/ mix).

Table 5.6: Mix proportions of hemp concrete with different hemp content for Task III

Binder Type	Mix composition (% by wt.)	w/b	Hemp abs. (%)	w/b (Including abs.)	B/H (By wt.)
Cement-Lime based binders	50% C+ 50% Li+ 20% S4-FR	0.625	200	1.02	5.0
	50% C+ 50% Li+ 40% S4-FR		200	1.43	2.5
	50% C+ 50% Li+ 50% S4-FR		200	1.62	2.0
	50% C+ 50% Li+ 67% S4-FR		200	1.96	1.5
	50% C+ 50% Li+ 100% S4-FR		200	2.63	1.0

The three components of hempcrete were mixed following similar techniques as Gourlay and Taoukil [3][31]. The hemp hurds were mixed for 1 min, and then 1/3 of water was added for wetting the hurds. Next, the binder was poured gradually and mixed for 2 mins. Finally, water was adjusted until it reached a homogeneous mixture and mixed for 2 mins. The mixture was cast in cubic and disc molds and tamped with a 6 mm rod, as shown in Figure 5.12. Samples were cured in a humid room for 28 days and then tested for wet and oven-dry conditions.

Figure 5.12: Mixing, casting, and demolding hempcrete samples for each mixture

5.4 Testing

5.4.1 Strength

Three cubes measuring 50mm/mix were prepared and subjected to compressive strength testing. In this study, the compressive strength machine had an adjustable load rating expressed in kPa/s. The loading rate was adjusted accordingly to ensure that each sample took at least 2 minutes to fail. A load rating of 50 kPa/s was selected for this purpose, following the guidelines specified in ASTM D4832 [39].

5.4.2 Porosity

Hemp concrete exhibits a highly porous microstructure, with an open porosity (interconnected pores) varying between 60% and 90%. Various methods were employed to measure the open porosity of hempcrete, including mercury intrusion porosimetry (MIP) [9][40], air porosimeter [3],

water displacement pycnometer [32], and helium pycnometer [41][42][43]. In this study, A Helium pycnometer is specifically designed to determine the skeletal or apparent volume of solid materials by utilizing Helium as a displacing fluid to infiltrate the smallest open pores (<10^{-4} μm) [44][45], as shown in Figure 5.13.

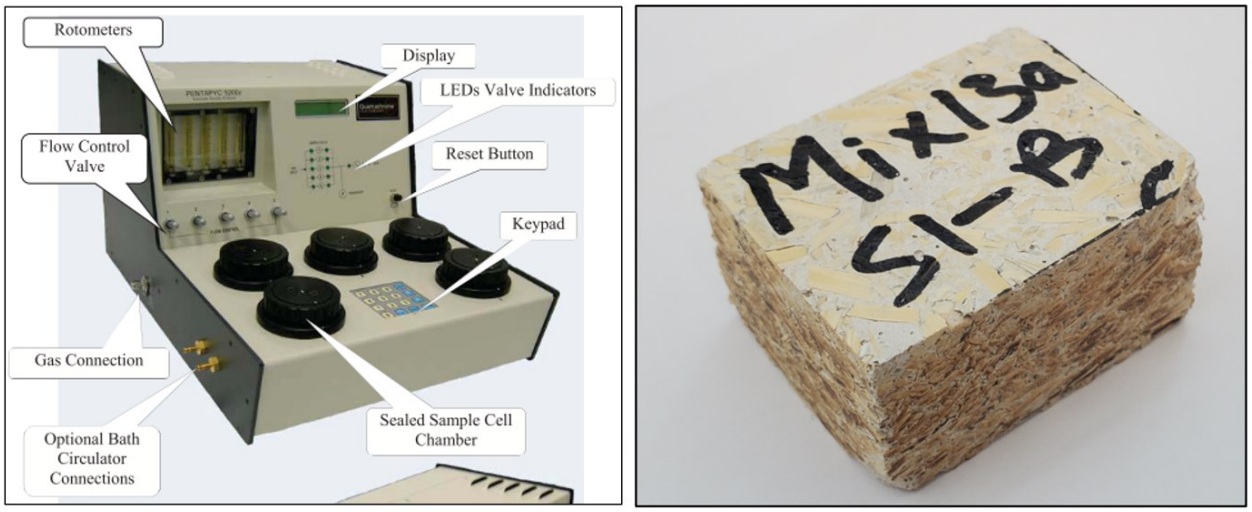

(a) (b)

Figure 5.13: (a) Pentapyc 5200e instrument; (b) Hemp concrete sample

The actual volume was measured 4-6 times for each sample with Eq- 5.1 [46][47].

$$V_{apparent} = V_c + \frac{V_A}{1 - \frac{P_2}{P_3}} \qquad \textbf{Eq-5.1}$$

where $V_{apparent}$: Apparent volume of sample; V_c: Empty sample cell volume; V_A: Added volume; P2: Stabilize pressure; P3: Falling pressure.

The open porosity was calculated according to Eq- 5.2 [3].

$$Porosity \quad \% = \left(1 - \frac{V_{apparent}}{V_{bulk}}\right) * 100 \qquad \textbf{Eq- 5.2}$$

The water displacement method can be utilized to measure the open porosity of hempcrete [9][45]. To ensure water accessibility to the open pores of hempcrete and prevent it from floating, a vacuum

of 100 mm Hg (Torr) was applied for 15 minutes, as shown in Figure 3.13. Hence, the open porosity could be found with the known V_{1water} and V_{2water} according to Eq- 3.2.

$$Porosity \quad \% = \left(1 - \frac{V2_{water} - V1_{water}}{V_{bulk}}\right) * 100 \qquad \textbf{Eq- 5.3}$$

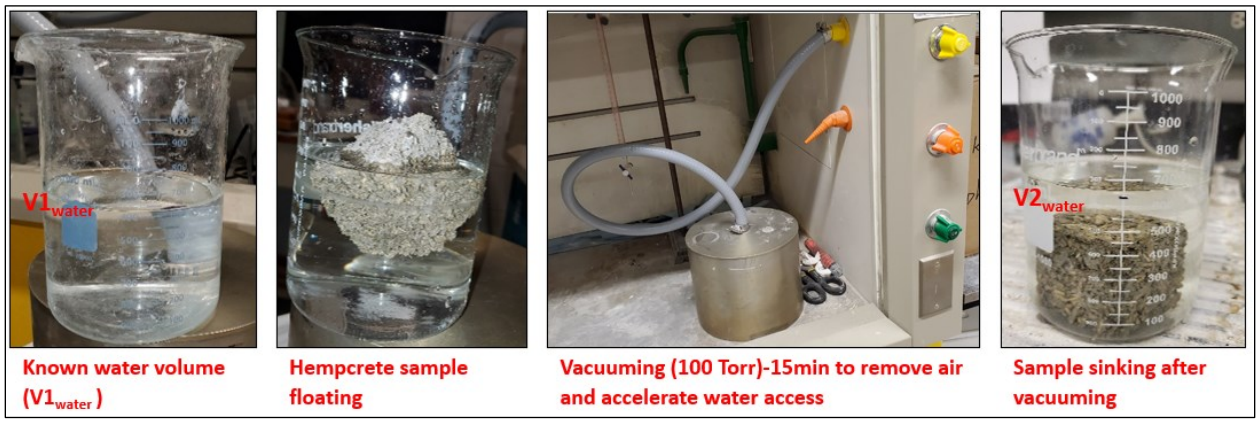

Figure 5.14: Measuring porosity of hempcrete cubes using water displacement method with vacuuming [48]

5.4.3 Thermal properties

The thermal properties, including thermal conductivity, heat capacity, and thermal diffusivity, were assessed for wet and dry conditions using the Hot Disk Method (HDM) [49]. The thermal constants of the prepared samples of hemp concrete were measured in this study using the Hot Disk TPS 1500 (Thermal Constants Analyzer), which provided an accuracy better than 5% as per ISO 22007-2 standards [49]. As shown in Figure 5.15, The main components of the setup are the TPS-1500, a PC, and a hot disc probe. The hot disc probe is horizontally embedded between two halves of the tested specimen.

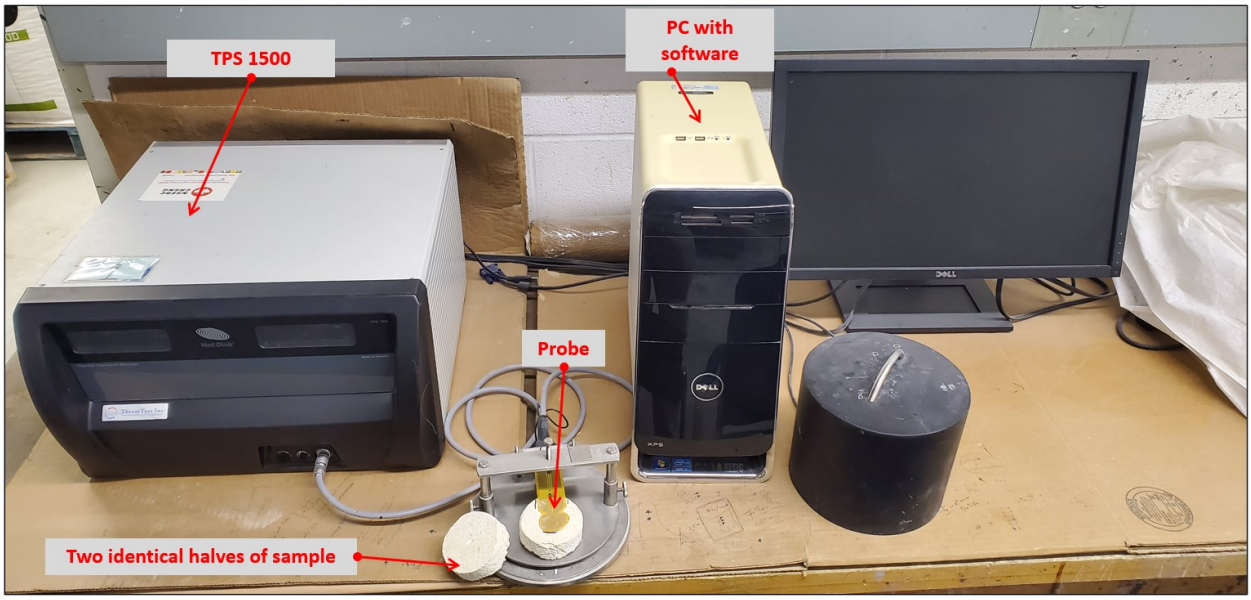

Figure 5.15: TPS 1500- Thermal Constant Analyzer

The Hot Disk Method operates on the principle of generating a heat pulse using an electrical current. This pulse is applied to the hot disk sensor, creating a dynamic temperature field within the two halves of the specimen. The average temperature increase of the hot disk probe is measured over time by monitoring the electrical resistance of the probe (sensor or adaptor) [49][50]. Compatible software with the device measured the thermal conductivity, thermal diffusivity, and volumetric heat capacity with a detailed process explained in the manual [49][50].

5.5 Results and Discussion

This study investigated two variables: hemp size and hemp content for hempcrete. 50mm cubes were tested for strength, and 75mm discs were examined for thermal properties, including thermal conductivity, heat capacity, and thermal diffusivity.

5.5.1 Effect of Hemp Size

In this task, four hemp sizes were used with a composition of binders of (50% Lime + 50% Cement), and the same binder-to-hemp ratio (2.50) to produce cubes and discs. As shown in Figure

5.16, the distribution of hemp particles into the composite is seen for the four sizes of hemp, in which the integration between hemp and binder seems to be stabilized and attractive. The difference among the four sizes is visually noticed, in which the small particles fill the gaps among the larger ones. However, S3 hemp particles are the finest, and many hemp seeds can be seen on S2 hemp size. The particle size of French hemp (S4-FR) looks in between Canadian hemp sizes (S1-CA and S3-CA).

Figure 5.16: The smoothed surface of hempcrete with four hemp sizes was used in this study.

As shown in Figure 5.17, the cubic densities are varied between 927-1240 kg/m^3 and 434-566 kg/m^3 for wet and dry samples, respectively. Wet densities are significantly higher than dry ones (47-56%) due to the high-retained moisture content in the 47-56% range, as shown in Figure 5.17. The finest hemp shives (S3-CA) showed the highest wet and dry densities, 1240 and 567 kg/m^3, respectively, which may be ascribed to increased water absorption (about 300%), and the high bulk density of S3-CA hemp (145 kg/m^3), and less porous composite relatively to other mixtures due to finer particles (similar findings [21]). Further, wetting the fine hemp particles and compaction leads to a denser mixture rather than the compaction of dry hemp hurds. However, larger hemp particles could not be compacted well due to their flaky shape, forming gaps between them, leading to a porous structure with lower density, as translated by S1 and S2. Hemp size S1 showed slightly higher density than S2 by about 6-14% for wet and dry samples, which ascribed to better particle size distribution of S1 relative to S2. However, the width and length of hemp particles clearly showed a similar hemp particle size between S1 and S2, as shown in Figure 5.5. French hemp size showed the least wet density with about 926 kg/m^3 due to the least water absorption relative to

other sizes (about 200%). However, the dry density is relatively higher due to the highest bulk density of S4 hemp hurds (about 164 kg/m^3) and the least porosity (about 40%), showing better hemp size analysis. As similarly found by many authors, the fine hemp hurds were found to increase the density of hempcrete due to filling the pores with the fine particles, reducing porosity [23][24][25]. Generally, the highest dry density was achieved by the finest hemp particles (S3-CA), then French hemp size (S4-FR) with coarser hemp particles, which ascribed the well-graded particles, leading to lower porosity.

As shown in Figure 5.17, the compressive strength varied between 0.18-0.77 MPa and 0.25-1.33 MPa for wet and dry samples at seven days, respectively. The dry samples showed a higher strength relative to wet samples (28-42%), which may be ascribed to the higher stiffness of the binder and interface zone. The French hemp (S4-FR) achieved the highest strength, 1.33 and 0.77 MPa, for dry and wet samples, respectively, which ascribed to the best hemp particle size distribution (As Figure 5.5) and their distribution into the composite leading to the least porosity (about 40%). Hemp size S3-CA exerts about half the strength of S4-FR due to the higher surface area (i.e., needs more binder). Further, the interfacial area between binder and hemp hurds increased with the usage of finer hemp particles, at which the debonding and microcrack propagation takes place under loading. Hemp sizes (S2-CA) showed the lowest strength (almost half strength of S1-CA hemp size) due to the highest porosity achieved (60%) caused by the lengthy/flaky hemp shives, disordered arrangement of particles, and poor gradation (Similar findings [19][20][51]). In conclusion, most hemp hurd sizes should be in the range of <3mm in width and 10mm in length (As described in Figure 5.5) to achieve well-graded hemp hurds with lower porosity, to achieve a higher strength (similar findings [24][25]). However, very fine particles require higher binder content and increase the possibility of interfacial failure under loading, which diminishes the compatibility of the composite. Further, the lengthy hemp hurds disturb the arrangement due to the flaky shape, leading to a highly porous composite.

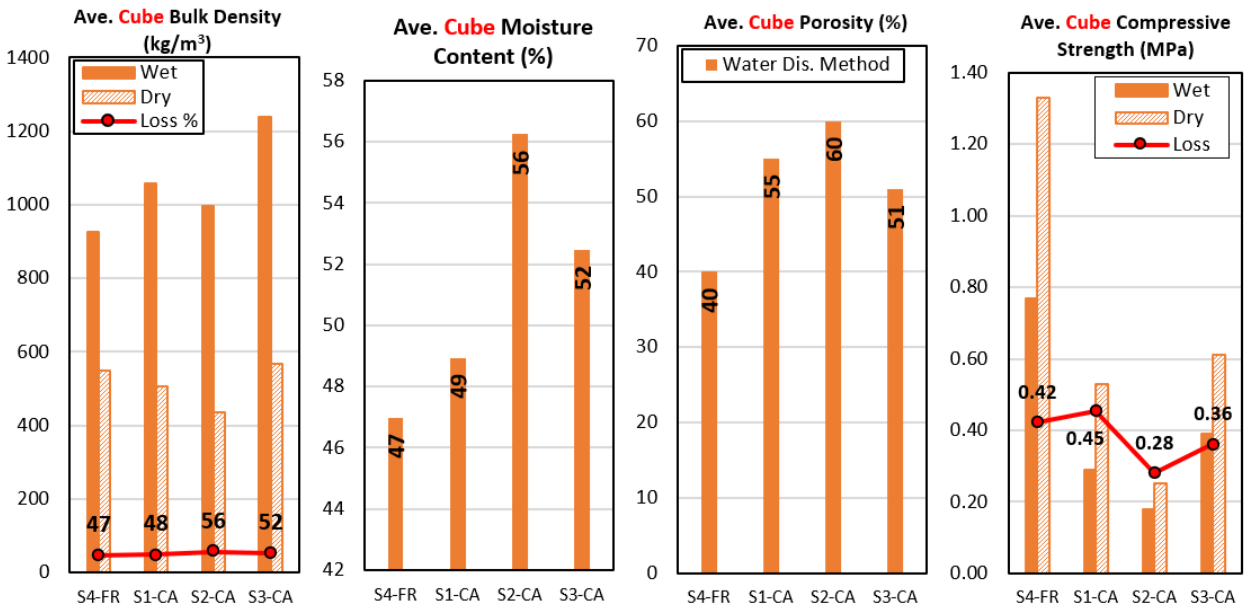

Figure 5.17: Physical and strength properties of hemp concrete cubes with four hemp sizes at seven days (Loss%= Loss*100)

As noticed in Figure 5.18, the disc density increased with decreasing hemp size from 925 to 1095 kg/m^3 for the wet sample, while the dry ones started from 505 to 567 kg/m^3. Similarly, the finest hemp sizes delivered the highest wet and dry densities, while S2 showed the lowest due to the highest porosity (about 80%). The moisture content of disc samples varied between 44-58%, and Helium pycnometer porosity was between 69-80%, as shown in Figure 5.18.

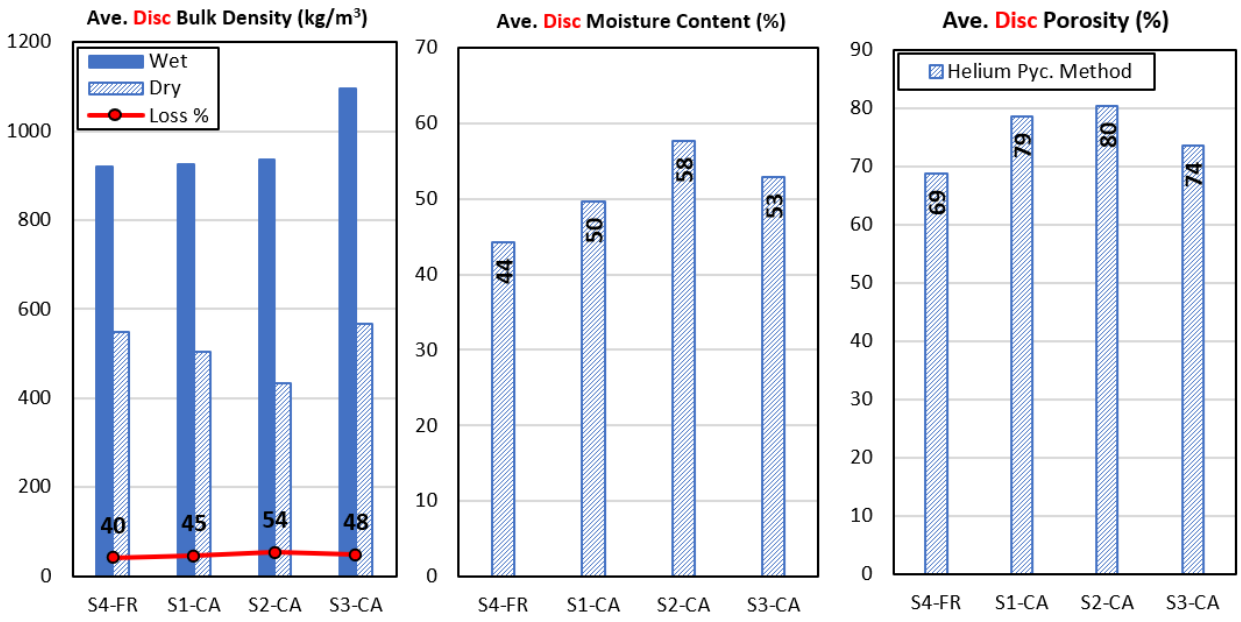

Figure 5.18: Physical and strength properties of hemp concrete discs with four hemp sizes at seven days

As shown in Figure 5.19, the thermal conductivity varied between 0.542-0.600 W/m K and 0.074-0.131 W/m K for wet and dry samples, respectively. The high moisture content in hempcrete samples (44-58%) increased the thermal conductivity significantly (76-87%) due to the higher conductivity of water. The thermal conductivity increased with increasing the density for wet and dry samples with all hemp sizes (Similar finding found [24][25]). The long hemp shives for S1 and S2 (Max sizes 53 and 43 mm) disturbed the arrangement of hemp hurds during compaction, forming the air voids, reducing density (i.e., porosity increased) and thermal conductivity. However, S2 showed the least conductivity due to the achieved least density. Although the density of S3 is relatively higher than S1 of dry samples, the conductivity of S3 is slightly lower than S1 due to more interface areas hindering heat conduction. The French hemp showed the least porosity (i.e., well gradation). Thus, the density and thermal conductivity were relatively high compared to other hemp sizes in this study. S3-CA showed higher density and lower conductivity relative to S4-FR, which may be explained by the microcracks, debonding, and interface zone leading to lower conductivity for S3. In summary, hemp sizes are affecting thermal conductivity significantly, in which coarse particles showed lower values due to higher porosity, and fine

particles showed higher conductivity relative to coarse ones (similar finding [16]). However, the well-graded hemp hurds form a denser composite and higher conductivity values, such as S4-FR.

Figure 5.19 shows the wet thermal diffusivity in the range of 0.359-0.449 mm^2/s, and the oven-dry ones are between 0.109 to 0.138 mm^2/s. Again, the wet thermal diffusivity is significantly higher than dry ones due to the high moisture content of hempcrete (44-58%, as shown in Figure 5.18), which requires a higher input heat energy, as explained in the thermal testing section. S3 hemp size showed the least dry thermal diffusivity, while S1 achieved the highest ones with a variation of 27% for dry conditions. This might be ascribed to the finer hemp particles, which reduce the rate of heat diffusion through the slippage at the interface zone (due to the higher surface area) relative to coarser particles (Similar findings [23]). In summary, fine hemp particles hinder heat diffusion due to the slippage at interface zones. In contrast, coarse particles might achieve similar outcomes due to the higher porosity (i.e., lower thermal diffusion). However, well-graded particles (such as S4-FR) may result in relatively higher diffusion, reaching 24%.

As shown in Figure 5.19, the volumetric heat capacity varied between 1.263-1.661 MJ/m^3 K and 0.677-0.970 MJ/m^3 K for wet and dry samples, respectively. The wet C_v values are higher than the dry ones, with 17-58% percentages due to high moisture content. However, the higher increments of thermal conductivity relative to the thermal diffusivity led to higher C_v values for wet samples than dry ones ($C_v=k/\alpha$). S3 hemp size showed the highest dry C_v value (about 0.887 MJ/m^3 K). In comparison, the lowest one for S2 with 0.677 MJ/m^3 K is due to the lowest dry density (i.e., dry C_v increases with increasing density since the heat capacity of hemp is much higher than air, similar findings [3][5]).

Interestingly, the specific heat capacity of dry samples is similar (1558 -1769 J/kg K), while the wet samples showed a difference reaching 26% (1365-1719 J/kg K) ascribed to the moisture content. The values of C_p are mainly affected by the wet and dry density (i.e., $C_p= C_v/\rho$), hence the higher densities leading to lower values of C_p.

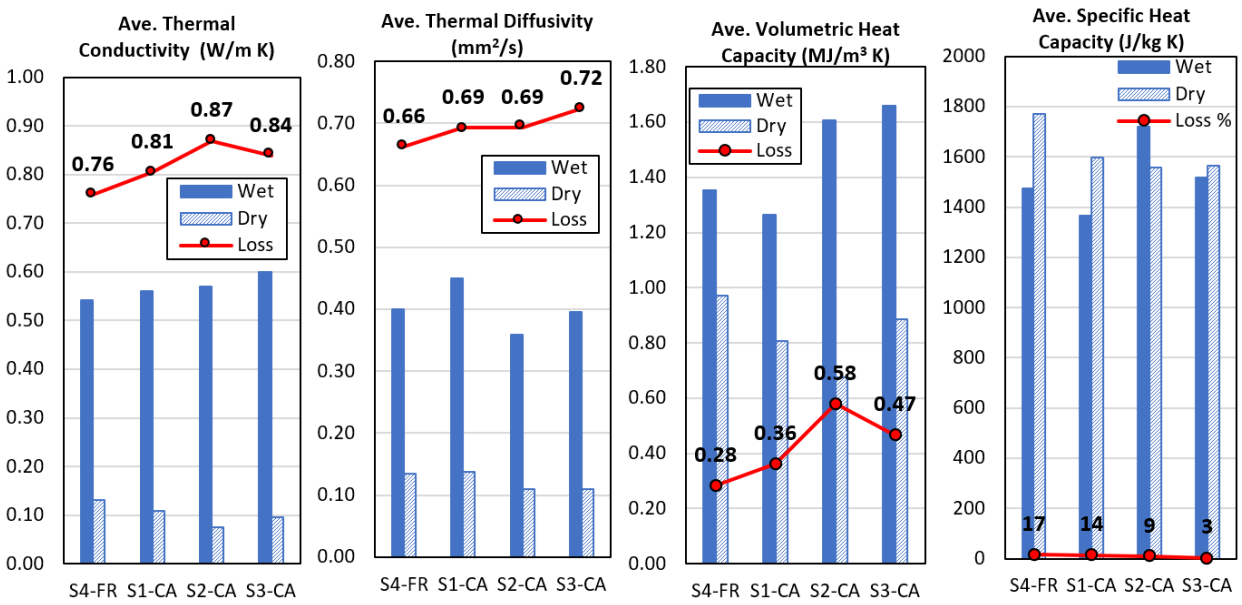

Figure 5.19: Thermal properties of hemp concrete with four hemp sizes at seven days (Loss%= Loss*100)

Figure 5.20 shows the thermal conductivity of dry hempcrete samples with four hemp sizes, R and U values for the same samples with a thickness of 0.20 for dry conditions. The R values varied between 1.53-2.69 m^2 K/W, while U values were 0.37-0.66 W/m^2 K. S2-CA achieved the highest R values, and S4-FR observed the lowest one.

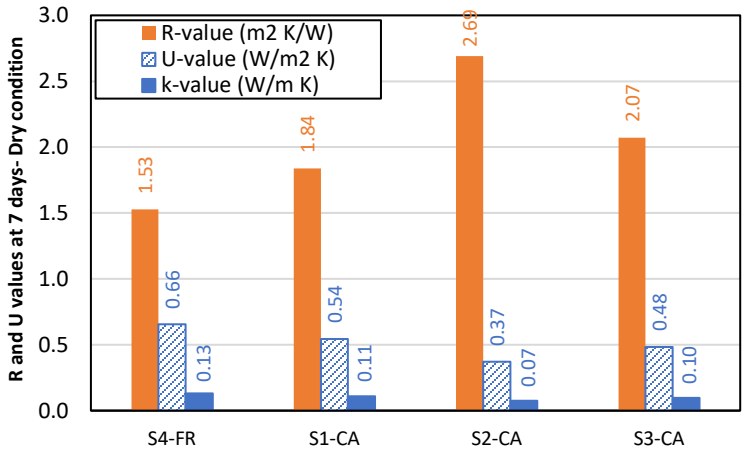

Figure 5.20: Thermal properties of hempcrete with four hemp sizes at seven days

5.5.1.1 Analysis of variance

Similarly, an ANOVA test (one factor, which is hemp size) is used to check for a difference between four hemp sizes by studying the means (i.e., compare the mean of each hemp size to the overall mean of all hemp sizes). Table 5.7 shows the P-values, significance, and Tukey analysis for dry and wet conditions of hempcrete with four different hemp sizes. The study showed no significant difference between the four hemp sizes regarding moist thermal conductivity and dry C_p. The means of most cases indicated a statistical difference between the hemp sizes in this study. Thus, there is a significant difference between the four hemp sizes since there is a difference in at least one factor.

Table 5.7: ANOVA and Tukey's analysis for thermal properties and strength of hempcrete experimental data with four hemp sizes (Dry and wet conditions)

Dependent Factor		Hemp size	P-value	Significance	Dependent Factor		Hemp size	P-value	Significance
k @ dry	S4-FR	S1-CA	0.002	Yes	k @ wet	S4-FR	S1-CA	0.862	No
		S2-CA	0.000	Yes			S2-CA	0.641	No
		S3-CA	0.000	Yes			S3-CA	0.182	No
	S1-CA	S2-CA	0.000	Yes		S1-CA	S2-CA	0.972	No
		S3-CA	0.053	Yes			S3-CA	0.480	No
	S3-CA	S2-CA	0.002	Yes		S3-CA	S2-CA	0.713	No
Cp @ dry	S4-FR	S1-CA	0.845	No	Cp @ wet	S4-FR	S1-CA	0.077	Yes
		S2-CA	0.994	No			S2-CA	0.000	Yes
		S3-CA	1.000	No			S3-CA	0.006	Yes
	S1-CA	S2-CA	0.720	No		S1-CA	S2-CA	0.010	Yes
		S3-CA	0.840	No			S3-CA	0.305	No
	S3-CA	S2-CA	0.995	No		S3-CA	S2-CA	0.128	No
α @ dry	S4-FR	S1-CA	0.037	Yes	α @ wet	S4-FR	S1-CA	0.052	Yes
		S2-CA	0.000	Yes			S2-CA	0.001	Yes
		S3-CA	0.000	Yes			S3-CA	0.003	Yes
	S1-CA	S2-CA	0.001	Yes		S1-CA	S2-CA	0.023	Yes
		S3-CA	0.001	Yes			S3-CA	0.198	No
	S3-CA	S2-CA	0.996	No		S3-CA	S2-CA	0.460	No
ρ @ dry	S4-FR	S1-CA	0.003	Yes	ρ @ wet	S4-FR	S1-CA	0.986	No
		S2-CA	0.000	Yes			S2-CA	0.757	No
		S3-CA	0.174	No			S3-CA	0.000	Yes
	S1-CA	S2-CA	0.000	Yes		S1-CA	S2-CA	0.909	No
		S3-CA	0.000	Yes			S3-CA	0.000	Yes
	S3-CA	S2-CA	0.000	Yes		S3-CA	S2-CA	0.000	Yes
Strength @ dry	S4-FR	S1-CA	0.000	Yes	Strength @ wet	S4-FR	S1-CA	0.000	Yes
		S2-CA	0.000	Yes			S2-CA	0.000	Yes
		S3-CA	0.000	No			S3-CA	0.000	Yes
	S1-CA	S2-CA	0.001	Yes		S1-CA	S2-CA	0.007	Yes
		S3-CA	0.336	No			S3-CA	0.022	Yes
	S3-CA	S2-CA	0.000	Yes		S3-CA	S2-CA	0.000	Yes

Figure 5.21 shows the mean values for thermal and strength properties obtained from SPSS for the experimental results of hempcrete with four hemp sizes. However, the difference might be indicated visually.

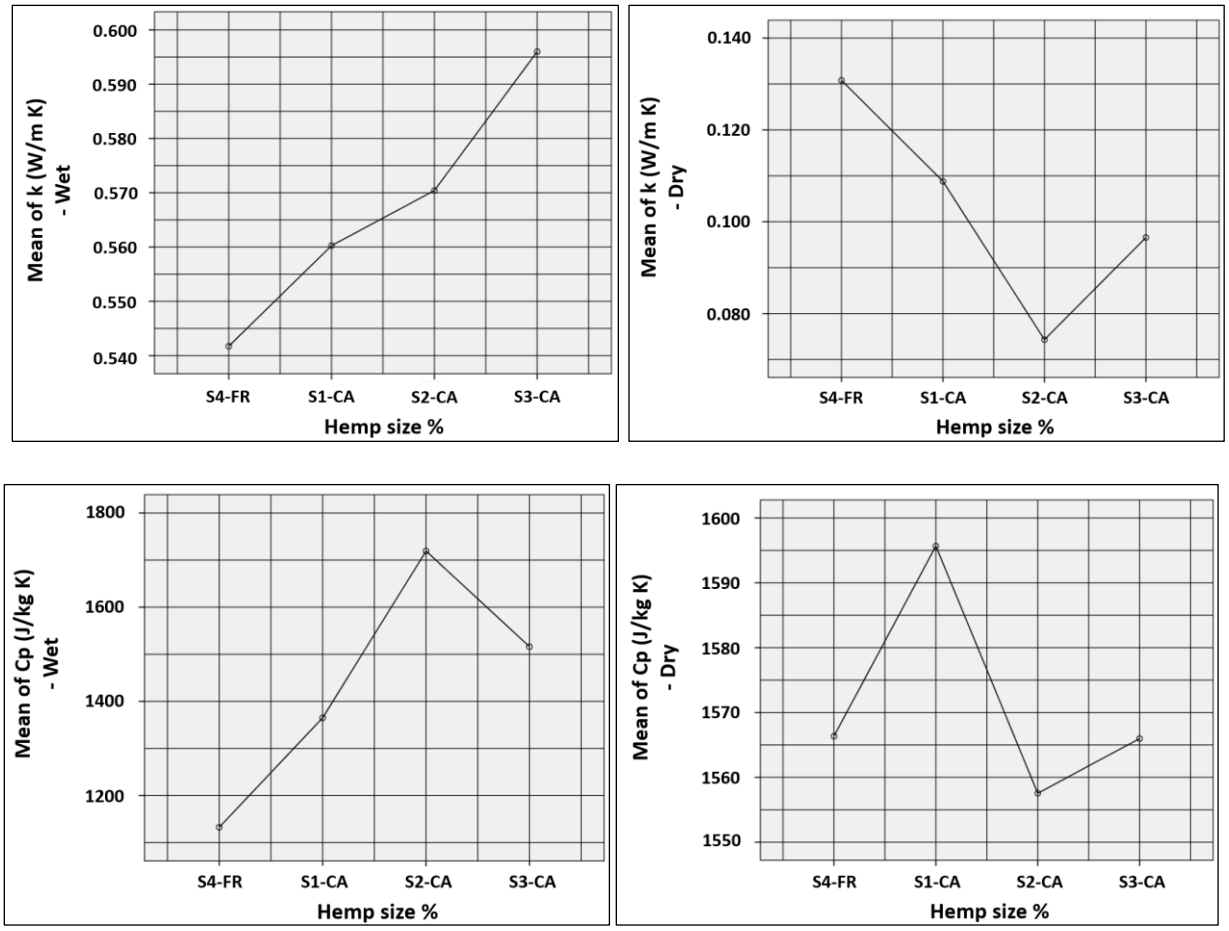

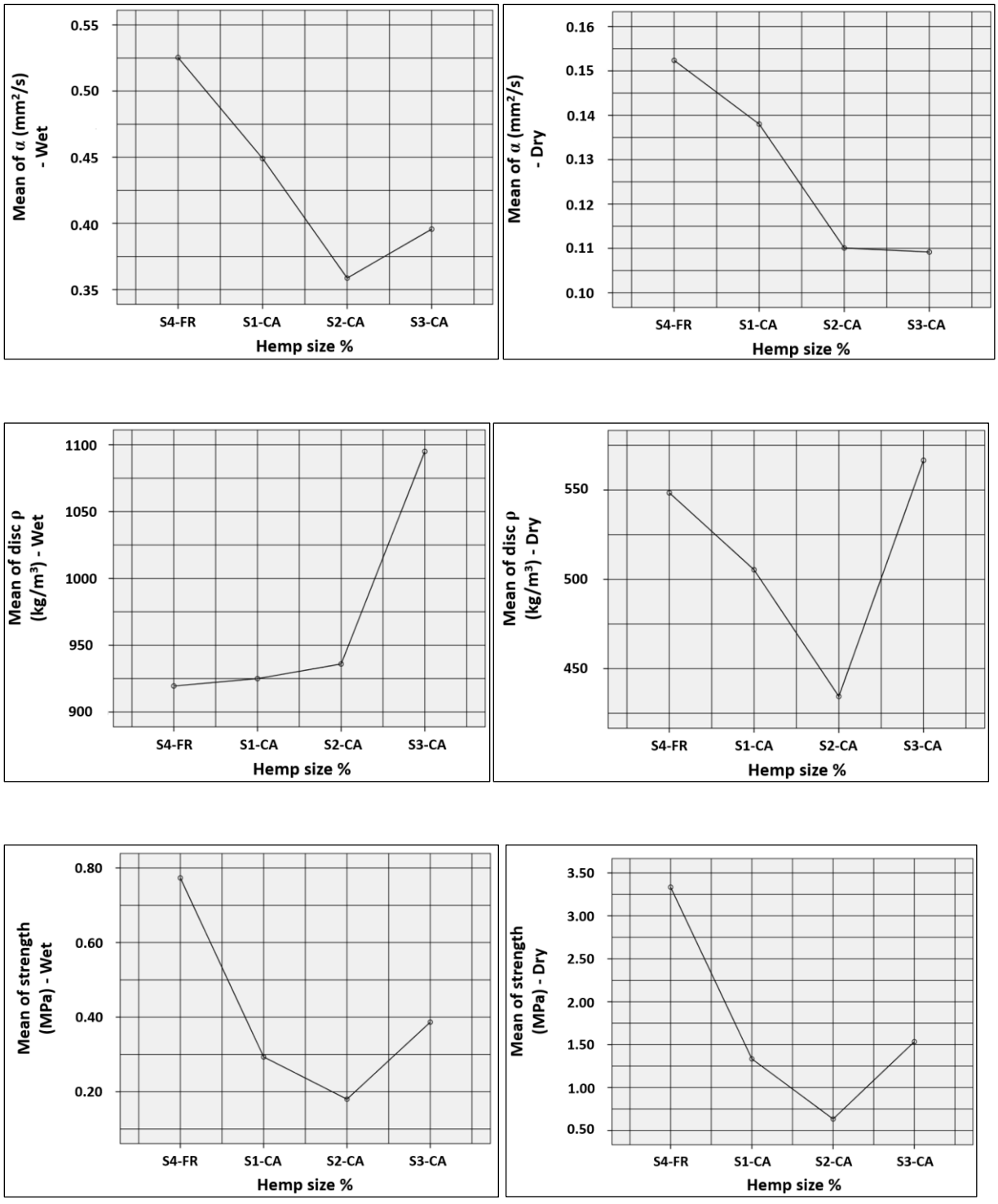

Figure 5.21: ANOVA and Tukey's analysis for oven dry and wet thermal properties and strength of hempcrete experimental data with four different hemp sizes

5.5.1.2 Linear regression analysis

Similarly, linear regression analysis was conducted using SPSS for the thermal properties of hempcrete samples with four hemp sizes to generate linear equations for predicting thermal diffusivity. Thermal diffusivity showed linear equations with the highest R^2 values (0.99-0.97) for dry and wet conditions, respectively, showing k, $C_{p,}$ and ρ as significant factors (Eq- 5.4 and Eq-5.5).

Table 5.8: Linear regression analysis for thermal properties of hempcrete experimental data (dry and wet conditions)

Dependent Variable	Independent Variable	P-value	Significance	R^2	Regression Equations	Eq No.
α @ dry (mm^2/s)	k (W/m K)	0.000	Yes	0.99	**α @dry**= 1.201 **k** – 0.000213 **ρ** – 0.000064 $\mathbf{C_p}$ + 0.214	**Eq-5.4**
	Cp (J/kg K)	0.011	Yes			
	ρ (kg/m^3)	0.000	Yes			
α @ wet (mm^2/s)	k (W/m K)	0.011	Yes	0.97	**α @wet**= 0.644 **k** – 0.000242 **ρ** – 0.000304 $\mathbf{C_p}$ + 0.738	**Eq-5.5**
	Cp (J/kg K)	0.000	Yes			
	ρ (kg/m^3)	0.010	Yes			

5.5.2 Effect of hemp content

In this task, five hemp contents were studied, including 20, 40, 50, 67, and 100% of hemp hurds by weight of binder. The hurds were mixed with one composed binder of cement and lime with equal percentages (50% C + 50% Li). As shown in Figure 5.22, increasing the content of hemp hurds increased the interlocking between the hurds and forming more visible pores starting at 50 to 100% of hurds (i.e., Blocking the pores and preventing filling the pores with binder). Thus, debonding, crack propagation, and hurds agglomeration are accompanied by the higher content of hurds. However, this task aims to balance binder/hemp ratio, strength, and thermal properties to achieve thermal insulation and acceptable strength of hemp concrete.

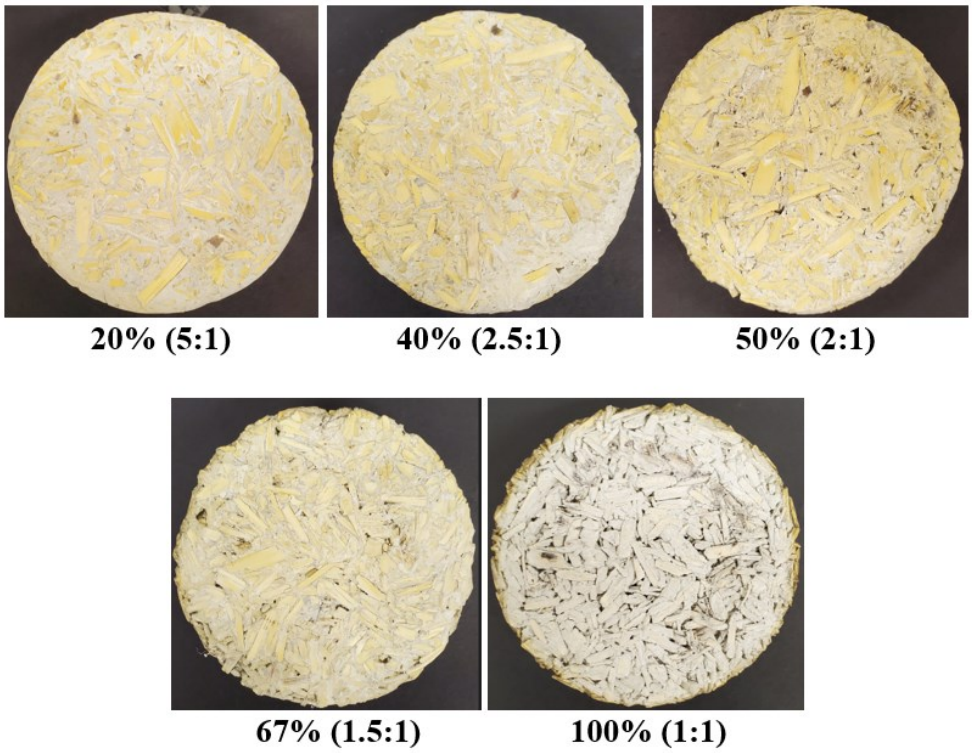

Figure 5.22: The smoothed surface of hempcrete samples with five hemp contents used in this study.

As shown in Figure 5.23, the density varied between 1208-638 kg/m^3 (difference <47%) and 704-258 kg/m^3 (contrast <63%) for wet and dry samples, respectively. Similar findings in literature could be found in references [5][14]. However, the density decreased with increasing hemp content due to the lower density of hemp (compared to binder) and increasing porosity. The moisture content increased with increasing hemp content (42-60%) due to the higher water absorption of hemp (Figure 5.23). Further, the porosity increased with increasing hemp content, reaching 37-71% because increasing hemp content leads to the interlocking of hemp particles forming higher pores (due to the flaky shape of hurds, as shown in Figure 5.22).

As shown in Figure 5.23, the compressive strength decreased with increasing the content of hemp hurds from 2.83-0.23 MPa for dry samples and from 1.51-0.23 MPa for wet samples. This reduction could be ascribed to lower binder and higher hemp content (i.e., higher hemp content means more surface area), leading to a loss of adhesion and decreased strength. The dry strength of hempcrete in this stage is significantly higher than that of wet samples, with a percentage of 37-

49%, ascribed to the sponge behavior of hemp hurds and crack development due to poor bonding (similar findings [52]). However, the binder-to-hemp ratio of 1:1 does not show a difference between wet and dry strengths, which the occurrence of quick debonding might explain due to the higher hemp content and lack of sufficient binder. The results obtained were comparable with the literature, as seen in references [16][15][17] for the 2:1 binder/ hemp ratio and [26][15] for the ratios of 3:1, 4:1. However, Walker et al. reported the same trend of strength reduction with increasing the hemp content due insufficient binder and weaker interface zone [53][26] (similar findings elsewhere [27]). The low content of hemp of 20% increased the strength significantly by about 49-53% relative to 40% of hemp hurds. However, the hemp composite became crumbling and showed a minimal strength for the binder to hemp ratio of 1:1 with a strength of 0.23 MPa. In summary, the strength decreases with increasing hemp content due to the lack of binder, which weakens the interface zone and the adhesion between hemp and binder matrix.

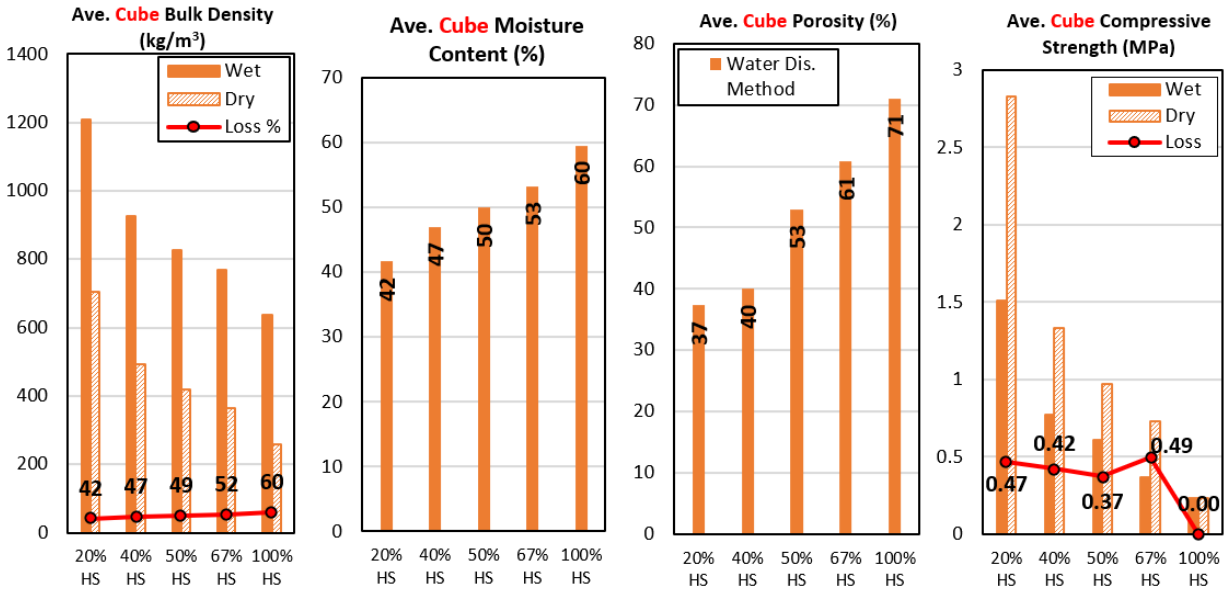

Figure 5.23: Physical and strength properties of hemp concrete cubes with five hemp contents at seven days

Similarly, for disc samples, the density decreased with increasing hemp content (20-100%) with values of 1084-593 kg/m^3 (difference of 45%) and 712-263 kg/m^3 (contrast of 63%) for wet and dry samples, respectively, as shown in Figure 5.24. With increasing the hemp content, the moisture

content increased from 36-56%, and porosity rose from 62-78%. However, samples with a binder/hemp ratio of 1:1 could not be prepared for the HE porosity test due to the fragile composite.

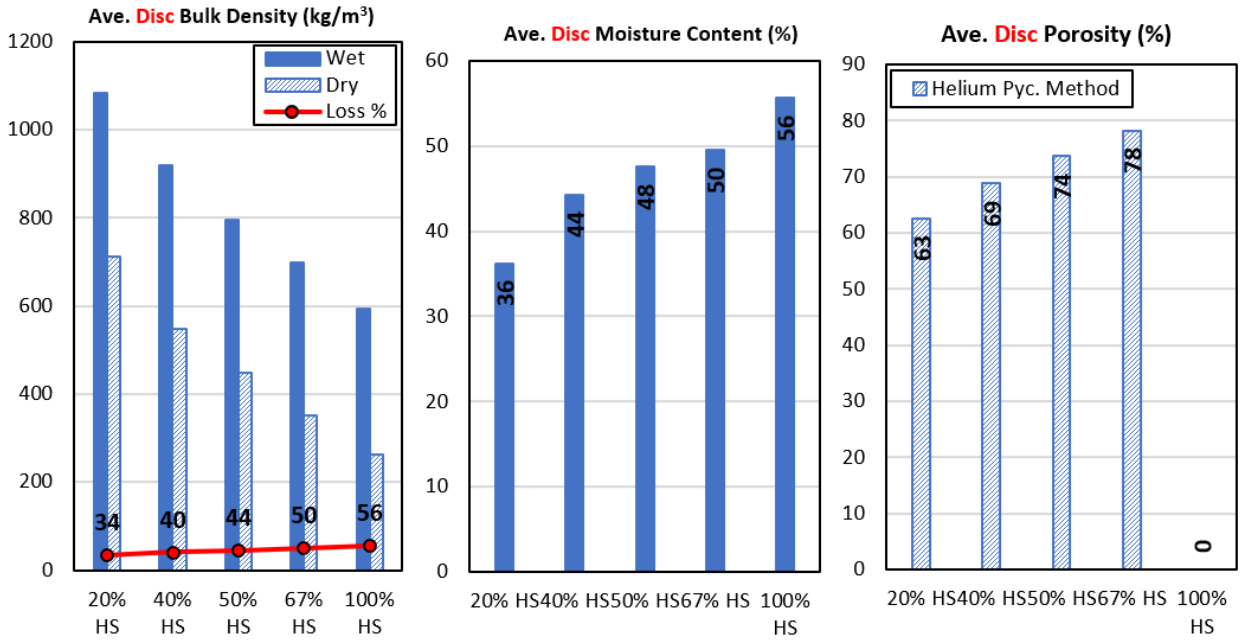

Figure 5.24: Physical and strength properties of hemp concrete discs with five hemp contents at seven days

As shown in Figure 5.25, the thermal conductivity varied between 0.669-0.349 W/m K (difference <48%) and 0.216-0.063 W/m K (difference < 71%) for wet and dry samples, respectively. The results showed that the conductivity significantly reduced with increasing hemp content. In the same trend, the conductivity of wet samples showed a substantially higher value than dry samples, with percentages of 68-82% due to the water effect. The highest conductivity values were observed with a hemp ratio of 5:1 (0.669-0.216 W/m K), while the lowest values were achieved by a hemp ratio of 1:1 (0.349-0.063 W/m K). Bruijn et al. found a similar trend for reducing conductivity (about 10%) with increasing binder/hemp ratio from 1:1.1 to 1:1.8 [5]. The reduction in thermal conductivity is ascribed to the higher content of hemp hurds and porosity (Similar findings elsewhere [25]). Further, binders have higher thermal conductivity relative to hemp; hence, increasing the content of a binder tends to increase the conductivity and strength (as similarly stated here [30]).

Similarly, the thermal diffusivity fell in the range of 0.527-0.380 mm^2/s (difference <28%) and 0.135-0.180 mm^2/s (difference <33%) for wet and dry samples, respectively, as shown in Figure 5.25. Similarly, the damp diffusivity values were significantly higher than those of dry samples, with 60-70% percentages due to high moisture. For wet samples, the diffusivity decreased by 16-27% for 40-50% of hemp hurds relative to 20% of hurds. However, the diffusivity showed similar values with 50, 67, and 100% hemp hurds in wet conditions. This behavior is ascribed to the change in conductivity and volumetric heat capacity ($\alpha = k/C_v$). As an example, the difference in k value and C_v is 19 and 5%, respectively, for 20 and 40% of hemp; hence, the diffusivity dropped roughly by 32% because the reduction in conductivity (19%) significantly higher than the reduction in C_v (4%). Therefore, the diffusivity mainly depends on each hemp content's conductivity behavior and volumetric heat capacity. Generally, diffusivity primarily relies on conductivity and heat capacity behavior simultaneously.

In the same trend, the volumetric heat capacity ranged between 1.354-0.936 MJ/m^3 K (difference 27%) and 1.200-0.419 MJ/m^3 K (difference 65%) for wet and dry samples, respectively, as shown in Figure 5.25. The C_v values were reduced with increasing hemp content for damp and dry conditions, which ascribed to a higher reduction of thermal conductivity with increasing hemp content than the change in thermal diffusivity ($C_v = k/\alpha$), as shown in Figure 5.25. Further, the decline in C_v values with increasing hemp content is ascribed to the mass reduction with increasing hemp content, as shown in Figure 5.24. However, the decrease in dry samples is significantly higher than wet ones due to the increment of porosity with increasing hemp content (C_v of air void < C_v of hemp, binder, and water). Therefore, compaction of hempcrete with a high range of hemp required sufficient force to compress the hemp hurds together and minimize the air voids to ensure higher diffusivity values.

The specific heat capacity differs between 1183-1579 J/kg K and 1596-1769 J/kg K for wet and dry samples. The dry values of C_p are considerably higher than wet ones due to the higher density of wet samples relative to dry ones ($C_p = C_v/\rho$). However, the C_p values increased with increasing hemp content for wet samples with a reduction in both C_v and density, which ascribed to a lower drop in C_v values relative to the decrease in density values with increasing hemp content. In

contrast, the dry C_p values decreased with increasing hemp content, similar to the trend of C_v values, which was attributed to the higher reduction in C_v values compared to the decrease in density values with increasing hemp content. In other words, the C_p values for dry samples decreased with increasing the content of hemp hurds because increasing hemp content tends to increase interaction between hemp particles and forming larger pores. Hence, the ability to store thermal energy by air is relatively lower than hemp (i.e., C_p values reduced with increasing hemp content) (Similar to the C_v trend). However, this behavior could be overcome by increasing compaction force to close the pores as much as possible, filling the spaces with hemp hurds, not air voids.

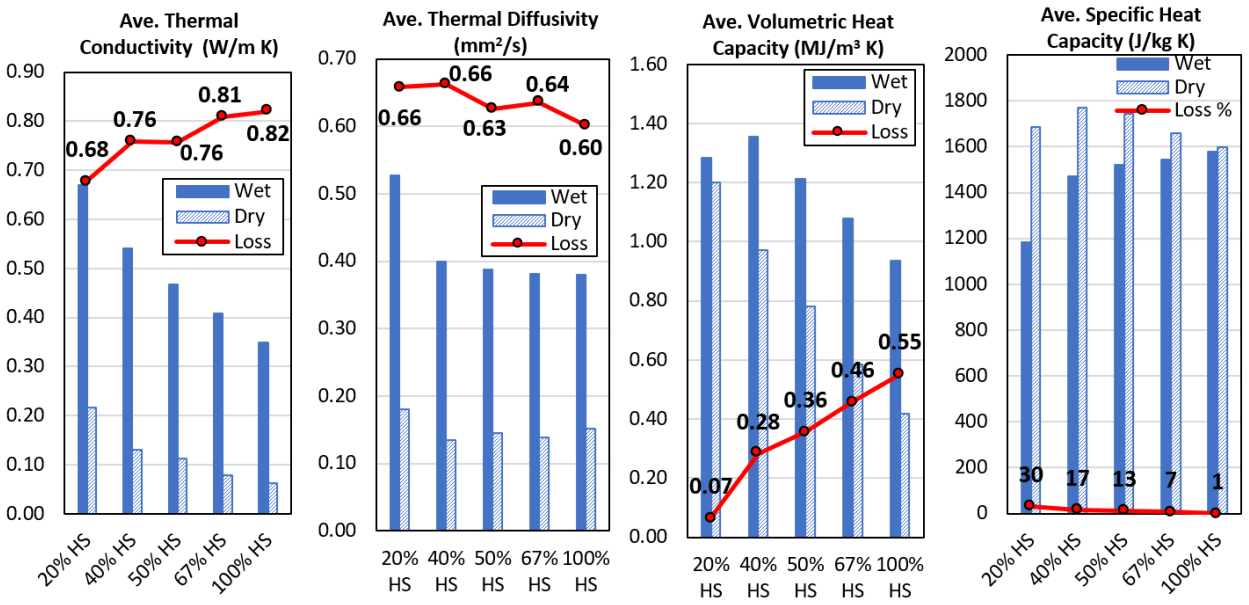

Figure 5.25: Thermal properties of hemp concrete with five hemp contents at seven days

5.5.2.1 Analysis of variance (ANOVA)

Similarly, an ANOVA test (one factor, which is hemp content) is used to check for a difference between five hemp contents by studying the means (i.e., compare the mean of each hemp content to the overall mean of all hemp contents). Tukey analysis was conducted for pairs of hemp contents for dry and wet conditions. The analysis showed no significant difference between the five hemp

contents regarding dry thermal conductivity and dry density, dry strength, and damp density, as shown in Figure 5.26. However, other cases showed significant and insignificant differences within each tested property, meaning that changing the hemp content generally showed a significant difference.

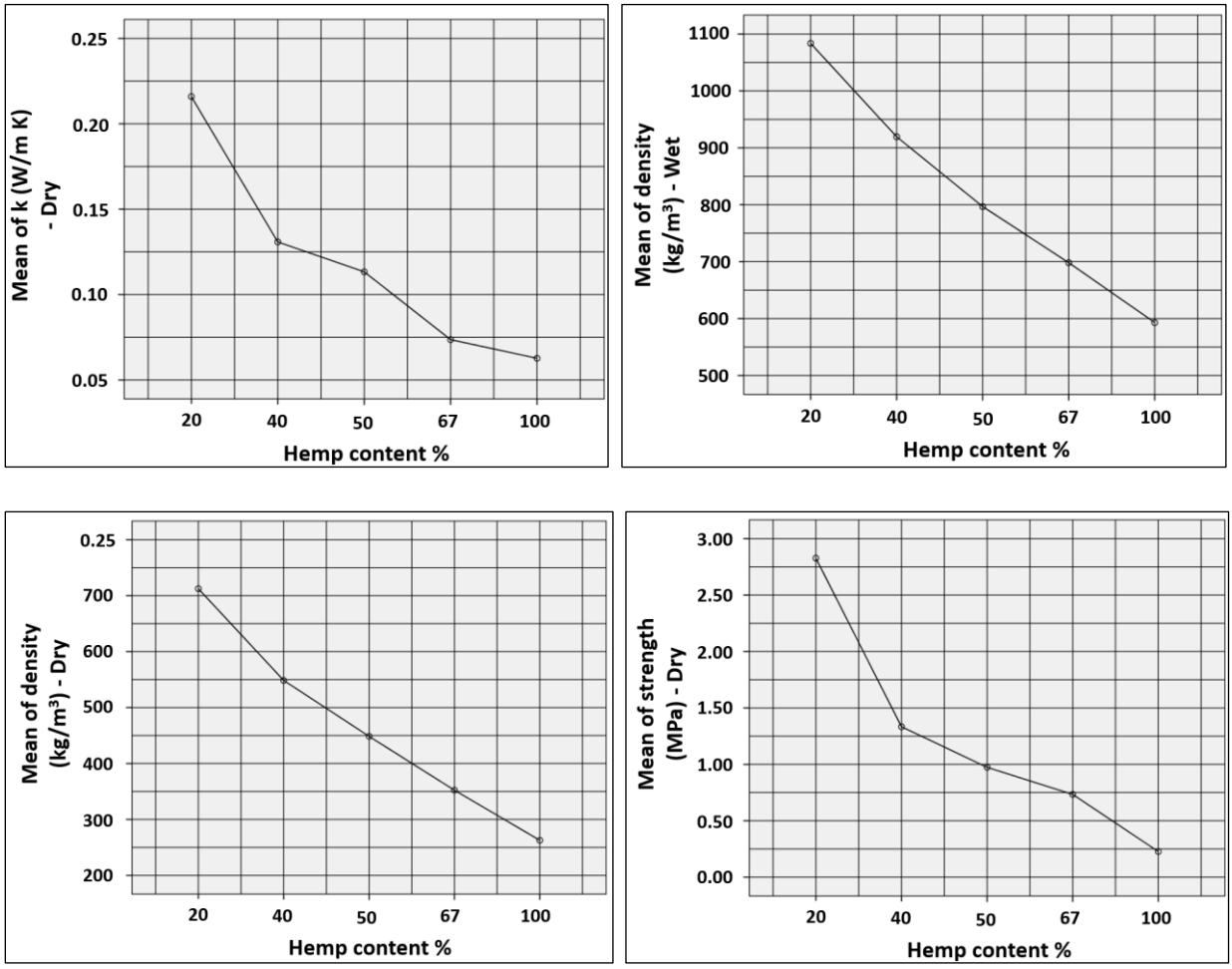

Figure 5.26: ANOVA and Tukey's results for properties showing no significant difference with five different hemp contents.

5.5.2.2 Linear regression analysis

Similarly, linear regression analysis was conducted using SPSS for the thermal properties of hempcrete samples with five hemp contents to generate linear equations for prediction. Thermal

diffusivity showed linear equations with the highest R^2 values (0.98) for dry and wet conditions, showing k, $C_{p,}$ and ρ as significant factors (Eq- 5.6 and Eq- 5.7). Further, compressive strength strongly correlated with hemp content as 0.80-0.81 R^2 values, as depicted in Eq- 5.8 and Eq- 5.9.

Table 5.9: Linear regression analysis for thermal properties of hempcrete experimental data (dry and wet conditions)

Dependent Variable	Independent Variable	P-value	Significance	R^2	Regression Equations	Eq No.
α @ dry (mm^2/s)	k (W/m K)	0.000	Yes	0.98	**α @dry**= 0.879 **k** – 0.000212 **ρ** – -0.00009 $\mathbf{C_p}$ + 0.295	**Eq-5.6**
	Cp (J/kg K)	0.000	Yes			
	ρ (kg/m^3)	0.000	Yes			
α @ wet (mm^2/s)	k (W/m K)	0.000	Yes	0.98	**α @wet**= 0.967 **k** – 0.001 **ρ** – 0.000302 $\mathbf{C_p}$ + 0.860	**Eq-5.7**
	Cp (J/kg K)	0.000	Yes			
	ρ (kg/m^3)	0.000	Yes			
Strength @ dry (MPa)	Hemp content %	0.000	Yes	0.81	**Strength @dry**= 2.849 – 0.029 Hemp content %	**Eq-5.8**
Strength @ wet (MPa)	Hemp content %	0.000	Yes	0.80	**Strength @wet**= 1.522 – 0.015 Hemp content %	**Eq-5.9**

5.6 Conclusions

This study examined two parameters, namely hemp sizes and hemp contents, to optimize the components of hempcrete. The hempcrete samples' thermal and strength properties were tested to achieve the desired optimization. Based on the results, the following conclusions were reached:

- Coarse hemp particles showed higher k values due to higher porosity, and fine particles showed higher conductivity than coarse ones. The well-graded hemp hurds form a denser composite and higher conductivity values, such as S4-FR.

- Fine hemp particles hinder heat diffusion due to the slippage at interface zones, while coarse particles might achieve similar outcomes due to the higher porosity. Well-graded particles (such as S4-FR) may have relatively higher diffusion values.
- Most hemp hurd sizes (about 80%) should be <3mm wide and <10mm long to achieve well-graded hemp hurds with lower porosity and higher strength. Very fine particles require higher binder content and increase the possibility of interfacial failure under loading, which diminishes the compatibility of the composite.
- Due to porosity, • Increasing hemp content reduces strength, density, thermal conductivity, and heat capacity. However, thermal diffusivity mainly depends on the behavior of conductivity and heat capacity simultaneously. Hence, the recommended hemp content depends on the targeted strength of the composite.
- Linear regression equations for thermal diffusivity were developed with high R^2 values for hempcrete with various hemp sizes and contents, showing k, $C_{p,}$ and ρ as significant factors.

6 CHAPTER 6: CHEMICAL TREATMENTS ON HEMP HURDS

Journal paper #5

Effect of Chemical Treatments on Hemp Hurds and Hempcrete Thermal and Strength Properties

Ahmed S. Al-Tamimi, Vivek Bindiganavilea, Yaman Boluk

Abstract

Hemp concrete is a new lightweight, non-structural concrete initiated in Europe in the early 1990s using hemp hurds as aggregate. Hemp composite shows superior thermal insulation properties with low conductivity and high heat capacity. However, machinal properties are poor due to bond and incompatibility problems between organic aggregates and inorganic binders. This study summarizes some literature treatments for woody aggregate for concrete and proposes some chemical treatments. Treatments aim to overcome the negative impacts of hemp on binder matrix, such as pectin and hydrophilicity. Hemp hurds were treated with three chemical solutions: NaOH, $Ca(OH)_2$, and Na_2SiO_3. Sodium hydroxide treatment partially removed the amorphous components, roughened the surface, and reduced particle size. Calcium hydroxide provides calcium ions that react with pectin and adhere to the hemp surface. Sodium silicate solution slightly roughens the surface, and silica bonded to enhance the interface zone. Finally, the treated hemp is used to produce hempcrete, measured for strength and thermal properties.

Keywords: Hempcrete, hemp hurds treatment, thermal properties, strength, hemp hydrophilicity

Abbreviations

C	Cement
HS	Hemp shives
k	Thermal conductivity (W/m K)
Li	Hydrated lime

S	Sand
ρ	Density (kg/m^3)

6.1 Introduction

The properties of hemp composite mainly depend on hemp hurd properties, binder matrix, and adhesion at the interface zone [1]. The hydrophilicity and chemical composition of hemp hurds are critical problems for the incompatibility between binder and hemp aggregates, which leads to low interface strength. Therefore, many research projects were devoted to enhancing the compatibility between bio-aggregates (filler) and binder matrix, thus improving the interface zone strength and adhesion by chemical and physical treatment [1][2][3]. Hemp hurds reported to retarding and disturbing the hydration of cement due to sugar, pectin, and high water absorption [4][5][6][7][8][9]. Therefore, there is a need to explore an economic and ecological method for hemp hurd treatment to match the requirements of building material applications. The following section summarizes the chemical composition of hemp hurds and the negative impacts on binder performance to navigate individual problems and think of proper solutions for overcoming them.

6.1.1 Hemp hurds composition

The hollow stem of the cannabis plant is mainly composed of fibers and hurds. The hurds are the woody parts, which include cambium and xylem layers [10], as shown in Figure 6.1.

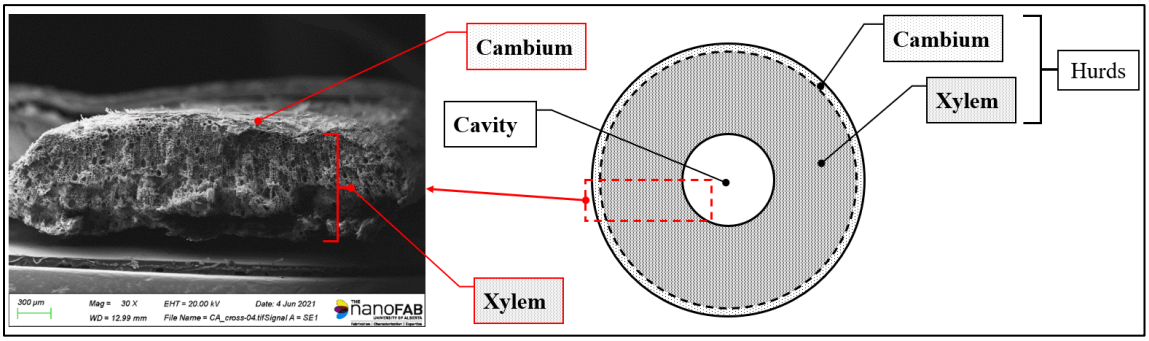

Figure 6.1: (a) SEM for hemp cross-section; (b) Sketch showing components of hemp cross-section.

The hemp hurds consist mainly of 40–48% cellulose, 18–24% hemicellulose, and 21–24% lignin, depending on their stage of growth, plant maturity, and plant variety [11][6][12]. Further, pectin (with some impurities such as wax and oil) exists on the surfaces with a small content of about 4% [13][12].

Cellulose has crystalline and amorphous constituents, while hemicellulose and lignin are completely amorphous structures [8][11]. The hydroxyl groups are strongly linked and inaccessible in the crystalline zone, while the hydroxyl groups are loosely connected and free to react in the amorphous area [8][14]. Pectin is a partially water-soluble constituent of hemp, which exists on the surface of hemp hurds with a small content of 4-6% [13][12][4], which delays the hydration and carbonation process, hence retarding the hardening of hemp concrete and reducing the strength. This is ascribed to the presence of pectin in hemp, which blocks calcium ions and forms a 3-dimensional gel network (insoluble salt residue in the solution), hence shortening the supply of ions for hydration and lowering the production of CSH gel (i.e., strength reduction) [9][15][5].

6.1.2 Effect of hemp on binder

Hemp hurds are bio-lightweight aggregates with superior thermal properties (low k, high Cp). However, using such aggregates with a binder to form hempcrete showed severe problems, affecting the bond, strength, and compatibility between hemp hurds and binder matrix, as summarized in Figure 6.2.

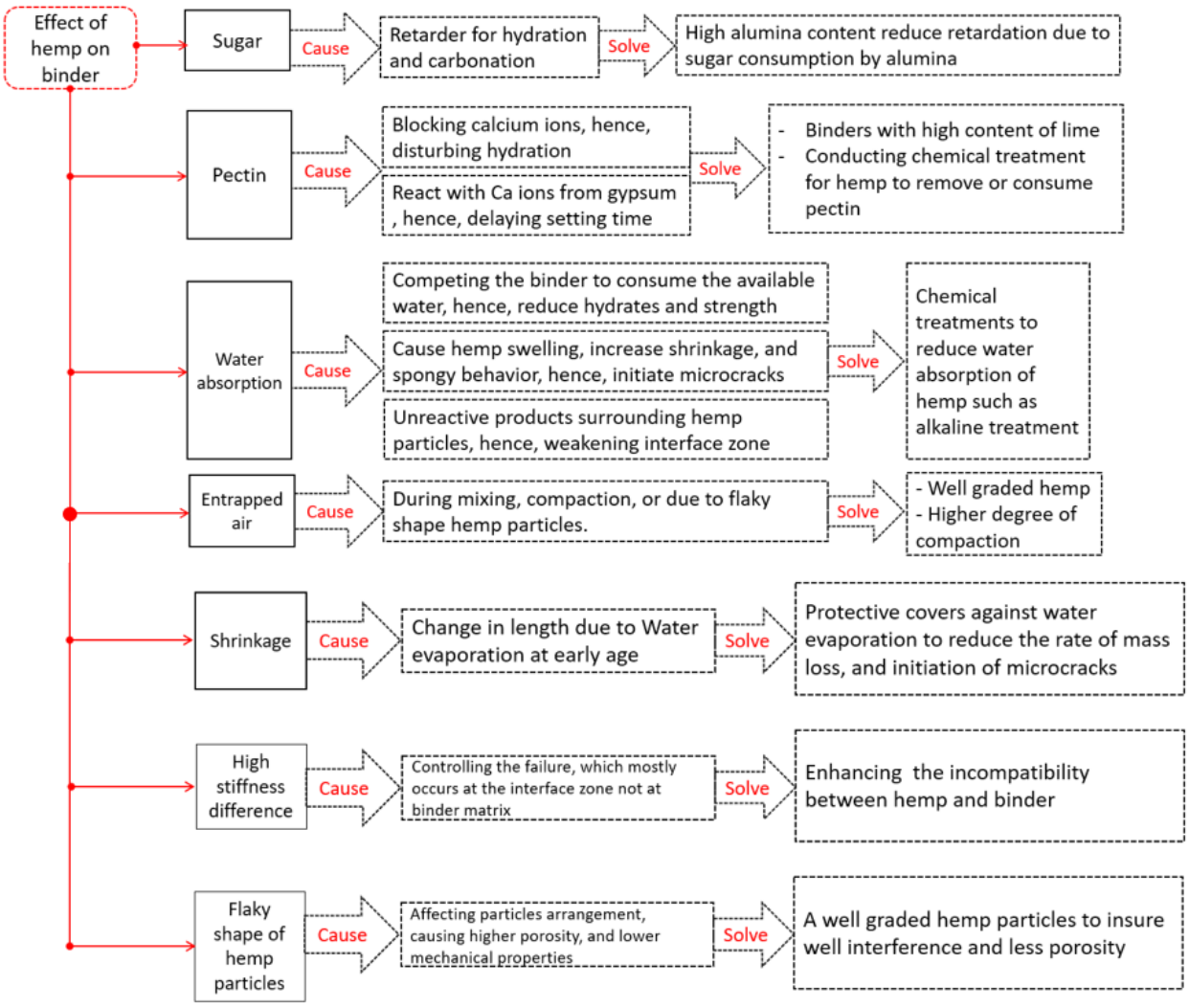

Figure 6.2: Effect of hemp hurds on binder matrix

Therefore, many research projects were initiated to overcome the negative impacts of hemp hurds in binder matrix, including physical and chemical treatments for hemp particles to enhance compatibility and mechanical properties [1][2][4][9][14][16].

6.1.3 Literature on hemp hurds treatment

The treatment of woody particles for application in concrete and construction materials is widely studied. Many treatments are found in the literature for hemp hurds, fibers, wood shives, and sawdust, including alkaline, acetylation, and coupling agents. The following section summarizes details of only alkaline treatments for hemp hurds and fibers, then the effect of such treated hemp on the binder matrix.

Alkaline treatment or mercerization (alkaline treatment for natural fibers) is a common chemical treatment for biomaterials, which uses an aqueous solution with different concentrations, times, and temperatures. Then, neutralized with water or acid and dried. As shown in Table 6.1, sodium and calcium hydroxides were mainly used as alkaline treatments for hemp fibers and hurds, resulting in chemical composition and morphology changes. NaOH treatment removes hydrogen bonding in the network structure, causing roughening surface and reducing hydrophobicity, as shown below [6][8][11][17][18][19]:

$$(\text{Biomaterial} - \text{OH}) + \text{NaOH} \longrightarrow (\text{Biomaterial} - \text{O}^- - \text{Na}^+) + \text{H}_2\text{O}$$

- Removes waxes, oils, and gummy impurities from the surface [11][14].
- Removes partially the amorphous materials, such as hemicelluloses, pectin, and lignin, from cellulose surfaces [6][8].
- Increases surface roughness and reduces the size, resulting in better mechanical interlocking [18].

Excess delignification (lignin removal) of natural fiber occurs at higher alkali concentrations, resulting in weaker or damaged fiber. The tensile strength of the composite decreased drastically after a specific optimum NaOH concentration [18]. The optimum percentage of NaOH is 4-6% [18], as further noticed in Table 6.1.

Hemp hurds delay the hydration and carbonation process, retarding the hardening of hemp concrete and reducing its strength. This is ascribed to the presence of pectin, which blocks calcium

ions and forms a 3-dimensional gel network (insoluble salt residue in the solution), hence shortening the supply of ions for hydration and carbonation [9][20]. In many studies, the usage of $Ca(OH)_2$ is a supplementary source for the continuity of hydration throughout providing Ca^{+2} ions into the system to be used for CSH production because pectin consumes and reacts with Ca^{+2} ions, in addition to the following [6][21][22][15]:

- Saturate hemp hurds with Ca^{+2} ions and enhance the interface zone.
- Removes slightly amorphous hemicelluloses due to alkalinity.
- Slightly remove amorphous constituents.

Table 6.1: Effect of alkaline treatment on hemp hurds/fibers

Hemp type	Treated with	Time (hr.)	Ref.	Treatment effect
Hurds	1.6 M (**NaOH**)	48	[6] [21] [22]	NaOH reacts with hydroxyl groups present in cellulose, forming water molecules: Fiber-OH + NaOH → Fiber-O-Na + H_2O The strongest defibrillation of fibrils. Partially remove amorphous materials, such as hemicelluloses, pectin, and lignin. The alkaline process cannot remove lignin. Waxes and oils disappear.
	1 wt. % (**NaOH**)	72	[11]	Reduces the diameter. Higher concentration leads to higher removal of amorphous. Enhance the surface exposure of cellulose to augment the number of potential reaction sites and interfering hydrogen boding.
	6 wt. % (**NaOH**)	48	[11]	
Fiber	6 wt.% **(NaOH)**	48	[23]	The surface of the fiber became rough.
	5 wt.% **(NaOH)**	4 Stirring	[24]	Partial removal of amorphous materials, such as hemicelluloses, pectin, and lignin.
	4-10 wt.% Na(OH) + Acetic acid	3 + 3 Soaking	[8]	The treatments had no impact on the cellulose structure of the fiber. Removing free water was more straightforward than removing bound water (connected to the cellulose). The removal of bound water necessitates higher temperatures (around 100°C).
Hurds	(Ca^{+2}= 0.02 M) **$Ca(OH)_2$**	48	[6] [21] [22]	Removes hemicellulose. Water absorption is significantly reduced due to losing hydrogen bonding.
			[15]	Saturate hurds with calcium ions. Pectin reacts with the calcium ions, forming insoluble salts.

As summarized in Table 6.2, hemp hurds were treated with Alkaline solutions, including NaOH and $Ca(OH)_2$. The alkaline treatment is supposed to increase the strength as stated by [25], which, against the findings found by Stevulova et al., might ascribed to the degradation of hemp in a binder alkaline medium [1].

The treatment using sodium silicate solution for sawdust increased the formation of ettringites due to the diffusion of sodium into cement paste, which increases chloride resistance and compressive strength [26]. The silica coating improves the chemical compatibility between hemp and binders, which are thermal shields and wash resistance [27][28]. The FTIR analysis demonstrated the formation of C–O–Si– covalent bonds between the hemp (cellulosic substrate) and silica coating [27].

Table 6.2: Effect of alkaline hemp hurd treatments on hempcrete thermal and strength properties.

Composite	w/b	b/h	Hemp treated with	Time (hr)	ρ (g/cm^3)	k (W/m K)	Water Abs. (%)	Comp. Strength (MPa)	Treatment effect	Ref
MgO cement + 40% HS	-	-	Reference	-	1.10	0.11	23	5.0	The treatment processes reduced the hydrophilicity and water absorption of hemp hurds. Partial removal of amorphous components surface impurities. Roughen and clean the surface only from impurities like waxes and oil.	[1]
			NaOH	48	1.20	0.07	11	2.0		
			$Ca(OH)_2$	48	1.0	0.08	9	2.0		
C + S + HS	0.48	6.25	Reference	-	1.41	-	16	3	Removes a particular portion of lignin. It leached out a portion of K_2O, which accelerated the setting. It hinders the sugar release from organic aggregates and decreases hygroscopicity and water absorption. Increased the hydration and formation of ettringite (i.e., increased compressive strengths).	[4]
			$Al_2(SO_4)_3$ + $Ca(OH)_2$	(18+1.5) min	1.42	-	15.5	14		
C + HS	0.32	4.0	Reference		0.819	0.103	-	1.67	Pectin reacts with Ca^{+2} in cement (i.e., more Ca^{+2} available for hydration from treatment).	[5]
			$Al_2(SO_4)_3$ + $Ca(OH)_2$	(18+1.0) min	0.993	0.137	-	5.55		

w/b = water/binder, b/h = binder/hemp, k: thermal conductivity, HS: hemp shives, C: Cement, S: Sand

6.2 Proposed Hemp Treatments

The properties of hemp concrete mainly depend on the chemical composition, morphology, and particle size of hemp, binder properties, and the adhesion between hemp and matrix [1]. As shown in Figure 6.1, the main problems with using hemp hurds with binder are their heterogeneity and hydrophilicity, resulting in high water absorption and incompatibility with the matrix [1]. The incompatibility is due to using bio-materials (hemp particles) with inorganic binders because of their morphology and chemical composition, which leads to loss of the bond at the interface zone and reduces the strength [1]. As presented earlier, many studies focused on physical and chemical treatments for hemp to improve the adhesion with the matrix and reduce hydrophilicity by removing impurities and amorphous components (pectin, lignin, hemicelluloses), roughening the surface separating the bundles of fibers. Therefore, three hemp chemical treatments were selected in this study to improve the morphology, hygroscopicity, and compatibility of hemp hurds with the binder matrix, including NaOH, $Ca(OH)_2$, and Na_2SiO_3, as shown in Figure 6.3. Therefore, each treatment will overcome a specific issue with hemp hurds, so comparing the three treatments will indicate the seriousness of the individual negative impacts of hemp, such as the pectin effect and hydrophilicity.

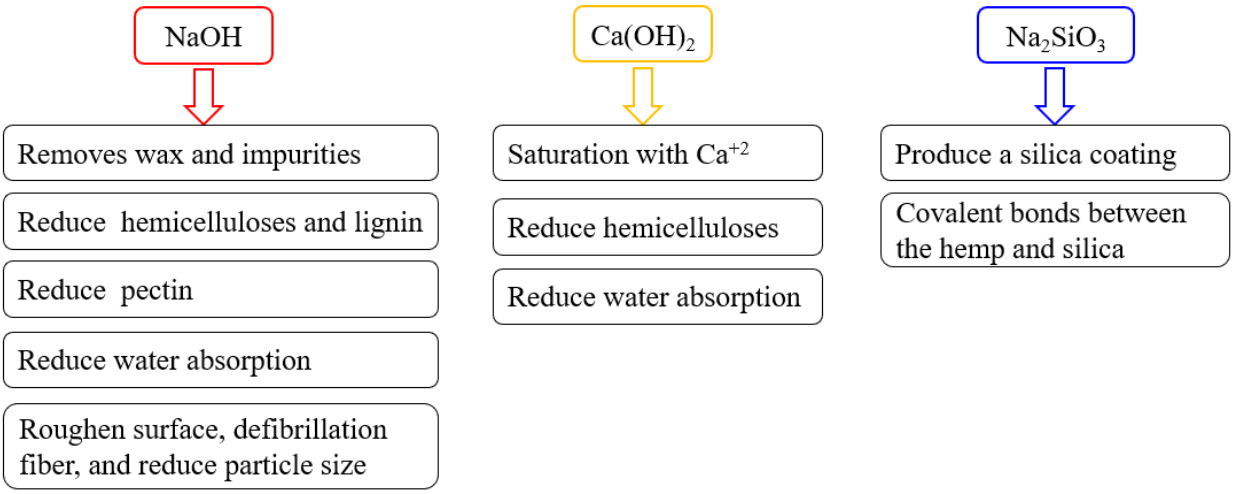

Figure 6.3: Flowchart showing this study's chemical treatments for hemp hurds.

6.3 Materials and Hempcrete Preparation

6.3.1 Materials

Hempcrete was prepared with three main components: binder (50% C + 50% Li), hemp hurds (S4-FR), and tap water. Binder composition was selected from the previous stage of this study with GU cement and hydrated lime type N (CaO = 99.5%). Hemp hurds (S4-FR) were supplied by LCDA in France according to the technical standards of French hemp. The bulk density, moisture content, and water absorption after 24 hours of hemp hurds are 164 kg/m^3, 9 %, and 350%, respectively. For treatments, NaOH pellets and sodium silicate solution (Na_2SiO_3) were supplied by BASAF with a specific gravity of 2.13 and 1.40, respectively. The PH value of sodium silicate solution is 11.2, and the molar ratio of water glass is >3.2 with 40% sodium silicate and 60% water.

6.3.2 Treatment procedures

Three treatments were conducted with sodium hydroxide, calcium hydroxide, and sodium metasilicate. Figure 6.4 shows the procedures followed for the treatment process. In the first step, solutions were prepared with three different concentrations; then, hemp was soaked into a solution for 48 hours. Next, the hemp was raised and dried in the oven for 48hrs at 60ºC. Finally, the treated hemp was stored in sealed bags to avoid gaining atmospheric moisture. The concentration of each solution is randomly chosen based on literature solution concentration to show any potential from each treatment, as depicted in Table 6.1. Then, the solution concentration optimization process might be holding on with the high potential treatment. SEM and EDX analysis for treated hemp will show the treatment modification of hemp surface along with the compressive strength of hempcrete samples with treated hemp.

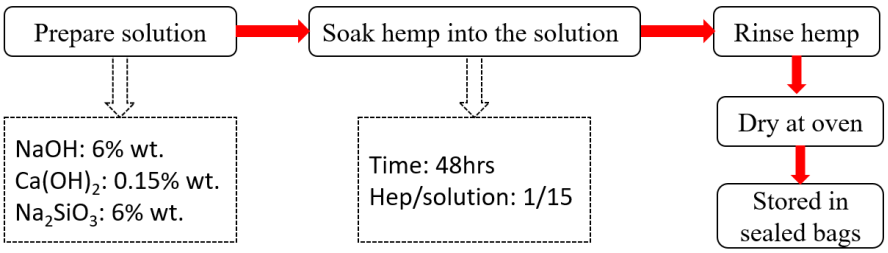

Figure 6.4: Hemp treatment procedures

6.3.2.1 Sodium hydroxide (caustic soda) – NaOH

In this study, a solution of NaOH was prepared with 6% wt. (1.50 M) of NaOH pallets. The PH of the prepared solution is 12.51, and the temperature is 30.33°C. The hemp hurds were soaked into the solution for 48 hours (hemp/solution 1:15, as similarly found [24]), then washed till the PH of rinse water was almost 7.0. The wet hurds were dried inside the oven for 48hrs at 60°C. The untreated hemp hurd weight is 400gm, while the weight reduces to 283gm after NaOH treatment with a weight reduction of about 30%. The dried hurds were stored in a sealed plastic bag to avoid atmospheric moisture contamination to be used in the hemp mixture in the next stage.

6.3.2.2 Calcium hydroxide (lime) – $Ca(OH)_2$

In this study, a $Ca(OH)_2$ solution was prepared with 0.15% by wt. (0.02 M) of lime powder. The PH of the prepared solution is 12.64, and the temperature is 17.24°C because the distilled water cooled down to 10°C to increase the solubility of calcium hydroxide. The hemp hurds were soaked into the solution for 48 hrs. (hemp/solution 1:15, as similarly found [24]), and then the hurds were washed and dried again. The weight difference between untreated and oven-dried treated hemp samples is about 11% due to losing the impurities, small particles, and moisture content.

6.3.2.3 Sodium metasilicate (water glass) – Na_2SiO_3

Water glass treatment is an inexpensive and eco-friendly chemical treatment that allows the production of a silica coating around the bio-materials [27][28]. Therefore, in this study, the covalent bond aimed to act as a bridge between hemp and the binder matrix rich in silica bonds

(i.e., improving the compatibility between organic and inorganic components of hemp concrete). The chemical equations (Eq- 6.1 and Eq- 6.2) show the process of the silica covalent formation starting with the dissolution of water glass into water, followed by the condensation process.

$$Na_2SiO_3 + H_2O \longrightarrow Si(OH)_4 + NaOH$$ **Eq-6.1**

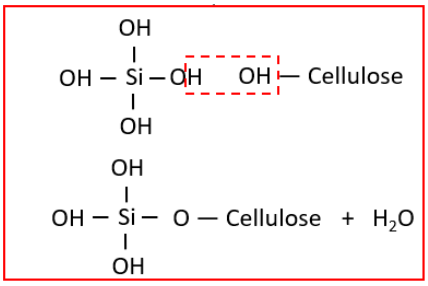

Eq-6.2

This study prepared the water glass solution with 6% wt. (0.71 M) of Na_2SiO_3 solution. The PH and temperature of the designed solutions are 11.18 and 21.8°C, respectively. Similarly, the hemp hurds were soaked in solution for 48 hrs. (hemp/solution= 1:15, as again found [24]), then rinsed and dried. The reduction of hemp weight due to water glass treatment is about 6%.

6.3.3 Preparing hempcrete with treated hemp hurds

In this task, three mixes were prepared with the treated hemp shives (S4-FR) and cement-lime-based binder to evaluate the effect of treatment on thermal and strength properties, as shown in Table 6.3. Similarly, the water absorption was assumed to be 150%, and then water was adjusted until reaching a homogeneous mixture.

Table 6.3: Mix proportions of hemp concrete with treated and untreated hemp.

Binder Type	Binder composition (% by wt.)	Hemp type	w/b	Hemp abs. (%)	w/b (Including abs.)	b/h (By wt.)
Cement-Lime based binders	50% C+ 50% Li+ HS-**Untreated**	S4-FR	0.625	200	1.43	2.50
	50% C+ 50% Li+ HS-treated with **NaOH**			220	1.51	
	50% C+ 50% Li+ HS-treated with **$Ca(OH)_2$**			200	1.43	
	50% C+ 50% Li+ HS-treated with **Na_2SiO_3**			200	1.43	

w/b: water/binder, w/h: water/hemp

The following procedures were followed during the mixing process for all hemp concrete mixtures produced in this work, which are similarly followed by Gourlay and Taoukil [29][16]:

- Mixing hemp hurds for 1 min to separate hemp particles agglomerates.
- Add 1/3 of the total water amount and mix for 2 min to wet the hemp.
- Addition of binder, and mix for 2 min.
- Adjust the water and mix for 2 min until it becomes homogeneous.

The components were mixed in a rotating pan mixer (EIRICH RV02E) with 8-10 Liter capacity for 7 min/mix. Six 50mm cubes were cast for strength and density for each batch, and six 75mm dia. discs for thermal properties, as shown in Figure 6.5. Samples were cured in a humid room for seven days. Samples were tested in wet condition, then dried in an oven for 24 hours at 60°C to be tested in dry condition.

Figure 6.5: Hempcrete samples after demolding

6.4 Results and Discussions

6.4.1 Properties of treated hemp

Hemp hurds were treated with three different chemical treatments to explore the effect on enhancing the properties of hempcrete. The modifications were examined for the treated hemp hurds using SEM and EDX. Then, the treated hemp hurds were used to produce hempcrete samples, which tested for strength and thermal properties.

6.4.1.1 Hemp size and water absorption

Figure 6.6 shows the particle size of untreated and treated hemp hurds to demonstrate the visual surface and size changes with the treatments. The treated hemp hurds with NaOH look bleached, defibrillated (partial separation of fibers), corroded (degraded), became thinner, and the companied hemp fibers disappeared (similar findings [11][6]). However, treated hemp with lime and water glass does not show a significant change in particle size. Most fibers might be lost during the rinse process until they reach neutral.


1.30 cm
Untreated hemp hurds
1 cm
Treated hemp hurds with NaOH
1.20 cm
Treated hemp hurds with Ca(OH)2

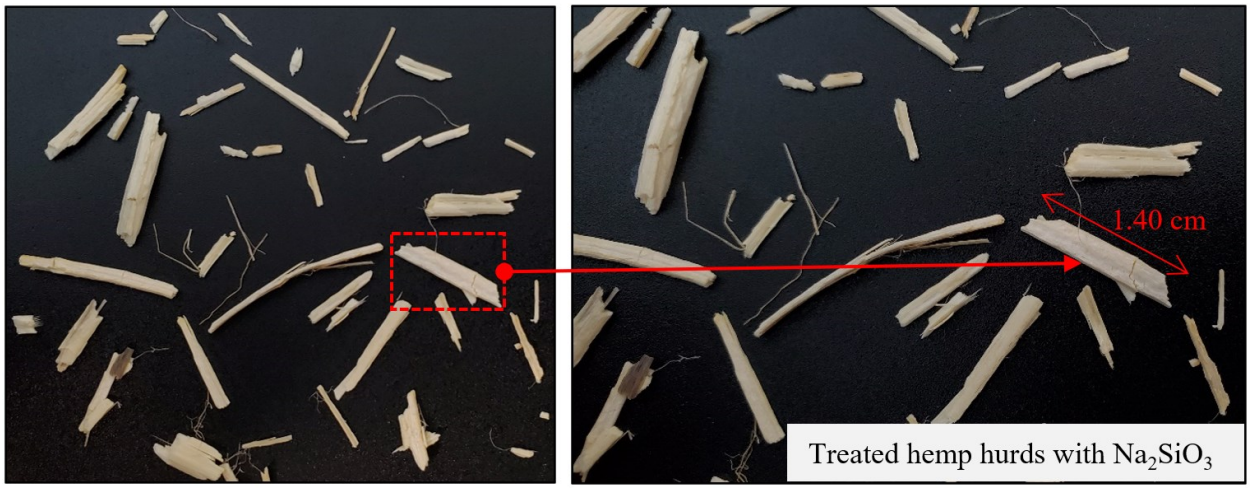

Figure 6.6: Zoomed images for visual evaluation of treated hemp hurds.

Most of the water absorption of untreated and treated hemp hurds occurred at the first hour, then increased slightly towards the second measuring point at 24 hours. As shown in Figure 6.7, the treatment with sodium hydroxide increased the amount of water absorption by 40% and 20% for one and 24 hours, respectively, compared to untreated hemp hurds. This may be ascribed to the thinner hemp particles treated with NaOH (i.e., more surface area) requiring more water. Further, water absorbed in cellulose increases slightly due to the linked water formed on the hemp surface [14][8]. However, water absorption of treated hemp with $Ca(OH)_2$ and Na_2SiO_3 was slightly affected compared to untreated hurds, which may be ascribed to the slight effect of treatments on removing amorphous constituents of hemp.

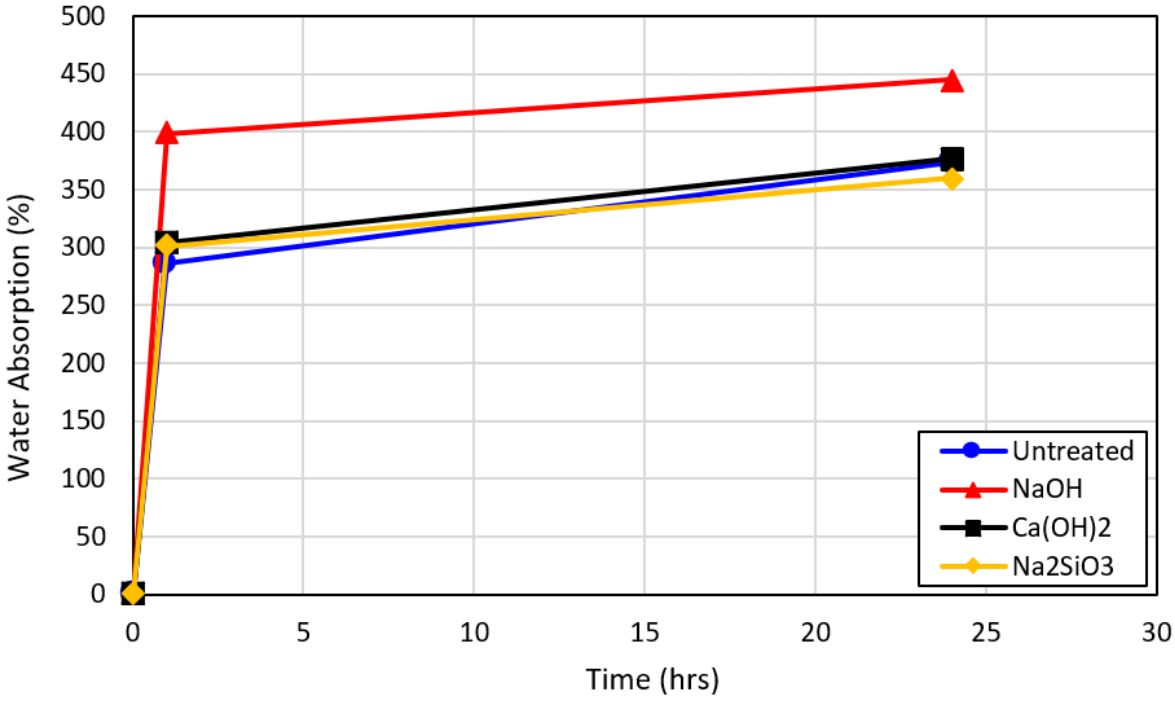

Figure 6.7: Water absorption of treated hemp after soaking for 24hrs.

6.4.1.2 SEM and EDX

Scanning Electron Microscope (SEM) images were taken using Zeiss Sigma FESEM w/ EDX & EBSD with an in-lens secondary electron (SE) detector and a backscatter (BSD) detector. A 20-nanometer gold layer was applied to the hurds to enhance conductivity, prevent charging, and achieve more distinct images. The images were captured using a leisurely scanning rate, spanning diverse magnifications from 300 to 2500, and with an acceleration voltage set at 20kV. The SEM images (micrographs) were utilized to examine the surface morphology (texture) of the hemp hurds and assess the influence of the treatments [23][24][4].

As shown in Figure 6.8, the surface of untreated hemp hurds is covered with pectin, lignin, and impurities such as wax and oil (similar findings [11][23]). The images of treated hemp hurds with NaOH show the removal of surface impurities, lignin, pectin, and hemicellulose. Further, the micro-images show fibrillation of hemp hurds due to revealing fibrils, which makes the rough

surface of hemp hurds after alkaline treatment [6][11][24]. Therefore, modifying hemp hurd morphology may enhance the bond with binders due to the availability of voids and more surface area. In summary, NaOH treatment cleans the hemp hurd surface, itches hemicellulose, lignin, and pectin, and roughens the surface.

The SEM images of the treated hemp hurds with $Ca(OH)_2$ clearly show a bunch of agglomerated calcium crystals spread over the surface, proofing the reaction with pectin and adhering to the surface, as shown in Figure 6.8. However, the EDX analysis shows a higher percentage of calcium on hemp surface (about 2.42%), relatively higher than reference and other treatments. Therefore, such treatment leads to the saturation of hemp hurds with calcium ions, which might be available for hydration and carbonation with a binder matrix [6]. Further, the surface of treated hurds shows partial removal of impurities, hemicellulose, and lignin (relatively lower to NaOH treatment), which is ascribed to the high alkalinity of solution (about 12.64) and a reduction of about 11% by wt. after treatment [6]. As a summary, the treatment of hemp hurds with calcium hydroxide solution partially cleaned surface, slightly itched amorphous components (hemicellulose and lignin), saturated hemp hurds with calcium ions, the reaction of Ca^{+2} with pectin, and adherend calcium hydroxide crystals on hemp surface.

The treatment of hemp hurds with sodium silicate slightly bleached the surface and partially itched the amorphous components due to high solution alkalinity (about 11.18) but relatively lower to NaOH and higher than $Ca(OH)_2$, as shown in Figure 6.8. Silica coating could be observed at higher magnification (about 1200-2500x), which adhered to hemp hurds surface, forming a silica bond (similar findings [27][28]). However, a higher content of silica was observed by EDX analysis on hemp surface treated with sodium silicate solution, which may act as a bridge between hemp and binder matrix.

Looking into EDX analysis for all treated hemp hurds, the results do not show a significant difference in composition to untreated hemp, which validated the minimal effect on structure modification with alkaline and sodium silicate treatment.

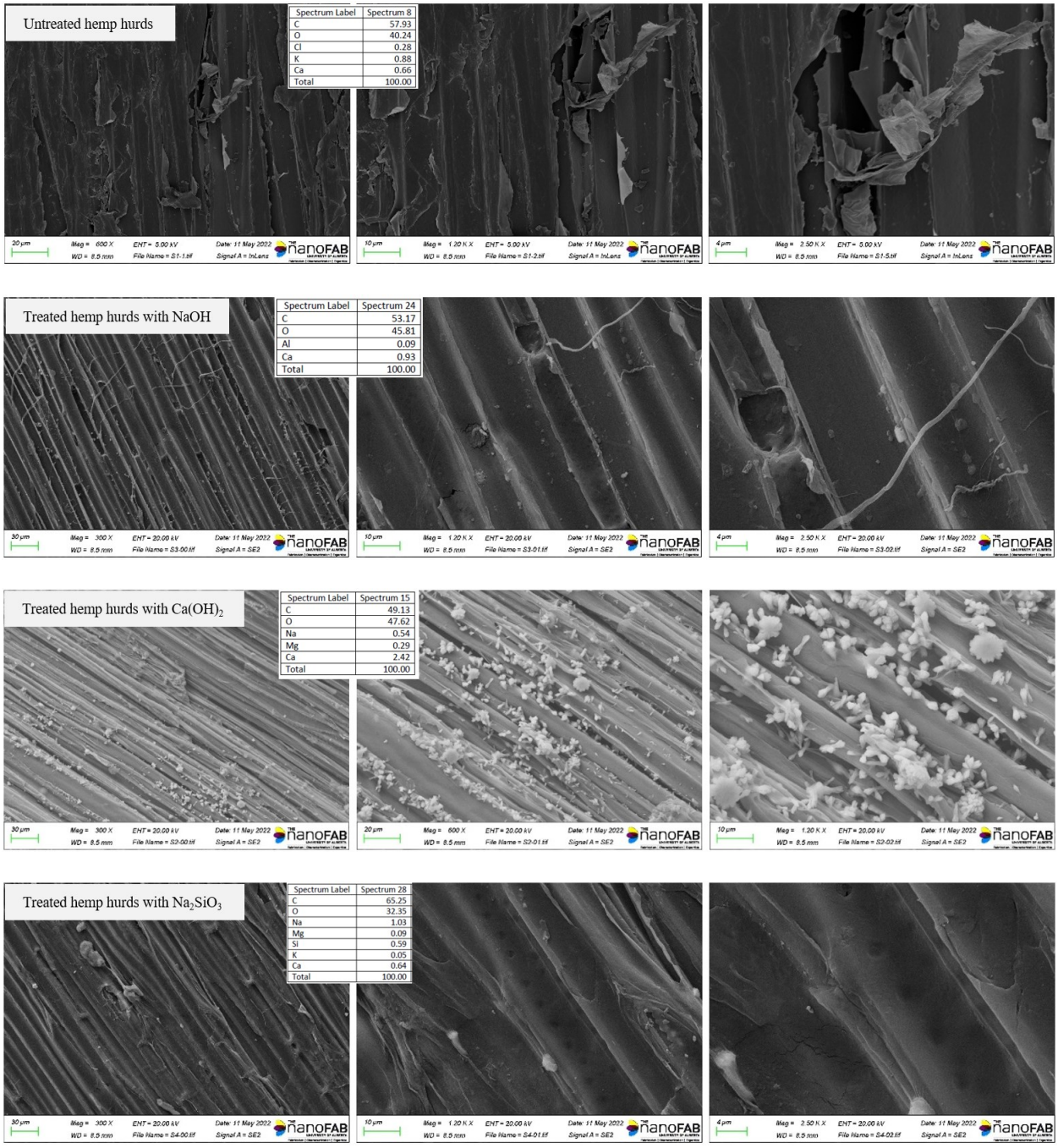

Figure 6.8: SEM and EDX for treated and untreated hemp hurds

6.4.2 Properties of hempcrete with treated hemp

The cube bulk densities of hempcrete with treated hemp hurds varied between 908-1270 kg/m^3, while oven-dry cubes were in a lower range as 491-611 kg/m^3 (difference between wet and dry 43-52% primarily due to the moisture content), as shown in Figure 6.9. The compressive strength of wet samples was 0.77-1.12 MPa, which might be ascribed to the dimensional instability (significant swelling) of hemp with higher water absorption ability [14]. However, the strength of oven-dry samples increased significantly to 1.33-1.56 MPa, which is ascribed to the higher binder stiffness-enhancing bonding with contraction of hemp due to the drying process; hence, more energy required for cracks initiation leading to failure at the interface zone at higher loading capacity (as similarly found for paste [30]). Samples with NaOH treatment showed the highest strength for wet and dry conditions, with about 45 and 15%, respectively, compared to untreated samples. This increment could be ascribed to bleaching and roughening hemp surface with NaOH treatment, which enhanced the bond and increased surface area (due to roughening the surface and reducing hemp size) with binder matrix. The treatment with $Ca(OH)_2$ enhanced the strength compared to untreated hemp by about 15 and 8% for wet and dry conditions, respectively, due to consuming pectin during treatment. Thus, hydration and carbonation hardening processes were barely disturbed. However, the enhancement is not as high as NaOH treatment due to the higher presence of lime in the binder matrix (50% wt.), which participates in minimizing the pectin effect. Further, the presence of calcium over the hemp surface (as shown in SEM-Figure 6.8) might work as the first line of defense for binder calcium. Additionally, the treatment with Na_2SiO_3 enhanced the strength considerably for wet and dry samples by about 25 and 10%, respectively, relative to untreated samples, which ascribed to the rich silica bonds formed with sodium silicate solution treatment (as silica coating shown in SEM-Figure 6.8) (similar findings found for treated sawdust with water glass [26]). The treatment with NaOH showed the highest strength improvement relative to other treatments (10-15%), ascribed to the higher removal of amorphous components, bleaching, and surface roughening. Another reason could be the higher bonding sites to cellulose with NaOH treatment enhancing the interface zone (as interpreted [1][11][14]).

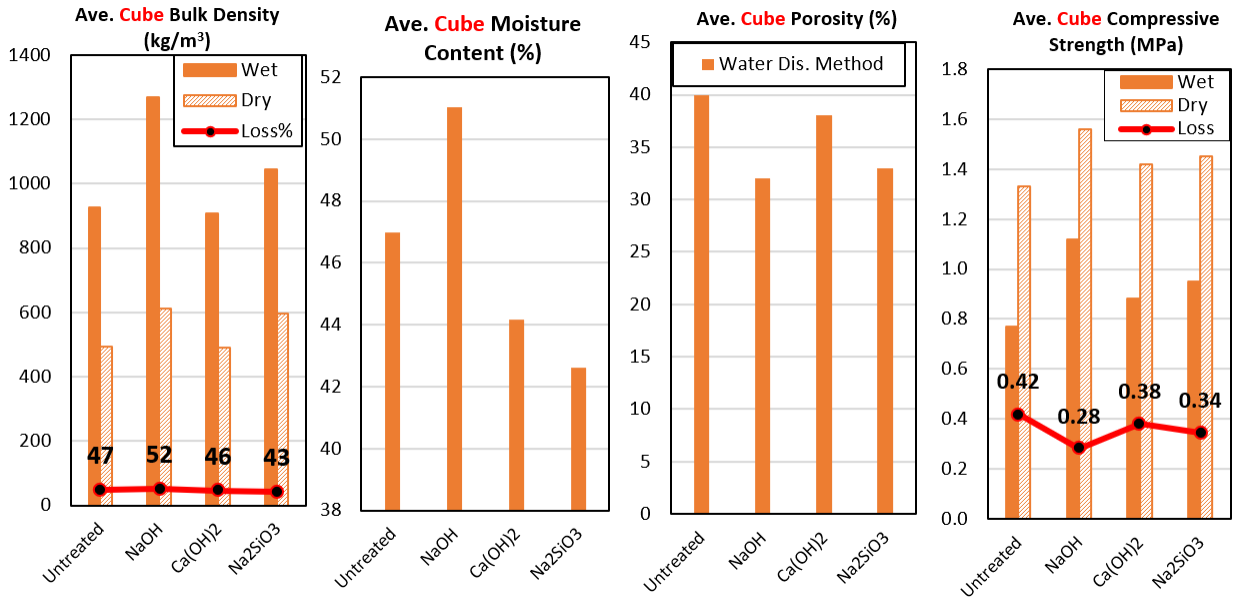

Figure 6.9: Physical and strength properties of hempcrete cubes with treated hemp at seven days (Loss%= Loss*100)

Thermal properties were measured for disc samples, and the physical properties for disc samples were presented in Figure 6.10. Similar densities of disc samples to cube ones are 849-1095 kg/m^3 for wet samples and 493-625 kg/m^3 for dry samples. Moisture content varied between 39-47%, showing a slight reduction with treated hemp hurds, indicating a higher reaction rate and lower porosity, as illustrated in Figure 6.10.

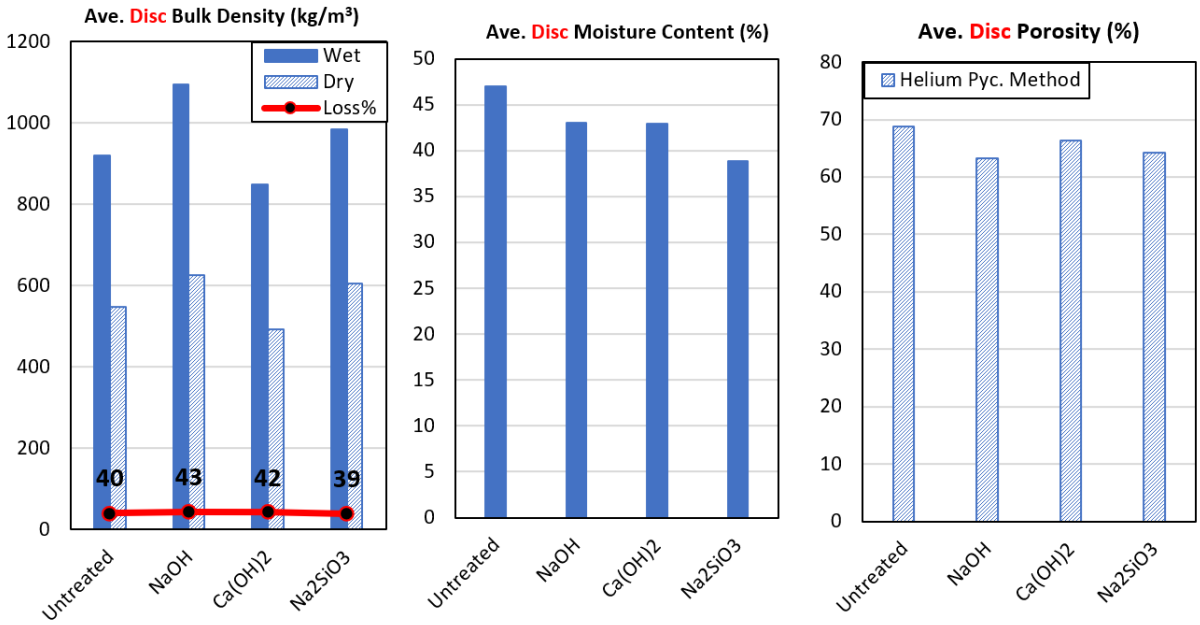

Figure 6.10: Physical properties of disc hempcrete samples with treated hemp at seven days.

Thermal properties were measured using the transient plane source (TPS) method using the TPS1500 machine according to ISO 22007-2 [31]. The hot disk probe is placed between two identical halves of one sample with a smooth surface to minimize losing thermal energy. Three readings were recorded for each sample, and the average of three samples represents each mixture with COV less than 10%.

As shown in Figure 6.11, the thermal conductivity of wet disc samples is in the range of 0.50-0.65W/m K. In contrast, dry samples show values between 0.11-0.21 W/m K. Hempcrete samples with NaOH-treated hemp showed the highest k values with about 20-40% increment as compared to untreated samples, which may be ascribed to the highest density and corroded hemp size. Calcium hydroxide treatment showed the lowest conductivity values with a reduction of 7-27% relative to control, which was attributed to the lowest density and more amorphous hydration products with the availability of extra calcium on the hemp surface. Sodium silicate treatment increased thermal conductivity compared to untreated cases by about 7-17% due to the higher density.

The thermal diffusivity with all treatments shows values of 0.40-0.45 mm^2/s for wet conditions and 0.12-0.17 mm^2/s for dry conditions, as depicted in Figure 6.11. The α values of wet conditions for the treated samples are similar but higher than untreated ones by about 13%. However, treatment with $Ca(OH)_2$ showed the least thermal diffusivity for dry conditions with about 14% reduction, compared to untreated one. The untreated and treated samples with Na_2SiO_3 showed almost the same values. However, density, conductivity, and Cp values are varied. NaOH showed the highest value with about 20% increment relative to untreated samples, which might be attributed to the higher increment of k relative to ρxCp. Generally, wet samples showed a significantly higher value than dry samples (about 62-72%) because moist samples require higher input thermal energy than dry ones.

The specific heat capacity varied between 1769-1987 J/kg K and 1334-1473 J/kg K for dry and wet conditions, respectively, as shown in Figure 6.11. However, the difference between all cases does not exceed 12%, indicating an increment in dry Cp values for treated samples and a reduction in moist Cp values, which may be ascribed to the un-monotonous behavior of Cp with moisture content. Generally, Cp values were calculated from diffusivity, conductivity, and density ($Cp= k/\alpha\rho$). Thus, higher Cp values for dry conditions indicate a higher proportion of $k/\alpha\rho$ than wet conditions.

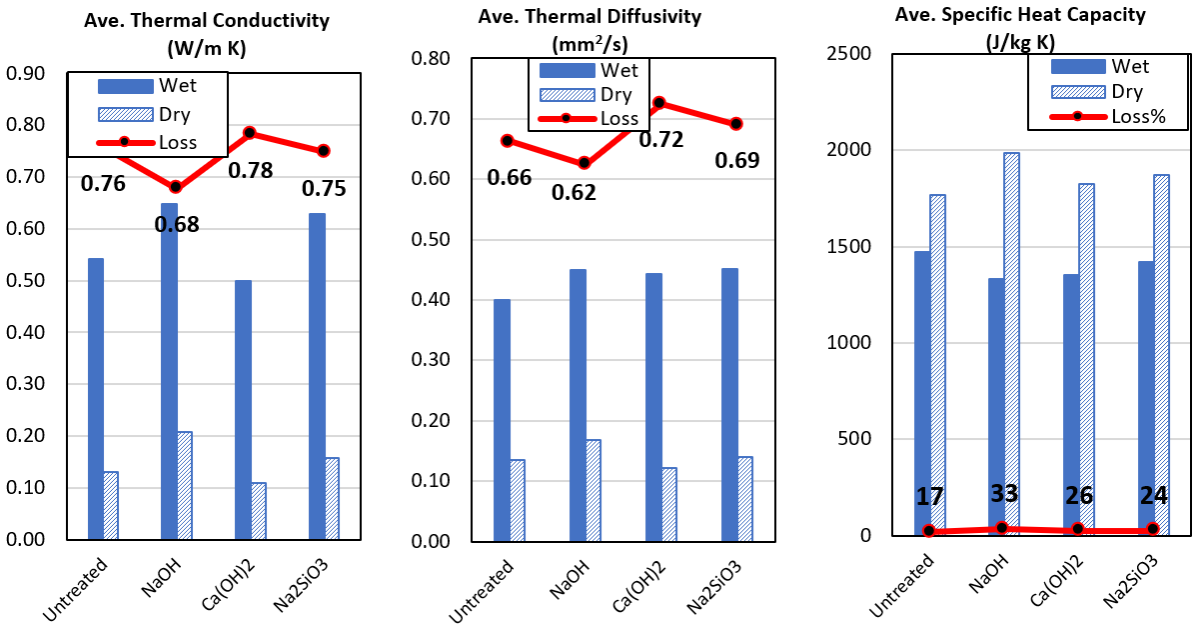

Figure 6.11: Thermal properties of hempcrete with treated hemp at seven days (Loss%= Loss*100)

6.5 Conclusions

The usage of hemp hurds as aggregates to produce hempcrete has dramatically increased due to its superior thermal properties. The incapability between such bio-aggregate and binder matrix is due to hydrophilicity, sugar, and pectin negatively affecting the bond and strength properties. Thus, chemical treatments were used in this study to explore the impact on the thermal and strength of hempcrete with the same hemp size and content. Three chemical treatments were used in this study with a solution of NaOH, $Ca(OH)_2$, and Na_2SiO_3 and a conclusion could be drawn as follows:

- Sodium hydroxide treatment bleached, fibrillation roughened hemp surface, which improved bond and strength by about 15-45% for dry and wet conditions, respectively, along with an increment in thermal conductivity (20-40%) and diffusivity (13-20%).
- Calcium hydroxide treatment minimized pectin content, and crystals adhered to the hemp surface, providing extra calcium ions for hydration and carbonation. The compressive strength

of hempcrete increased (8-15%), thermal conductivity reduced (7-27%), and thermal diffusivity reduced by 14% for dry conditions.

- Sodium silicate treatment increased silica content on the hemp surface, which enhanced the strength by 10-25% and thermal conductivity (7-17%) due to the higher density. However, the diffusivity is similar to untreated samples.
- The difference between all cases in heat capacity does not exceed 12%, showing an increment in dry Cp values for treated samples and a reduction in moist Cp values.

7 CHAPTER 7: PARAMETRIC STUDY (PART I: TRADITIONAL WALLS)

Journal paper #6

Thermal energy storage and losses in various types of masonry concrete walls

Naef A.A. Qasem, Ahmed S. Al-Tamimi, Vivek Bindiganavile

Published in Journal of Energy Storage, May 2023

Abstract

This study investigates the thermal performance of various masonry walls, with and without plaster, for cold zones regarding energy storage and loss. Besides a traditional concrete mixture, twenty-five additional combinations were selected from among 400 mixtures reported in the literature. A computational fluid dynamic (CFD) model that was implemented using ANSYS Fluent is employed here to study the heat transfer from a reference room condition (20 ºC) to a cold ambient state (-20 ºC) throughout 6, 12, and 24 hours to facilitate the comparison between different walls. The model was validated using a reported experimental test *via* a hot plate setup. The results show that among the investigated walls, a mixture with wood shives (WS1) has the maximum stored energy (92% over 24 hr) and the minimum energy loss (8%) in the total heat transfer from the reference room to the ambient. On the other hand, the minimum energy storage (40%) and maximum loss (60%) were observed for hempcrete (HC11). It was found that the combination of thermal properties (thermal conductivity, specific heat capacity, and thermal diffusivity) governs the thermal behavior of each type of concrete. The stored energy inside the wall is drastically influenced by the production of density and heat capacity and secondarily by thermal conductivity. In contrast, the energy loss is significantly affected by thermal conductivity and diffusivity and secondarily by the heat capacity and density as they raise the wall temperature. It is noted that the plaster reasonably reduces energy loss but does not impact energy storage.

Keywords: Masonry walls; enhanced concrete; thermal performance; plaster; cold weather

Nomenclature

Abbreviations

C	Cement
CWM-F	Crushed waste marble-fine
DPF	Date palm fiber
F	Foam
FA	Fly ash
GGBS	Ground granulated blast furnace slag
HC	Hempcrete
HS	Hemp shives
Li	Hydrated lime
MK	Metakaolin
NC	Normal concrete
NHL	Natural hydraulic lime
NP	Non-plastered wall
P	Plastered wall
PL	Perlite
PNC	Prompt natural cement
S	Sand
SD	Sawdust
TES	Thermal energy storage
SF	Silica fume
Vc	Vermiculite
WS	Wood shives

Symbols

Cp	Specific heat capacity (J/kg K)
E_{in}	Energy inflow (J)

E_{out}	Energy outflow (J)
E_{st}	Stored Energy (J)
h_{film}	Film coefficient (W/m^2)
k	Thermal conductivity (W/m K)
Nu	Nusselt number
Pr	Prandtl number
Ql	Lost thermal energy (MJ/m^2)
Qs	Stored thermal energy (MJ/m^2)
q_x	Heat rate (W)
q_x"	Heat flux (W/m^2)
Ra	Rayleigh number
RH	Relative humidity (%)
T_{amb}	Ambient temperature (^oC)

Greek letters

α	Thermal diffusivity (mm^2/s)
ρ	Density (kg/m^3)

7.1 Introduction

Building quality has improved significantly in recent decades with growing living standards and the availability of advanced construction materials. Therefore, standards were initiated for buildings' excellence in indoor air quality and acoustic and thermal insulation. The thermally comfortable environment is mainly controlled by heating and cooling systems to maintain the desired indoor temperature. Thus, much energy is consumed to satisfy comfortable indoor conditions, which differ from country to country.

The various components of the building envelope, including the exterior walls, windows, cladding, exterior structural members, thermal bridges, etc., are the most critical elements affecting heat exchange between the interior and the exteriors. Therefore, a comprehensive analysis is needed

for building envelopes to identify the poor thermal behavior and improve design and construction decisions for sustainability. Buildings in the European Union account for about 40% of the total power consumption. Out of these, space heating alone accounts for between 60-80% [1]. In Canada and the USA, the value reaches 63% [2] and 42% [3], respectively. Thus, a considerable energy expense may be saved if the parameters that affect a building envelope's thermal properties (such as thermal conductivity, diffusivity, density, and specific heat capacity) are suitably modified. Note that masonry blocks are widely used as building envelopes in building exteriors worldwide. Concrete masonry units account for an annual production of about 4.3 billion units in the USA and Canada [4]. Minimum requirements for energy and thermal performance of buildings and construction materials, especially thermal insulation of building envelopes, are included in the European Parliament [5], Canadian Standards Association (CSA) (A165 SERIES-14- R2019) [6], and the American Society for Testing and Materials (ASTM) [7].

Thermal insulation materials are used in wall construction for solid and hollow masonry blocks or block-filling cavities to minimize equivalent thermal conductivity. Prior experimental and numerical studies exist to aid in designing masonry blocks to adapt to the thermal requirements of energy-efficient building envelopes. Various numerical approaches have been employed, including computational fluid dynamics (CFD) [8]. Al-Awsh et al. [9] conducted a thermal model for hollow masonry block walls to evaluate the heat transfer with different material components. The study considered conduction in the solid components and both convection and radiation for the cavities, exteriors, and interiors. The boundary conditions were considered external solar radiation and the ambient interior and exterior temperatures. The surface temperature, heat flux, and wall resistance were found for each case. Results showed an improvement in the thermal resistance by about 15% over the reference mixture for hollow blocks that contained volcanic aggregates. A study in China showed that sintered coal hollow block ($k = 0.57$ W/m K) reduced the thermal conductivity by 65% relative to an ordinary clay block ($k = 0.76$ W/m K) [10].

Marcos et al. [4] assessed different layouts in hollow masonry units by considering air cavities and insulation materials such as cardboard, EPS, and foam. The boundary conditions included convection and radiation on both block surfaces (T_{amb}, h_{film}, ε), which were similar to the boundary

conditions applied to a 2-D numerical study using the finite element method (FEM) for a hollow block with cylindrical cavities that was filled with three different phase change materials [11]. The model adequately predicted the experimental outcomes. It confirms that, especially for air cavities, it is essential to consider all heat transfer mechanisms: conduction, convection, and radiation. Further, research outcomes emphasized that the layout of holes and, where possible, filling them with insulation materials could dramatically improve the thermal insulation of masonry blocks by up to 400%. Utilizing phase change materials yielded benefits to energy storage [12–17]. Wernery et al. [18] investigated the effect of filling cavities in hollow clay bricks, firstly with perlite and later with an aerogel compound. The thermal conductivity for the resulting bricks was lower by 80% and 92%, respectively, over the un-filled cavity. Blanco et al. [8] studied three types of hollow blocks with empty and filled cavities, showing enhanced block thermal resistance. Su et al. [19] measured blocks' thermal conductivity and resistance at steady-state conditions using the hot box setup.

Al-Tamimi et al. [20] thermally investigated different cavity layouts of hollow masonry blocks, involving all heat transfer mechanisms. According to ISO 6946, as detailed in [15], both convection and radiation inside the cavities were significant. The results demonstrated the optimum cavities layout with different insulation materials [21]. Real et al. [1] investigated the effect of four structural lightweight concrete mixtures on reducing thermal bridges and energy consumption. The measurements indicated a reduction reaching 50% in thermal conductivity and diffusivity relative to a normal concrete mixture and about a 40% increase in the specific heat capacity. The results also predicted a reduction in energy needs reaching about 20% for lightweight concrete, compared to normal weight concrete, for an apartment in Lisbon, Portugal. However, the percentage of improvement was likely to differ with changes in location and climate conditions.

Haika et al. [22] measured the energy consumption for buildings made of lime hempcrete, hollow concrete blocks, and expanded polystyrene. The results showed a dramatic reduction in total energy consumption, 90% lower than hollow concrete blocks, for heating and cooling. Concrete was used as a thermal energy storage (TES) medium in many applications to store thermal energy in solar energy plants, in which concrete under thermal cycle was used as thermal energy storage

(TES) [23][24]. For such an application, heat capacity and thermal conductivity must be sufficiently high to extend the period and charging time to back up at low insolation.

As illustrated above, the existing literature shows different ways and materials to improve the thermal performance of masonry walls. However, each of these prior studies applied uniquely to its specific conditions. So, to the best of the authors' knowledge, no study compares various types of masonry walls under the same conditions. Thus, the novelty of the current study is to investigate multiple concrete types for cold-weather building envelopes under the same conditions and to evaluate the thermal performance in terms of thermal storage and losses. The study assesses the energy storage inside the wall and energy loss from walls to the ambient to suggest the best walls for energy saving in cold regions. Thus, materials for building envelopes are required to show high storage energy and thermal resistance. Materials with low thermal conductivity and high heat capacity (i.e., low thermal diffusivity) are expected to minimize energy loss to the exterior and store more energy. A transient thermal model is implemented to assess the thermal performance over 24 hours for different concrete mixtures to be used for building envelopes to save thermal energy. The model is developed using ANSYS Fluent [25] and validated against an experimental study of a hot plate setup to evaluate the performance of the walls. The combination of the thermal properties (ρ, Cp, and k) for transient heat flow on stored and lost energy is studied. Further, the effect of adding plaster to the internal and external surfaces of the wall is considered for evaluating both energy storage and loss. The study assumes cold weather outside conditions with constant temperature (- 20 ^{o}C) to compare different walls, while inside conditions are kept at 20 ^{o}C. Twenty-five walls are investigated and compared with the traditional concrete wall.

7.2 Research methodology

To achieve the objectives of the parametric study, the following methodology was employed, as shown in Figure 7.1. First, the authors investigated the literature for thermal models in building envelopes and used input parameters to identify the specific boundary conditions. Thus, the properties needed in the model were collected from experimental data of different concretes. The model was validated with hot plate experimental data from the literature. A parametric study was

carried out to understand and analyze the heat transfer through masonry walls by evaluating the amount of stored and lost thermal energy in the walls. Different walls, with and without plaster layers, were compared based on their thermal performance.

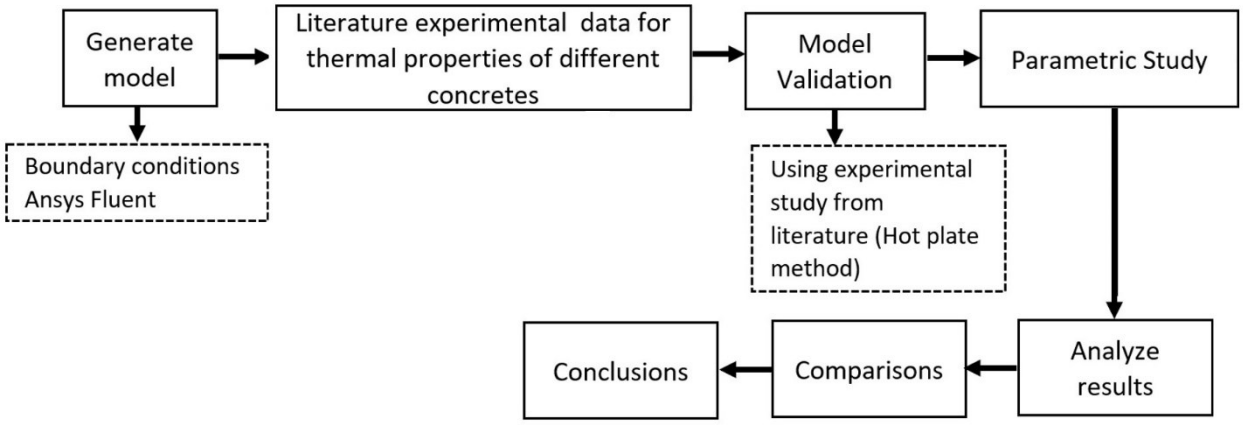

Figure 7.1: Methodology of parametric study

7.3 Mathematical Model

Walls consisting of bricks with and without plaster are considered in this study. The modeled wall is shown in Figure 7.2 and Figure 7.3. A three-dimensional (3-D) thermal simulation using the finite volume method with the help of ANSYS Fluent [25] was generated to investigate the thermal performance of masonry walls with solid blocks having different materials, as shown in Figure 7.2. The model was based on the energy conservation equation under transient conditions. The heat transfer is considered transient to investigate the thermal performance with time, during 24 hours to investigate the heat stored in and lost from the walls. Both convection and radiation were assigned as boundary conditions across the external and internal wall surfaces. The mortar layers connected by masonry units are considered one body with different thermal properties at each layer. However, the model assumes a perfect bond with no gaps or friction at joint zones [9].

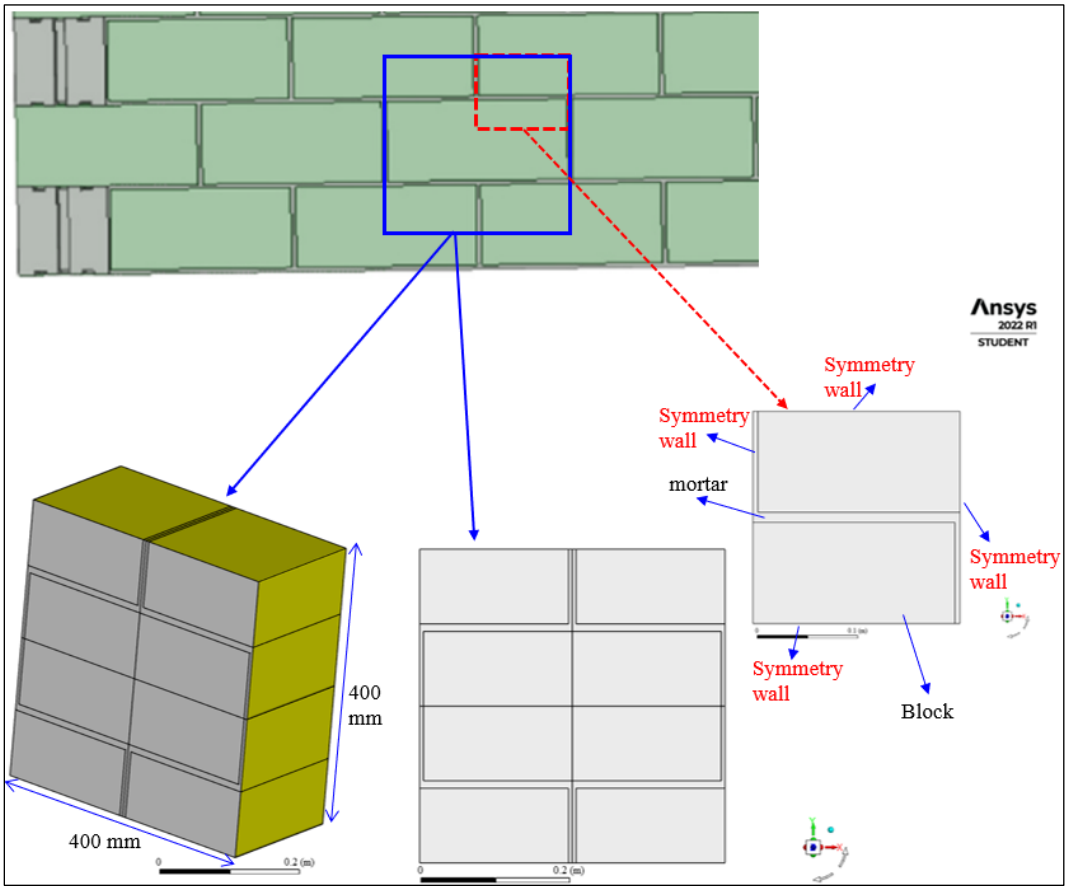

Figure 7.2: Masonry wall and symmetric part used in the model.

7.3.1 Governing equations

The transient thermal model is governed by an energy equation as follows [26]:

$$E_{st} = E_{in} - E_{out} \qquad \textbf{Eq- 7.1}$$

Where E_{st} is the stored energy in the wall, E_{in} is the heat transfer from the room (higher temperature) to the wall, and E_{out} is the heat lost from the wall to the cold ambient temperature in the exterior.

The heat stored in the wall could be expressed as [26]:

$$E_{st} = C_p\,\rho\,\frac{\partial T}{\partial t}\,dx\,dy\,dz \qquad \textbf{Eq- 7.2}$$

Conduction heat rates through the wall (in W) can be evaluated as [26]:

$$q_x = -k\,(dA\,\nabla T) = -k\,(dy\,dz\,\frac{\partial T}{\partial x} + dx\,dz\,\frac{\partial T}{\partial y} + dx\,dy\,\frac{\partial T}{\partial z}) \qquad \textbf{Eq- 7.3}$$

Now, the heat transfer equation, including storage and conduction inside the brick, is [26]:

$$C_p\rho\,\frac{\partial T}{\partial t} = k\,\nabla^2 T \qquad \textbf{Eq- 7.4}$$

And in terms of thermal diffusivity is given by [26]:

$$\frac{\partial T}{\partial t} = \alpha\nabla^2 T \qquad \textbf{Eq- 7.5}$$

7.3.2 Boundary conditions

The heat transfer to/from the wall surface, which faces external conditions, accommodates both convection and radiation. It can be expressed as [9]:

$$k_w\left(\frac{\partial T_{w,ext}}{\partial x}\right) = h_{ext}\left(T_{w,ext} - T_{amb,ext}\right) + \varepsilon_{ext}\sigma\left(T_{w,ext}^4 - T_{amb,ext}^4\right) \qquad \textbf{Eq- 7.6}$$

where k_w is the thermal conductivity of the wall (W/m K), h is the convection heat transfer coefficient (W/m^2 K), $T_{w,ext}$ is the exterior wall surface temperature (K), $T_{amb,ext}$ is the external ambient temperature (K), ε_{ext} is the emissivity of the outer wall surface, and σ is the Stefan–Boltzmann constant (5.6703 x 10^{-8} W/m^2 K^4). Similarly, for the internal wall [9],

$$k_w\left(\frac{\partial T_{w,int}}{\partial x}\right) = h_{int}\left(T_{w,int} - T_{amb,int}\right) + \varepsilon_{ext}\sigma\left(T_{w,int}^4 - T_{amb,int}^4\right) \qquad \textbf{Eq- 7.7}$$

The heat transfer coefficient at the vertical walls can be calculated from the Nusselt number using the following equation [26]:

$$h = \frac{Nu * k_{air}}{L} \qquad \textbf{Eq-7.8}$$

Where k_{air} is the thermal conductivity of the air, L is the vertical length of the wall, and Nu is the Nusselt number calculated using the following empirical correlation for external free convection on vertical surfaces and laminar flow [26]:

$$Nu = 0.68 + \frac{0.67Ra^{0.25}}{\left(1 + \left(\frac{0.49}{Pr}\right)^{9/16}\right)^{4/9}} \qquad \textbf{Eq- 7.9}$$

where Pr is the Prandtl number of the air atmospheric pressure and defined as the ratio of momentum to thermal diffusivity of air, and Ra is the Rayleigh number (for laminar flow: $10^4 < Ra < 10^9$), as follows for external free convection on vertical surface [26]:

$$Ra = \frac{g\beta L^3\left(T_{w,surf} - T_{amb,air}\right)}{v\alpha} \leq 10^9 \qquad \textbf{Eq- 7.10}$$

Here, the thermophysical properties of air at atmospheric pressure (Table A.4 [26]) include β, v, α, Pr, and k. The previous equations calculated the heat transfer coefficients at the interior and exterior wall surfaces as 3 and 3.5 W/m^2 K, respectively. The detailed boundary conditions are shown in Figure 7.3. It is worth noting that the wind speed is ignored, besides assuming constant temperature interior and exterior to facilitate the compression of different walls. Variable and accurate conditions are essential for energy consumption estimation, which is not the focus of this paper.

The symmetric wall conditions, as applied to the side walls, can be expressed as [9]:

$$\nabla T = 0 \qquad \textbf{Eq- 7.11}$$

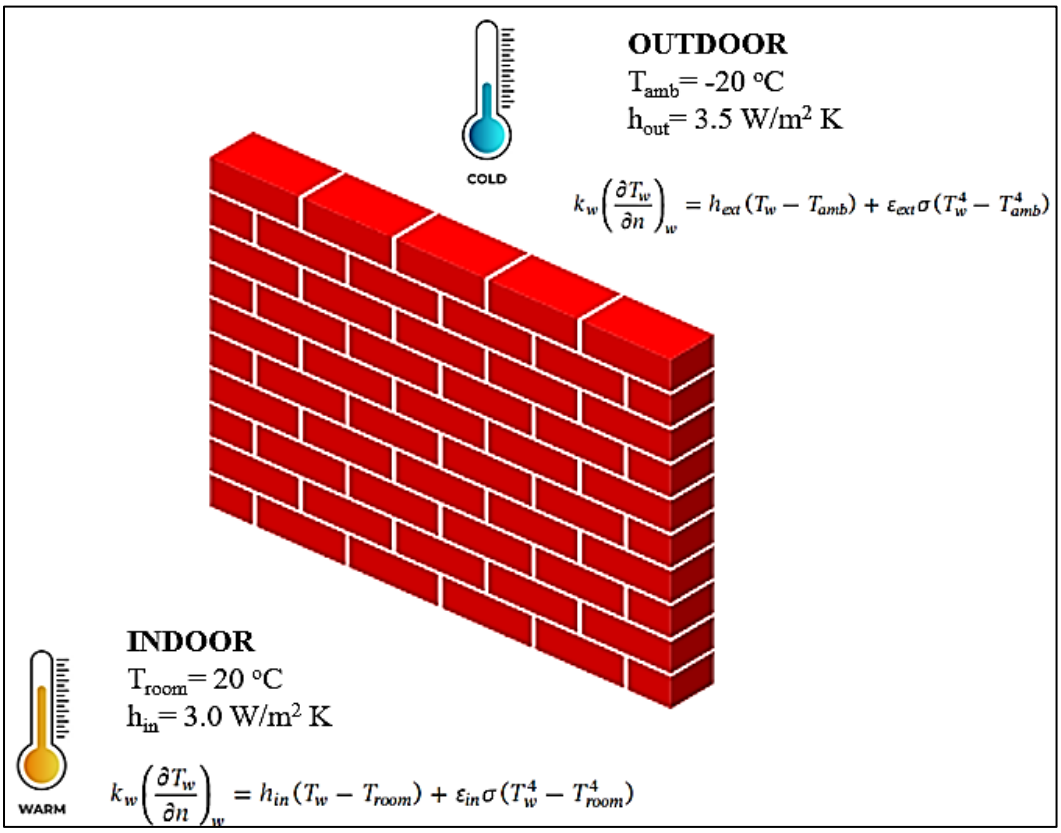

Figure 7.3: Boundary conditions for the thermal model used in this study.

7.4 Mesh independence

A mesh verification was conducted to maintain the stabilization of results. Thus, nine mesh sizes were modeled with the number of cells as 400, 1000, 7000, 16000, 31000, 73000, 128000, 250000, and 411000, respectively. The structured mesh was used, as shown in Figure 7.4(a). The outcomes of mesh independence were tested regarding the masonry wall's inner surface temperature (Tin) with flow time and cell size, as depicted in Figure 7.4(b). Therefore, a cell size of 3.40 mm (number of cells = 411000) was selected to verify the independence of the mesh. It is noted that a smaller mesh size could also be acceptable. However, a larger mesh size ensures mesh independence for all studied cases.

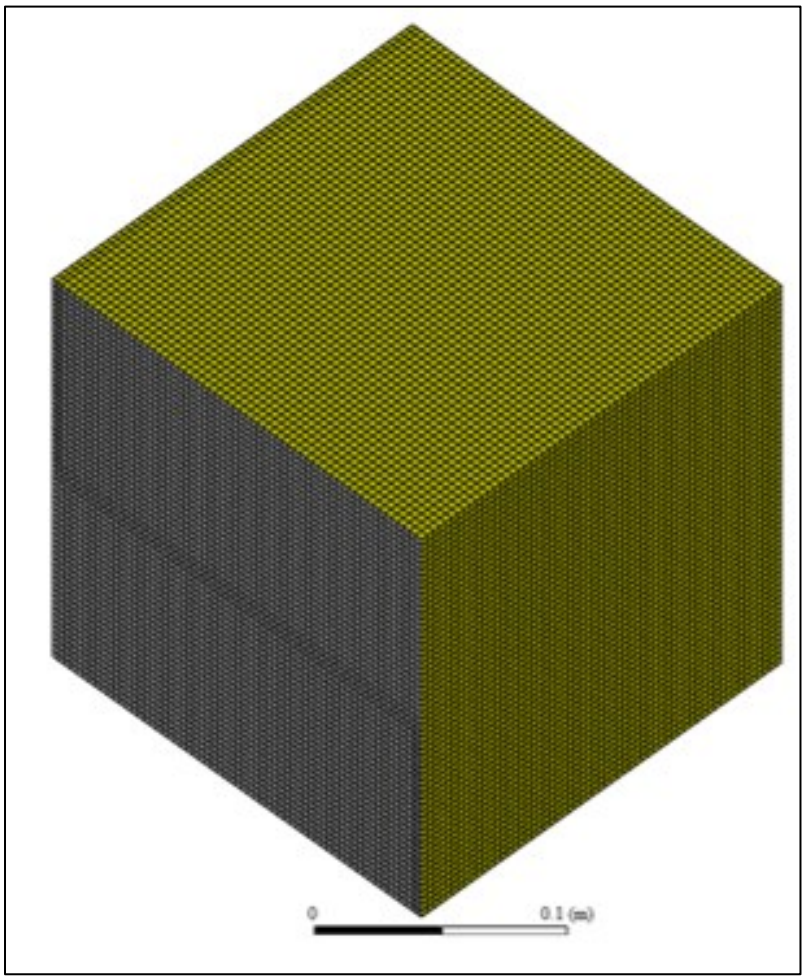

(a)

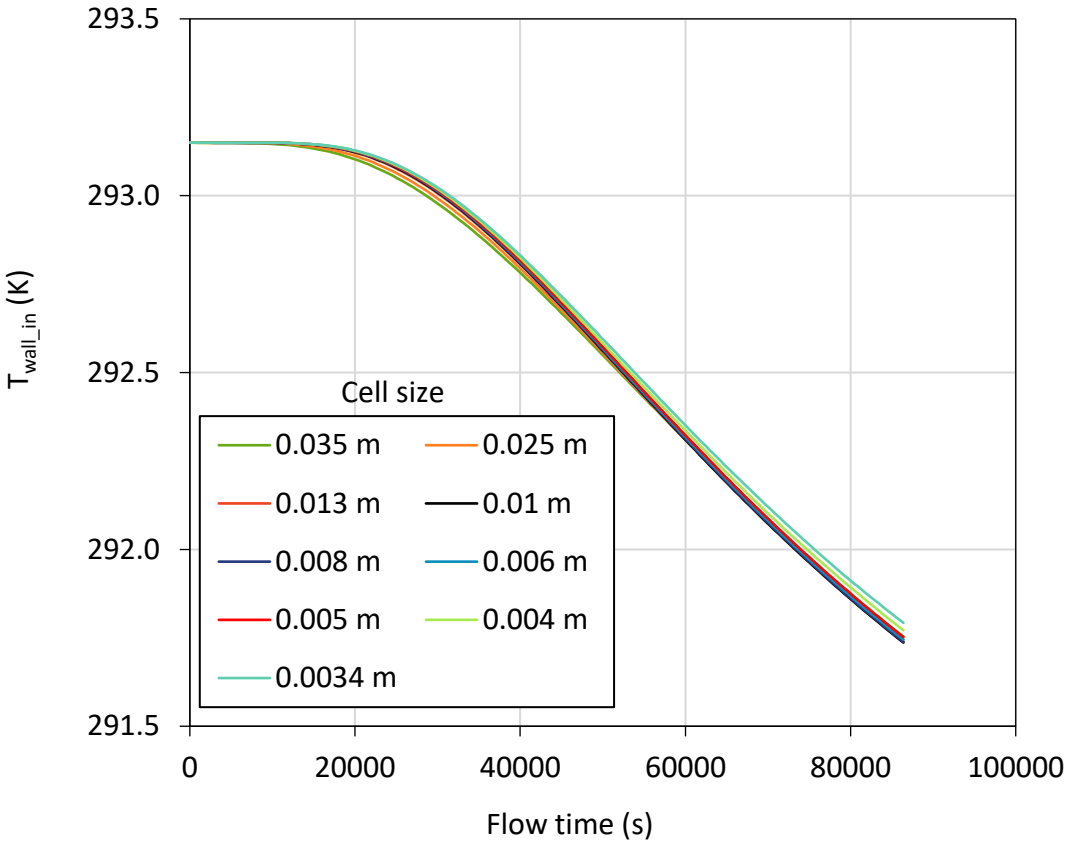

(b)

Figure 7.4: Mesh independence study: (a) mesh scheme and (b) mesh independence in terms of inner wall temperature.

7.5 Model Validation

An experimental study [27] was used to validate the model, in which a lime hemp wall of 0.90 m x 0.90 m and a thickness of 0.30 m was tested using the hot plate method to measure the thermal conductivity of the wall [27]. The setup of the hot plate and the tested sample is shown in Figure 7.5. Thermocouples and heat flux sensors were fixed into both sample surfaces to monitor the surface temperature and flux.

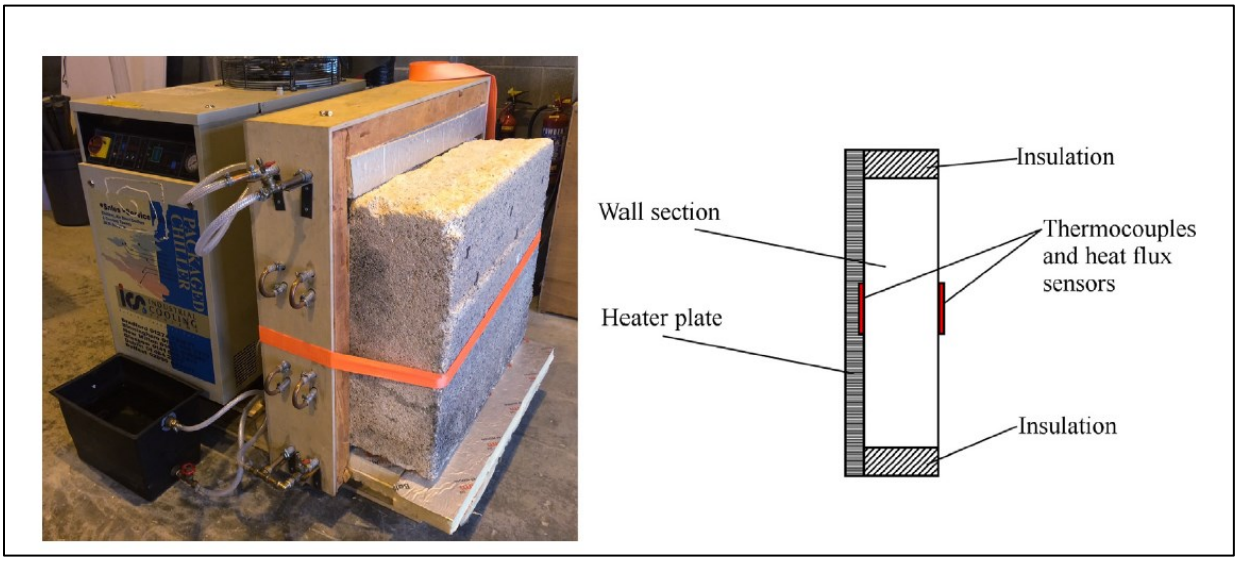

Figure 7.5: Setup of the hot box with lime hemp concrete sample [27].

The heater was set at a temperature of 60 ºC, and the heat flowed to the cold side. The temperature was measured for hot and cold wall surfaces (T_{hot}, T_{cold}), and the flux at the cold surface was mapped, as shown in Table 1 and Figure 7.6, respectively. Additionally, as listed in Table 5.7, the experimental data and the model predictions were compared for identical experimental conditions, as shown in Figure 7.6. It can be seen that the predicted flux is in agreement with the experimental data (difference <5%). Convection and radiation on both surfaces are not considered because both surface temperatures were defined. However, convection and radiation were included for actual walls, as shown in Figure 7.3.

Table 7.1: Model input parameters

Sectional Properties	**Thermal Properties**	**Boundary Conditions**
Wall thickness = 0.30 m	k = 0.129 W/m K	T_{hot} = 51 ºC
Wall area= 0.90x0.90 m	Cp = 1627 J/kg K	T_{cold} = 20 ºC
	ρ = 508 kg/m^3	Transient time = 300,000 s

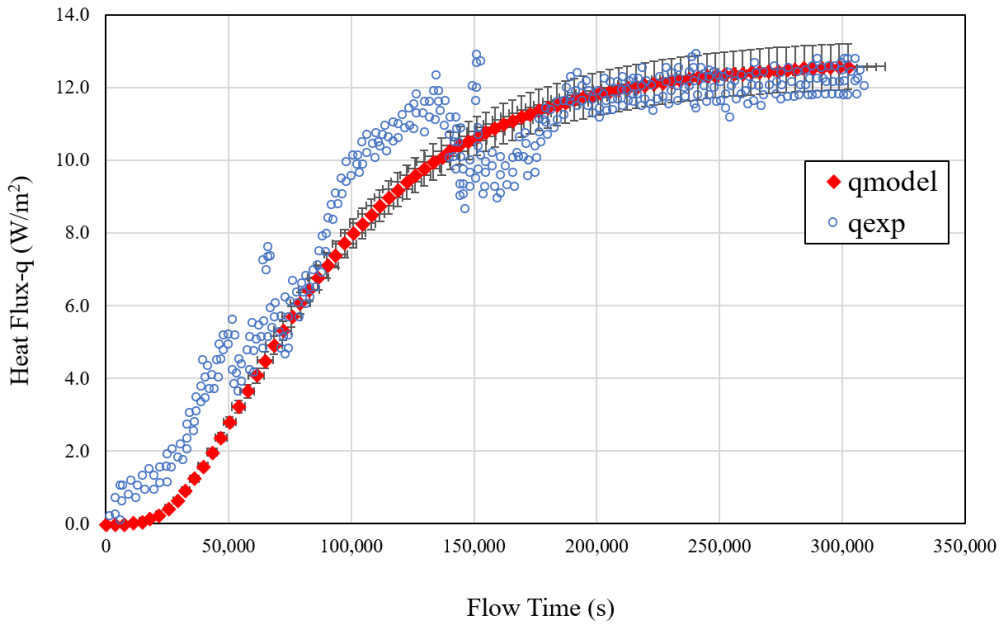

Figure 7.6: Validation of the CFD model against the experimental data of [27] regarding temporal heat flux at the interior surface (cold surface).

7.6 Materials and Data

In the model, blocks with a dimension of 40 cm x 40 cm x 20 cm were assembled to build a wall. It was assumed that the blocks were connected with two types of mortars, one of which was a Portland cement mixture while the other was a lime mortar. Data from 400 mixtures were collected from the literature for different types of concretes tested for their thermal properties, including thermal conductivity, specific heat capacity, and thermal diffusivity. This data was assembled and sorted four times: three resulting in ascending order for k, α, and ρ, respectively, and in descending order for Cp. This led to identifying the concrete mixture that offered the lowest k, α, and ρ, and similarly, with the highest Cp. Each group selected the first ten concrete mixtures for this study to illustrate the effect of k, Cp, ρ, and α on thermal performance. This is summarized in Table 7.2.

Table 7.2: Thermal properties of different concretes from literature

Mix ID	Mix Components	ρ kg/m^3	k W/m K	Cp J/kg K	α mm^2/s	Ref
HC11	PNC + HS-fibered (S1<10mm) - Light compaction	351	0.105	650	0.46	[28]
HC9	PNC + HS-un-fibered (S2<S1)- Light compaction	340	0.103	750	0.40	
HC13	PNC + HS-fibered (S1<10mm)- Heavy compaction	415	0.110	690	0.38	
HC12	PNC + HS-un-fibered (S2<S1) - Heavy compaction	410	0.115	760	0.37	
HC6	75% Li + 15% NHL5 + 10% FA + HS (RH=15%)	1001	0.094	333	0.28	[29]
HC8	75% Li + 15% NHL5 + 10% FA + HS (RH=65%)	1111	0.100	300	0.30	
HC10	75% Li + 15% NHL5 + 10% FA + HS (RH=15%)	995	0.105	385	0.27	
HC7	Hempcrete	413	0.100	1000	0.24	[30]
HC4	Commercial hempcrete for Ext. wall	275	0.060	1500	0.15	[31]
HC3	Commercial hempcrete for floor	330	0.070	1550	0.14	
HC2	Standard mix of TRADICAL hempcrete	275	0.060	1800	0.12	
PL1	C + S + 75% PL	400	0.09	1720	0.13	[32]
VC	C + Vc	450	0.11	1800	0.14	
Foam	C + 49.4% ECA + F	739	0.228	1136	0.27	[33]
WS2	C + S + 8% WS	1547	0.25	1077	0.15	[34]
SD1	C + S + 10% SD	1427	0.26	1301	0.14	
SD2	C + S + 8% SD	1484	0.29	1261	0.15	
WS1	C + S + 10% WS	1495	0.24	1574	0.10	
DPF1	Gy + Li + S + G + 1% DPF	1150	0.894	1700	0.46	[35]
DPF2	Gy + Li + S + G + 1.5% DPF	1120	0.864	1800	0.43	
DPF3	Gy + Li + S + G + 2% DPF	970	0.764	2200	0.36	
PL2	C + 45% PL + 40% S + 60% CWM_F	1124	0.87	1879	0.41	
PL3	C + 45% PL + 20% S + 80% CWM_F	1144	0.95	1909	0.44	
PL4	C + 45% PL + 80% CWM_F	1164	1.1	1989	0.48	
NC	C + S + G	2450	1.687	1111	0.62	[36]

As listed in Table 7.3, cement-based and lime-based mortars were used for block connections. The two mortar mixtures were used with the same concrete mixture in the block. Finally, the masonry

walls were plastered on both sides with lime plaster for the interior and stucco for the exterior, as shown in Table 7.3. Note that the emissivity coefficient varies with the mixture and color of the concrete surface. However, it is assumed here to be the same for all walls due to a lack of reported data for each case. Based on the literature reviewed, the emissivity coefficients for masonry surfaces lie in the range of 0.85 – 0.95. Thus, this study takes the average value as 0.90 across walls [4].

Table 7.3: Thermal properties of mortars and plasters used in this study.

	Thickness (mm)	Material	ρ (kg/m^3)	k (W/m K)	Cp (J/kg K)	α (mm^2/s)	ε	Ref
Mortar	10	Cement mortar	2143	0.42	570	0.34	0.90	[4]
		Lime mortar	1251	0.25	960		0.90	
Indoor plaster	10	Li + S	1745	0.65	817	0.46	0.92	[37]
Outdoor plaster	20	Stucco	2659	0.721	837	0.32	0.88	[38]

7.7 Results and discussions

This parametric study aims to assess the thermal performance of different wall systems for storing and losing heat energy, calculated by the model and not experimentally. The input thermal parameters (k, Cp, and ρ) were obtained from the experimental test. The time factor is evaluated at 6, 12, 18, and 24 hours. The wall thickness was 200 mm, and interior and exterior temperatures were assumed constant for model simplicity.

The CFD model predicts the internal surface temperature, the external surface temperature, the average wall temperatures, and the heat flux. Such that the stored and lost energy can be estimated. Figure 7.7 shows some representative 3-D plots for two masonry block walls built with concrete

made of wood shives and cement binder (Mix WS1) and normal concrete (Mix NC). The figure shows a concentrated temperature gradient and heat flux at connection zones (mortar) with values higher than in the blocks. This scenario was revealed in the case of normal concrete blocks because the thermal properties of NC are higher than cement mortar, as listed in Table 7.3. The NC wall's heat flux values are higher since hempcrete has a higher thermal resistance.

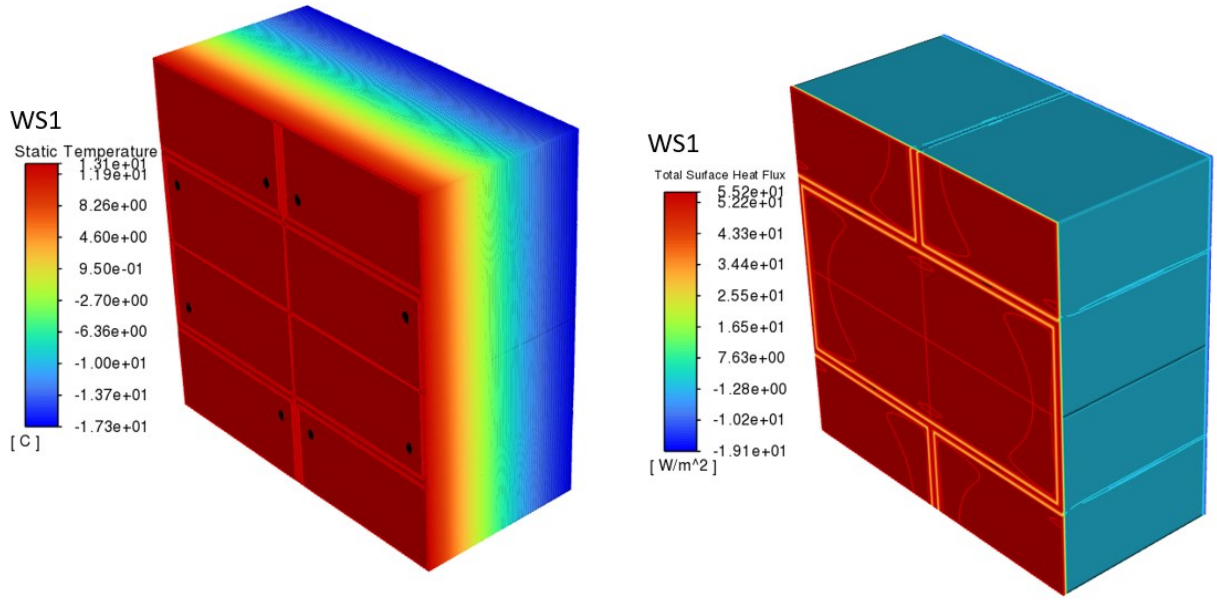

(a)

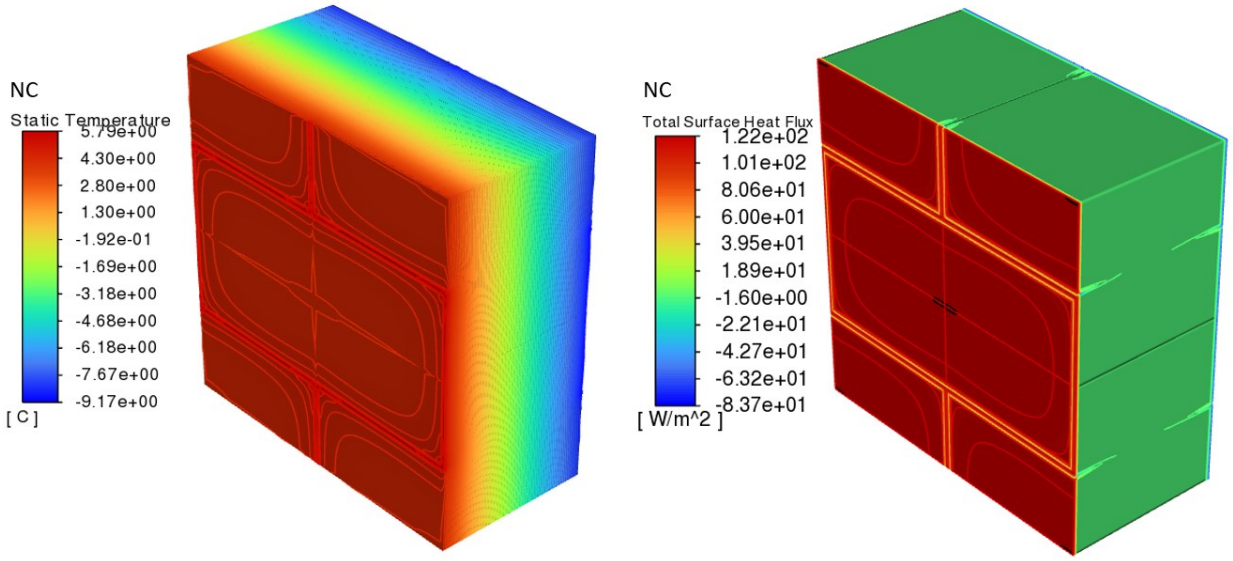

(b)

Figure 7.7: Typical 3-D plots for temperature and heat flux; (a) Mix WS1, (b) Mix NC.

7.7.1 Stored energy for unplastered concrete walls

Figure 7.8 depicts that the amount of stored energy increases with time for all concrete types. However, the increase differs depending on the properties of the concrete. Since the volume is constant, the amount of stored heat depends on the production of density and specific heat capacity (similar findings of [39]), while charging time mainly depends on thermal conductivity. For example, the rise in stored energy for hemp concretes is significantly lower than that of others, which indicates a shorter period to reach saturation because the hemp concrete walls have a lower density. So, the heat capacity product ($C = \rho \times C_p$) is small. Further, the lower thermal conductivity of hempcrete accounts for slower charging, as compared to other concretes with higher k values (as similarly found by John [23][40]). In this regard, the hemp concretes show a stored energy of about 1 – 2 MJ/m^2 after 24 hr, while the other concrete walls indicate stored energy between 3 – 10 MJ/m^2 due to their higher $\rho \times Cp$. Additionally, it can be noticed from Figure 7.8 that most stored energy charging occurs in the first six hours for most walls owing to its reaching the highest

thermal capacity level. Based on the stored energy value (over 24 hours), Figure 7.8 walls would be classified into three groups to show the capability of walls to store energy, as follows:

- Group I (Qs < 2MJ/m^2): Walls H3 – H11,
- Group II (Qs = 2 – 4 MJ/m^2): Walls PL1, VC, Foam
- Group III (Qs = 5 – 10 MJ/m^2): Walls WS2 – NC

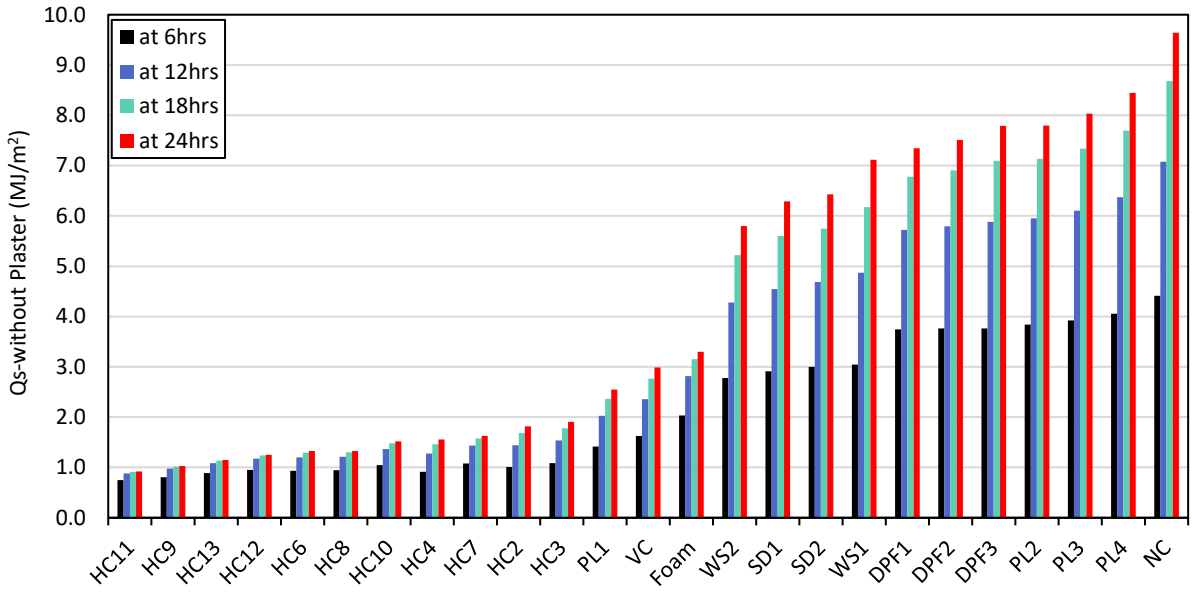

Figure 7.8: Stored energy for unplastered walls built with different concrete types.

The hemp concrete mixtures were suggested for the cold regions in the literature [41][42], as they suit their low conductivity and high heat capacity. However, they perform inefficiently for stored energy due to their lower density. Further, the charging time is significantly lower than other concretes with lower storage capability. Table 7.4 lists the hempcrete walls classified based on their thermal diffusivity as high, medium, and low values. The stored energy increases with decreasing thermal diffusivity for hempcrete due to high C_p and low k values (i.e., ρ x C_p is relatively higher). Furthermore, the percentage of Qs from all heat transfer from the room is high (63-81%) for walls HC 2, 3, 4, and 7 that have lower diffusivity values (high ρ x C_p values) – that implies the lost energy to the ambient is lower. In summary, high ρ x C_p values lead to lower

diffusivity and a higher percentage of stored energy (i.e., lower lost energy at the wall serves as a thermal capacitor more than a thermal conductor). Further, higher thermal conductivity reflects less time for charging and vice versa.

Table 7.4: Effect of Cp, ρ, and k on thermal diffusivity values

Model ID	ρ kg/m^3	Cp J/kg K	k W/m K	α mm^2/s	Qs over 6hr MJ/m^2	Qs over 24hr MJ/m^2	Qs over 24hr %*
HC 11, 9, 13, 12	Low (340-415)	Low (650-760)	High (0.103-0.115)	High (0.37-0.46)	0.75-0.95	0.92-1.25	40-48
HC 6, 8, 10	High (995-1111)	Lower (300-385)	Low (0.094-0.105)	Medium (0.27-0.30)	0.93-1.05	1.33-1.52	56-59
HC 4, 7, 2, 3	Low (275-413)	High (1000-1800)	Lower (0.06-0.10)	Low (0.12-0.24)	0.91-1.08	1.56-1.91	63-81

*The percentage of stored energy inside the wall from the total heat released from the room to the wall.

Another classification of the walls in the literature is based on the diffusivity values. Even though the diffusivity value is the same for some walls, as listed in

Table **7.5**, the performance is not the same as Cp, ρ, and k vary. Walls SD1 and HC3 have the same α (0.14 mm^2/s), but the stored energy differs. The higher density and Cp resulted in higher Qs for SD1 compared to smaller values for HC3. High thermal diffusivity values could be obtained either by high k (as DPF1) or low ρ and Cp (as HC11). However, the high thermal diffusivity values do not reflect higher storing energy directly. The k-value's effect appears when the two walls have the same or closer ρ x Cp product since the low k-value indicates more resistance to heat passing through the wall (i.e., that increases the charging time and reduces the heat losses).

Table 7.5: Comparison between models with the same diffusivity values in Qs.

Model ID	ρ kg/m^3	Cp J/kg K	k W/m K	α mm^2/s	Qs over 6hr MJ/m^2	Qs over 24hr MJ/m^2	Qs over 24hr %
VC	400	1720	0.09	0.14	1.63	2.99	80
HC3	330	1550	0.07	0.14	1.08	1.91	78
SD1	1427	1301	0.26	0.14	2.91	6.29	86
HC4	275	1500	0.06	0.15	0.91	1.56	75
WS2	1547	1077	0.25	0.15	2.78	5.80	84
SD2	1484	1261	0.29	0.15	3.00	6.43	84
HC11	351	650	0.105	0.46	0.75	0.92	40
DPF1	1150	1700	0.894	0.46	3.74	7.34	68

7.7.2 Stored energy for plastered concrete walls

In this numerical exercise, the plaster's thickness and material were kept the same for all the walls. Note, however, that the effect of plastering on the energy stored varies based on the material in the wall and the storing period, as depicted in

Figure **7.9**. After 6 hours, the energy stored in the plastered walls was mostly lower than in the unplastered walls. This may be attributed to the plaster, a barrier against heat transfer. The walls built with WS1, WS2, SD1, SD2, DPF2, DPF3, and DPF4 were exceptions, registering higher Qs for the plastered walls by about 7 – 9%. This was due to the higher wall thickness (at 0.23 m) and

consequent increase in the wall mass that stores energy. However, the effect of plaster to hinder heat transfer reduced with time as the wall temperature was raised. Thus, the stored energy increases in the wall and plaster system were higher than in the unplastered walls. Most hempcrete walls show reduced stored energy for plastered walls due to the lower product of ρ×Cp. The stored energy for the unplastered PL2-4 walls shows higher values, reaching 12% compared to plastered walls at 24 hours, which may be ascribed to these walls having higher thermal conductivity and the ρ×Cp of the unplastered wall being higher than that of the plaster, affecting the stored energy. Generally, the effect of plastering on stored energy is insignificant because of the small plaster thickness (3 cm), and ρ×the Cp of the plaster is lower than that of some walls. It is expected to reduce heat loss, as discussed in the next section.

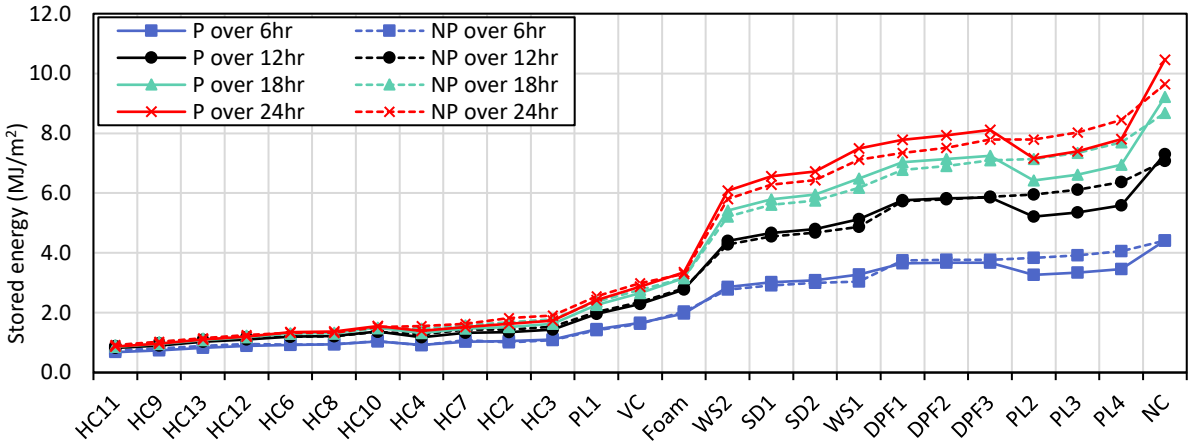

Figure 7.9: Interior and exterior plasters affect wall stored energy (Qs). The connecting curves only show the difference between plastered (P) and unplastered (NP) values.

7.7.3 Lost energy for unplastered concrete walls

The walls lose thermal energy due to convection and radiation heat transfer from the exterior wall surface to the ambient. As expected, the energy losses increase with time during the 24 hours, see Figure 7.10. It is noticeable that the lost energy in the first 6 hours is smaller than the loss at later hours. This is attributed to a slight increment in outer surface temperature in the first 6 hours when

it reaches -16.5 ºC. The walls have a higher ability to store energy during this period. At the 24-hour mark, the least energy loss, Ql, was for HC2 (hempcrete) at 0.44 MJ/m^2, while the highest loss was seen for the normal concrete with 4.11 MJ/m^2 (i.e., increment of about 90%). The concrete walls could be classified in terms of lost energy over 24 hours into four groups as follows:

Group I (< 0.5 MJ/m^2): HC2

Group II (0.5-1.0 MJ/m^2): HC3, HC4, HC5, WS1, PL1, VC, HC7, HC6,

Group III (1.0-2.5 MJ/m^2): SD1, HC8, HC10, WS2, SD2, HC9, HC13, HC12, HC11, Foam

Group IV (2.5-4.5 MJ/m^2): DPF1-NC

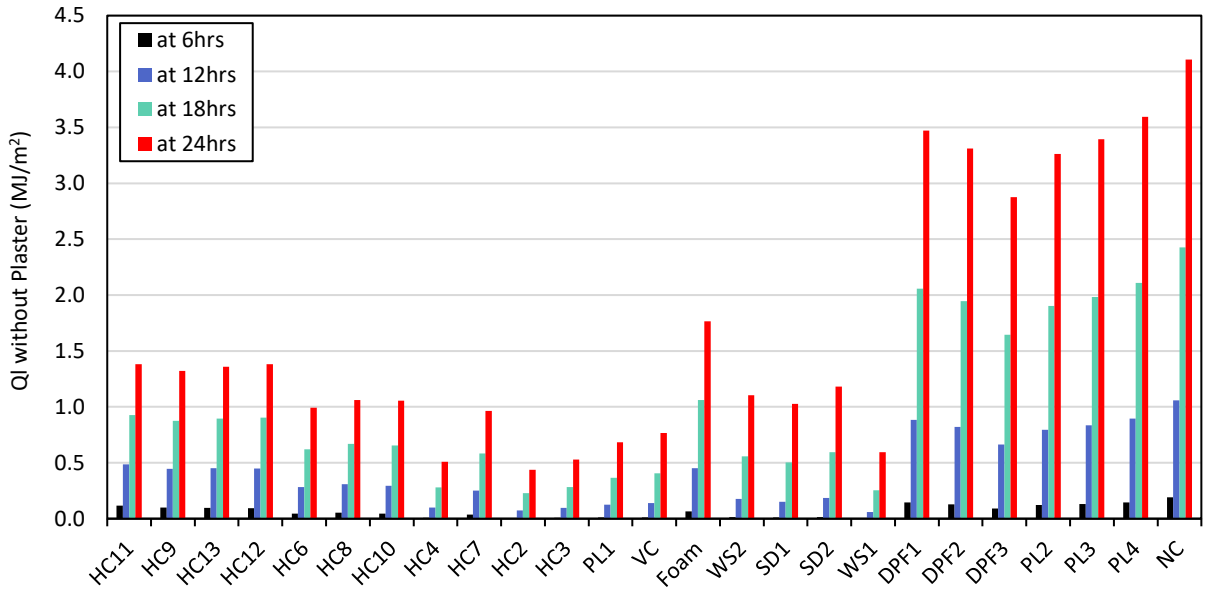

Figure 7.10: Lost energy for unplastered walls built with literature concrete types.

The amount of energy escaping to the exterior environment increases with increasing diffusivity (similar findings [24]), conductivity, and outer surface temperature (i.e., Ql increases with increasing T_{out}). Therefore, walls with higher α and k values result in higher T_{out} and Ql, as the wall thermal resistance minimizes, as shown in Figure 7.11. Lower T_{out} values (closer to ambient temperature) show lower Ql values for the higher resistive walls.

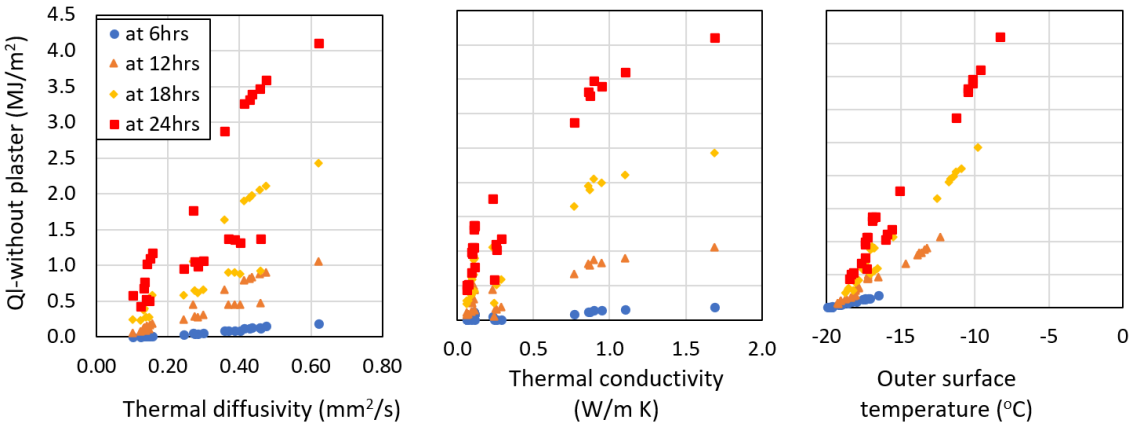

Figure 7.11: Relation between lost energy and thermal properties for unplastered wall

As an extension to Table 5 for storage energy, Table 7.6 shows the heat losses compared to unplastered walls having the same thermal diffusivity. Walls VC and HC3 have the same diffusivity (0.14 mm^2/s), but the energy loss varied by about 30% at 24 hours. This is attributed to lower thermal conductivity for HC3 compared to VC. Moreover, SD1 shows twice the loss of HC3 due to its higher thermal conductivity (about 75%). A similar comparison may be made between HC4 and SD2. Again, HC11 and DPF1 showed the same high thermal diffusivity values, with significantly different ρ, Cp, and k. However, the lost energy of DPF1 is dramatically higher (150% at 24 hr), resulting from higher thermal conductivity (about eight times) relative to HC11, which accounts for conduction heat transfer. Heat loss is a vital function of thermal conductivity as the wall is a conductor between the interior room and the external environment. For example, the product of ρ x Cp is high for SD1, which is expected to decrease the heat loss compared to VC, but the heat loss is higher for SD1 due to higher thermal conductivity. The effect of Cp and density

comes in second for the same or closer thermal conductivity values since the product of ρ x Cp helps increase the wall temperature and thus increases the potential of heat loss from the external surface to the ambient.

Table 7.6: Comparison between walls with the same diffusivity values in terms of lost energy, Ql.

Model ID	ρ kg/m^3	Cp J/kg K	k W/m K	α mm^2/s	Qs over 6hr (MJ/m^2)	Qs over 24hr (MJ/m^2)	Ql over 6hr (MJ/m^2)	Ql over 24hr (MJ/m^2)
VC	400	1720	0.09	0.14	1.63	2.99	0.01	0.77
HC3	330	1550	0.07	0.14	1.08	1.91	0.01	0.53
SD1	1427	1301	0.26	0.14	2.91	6.29	0.01	1.03
HC4	275	1500	0.06	0.15	0.91	1.56	0.01	0.51
WS2	1547	1077	0.25	0.15	2.78	5.80	0.01	1.10
SD2	1484	1261	0.29	0.15	3.00	6.43	0.01	1.18
HC11	351	650	0.105	0.46	0.75	0.92	0.12	1.38
DPF1	1150	1700	0.894	0.46	3.74	7.34	0.15	3.47

7.7.4 Lost energy for plastered concrete walls

Figure 7.12 exhibits that the implementation of wall plastering reduces the lost energy significantly. For example, the lost energy over 6 hr of plastered HC11 is 0.05 MJ/m^2, which jumped to 0.12 MJ/m^2 for the unplastered wall (i.e., an increment of about 140%)—the lost energy increases differently over time. Over 12 hr, the plastered and unplastered HC11 has Ql values of 0.33 and 0.49 MJ/m^2, respectively (i.e., the increment is about 50% compared to 6 hr). A similar

trend is found for 18 hr (0.74-0.93 MJ/m^2) and 24 hr (1.18-1.38 MJ/m^2), showing a lower increment in lost energy by about 25% and 17%, respectively, between plastered and unplastered walls. Therefore, the lost energy is increased for both cases (plaster and unplastered), with lower values for plastered walls. This reduction is because of the increase in the thermal resistance of the wall (by both k and wall thickness) and hence reduces the outer temperatures, as shown in Figure 7.13. Generally, plaster layers enhance the wall's performance in cold zones. Walls such as HC2, HC4, and WS1 exhibit the lowest values of Ql, as shown in Figure 7.12, resulting from either low thermal conductivity or diffusivity of the wall itself in addition to the plaster layer.

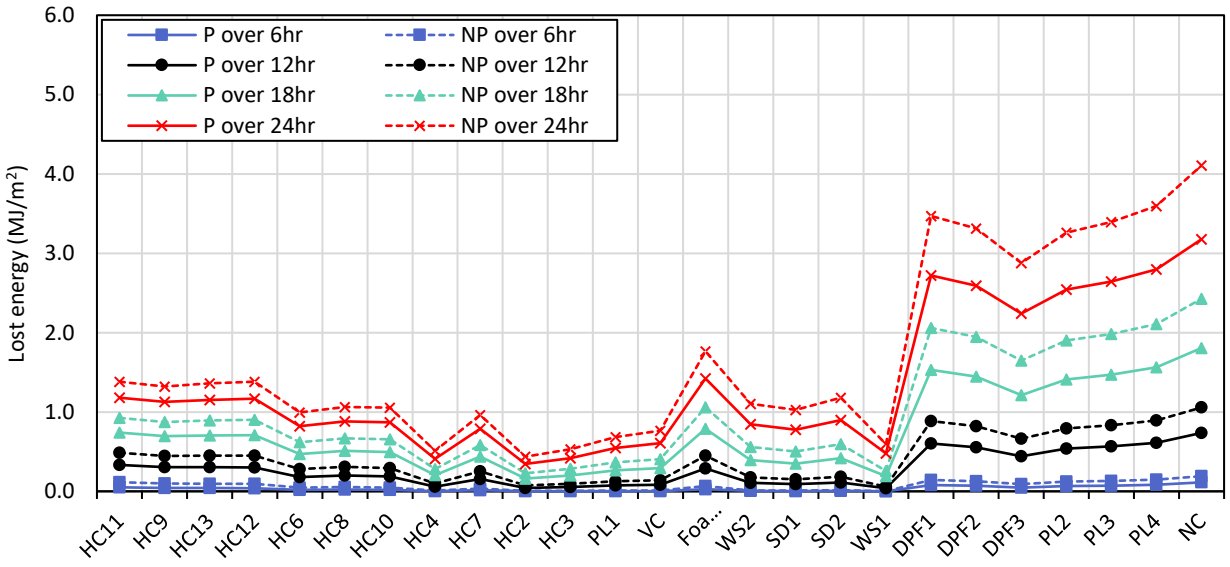

Figure 7.12: Effect of interior and exterior plasters on wall lost energy (Ql). The connecting curves only show the difference between plastered (P) and unplastered (NP) values.

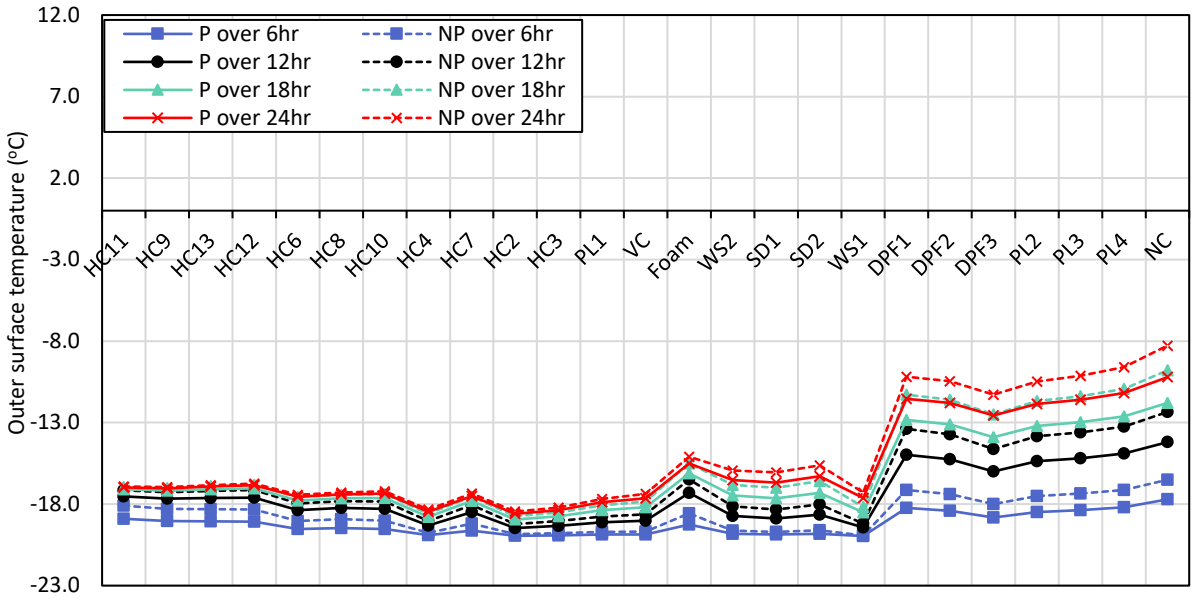

Figure 7.13: Outer surface temperature for plastered and non-plastered walls. The connecting curves only show the difference between plastered (P) and unplastered (NP) values.

Figure 7.14 summarizes the lost energy of plastered and unplastered walls. The plastered walls have lower heat losses by about 2 - 7% than the unplastered ones. Wall HC11 has the highest heat loss, while wall WS1 has the lowest. However, stored and lost energies should be considered to determine the best wall for cold weather based on this study's thermal performance, as discussed in the following section (Section 3.5).

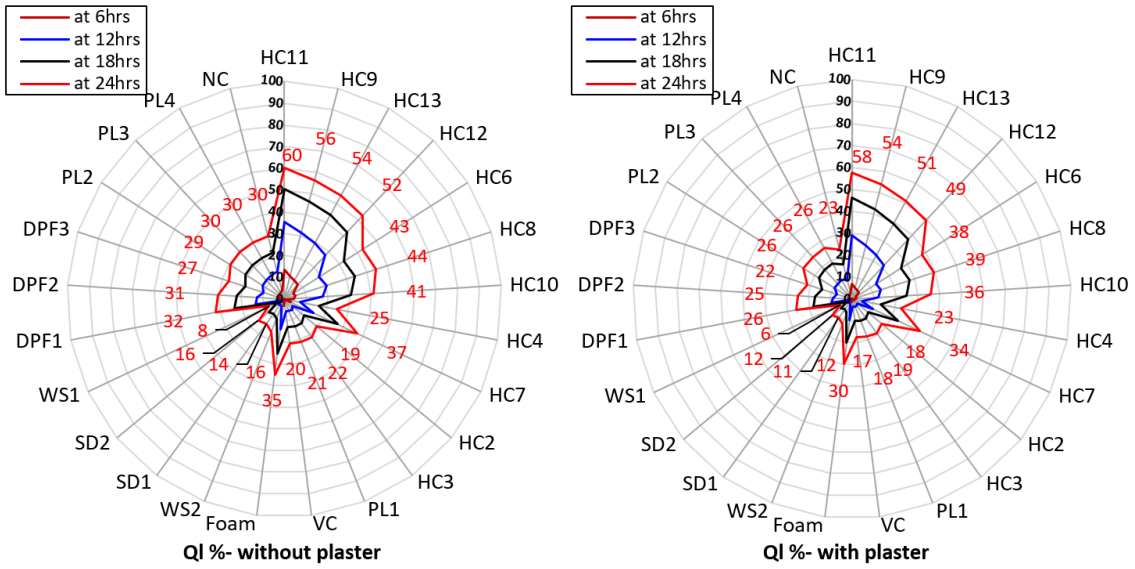

Figure 7.14: Lost energy for plastered and unplastered walls as a percentage.

7.7.5 Comparison between walls in terms of both stored and lost energy

The dual criteria for assessing different wall systems were the percentages of stored energy and the lost thermal energy from the total heat transfer from the room (i.e., the conditioned space) to the wall. Hence, the best candidate for a cold weather environment is one that maintains the highest stored energy and minimal loss. Figure 7.15 compares walls based on the percentage of energy storage and loss. The minimum energy loss was 8% for WS1, 14% for SD1, and 16% each for SD2 and WS2. That means these walls store higher thermal energy than the energy lost because of their relatively high ρ x Cp and low k. In other words, higher production of ρ x Cp leads to higher Qs, and lower k values result in lower Ql (which results in increased charging and discharging time). The hempcrete walls show massive variation in lost energy from 19 – 60% for HC11 – HC2 for the lower and upper limits, respectively. HC2 showed very high Cp values (1800 J/kg K) and low k value (0.06 W/m K), while Cp and k values for HC11 are 650 J/kg K and 0.105 W/m K, respectively, as shown in Table 7.2. This study predicts that the most efficient wall in cold climates is WS1, while the least efficient is HC11. Wall WS1 stores 92% of the energy transferred from the conditioned room to the wall, with only 8% losses over 24 hours. The simulation shows

that this wall performs even better over shorter periods. It is worth noting again that this study only focused on the thermal performance of the walls.

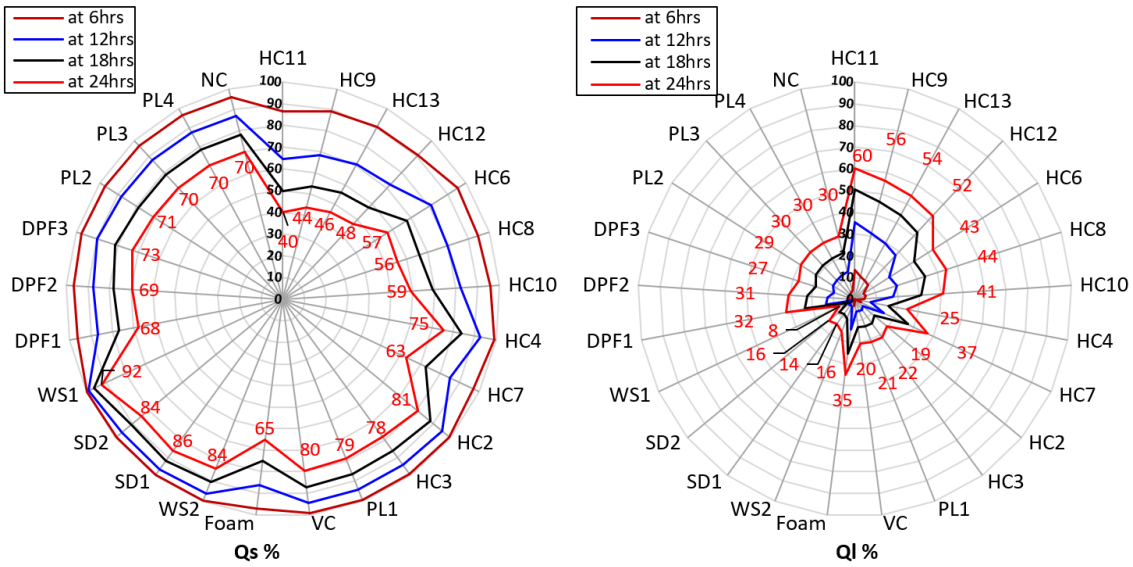

Figure 7.15: Comparison between stored and lost heat energy for investigated walls as percentages.

7.8 Concluding remarks

In this study, twenty-five different masonry walls (both with and without plaster) were selected from 400 wall elements described in the literature to be thermally assessed for their stored and lost energy in cold regions. A model was developed using ANSYS Fluent for simulating the heat transfer through walls. Experimental data mined from the literature was used to validate the proposed model. Based on the conditions examined by this study, the following conclusions may be drawn:

- The stored energy inside the walls is directly proportional to the product of density and heat capacity ($\rho \times C_p$) while inversely proportional to their thermal conductivity.
- The energy loss significantly increases with an increase in the thermal diffusivity and conductivity. A higher k-value makes the wall a good thermal conductor that transfers heat

from the conditioned room to the cold ambient exterior. The study confirms the preference for walls with low k-value. On the other hand, increased heat capacity and density led to higher heat loss by raising the wall temperature.

- Plastering does not impact the stored energy due to its small thickness. However, energy loss is reduced due to a slight reduction in the outer surface temperature of the walls.
- The study predicts that wall WS1, made with Portland cement + sand + 10% wood shives, performs best with 92% heat transferred from the conditioned room to the wall over 24 hours and only 8% losses to the ambient exterior. This is followed by wall SD1 (Portland cement + Sand + 10% sawdust), with 86% stored energy and 14% losses. Conversely, wall HC11 registers the minimum stored energy at 40% against maximum energy loss at 60%.
- High thermal diffusivity values do not directly reflect higher storing energy.

For future studies, estimating the energy consumption in actual buildings using the suggested walls in this paper and comparing performance with those with traditional walls is recommended. Also, it is recommended to experimentally evaluate the effect of hollow blocks to store and lose thermal energy and compare the performance to the filled cavities with insulation materials such as polystyrene and foam.

8 CHAPTER 8: PARAMETRIC STUDY (PART II: HEMPCRETE WALLS)

Journal paper #7

Experimentally and numerically thermal performance evaluation of hempcrete masonry walls

Ahmed S. Al-Tamimi, Naef A.A. Qasem, Vivek Bindiganavile

Journal of Energy Storage, Under review

Abstract

This work targeted the thermal performance of hempcrete walls due to the superior thermal properties, including the low thermal conductivity and high heat capacity (i.e., low thermal diffusivity). Twenty-five hempcretes were experimentally produced and thermally characterized. The thermal assessment also includes some hemp concretes from the literature for comparison purposes. A transient thermal model was developed using ANSYS Fluent to thermally assess the hempcrete walls to evaluate the energy storage and losses in cold weather (e.g., -20 ºC). Results showed that stored energy is mainly affected by the production of ρ x Cp, while lost energy depends on thermal conductivity and diffusivity. The highest stored energy, over 24 hours, observed in this study is 1.91 and 5.54 MJ/m^2 for HC3 (literature) and AAFA-NaOH (experimentally tested in this study), respectively, with a difference of 190 %. Further, the lowest value for lost energy is 0.44 and 0.42 MJ/m^2 for HC2 and S2-CA, respectively, representing lost percentages of 19 and 12 %. However, the stored energy for S2-CA is significantly higher than HC2, reaching 70 %. Thus, the S2-CA wall shows the best thermal performance among all walls investigated in this study regarding stored and lost thermal energy. Generally, hempcrete produced in this study (hempcrete II) shows a high potential due to the thermal performance with lower lost energy of 12 and 24 %. The literature on hempcrete (hempcrete I) shows losses between 19 and 60 %. Finally, increasing hemp content was noticed to increase stored energy (73 – 86 %) and reduce lost energy (14 – 27 %) due to high Cp and low k values of hemp aggregates.

Keywords: Hempcrete; masonry walls; thermal performance; cold weather; thermal energy

Nomenclature

Abbreviations

AAFA	Alkali activated fly ash
AAMK	Alkali activated metakaolin
C	Cement
FA	Fly ash
GGBS	Ground granulated blast furnace slag
HC	Hempcrete
HS	Hemp shives
Li	Hydrated lime
MK	Metakaolin
NHL	Natural hydraulic lime
PNC	Prompt natural cement
S	Sand
SF	Silica fume

Symbols

Cp	Specific heat capacity (J/kg K)
E_{in}	Energy inflow (J)
E_{out}	Energy outflow (J)
E_{st}	Stored Energy (J)
h_{film}	Film coefficient (W/m^2)
k	Thermal conductivity (W/m K)
Nu	Nusselt number
Pr	Prandtl number
Ql	Lost thermal energy (MJ/m^2)

Qs	Stored thermal energy (MJ/m^2)
q_x	Heat rate (W)
q_x"	Heat flux (W/m^2)
Ra	Rayleigh number
RH	Relative humidity (%)
T_{amb}	Ambient temperature (^oC)

Greek letters

α	Thermal diffusivity (mm^2/s)
ρ	Density (kg/m^3)

8.1 Introduction

In recent decades, the quality of buildings has improved significantly with growing living standards and enhancing construction materials. Therefore, standards were initiated for building excellence in indoor air quality and acoustic and thermal insulation. The thermally comfortable environment is mainly controlled by heating and cooling systems to maintain the desired indoor temperature. Thus, the outdoor weather conditions and indoor climate need lead to various energy requirements and costs, which differ from country to country.

The building envelopes, including exterior walls, windows, cladding, exterior structural members, thermal bridges, etc., are the most critical elements affecting heat exchange between interiors and exteriors, hence affecting the energy consumption of the building. Therefore, a comprehensive analysis is needed for building envelopes to identify the poor thermal behavior and, in accordance, improve design and construction decisions for sustainable buildings and saving energy. Facilities in the European Union consumed about 40% of total energy, in which space heating substituted about 60 – 80 % of total buildings consumption in the European Union [1], 63% in Canada [2], and 42% in the USA [3]. Consequently, massive energy could be saved if the thermal properties of the building envelope sufficiently improved, including thermal conductivity, diffusivity,

density, and specific heat capacity. However, this study focused on masonry blocks as building envelopes since blocks are widely used for building exteriors worldwide. Concrete masonry units are widely used as a construction material for the masonry industry, with an annual production of about 4.3 billion units in the USA and Canada [4]. Further, governments established minimum requirements for energy and thermal performance of buildings and construction materials such as thermal insulation of building envelopes, including European Parliament [5], Canadian Standards Association (CSA) (A165 SERIES-14- R2019) [6], American Society for Testing and Materials (ASTM) for concrete masonry units [7].

Massive experimental and numerical studies focused on developing and designing masonry blocks to adapt to the thermal requirements of building envelopes to minimize energy consumption. However, computational fluid dynamics (CFD) is commonly used in many areas of engineering due to the ability to model structures with different materials, shapes, scales, and boundary conditions [8]. Therefore, the thermal behavior of walls is widely modeled, and estimations are demonstrated by real testing for validation [8]. Thermal insulation materials are used in wall construction for solid and hollow masonry blocks or block-filling cavities to minimize equivalent thermal conductivity.

Many literature studies conducted thermal models using ANSYS due to the powerful tools to apply boundary conditions for conduction, convection, and radiation for exposed and closed surfaces [9][10]. Blocks with different types and materials were modeled in ANSYS to evaluate the thermal performance as solid, hollow, and filled cavities with insulation materials, as shown in Figure 8.1. Al-Awsh et al. [9] assessed hollow concrete blocks with different insulation materials in the mixture (not filling the cavities), such as low-density polyethylene (LDPE), expanded polystyrene beads (EPS), vermiculite (VL), and volcanic scoria aggregate. The block has the same cavities arrangement layout and dimensions, tested experimentally using a hot plate device for the equivalent thermal conductivity. The thermal Ansys model simulated the test setup of the insulation blocks at steady state, which matched the experimental outcomes and proved about 15% enhancement on the volcanic block's thermal resistance compared to the control block without insulation materials (same cavities layout and dimensions). The boundary conditions were

conduction, convection, and radiation on both wall surfaces, and cavities were considered filled with air; thus, convection and radiation were included in holes. Similar boundary conditions were applied by Hongxia et al. [10] to evaluate the sintered coal hollow blocks with ordinary clay blocks in terms of thermal conductivity; thus, the model was conducted at a steady state, which proved an enhancement of coal block with about 65%.

The effect of filling cavities of hollow blocks with insulation materials was investigated numerically (using BISCO) and experimentally (using a hot-guarded plate) by Wernery et al. [11]. The experimental data showed a significant reduction in thermal conductivity for the hollow blocks filled with aerogel than perlite by about 12%. However, the decline in thermal conductivity of blocks with filled cavitied with perlite and aerogel could reach 80 and 92%, compared to unfilled cavities. The two-dimensional model with BISCOO showed an acceptable matching with test results with a difference of less than 12%. Hollow concrete blocks with an embedded insulation layer of extruded polystyrene were thermally evaluated using the hot box method (steady state) by Su et al. [12]. The test was simulated using ANSYS with the same boundary condition as previous authors, which showed an acceptable matching with an error of less than 6%.

The hybrid cases of the cavities for the hollow block were targeted by Marcos et al. [4] experimentally and numerically, in which holes were filled with air or insulation materials (cardboard, EPS, and foam). The experimental data was extracted from the hot box test, while the simulation was generated using ANSYS Fluent. The model and experimental results emphasized the importance of convection and radiation, which occurs inside the cavities, on the overall thermal performance of hollow blocks with empty cavities. The results proved the importance of filling the cavities with insulation materials, dramatically improving the blocks' thermal performance, reaching four times. Similar studies include the two scenarios of holes, such as Kant et al. [13] and Blanco et al. [8], to focus on the improvement and simulation capability of such cases using ANSYS and other thermal tools.

Interestingly, the cavities layout (arrangements and dimensions) of hollow blocks were explored by Al-Tamimi et al. using ABAQUS [14] to find out how cavities affect heat transfer and optimize

cavities layout for better thermal performance. Convection and radiation inside the holes were applied using ISO standards 6946, and ambient temperatures with exterior solar radiation were utilized as boundary conditions. The resultant cavities layout was patented and optimized for standard block dimensions [15].

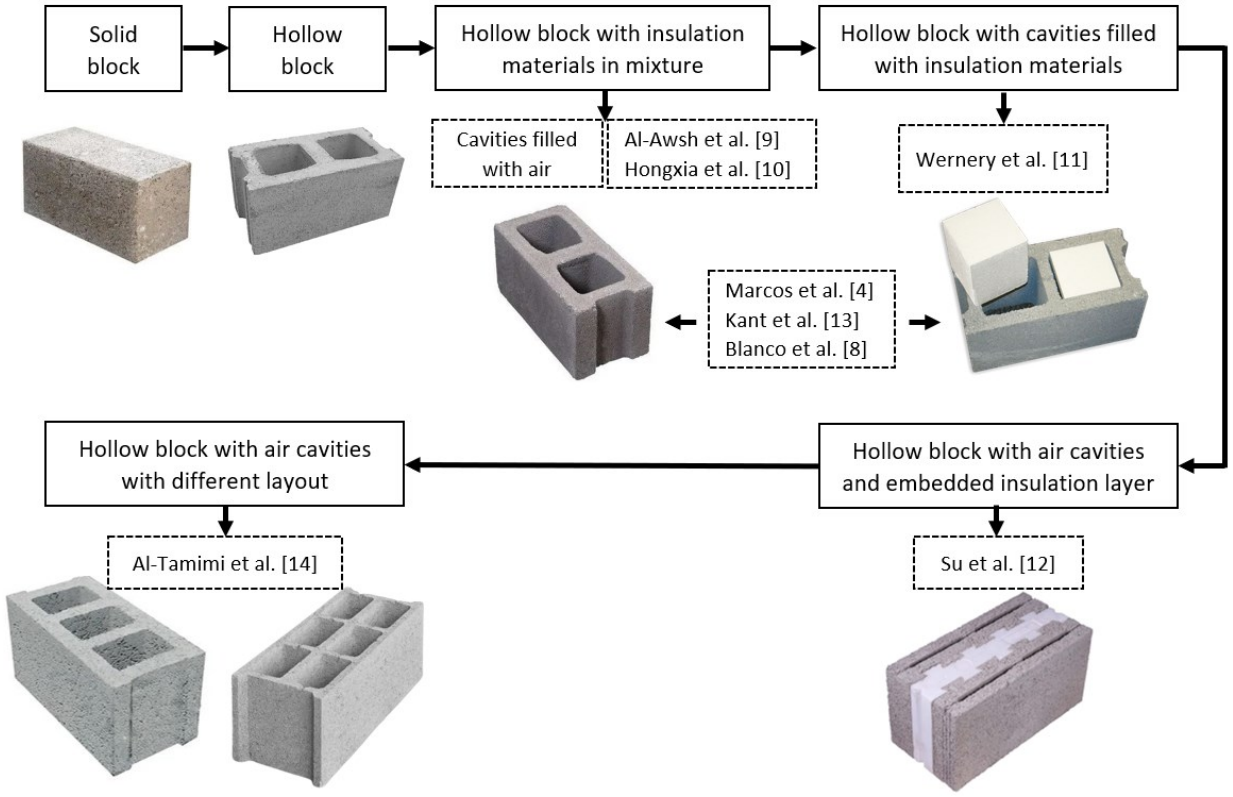

Figure 8.1: The literature methods on thermal models with different types of masonry blocks.

The lost energy and required energy were measured using a thermal model in 2-D (using the *Therm* program) and 3-D (using *EnergyPlus*) for an apartment assumed to be located in Lisbon (Portugal) by Real et al. [1]. Four different types of structural lightweight concrete were used in the model to investigate the effect of reducing thermal bridges. However, the thermal properties of the four concretes were measured experimentally in the lab, which are major inputs for the model with the inclusion of boundary conditions. Model outcomes proved a reduction of losing thermal energy

between 11-19%, compared to thermal bridging with normal concrete, while the required energy was reduced by about 20%. However, this percentage will change with changing climate conditions (location) worldwide. A similar full-scale model was generated for a building using EnergyPlus by Haika et al. [16] to measure the energy consumption of such a building made of lime hempcrete, hollow concrete blocks, and expanded polystyrene. The thermal model was supported with full-scale experimental work for the three buildings, which validated the model to a great degree of confidence. Lime hempcrete showed a promising result with about 82 90% reduction in the required energy for cooling and heating, compared to hollow concrete blocks.

This study targets the thermal performance evaluation of hempcrete on storing and losing thermal energy in cold weather countries such as Canada due to the promising thermal properties and potential noticed from literature about hempcrete. Two groups of hempcrete data were explored, including some reported in the literature and some produced experimentally in the present study. The ANSYS Fluent model is developed and validated against hot plate experimental data to evaluate the energy loss and storage. The study explores the effect of hempcrete's thermal diffusivity (i.e., ρ, Cp, k) on transient heat transfer to suggest the best hempcrete for cold weather conditions. Plaster addition to the wall is also investigated.

8.2 Research methodology

Figure 8.2 shows the followed methodology to achieve the objectives of this study. First, the authors explored thermal models in literature for building envelope assessment, the available thermal simulation software, boundary conditions, and preferred results. Then, the thermal transient model was created and verified with literature experimental data for the hot plate test. Towards the goals of this study, two groups of data were collected, as illustrated in Section 8.6. Finally, the model results were summarized, analyzed, and compared to attain inferences about stored and lost thermal energy in/from the building envelope and a richer understanding of the influencer factors.

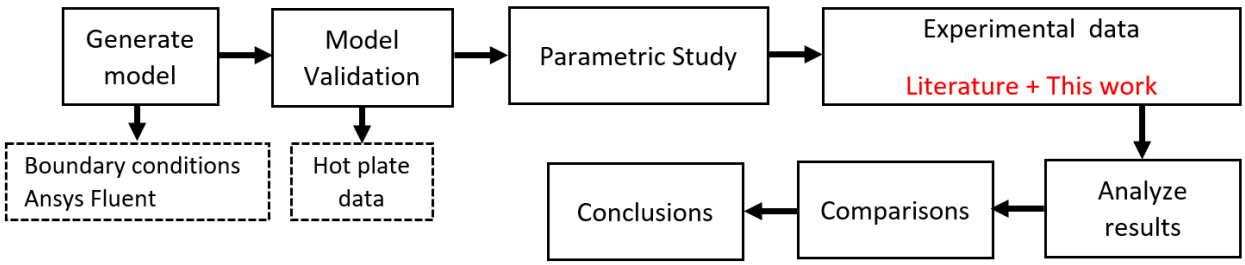

Figure 8.2: Methodology of parametric study

8.3 Mathematical model

As shown in Figure 8.3, a 400 x 400 mm wall was duplicated of part 200 x 200 mm using ANSYS Fluent to assess the thermal performance of hempcrete as a masonry wall with solid blocks. The energy conservation equation and transient heat transfer governed the model. Thus, hempcrete walls could be evaluated for the stored and lost thermal energy over the day (24 hrs). The heat transfer by convection and radiation was considered on both wall surfaces. Mortar is connected to block units as one body with different thermal properties. However, the connection zones were considered perfect bonds with no gaps or friction (similar consideration by [9]).

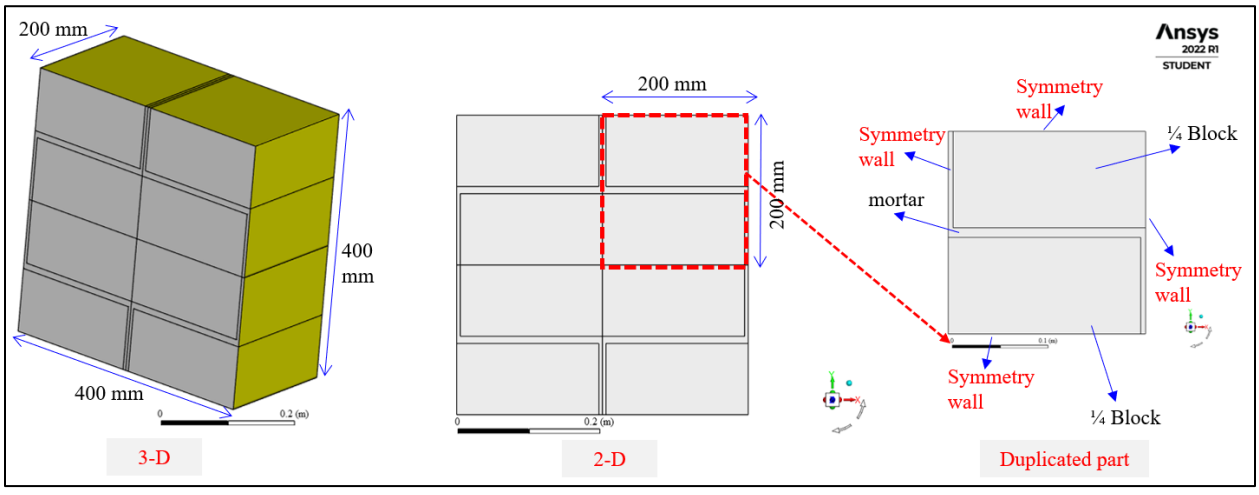

Figure 8.3: Masonry wall and symmetric part used in the model.

8.3.1 Governing equations

As shown in Eq- 8.1, the energy equation without radiation in one direction governs the transient heat flow [17].

$$E_{stored} = E_{in} - E_{out} \qquad \textbf{Eq- 8.1}$$

Eq- 8.2

Estored is the stored energy inside the wall, Ein is the energy flowing from the room (warm place) to the wall, and E_{out} is the energy escaping from the wall to the exterior cold environment.

The amount of stored thermal energy in the wall system could be stated as follows:

$$E_{stored} = C_p\, \rho \frac{\partial T}{\partial t} dx\, dy\, dz \qquad \textbf{Eq- 8.3}$$

The rate of thermal conduction (q_x W or J/s) can be estimated from Fourier's law (Eq- 8.4):

$$q_x = -k\, dy\, dz \frac{\partial T}{\partial x} \qquad \textbf{Eq- 8.4}$$

Now, the transient heat transfer equation in the x-direction (1-D), incorporating stored energy and conduction through the wall (Eq- 8.5):

$$C_p \rho \frac{\partial T}{\partial t} = k\, \frac{\partial}{\partial x}\left(\frac{\partial T}{\partial x}\right)$$

Eq- 8.5

Equation Eq- 8.5 could be expressed in terms of thermal diffusivity, as in Eq- 8.6:

$$\frac{\partial T}{\partial t} = \alpha \frac{\partial^2 T}{\partial^2 x^2} \qquad \textbf{Eq-8.6}$$

8.3.2 Boundary conditions

The heat exchange between both wall surfaces and the corresponding ambient environments occurs due to convection and radiation separately on both surfaces, as expressed in Eq- 8.7 and Eq- 8.8 [9].

$$k_w \left(\frac{\partial T_{w,ex}}{\partial x}\right) = h_{ex}\left(T_{w,ex} - T_{amb,ex}\right) + \varepsilon_{ex}\sigma\left(T_{w,ex}^4 - T_{amb,ex}^4\right) \qquad \textbf{Eq-8.7}$$

where k_w is the thermal conductivity of the wall (W/m K), h is the convection heat transfer coefficient (W/m^2 K), $T_{w,ex}$ is the exterior wall surface temperature (K), $T_{amb,ex}$ is the external ambient temperature (K), ε_{ex} is the emissivity of outer wall surface, and σ is the Stefan–Boltzmann constant (5.6703x10^{-8} W/m^2 K^4). Similarly, for the internal wall,

$$tightk_w \left(\frac{\partial T_{w,in}}{\partial x}\right) = h_{in}\left(T_{w,in} - T_{amb,in}\right) + \varepsilon_{in}\sigma\left(T_{w,in}^4 - T_{amb,in}^4\right) \qquad \textbf{Eq-8.8}$$

The film coefficients at the vertical walls were estimated using Eq- 8.9, and more details about calculations could be found [17]:

$$h = \frac{Nu * k_{air}}{L} \qquad \textbf{Eq-8.9}$$

Where k_{air} is the thermal conductivity of the air, L is the vertical length of the wall, and Nu is the Nusselt number.

The film coefficients for interior and exterior wall surfaces were calculated using the previous equations as 3 and 3.5 W/m^2 K, respectively. Figure 8.4 shows the thorough boundary conditions on the wall.

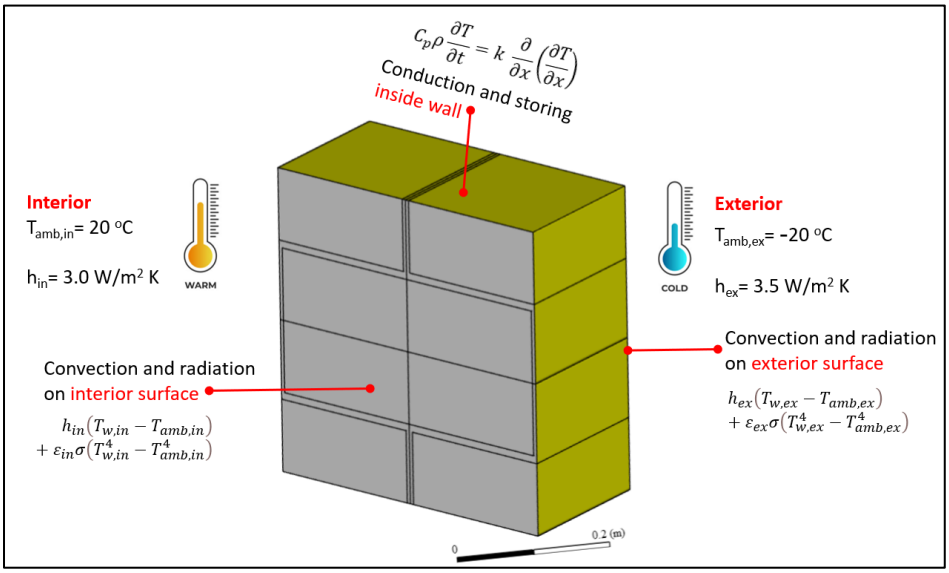

Figure 8.4: Boundary conditions for the thermal model used in this study.

8.4 Mesh independence

Mesh was verified in this study to ensure the quality of model results. Thus, nine trials with various numbers of cells (0.40, 1.0, 7.0, 16.0, 31.0, 73.0, 128, 250, and 411 k) were examined, representing

cell sizes 35 – 3.4 mm, as illustrated in Figure 8.4. Mesh verification was assessed regarding the walls' exterior surface temperature (Tex), flow time, and cell size, as presented in Figure 8.5. The external temperature stabilized with reduced cell size, reaching 0.02 % at a cell size of 3.40 mm with several cells equal to 411 k, which was chosen for further models.

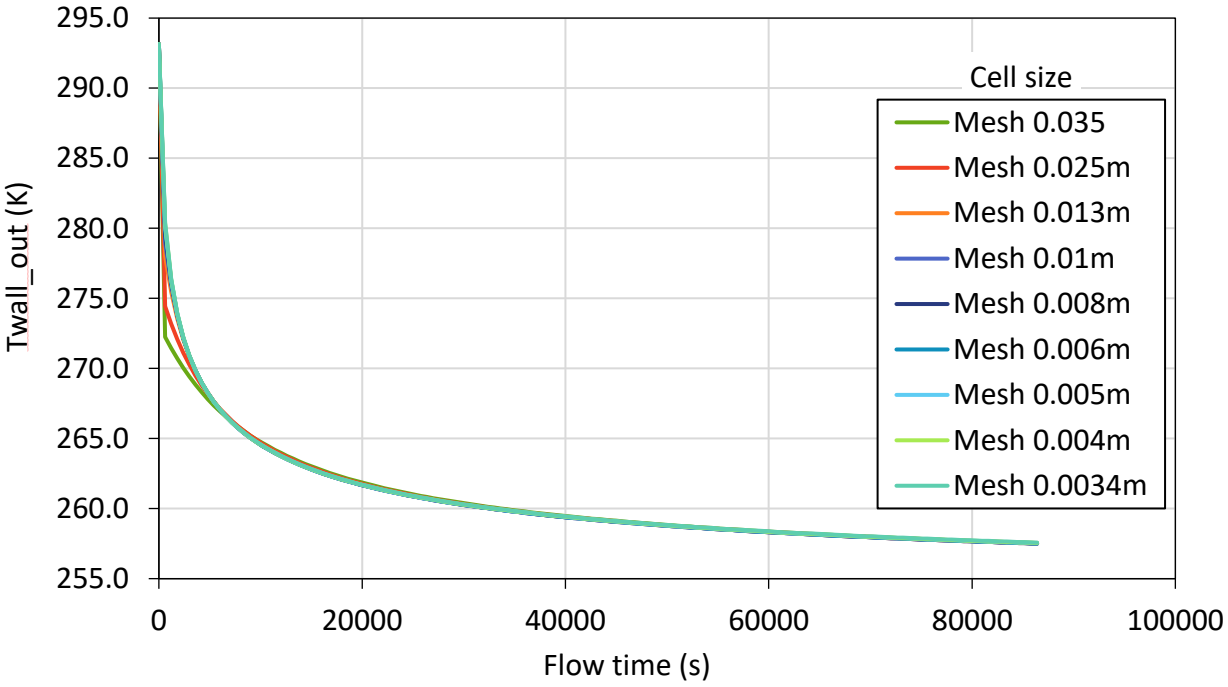

Figure 8.5: Mesh independence study.

8.5 Model validation

For model validation, an experimental study was selected from the literature about testing hempcrete walls for thermal conductivity using the hot plate method [18]. As shown in Figure 8.6, a hempcrete wall of 0.90 m x 0.90 m and a thickness of 0.30 m was installed on the test setup, where the hot plate was in contact with the wall surface and the other wall surface was exposed to ambient conditions [18]. Further, thermocouples and heat flux sensors were attached to both wall surfaces to observe surface temperature and flux.

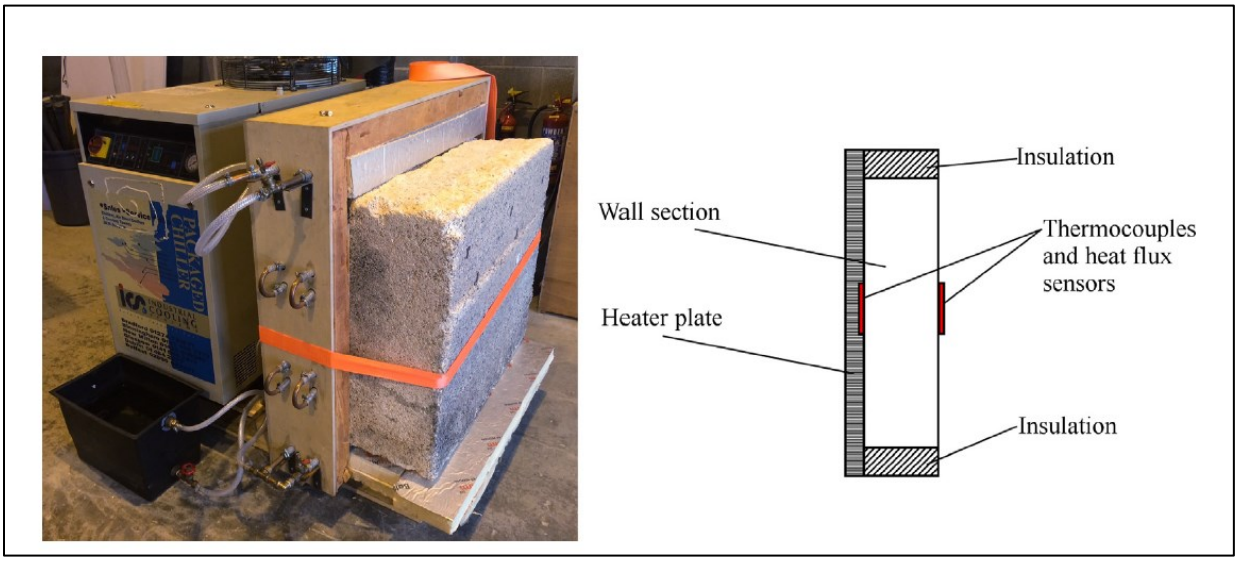

Figure 8.6: Setup of the hot plate device with lime hemp concrete sample [18]

Testing started with setting the heater temperature at 60ºC, heating the wall surface, causing a temperature gradient, and flowing heat toward the cold side of the wall (ambient). The temperature and heat flux were monitored on both wall surfaces to ensure reaching a steady state, which was achieved after about 40 hours. The experimental data in Table 8.1 was used for model verifications, which attained a reasonable agreement with the experimental data, as shown in Figure 8.7.

Table 8.1: Model input parameters

Sectional Properties	Thermal Properties	Boundary Conditions
Wall thickness = 0.30 m	K = 0.129 W/m K	T_{hot} = 51ºC
Wall area= 0.90x0.90 m	Cp = 1627 J/kg K	T_{cold} = 20ºC
	P = 508 kg/m^3	Transient time = 300,000 s

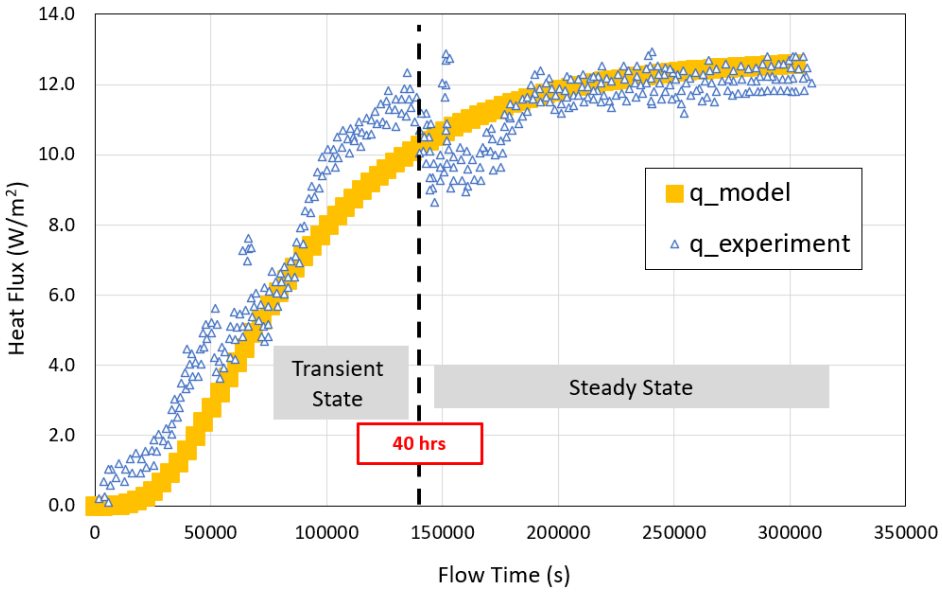

Figure 8.7: Validation of the CFD model against the present experimental data regarding temporal heat flux.

8.6 Materials and data

This study used two categories of materials, including literature concretes and hemp concretes, produced and tested in the lab for their thermal properties. In the model, blocks with a dimension of 40 cm x 40 cm x 20 cm were drawn and assembled to build a wall of 1 m x 1 m, which connected with two types of mortars (cement or lime mortars) depending on the kinds of concrete binder.

8.6.1 Hempcrete I: From Literature

A lot of data was collected from the literature for different types of concretes tested for their thermal properties, including density, thermal conductivity, specific heat capacity, and thermal diffusivity (about 400 mixtures). Then, all data are assembled and sorted four times: ascending for k, α, and ρ; descending for Cp to ensure considering concrete with the lowest k, α, and ρ; and

with the highest Cp. After that, from each group, ten concretes were selected for modeling. Hempcretes were assembled, as summarized in Table 8.2.

Table 8.2: Thermal properties of different concretes from literature

Mix ID	Mix Components	B/H	ρ	k	Cp	α	Ref
			kg/m^3	W/m K	J/kg K	mm^2/s	
HC11	PNC + HS-fibered (S1<10mm) - Light compaction	2.0	351	0.105	650	0.46	[19]
HC9	PNC + HS-un-fibered (S2<S1)- Light compaction	2.0	340	0.103	750	0.40	
HC13	PNC + HS-fibered (S1<10mm)- Heavy compaction	2.0	415	0.110	690	0.38	
HC12	PNC + HS-un-fibered (S2<S1) - Heavy compaction	2.0	410	0.115	760	0.37	
HC6	75% Li + 15% NHL5 + 10% FA + HS (RH=15%)	1.10	1001	0.094	333	0.28	[20]
HC8	75% Li + 15% NHL5 + 10% FA + HS (RH=65%)	1.10	1111	0.100	300	0.30	
HC10	75% Li + 15% NHL5 + 10% FA + HS (RH=15%)	1.80	995	0.105	385	0.27	
HC7	Hempcrete	NA	413	0.100	1000	0.24	[21]
HC4	Commercial hempcrete for Ext. wall		275	0.060	1500	0.15	[22]
HC3	Commercial hempcrete for floor	NA	330	0.070	1550	0.14	
HC2	Standard mix of TRADICAL hempcrete		275	0.060	1800	0.12	

8.6.2 Hempcrete II: Present Experimental Data

An experimental program was conducted to study the thermal properties of hempcrete in the first phase of this study. Four groups of binders were investigated for strength and thermal properties, including cement-based, lime-based, cement-lime-based, and alkali-activated, as shown in Table 8.3. However, the binder-to-hemp ratio was fixed (2.50), and the hemp size was the same (S4-FR) supplied by LCDA in France and met all technical standards of French hemp building professional rules, as shown in Figure 8.8. The components were mixed (binder + hemp + water) using a rotary pan mixer; then, the homogeneous mixture was poured into a disc with a diameter of 75mm and a thickness of 30mm. Next, samples were cured for 28 days in a humidity room. After that, samples were dried in the oven for 24 hours at 60^{o}C. Finally, one surface was ground to flatten the surface (Figure 8.8) and be ready for the thermal test.

(a) **(b)**

Figure 8.8: (a) Hemp hurds aggregate; (b) Hempcrete samples disc for thermal properties measurements

The thermal diffusivity and conductivity were assessed using the transient plane source (TPS) measurement technique called Hot Disk Method (HDM) [23]. TPS 1500 has three probes: Kapton, Mica, and Teflon sensors. In this study, Hot Disk TPS 1500 (Thermal Constants Analyzer) was used to measure the thermal constants of the prepared samples of hemp concrete with an accuracy better than 5% according to ISO 22007-2 [23]. As shown in Figure 8.9, the setup mainly comprises a TPS-1500, PC, and Kapton-insulated probe with a radius of 14.60 mm, which is embedded horizontally between two halves of the tested specimen. The hot disk acts as a heat source and resistance thermometer to raise the sample temperature and record time-dependent temperature increases [23].

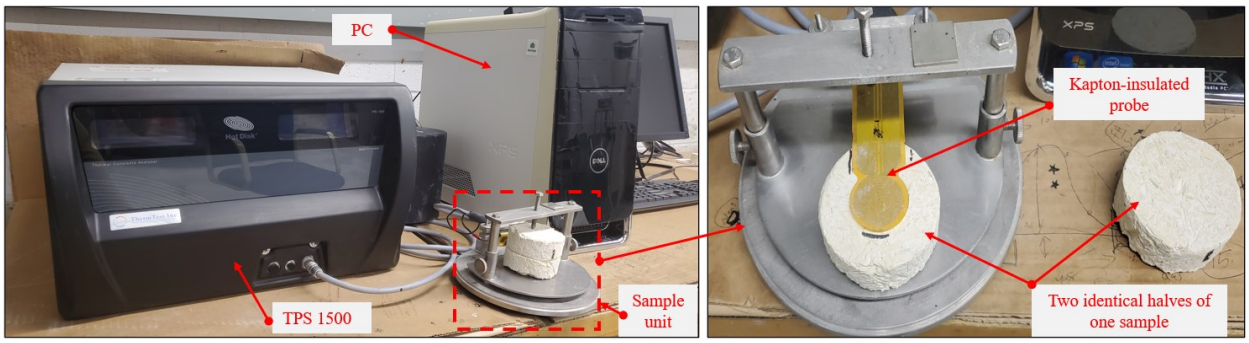

Figure 8.9: TPS 1500- Thermal Constant Analyzer with a sample unit.

The principle of the Hot Disk Method is to produce a heat pulse for a defined period (by electrical current) in the form of a stepwise function through a hot disk sensor to generate a dynamic temperature field within the specimen's two halves [23]. The increase in the average temperature of the hot disk probe is measured as a function of time by monitoring the electrical resistance of the probe (sensor or adaptor) [23][24]. The solution of the thermal conductivity equation is given by Eq- 8.10 and Eq- 8.11:

$$\Delta T_s(\tau) = \frac{P_o}{\pi^{1.5}\, rk} D(\tau) \qquad \textbf{Eq-8.10}$$

$$\tau = \sqrt{\frac{\alpha(t - t_c)}{r^2}} \qquad \textbf{Eq-8.11}$$

Where $\Delta T_s(\tau)$ is the temperature increase of the sample surface, P_o is the output power from the probe, r is the radius of the probe, k is the thermal conductivity of sample, $D(\tau)$ is a dimensionless specific time function [23], α is thermal diffusivity of sample, t is the total measurement time, t_c is time correction less than 0.5% of the total time because the development of full output power does not coincide exactly with t=0

To solve equation (Eq- 8.10), an iteration procedure with diffusivity (α) and time correction (t_c) is established, and a linear relationship between $\Delta T_s(t)$ and $D(\tau)$ is created. The values of α and t_c were obtained from the last step of iteration. Finally, thermal conductivity is the slope of the generated line.

The iteration (guessing values for α and t_c) continued until the temperature increase (ΔT) difference between every two constitutive points was less than 0.01°C. The values of the last iteration are the corresponding material results of α and t_c. To calculate the k value, the values of ΔT(τ) and D(τ) corresponding to the last iteration α and t_c were picked up and implemented into Eq- 8.10. Further, the slope of the generated chart between ΔT(τ) and D(τ) reflects the thermal conductivity value. Finally, the volumetric heat capacity (C_v) could be obtained by dividing thermal conductivity by thermal diffusivity.

$$C_v = \frac{k}{\alpha} \qquad \textbf{Eq- 8.12}$$

If the bulk density of samples is available, the specific heat capacity (C_p) could be calculated.

$$C_p = \frac{C_v}{\rho} \qquad \textbf{Eq- 8.13}$$

The thermal properties (k, α, C_p) were measured for three samples from each mixture and three readings for each sample. Thus, the measured properties are the average of nine readings (3 readings/sample) with less than 10% COV. The experimental results of hempcrete mixtures were summarized, as shown in Table 8.3.

Table 8.3: Thermal properties of experimental hempcrete in this study

Mix ID	ρ	k	Cp	α	Mix ID	ρ	k	Cp	α
	kg/m^3	W/m K	J/kg K	mm^2/s		kg/m^3	W/m K	J/kg K	mm^2/s
C	549.08	0.11	1578.88	0.13	C+Li+30%SF	533.37	0.10	1862.62	0.11
C+30%SF	527.94	0.11	1844.03	0.11	C+Li+30%FA	546.13	0.16	1798.82	0.16
C+30%FA	507.35	0.09	1719.17	0.10	C+Li+30%MK	617.64	0.19	1796.17	0.17
C+30%MK	511.34	0.09	1654.11	0.11	C+Li+30%GGBS	553.21	0.11	1485.41	0.14
C+30%GGBS	529.24	0.10	1559.81	0.12	AAFA-NaOH	836.82	0.22	1981.22	0.13
70%C+30%Li	534.44	0.11	2061.86	0.10	AAMK-NaOH	718.66	0.15	1512.48	0.14
Li	476.27	0.10	1863.79	0.11	AAFA-(Na2SiO3)	724.25	0.21	1990.91	0.15
Li+30%SF	445.61	0.09	1456.63	0.14	AAMK-(Na2SiO3)	724.70	0.16	1651.03	0.13
Li+30%FA	446.17	0.10	1571.34	0.15	AAFA+AAMK	773.35	0.21	1910.58	0.14
Li+30%MK	459.88	0.09	1782.59	0.11	S4-FR	548.45	0.13	1571.42	0.15
Li+30%GGBS	507.22	0.15	1624.93	0.18	S1-CA	505.34	0.11	1595.67	0.14
70%Li+30%C	542.83	0.18	2024.56	0.16	S2-CA	434.47	0.07	1557.55	0.11
50%C+50Li	527.07	0.13	1524.87	0.16	S3-CA	566.57	0.10	1565.99	0.11

As shown in Table 8.4, cement and lime mortars were used for block connections, which were used with the same block binder. However, the emissivity coefficient is assumed to be the same for all walls for model simplicity and lacks values for all concretes. Based on the literature, the emissivity coefficients for masonry surfaces are in the range of 0.85 – 0.95; thus, this study takes the average value as 0.90 for the whole research [4].

Table 8.4: Thermal properties of mortars and plasters used in this study

	Thickness (mm)	Material	ρ (kg/m^3)	k (W/m K)	Cp (J/kg K)	α (mm^2/s)	ε	Ref
Mortar	10	Cement mortar	2143	0.42	570	0.34	0.90	[4]
		Lime mortar	1251	0.25	960		0.90	

8.7 Results and discussions

The first step in this parametric study is generating the thermal model considering the proper boundary conditions and material properties. Then, the model validation process with experimental data from the literature using the hot plate method. Finally, the model with two groups of thermal data for hempcrete, including literature experimental data and this study's experimental data, is illustrated in Figure 8.10. The walls were not plastered in this case because the target is to evaluate the difference between the hempcrete of the literature and this study in terms of storing and losing heat capabilities.

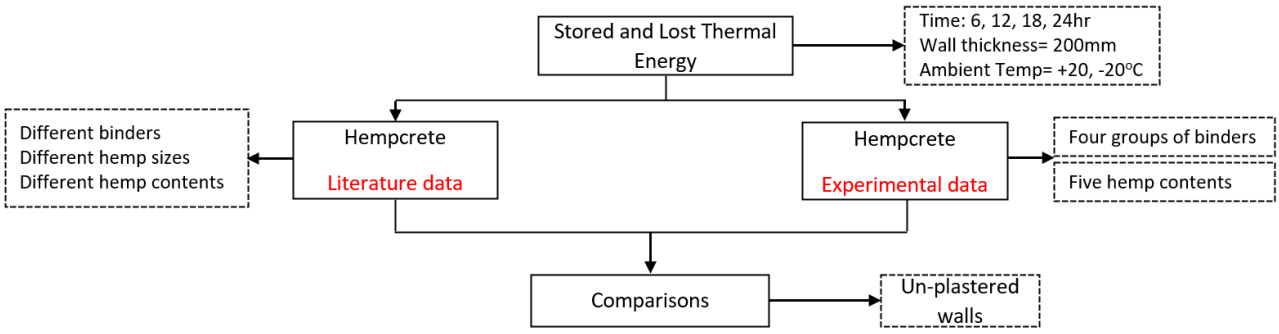

Figure 8.10: Milestones of parametric study

As shown in Figure 8.10, this study aims to assess the thermal performance of different wall systems for storing and losing thermal energy. Thus, the time factor is significant to be evaluated as 6, 12, 18, and 24 hr. The interior and exterior ambient temperatures were assumed to be constant

for model simplicity, and wall thickness was considered constant (200mm), and thickness variation is not targeted in this study.

The results obtained from the CFD model are internal surface, external surface, average wall temperatures, and heat flux. Such that the stored and lost energy can be estimated. Figure 8.11 shows some representative 3-D plots for masonry block walls built. The figure shows an increased temperature gradient and heat flux at connection zones (mortar) with values higher than blocks, ascribed to the thermal bridging of the mortar due to their relatively higher thermal properties.

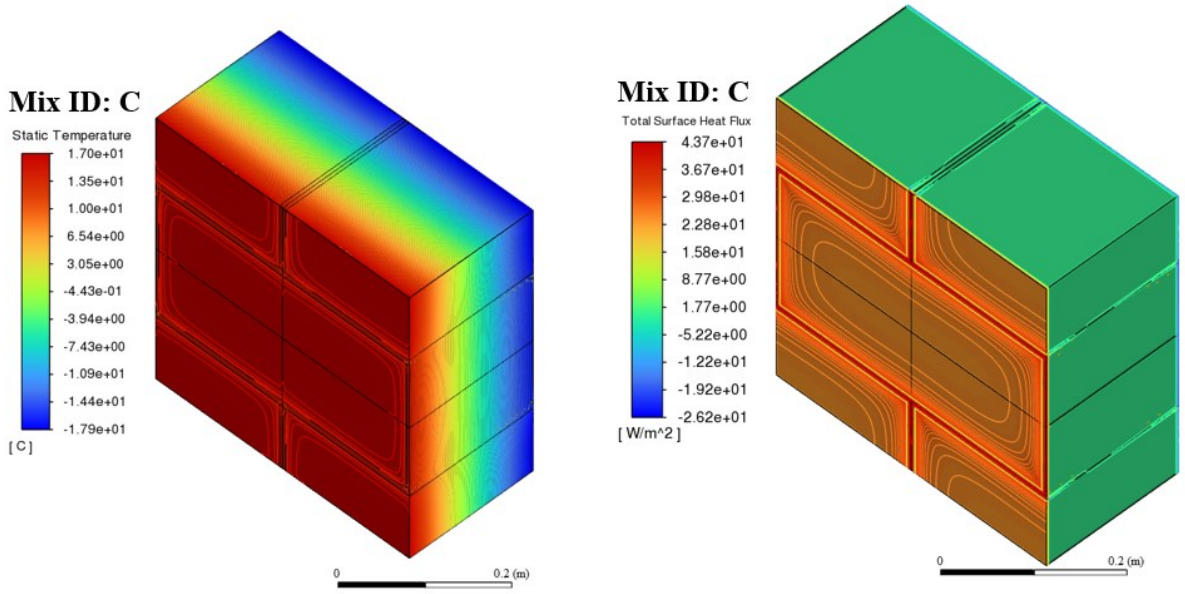

(a)

Figure 8.11: Typical 3-D plots for temperature and heat flux

8.7.1 Stored and lost heat energy for hempcrete walls II

The experimental data for thermal properties of hempcrete, including conductivity (0.07 – 0.22 W/m K), diffusivity (0.10 – 0.17 mm^2/s), Cp (1460 – 2060 J/kg K), resistance (0.90 – 2.69 m^2 K/W), and U-value (0.37 – 1.11 W/m^2 K) are shown in Figure 8.12 (a). The highest density is for wall AAFA-NaOH (837 kg/m^3), heat capacity for 70%C+30%Li (2060 J/kg K), and resistivity for S2-CA (2.69 m^2 K/W), while the lowest thermal conductivity is for S2-CA (0.070 W/m K), thermal diffusivity for 70%C+30%Li and 70%C+30%FA (0.10 mm^2/s), and transmittance for S2-CA (0.37 W/m^2 K). For the literature hempcrete, the range of measured properties is as follows: thermal conductivity (0.06 – 0.115 W/m K), diffusivity (0.12 – 0.46 mm^2/s), Cp (300 – 1800 J/kg K), and density (275 – 1111 kg/m^3), resistivity (1.74 – 3.33 m^2 K/W), and transmittance (0.30 – 0.58W/m^2 K), as shown in Figure 8.12 (b). As a comparison between the two groups, the least k values are similar, while Cp and α from group II are considerably higher, with about 13 % and 17 %, respectively. However, the highest wall resistivity with 200mm thickness is observed for HC2, about 24 % higher than S2-CA.

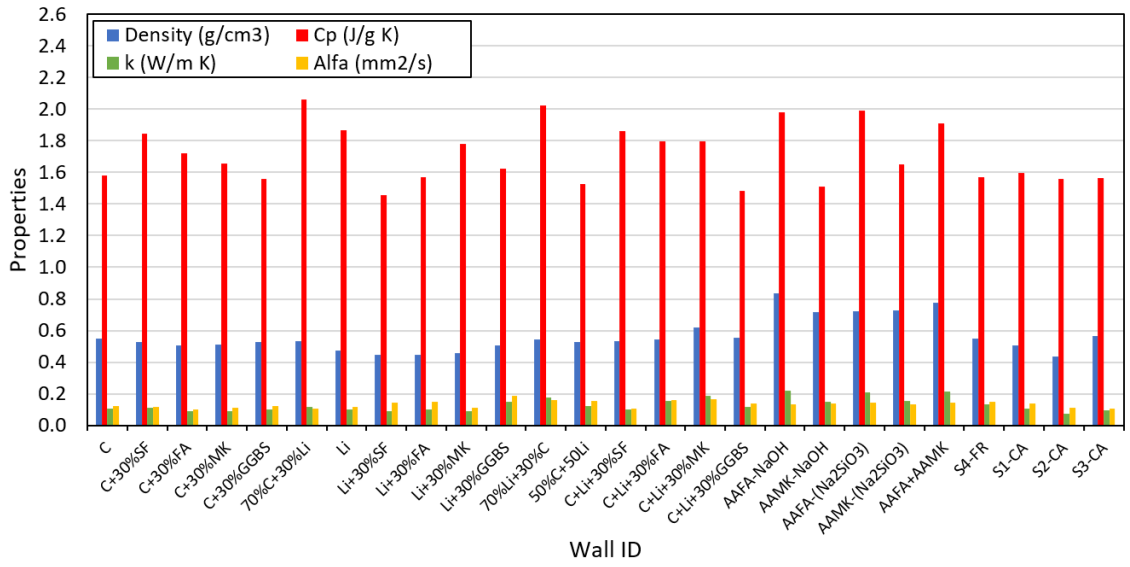

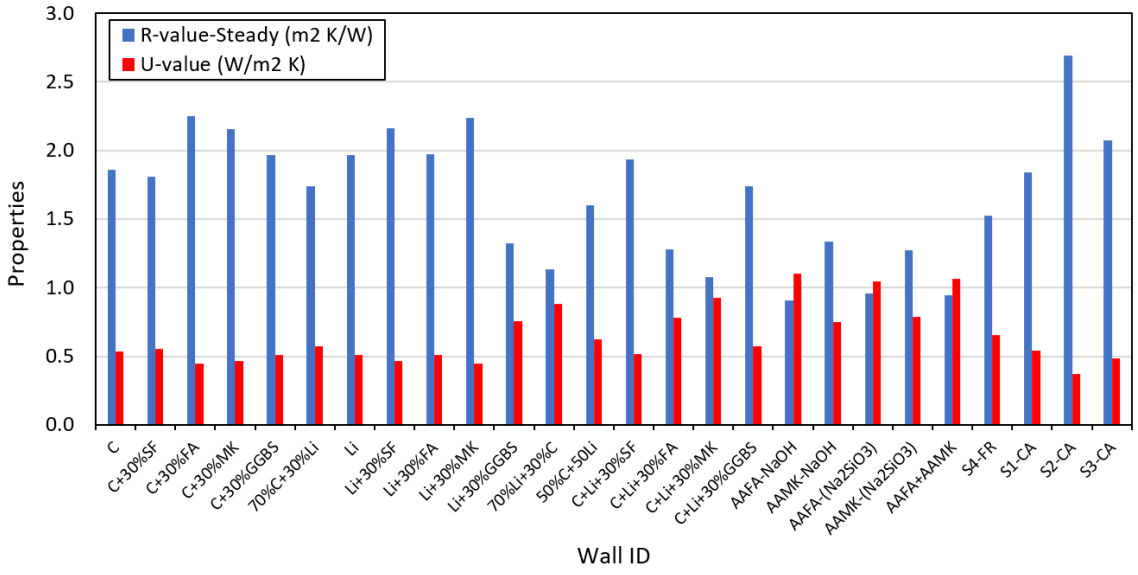

(a)

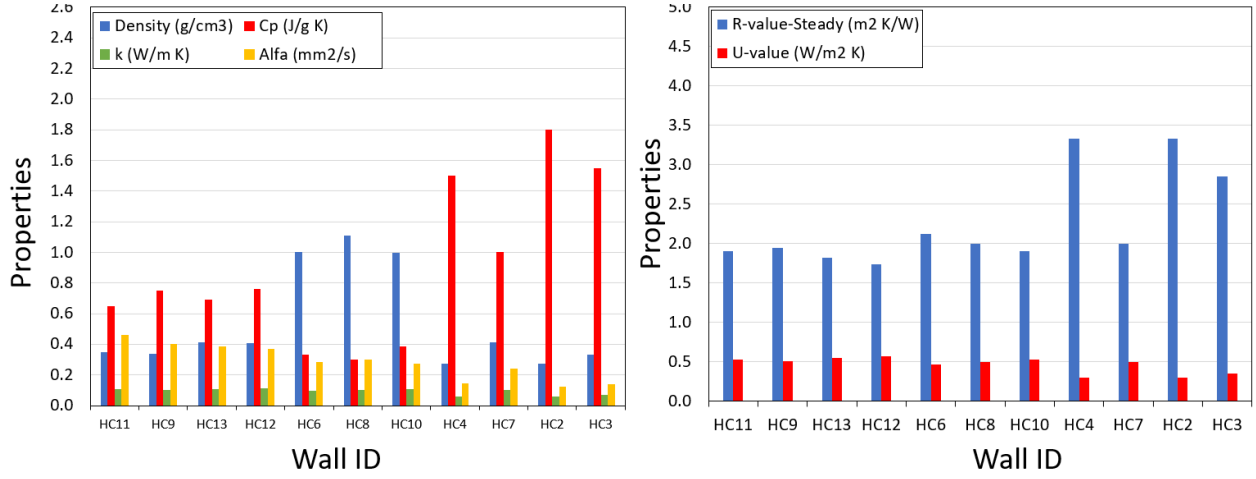

(b)

Figure 8.12: Physical and thermal properties of hempcrete walls: (a) Group II, (b) Group I

8.7.1.1 Stored energy

As shown in Figure 8.13, hemp concrete's stored energy varies between 2.38 – 5.54 MJ/m^2 after 24 hr. However, the values increase significantly with time in the 80 – 110 % range between 6 and 24 hr. The highest three values are 5.54, 5.08, and 4.98 MJ/m^2 for alkali-activated mixture walls

AAFA-NaOH, AAFA+AAMK, and AAFA-Na_2SiO_3, respectively, which ascribed to their higher r×Cp values, as shown in Figure 8.12. On the other hand, the least three Qs values are observed with lime-binders SF, FA, and MK representing 2.38, 2.57, and 2.84 MJ/m^2, respectively, due to the lower production values of r×Cp. In conclusion, the production r□Cp values directly affect the stored energy. Thus, higher density and heat capacity walls show higher stored energy values. The walls of hempcrete in Figure 8.13 could be classified in terms of stored energy into five groups based (on 24 24-hour) to evaluate the performance of individual walls:

- Group I (Qs = 2.30 – 3.30 MJ/m^2): 14 Walls,
- Group II (Qs = 3.31 – 4.30 MJ/m^2): 9 Walls
- Group III (Qs = 4.31 – 5.30 MJ/m^2): 2 Walls
- Group IV (Qs > 5.30 MJ/m^2): 1 Walls

Hempcretes show higher heat capacity values, as depicted in Figure 8.12, while the densities are relatively lower; hence, the Qs values are low, such as Group I walls. On the other hand, Group III and Group IV showed somewhat higher values (reaching 56%) due to the increment of density and heat capacity.

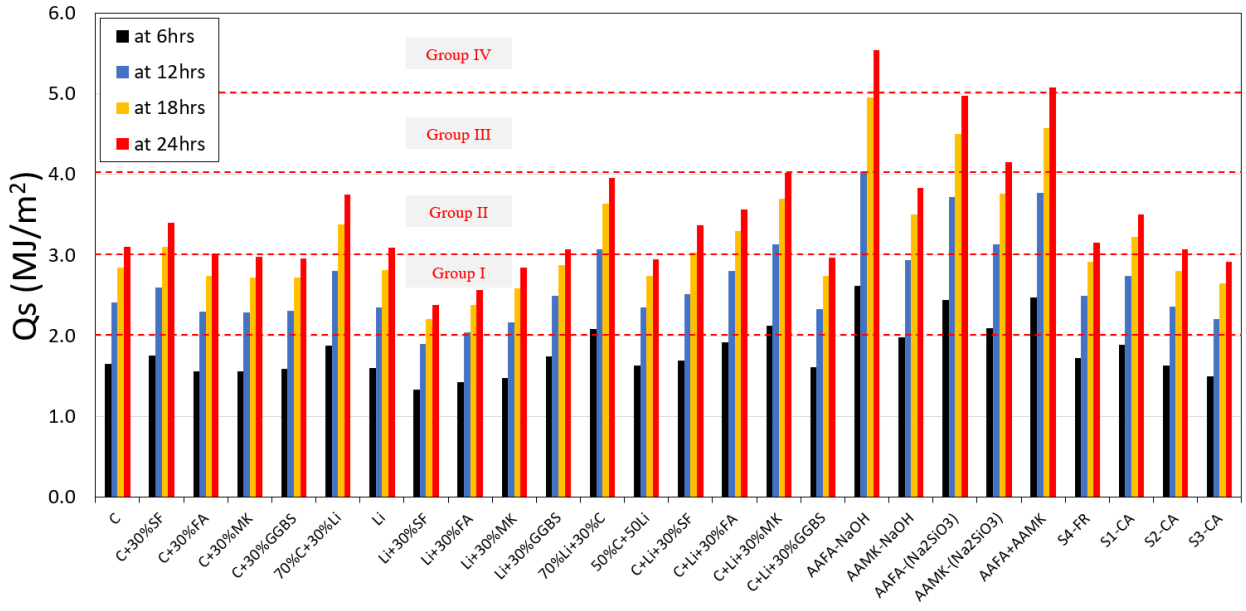

Figure 8.13: Stored heat energy into hemp concrete walls produced in this study.

8.7.1.2 Lost energy

The lost energy for hemp concrete showed little values not exceeding 1.0 MJ/m^2 after 24 hours, as shown in Figure 8.14. Surprisingly, the lost energy over the first 6hrs was negligible for all walls. Then, the values increased slightly, revealing a max value of 0.2 MJ/m^2 at 12hrs, while loss reached 0.55 MJ/m^2 at 18hr (i.e., about 175 % increment). The least value of Ql observed by S2-CA mixture with about 0.42 MJ/m^2 at 24hr due to the least k values (about 0.07 W/m K), as shown in Figure 8.12. The highest values observed by Li+GGBS and C+Li+MK with 0.99 and 1.0 MJ/m^2, respectively, which attributed to their highest values of conductivity (0.15-0.19 W/m K) and diffusivity (0.18-0.17 mm^2/s), as shown in Figure 8.12. The walls could be categorized into five groups for their lost energy:

- Group I (Ql = 0.40 – 0.50 MJ/m^2): 4 Walls,
- Group II (Ql = 0.51 – 0.60 MJ/m^2): 4 Walls
- Group III (Ql = 0.61 – 0.70 MJ/m^2): 7 Walls
- Group IV (Ql = 0.71 – 0.80 MJ/m^2): 4 Walls
- Group V (Ql > 0.8 MJ/m^2): 6 Walls

Four walls of Group I showed the least escaped energy due to the lower k-values (0.07, 0.10, 0.10, 0.09 W/m K), while the highest Ql observed for Group V with relatively higher k-values (0.18, 0.13, 0.16, 0.19, 0.15, 0.21, 0.21 W/m K).

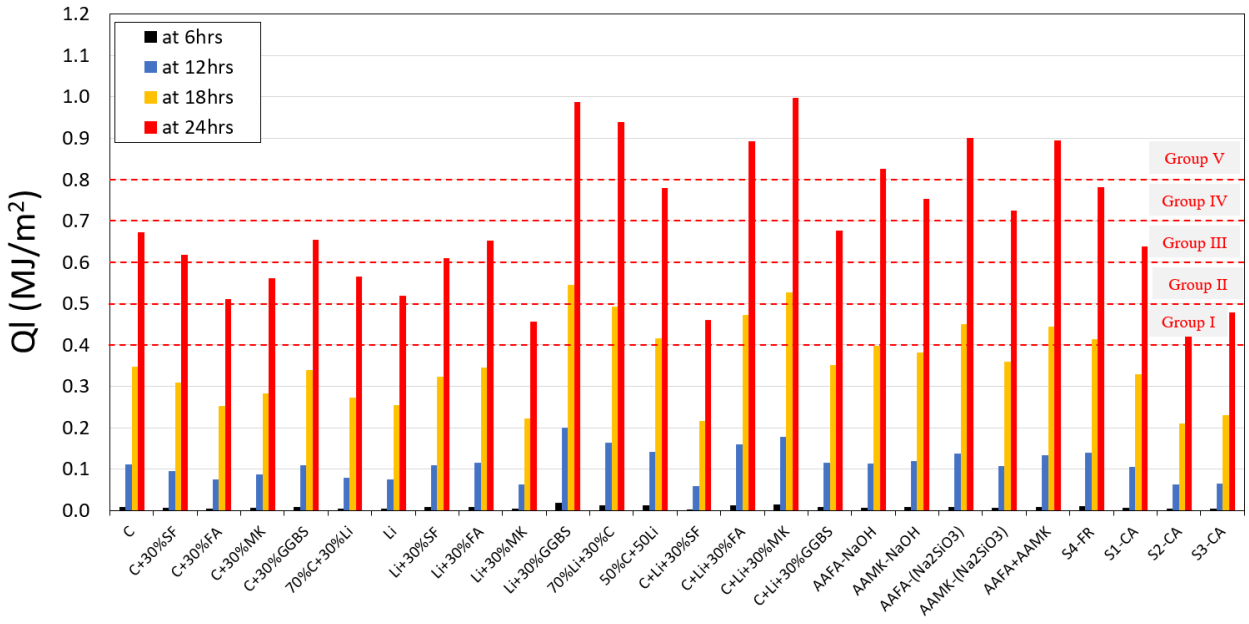

Figure 8.14: Lost heat energy in hemp concrete produced in this study.

As shown in Figure 8.15, the lost energy increases with increasing the values of thermal conductivity, diffusivity, and outer surface temperature. Thus, the walls with higher thermal properties (k, α) result in higher values of lost energy. Consequently, materials with lower thermal conductivity and diffusivity are desirable for building envelope and thermally efficient performance.

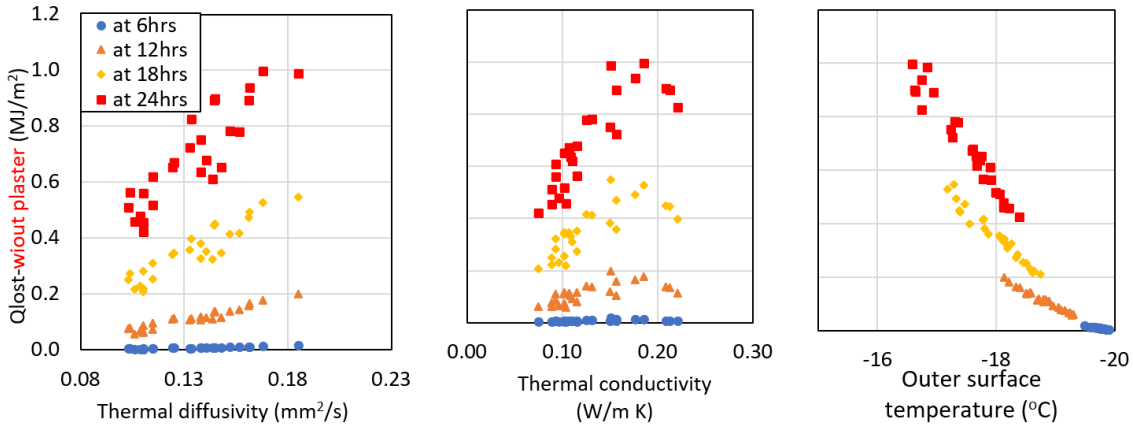

Figure 8.15: Relation between lost energy and thermal properties of hempcrete walls

8.7.1.3 Comparison between stored and lost energy

As a comparison between stored and lost thermal energy in hempcrete walls, Figure 8.17 shows interesting results illustrating no loss at the first 6hr and a minimal loss after 12hr, which proved the superior insulation property of hemp concrete with high storing ability reaching 4 MJ/m^2 at 12 hr. At 18 hr, the walls start losing considerable heat because of earning a higher storage capacity, which continues increasing heading the storing capacity limit. A comparison between percentages of stored and lost energy is carried out to assess each wall, which is presented in the next section.

8.7.1.4 Comparison between hemp concrete for walls (Literature and experimental data)

Figure 8.16 shows the stored and lost energy from the literature hempcrete (Hempcrete I) over 24 hrs. Most energy is stored in the first 6hrs and slightly continued charging until 24hrs, indicating a lower capacity than hempcrete II in Figure 8.13. Most walls lost some energy at the first 6hrs (3 walls showed almost zero), which hempcrete II similarly observes in Figure 8.14.

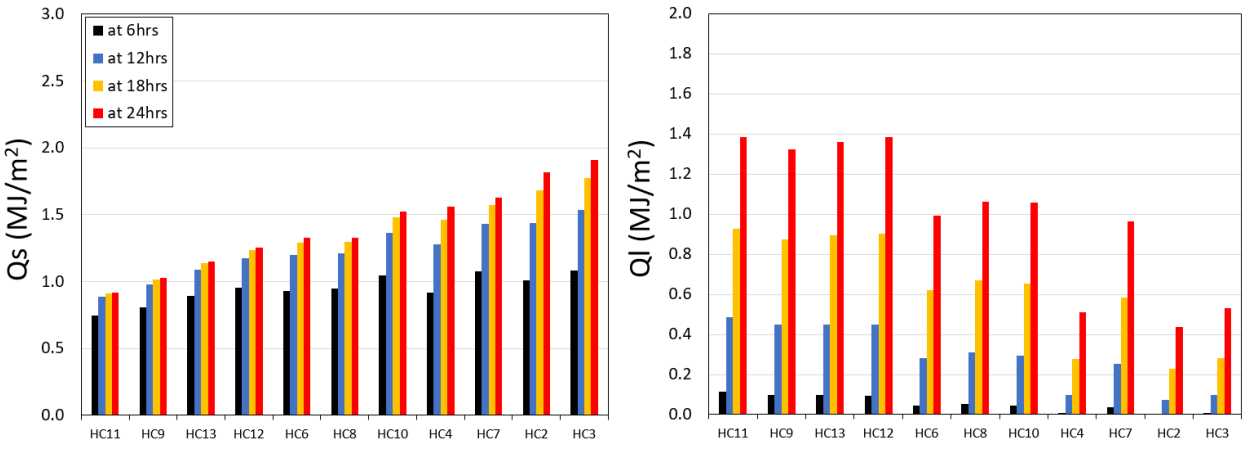

Figure 8.16: Stored and lost heat energy for hempcrete walls from literature

As summarized in Table 8.5, the stored energy recorded for hempcrete in this study (Hempcrete II) is significantly higher than literature hempcrete walls, reaching 160 – 190 % due to the relatively higher $\rho \times Cp$. Further, the lost energy of this study wall showed a substantially lower value (5 – 40 %) compared to the literature walls due to the lower conductivity, diffusivity, and higher heat capacity.

Table 8.5: Comparison between stored and lost thermal energy values for hempcrete in this study and the literature.

Time (hr)	Qs (MJ/m^2)		Ql (MJ/m^2)	
	This study	**Literature**	**This study**	**Literature**
Over 6	1.33-2.48	0.75-1.08	0.00-0.02	0.01-0.12
Over 12	1.90-4.04	0.88-1.53	0.06-0.20	0.07-0.49
Over 18	2.21-4.95	0.91-1.78	0.21-0.55	0.23-0.93
Over 24	2.38-5.54	0.92-1.91	0.42-1.00	0.44-1.38

For assessing the values of stored and lost thermal energy into/from different hempcrete walls, the percentages of stored energy and corresponding lost energy are calculated and presented in Table 8.6 and Figure 8.17. Hemp concretes produced in this study showed significantly higher stored energy and lower lost thermal energy at each time interval than literature hempcrete (Table 8.6 and Figure 8.17). This may be ascribed to smaller diffusivity values (0.10 – 0.18 mm^2/s) for hempcrete produced in this study relative to literature hempcrete (0.12 – 0.46 mm^2/s). However,

literature hempcrete has a conductivity of (0.06 – 0.12 W/m K) similar to produced hempcrete (0.07 – 0.18 W/m K).

Table 8.6: Comparison between stored and lost thermal energy percent for hempcrete in this study and the literature.

Time (hr)	Qs %		Ql %	
	This study	Literature	This study	Literature
Over 6	100	87-100	0	<13
Over 12	>95	64-94	>5	6-36
Over 18	87-93	50-88	7-13	12-50
Over 24	76-88	40-81	12-24	19-60

As shown in Table 8.6 and Figure 8.17, the stored energy after 6hr demonstrates about 100% storing energy (i.e., Ql= 0%), which proves the high thermal efficiency of hempcrete produced in this study (showing lower diffusivity values in Figure 8.12). However, the stored energy reached 76 – 88% after 24 hours (about 12 – 24 % losing energy), which is relatively higher than the literature hempcrete (40 – 81 %), as shown in Figure 8.17 (b). From group II data, the minimum percentage of Ql after 24 hours is 12%, representing hempcrete walls S2-CA and C+Li+30%SF with the same diffusivity value (0.11 mm^2/s). At the same time, the minimum Ql% from literature hempcrete is about 19 % for HC2 with a diffusivity value of 0.12 mm^2/s for the same time interval. Interestingly, higher thermal diffusivity hempcrete increased lost energy, as depicted with HC11-9-13 and 12 with diffusivities of 0.46, 0.40, 0.38, 0.37 mm^2/s, respectively, showing lost energy of 60, 56, 54, and 52 %, respectively. In conclusion, hempcrete produced in this study showed promising thermal performance for cold weather regions due to the lower lost energy, which is zero lost at 6 hours and not exceeding 24 % after 24 hours.

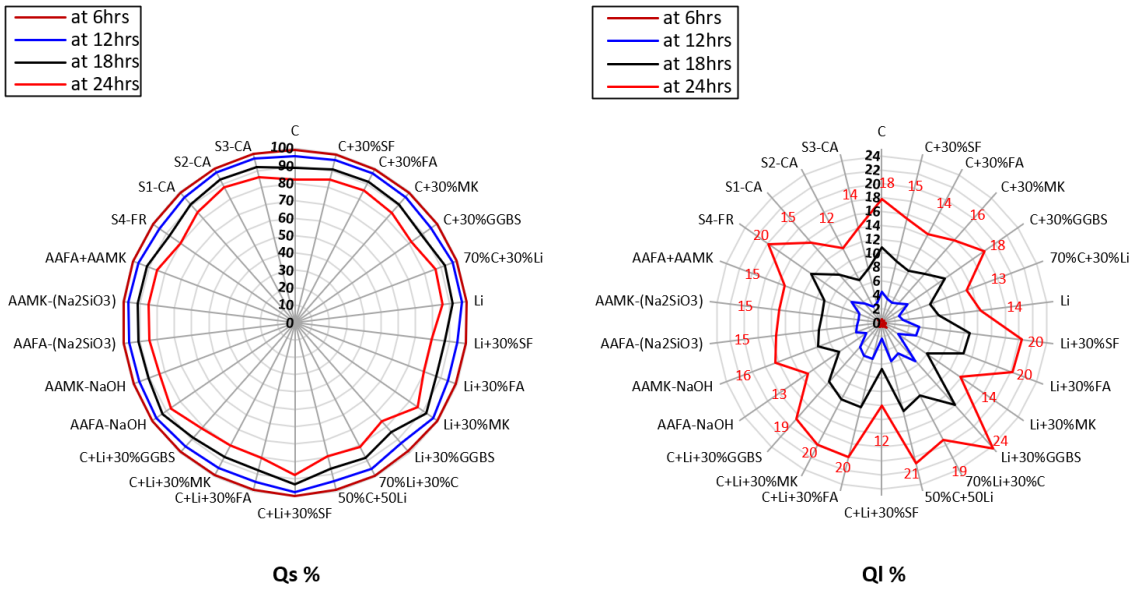

(a)

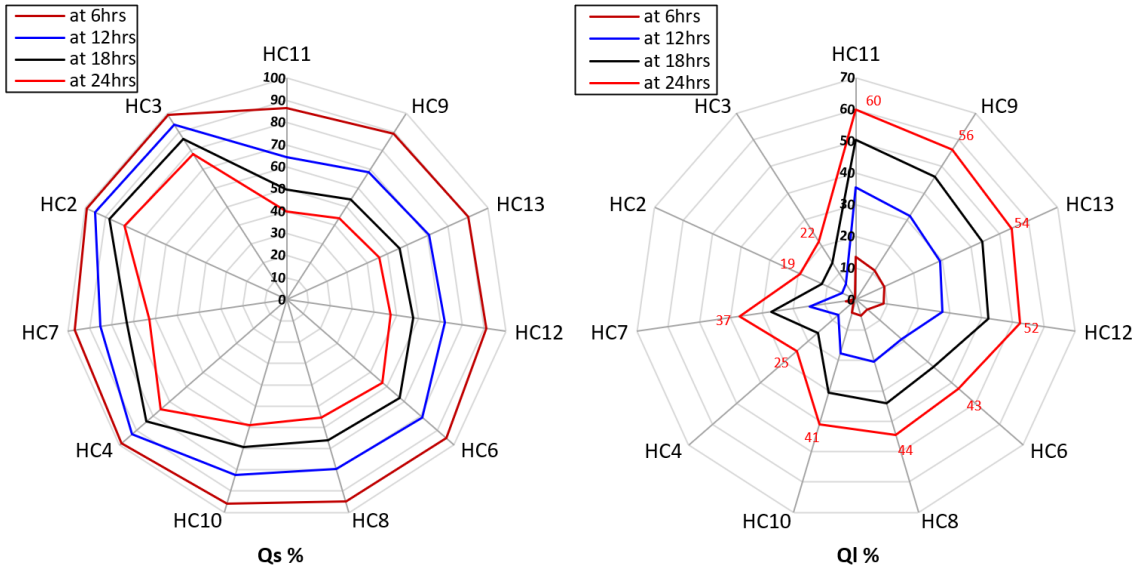

(b)

Figure 8.17: Comparison between stored and lost heat energy as percentages for hempcrete from (a) this study and (b) the literature

8.7.2 Effect of hemp content on stored and lost energy

The experimental data of hempcrete with varying hemp content were used in the model to address the effect of hemp content on stored and lost thermal energy. The results of Qs and Ql are presented as percentage and amount with their corresponding hemp contents in Figure 8.18. The stored energy increases significantly with time from 1.66 – 3.43 MJ/m^2, and the lost energy also increases from 0.01 – 1.14 MJ/m^2 between 6 and 24 hr. At 6hr, the stored energy is about 100% and minimal lost energy, showing superior thermal performance. At 24 hr, the stored energy decreased due to increasing lost energy, reaching a maximum percentage of 27 % for a hemp content of 20 %. On the contrary, the least lost energy is observed by 100 % of hemp content, with about 14 %. However, other hemp contents (40 – 67%) show a 15 – 18% lost energy. Noticeably, the lost energy significantly decreases from 27 % to 16 % with increasing hemp content from 20 % to 40 %, which may be attributed to higher Cp and lower k values, as shown in Figure 8.19. In summary, the lost energy dropped by 27 – 16% with increasing hemp content by 20 – 40%, then the change was relatively lower by 14 – 18% with higher hemp content by 50 – 100%.

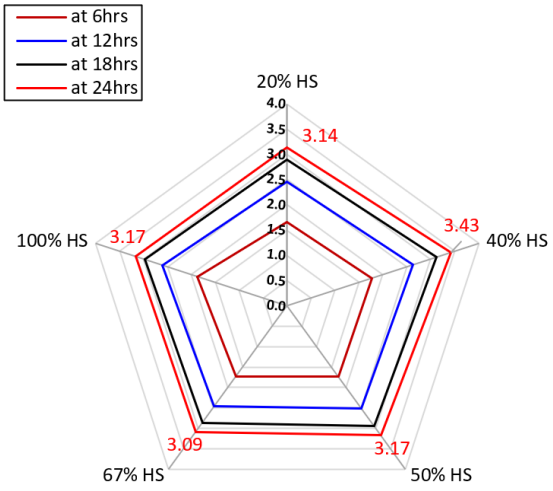

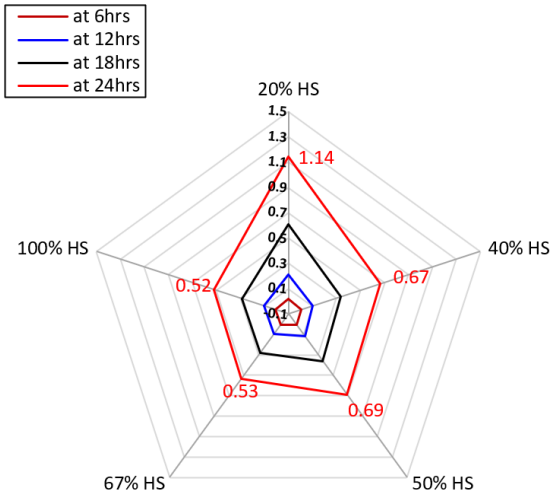

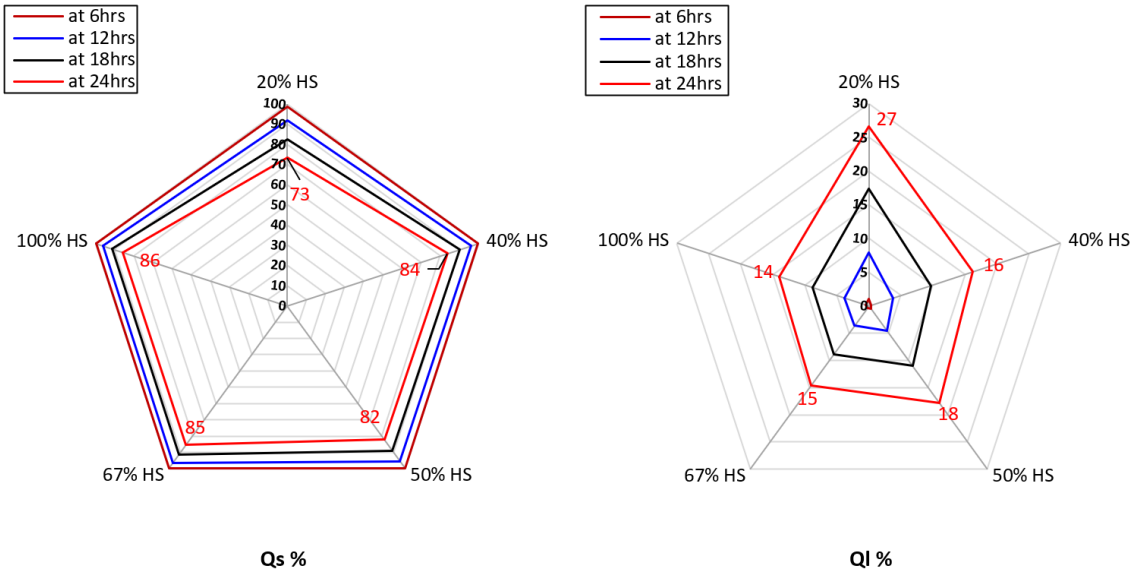

Figure 8.18: Stored and lost thermal energy for hempcrete with various hemp contents.

As shown in Figure 8.19, density and Cp values decrease with increasing hemp content 40 – 100 %, while the stored energy increases slightly from 84 – 86 %. This behavior is ascribed to the appreciable reduction in thermal conductivity 0.13 – 0.06 W/m K (about 120 %), leading to a slighter reduction in outer surface temperature. Thus, the lost energy decreased again slightly from 16 – 14 %. Interestingly, 40 % of hemp content showed higher stored energy (i.e., lower Ql) relative to 50 % due to the higher Cp values and the slight reduction in k values.

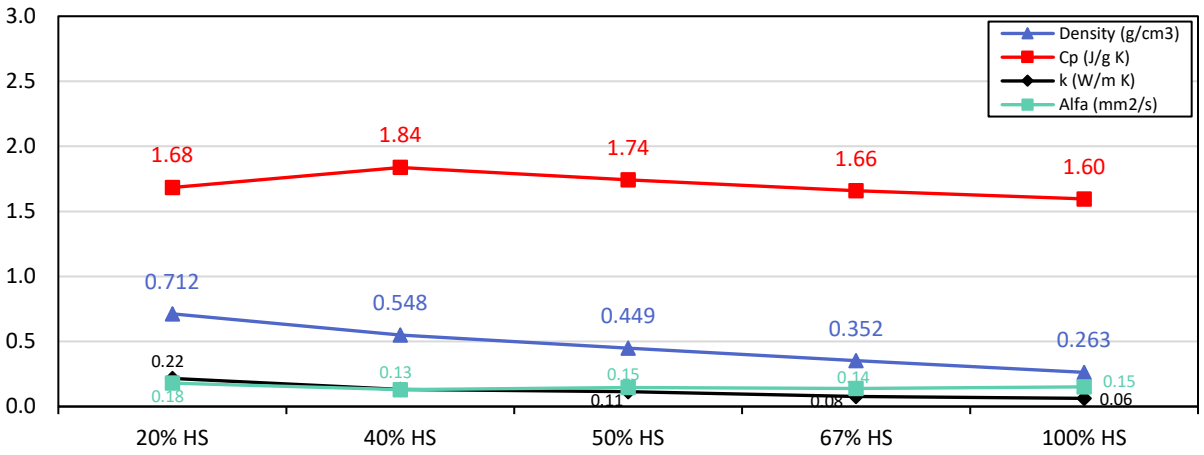

Figure 8.19: Thermal properties of hempcrete with different hemp contents

As shown in Figure 8.20, the stored energy increased with increasing hemp content over 6 and 12 hr. At the same time, the increment is not significant for time over 18 and 24 hours due to approaching the maximum capacity of the wall. On the other hand, lost energy decreases with increasing hemp content, showing a higher difference after 12 hours, which is ascribed to the increase in the thermal resistance of the walls. Therefore, the presence of more hemp hurds showed higher Qs and lowered Ql due to the enhanced thermal properties. However, the density tends to decrease with higher hemp content due to the light weight of hemp, leading to relatively lower stored energy.

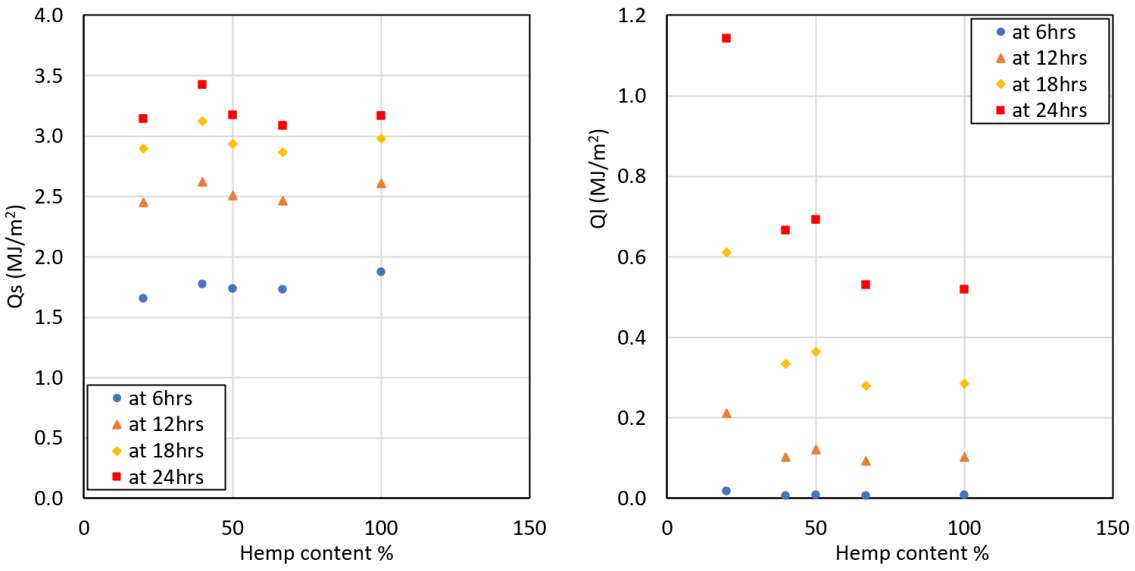

Figure 8.20: Correlation between Qs and Ql for hempcrete walls with different hemp content

8.8 Conclusions

This study evaluates the thermal performance of hempcrete masonry walls in terms of heat storing capability and escaped energy to the exterior environment to minimize thermal energy waste and electricity usage for heating purposes in cold zones. As hempcrete showed superior thermal insulation properties (low k and α values), the ANSYS Fluent model is developed to assess two categories of hempcrete data collected from the literature (Group I) and in this work. The outcomes of this parametric study could be summarized as follows:

- The stored energy is directly proportional to producing $\rho \times C_p$ of the hempcrete walls. Thus, the higher density and heat capacity leads to higher storage capacity.
- The thermal storing process was efficient in the first 6 hours (i.e., most energy stored over 6 hours), then Qs increased significantly with time in the range of 80 – 110 % between 6 and 24 hr. On the other hand, the literature hempcretes show quick full charge of walls within the first 6 hours and insignificant storing from 6 – 24 hrs due to the lower density and Cp values.

- Unfortunately, hempcrete is lightweight concrete with relatively more minor densities than normal concrete, which decreases its capability of storing higher energy. However, many hempcrete mixtures were produced in this study with alkali-activated binders showing relatively higher density, low k, and high Cp values. Hence, the increase in Qs values reaches 130% relative to other hempcrete in the same study.
- The activated binder group showed the highest stored energy, followed by cement-lime-based binders and lime-based binders, mainly affected by the density and heat capacity of the individual mixture.
- The highest Qs value for the literature hempcrete is 1.91 MJ/m^2 (HC3). In comparison, the highest value for hempcrete produced in this study is 5.54 MJ/m^2 (i.e., about 190 % higher) for alkali-activated fly ash with NaOH.
- For the literature data, the maximum lost energy observed is 1.38 MJ/m^2, while group II data showed the highest value of 1.0 MJ/m^2 (i.e., about 28% reduction).
- The lost energy is negligible at the first 6hrs, then slightly increased at 12hrs (>0.2 MJ/m^2); the most of energy lost occurs between 12 – 24hrs (with about 450 – 600 %). Literature hempcrete shows slightly lost energy over the first 6hrs (>0.12 MJ/m^2), dramatically increasing over 12, 18, and 24hrs due to early full charge in less than 6hrs.
- From group I, the least lost energy is achieved by the HC2 wall (0.44 MJ/m^2), while S2-CA showed the minimum Ql from group II data (0.42 MJ/m^2) with a difference <5 %. However, the stored energy of S2-CS is (3.07 MJ/m^2) while HC2 achieved 1.82 MJ/m^2 (i.e., a difference of about 70 %). As a percentage, the Ql of S2-CA and HC2 is 12 and 19 %, respectively, relative to Qs. Thus, the S2-CA wall shows the best thermal performance among the walls investigated in this study.
- Wall C+Li+30%SF shows about 12 % lost energy after 24 hrs (same as S2-CA) with a slightly higher value (0.46 MJ/m^2) and marginally higher stored energy of 3.36 MJ/m^2.
- Hempcretes produced in this study showed a promising thermal performance as the percentage of lost energy for all models is 12 – 24%, while Ql for the literature walls varies between 19 – 60 %.
- The lost energy increases with the rising values of k and α significantly.

- The percentage of stored energy increases with increasing hemp content from 73 – 86 %; hence, lost energy decreases from 27 – 14 % due to high Cp and low k values of hemp. The low density of hemp reduces the Qs values, but using proper binders increases the density significantly, e.g., alkali-activated binders.

9 CHAPTER 9: CONCLUSIONS AND RECOMMENDATIONS

9.1 Research Summary

This thesis is intended to optimize the components of hempcrete in the first stage, including the proper binder type, hemp size, and hemp content. Four groups of binders were explored with hempcrete for compressive strength and thermal properties. The results can be summarized as follows:

- Cement binders showed relatively lower strength and thermal properties due to a lower w/b ratio and workability, leading to a more porous structure.
- Lime binders require optimization for curing conditions to improve the hempcrete mixture's setting, hardening, and strength.
- Cement-lime binders improved the strength of hempcrete and considerably increased its thermal properties.
- Alkali-activated binders showed promising results in strength with an appreciable increment in thermal properties. Optimization for the alkali-activated is required to improve the strength and compatibility of the composite.
- Coarse hemp particles showed higher k values due to higher porosity, and fine particles showed higher conductivity than coarse ones. The well-graded hemp hurds form a denser composite and higher conductivity values, such as S4-FR.
- Fine hemp particles hinder heat diffusion due to the slippage at interface zones, while coarse particles might achieve similar outcomes due to the higher porosity. Well-graded particles (such as S4-FR) may have relatively higher diffusion values.
- Increasing hemp content reduces strength, density, thermal conductivity, and heat capacity. However, thermal diffusivity mainly depends on the behavior of conductivity and heat capacity simultaneously.

The second stage of this study is to improve the compatibility between hempcrete components with chemical treatments for hemp hurds. Hemp hurds were treated with NaOH, $Ca(OH)_2$, and

Na_2SiO_3 solutions, which improved the bond and strength of the hempcrete with treated hurds. A summary could be drawn as follows:

- Sodium hydroxide treatment bleached, fibrillation roughen hemp surface improved bond and strength by about 15-45% for dry and wet conditions. Thermal conductivity (20-40%) and diffusivity (13-20%).
- Calcium hydroxide treatment minimized pectin content, and crystals adhered to the hemp surface, providing extra calcium ions for hydration and carbonation. The compressive strength of hempcrete increased (8-15%), thermal conductivity reduced (7-27%), and thermal diffusivity reduced by 14% for dry conditions.
- Sodium silicate treatment increased silica content on the hemp surface, which enhanced the strength by 10-25% and thermal conductivity (7-17%) due to the higher density. However, the diffusivity is similar to untreated samples.
- The difference between all cases in heat capacity does not exceed 12%, showing an increment in dry Cp values for treated samples and a reduction in moist Cp values.

The final stage was devoted to the thermal performance assessment of hempcrete and other concrete in terms of thermal storing energy and losses from wall systems to use such concretes for building envelope material. The outcomes could be summarized as follows:

- The stored energy inside the walls is directly proportional to the product of density and heat capacity ($\rho \times C_p$) while inversely proportional to their thermal conductivity.
- The energy loss significantly increases with an increase in the thermal diffusivity and conductivity. High thermal diffusivity values do not directly reflect higher storing energy.
- Plastering does not impact the stored energy due to its small thickness. However, energy loss is reduced due to a slight reduction in the outer surface temperature of the walls.
- The study predicts that wall WS1, made with Portland cement + sand + 10% wood shives, performs best with 92% heat transferred from the conditioned room to the wall over 24 hours and only 8% losses to the ambient exterior.

- The thermal storing process was efficient in the first 6 hours (i.e., most energy stored over 6 hours), then Qs increased significantly with time in the range of 80 – 110 % between 6 and 24 hr. On the other hand, the literature hempcretes show quick full charge of walls within the first 6 hours and insignificant storing from 6 – 24 hrs due to the lower density and Cp values.
- Unfortunately, hempcrete is lightweight concrete with relatively more minor densities than normal concrete, which decreases its capability of storing higher energy. However, many hempcrete mixtures were produced in this study with alkali-activated binders showing relatively higher density, low k, and high Cp values. Hence, the increase in Qs values reaches 130% relative to other hempcretes in the same study.
- For the literature hempcrete data, the maximum lost energy observed is 1.38 MJ/m^2, while group II data showed the highest value of 1.0 MJ/m^2 (i.e., about 28% reduction).
- The lost energy is negligible at the first 6hrs, then slightly increased at 12hrs (>0.2 MJ/m^2); the most of energy lost occurs between 12 – 24hrs (with about 450 – 600 %). Literature hempcrete shows slightly lost energy over the first 6hrs (>0.12 MJ/m^2), dramatically increasing over 12, 18, and 24hrs due to early full charge in less than 6hrs.

9.2 Research Contributions

Hempcrete is a relatively new concrete developed in the 1990s and approved in Canada in 2012. Few research studies were found in the literature focusing on all thermal properties of hempcrete, including thermal conductivity, thermal diffusivity, and heat capacity. Thus, there is a need to explore such thermal properties because the actual heat transfer depends on all three properties, not only thermal conductivity. Hempcrete shows low thermal conductivity and high heat capacity (i.e., low thermal diffusivity), an advantage rarely reconciled with other concretes. The original contributions of this study could be drawn as follows:

- Providing the behavior of a variety of binders with hemp hurds on thermal and strength properties:
    - The presence of lime with hemp reduces the negative impact of hemp on the binder matrix through consuming pectin, the occurrence of carbonation, and reducing competition about water with hemp.
    - The effect of pozzolan with cement and lime binders was investigated.
    - The potential of using alkali-activated binders with hempcrete was explored.
    - The behavior of thermal conductivity, heat capacity, and density on thermal diffusivity of hempcrete was investigated using regression analysis.
- Exploring different hemp sizes provided by Canadian suppliers for strength and thermal properties of hempcrete. Thus, it's recommended that about 80% of hemp sizes should be with a width <3mm and a length <10mm. Therefore, this thesis is a valuable contribution and resource for future measures of Canadian hemp.
- Exploring the effect of hemp content on hempcrete's thermal and strength behavior.
- Providing a database for hempcrete thermal properties and strength with different components. Thus, proper hempcrete with the required strength and thermal behavior could be selected and modified.
- Developing linear regression equations for the thermal diffusivity of hempcrete.

- Developing a thermal transient model to assess the thermal performance of hempcrete and other concretes from literature. The walls of hempcrete produced in this study showed relatively higher stored energy and lower losses due to the superior material properties.

9.3 Recommendations & Future Research

In order to optimize hempcrete components, this study tested hempcrete samples' thermal properties and compressive strength with various binder types, hemp sizes, and hemp contents. However, this research was limited to the scope and can be further extended to tackle the following:

1. The effect of moisture content on concrete's thermal properties (k, Cp, and α) is not clear and varied at each moisture content. Future research could be conducted on microstructure to deeply understand the behavior of thermal properties with changing water content for the same sample.
2. Quantifying crystalline and amorphous phases of the binder matrix is highly recommended for future work showing the effect of hemp on the binder matrix and the impact on thermal properties.
3. The amount of lime and alumina differed in all binder compositions; thus, the amount needed to be identified to reduce the negative impact of hemp pectin and sugar without chemical treatment.
4. Optimization for curing conditions for lime and lime-pozzolan to achieve better mechanical properties for hempcrete due to the higher moisture content.
5. The degree of compaction needed to be unified for hempcrete using such a specific weight hammer due to the flaky shape of hemp hurds.
6. Future studies could be held into alkali-activated and cement-lime binders with hempcrete to optimize the binder composition and achieve higher strength and bond for the same hemp content.
7. Studying the effect of hemp hurds on the solution of alkali-activated binders, such as monitoring the absorption of the alkali-activated solution by hemp hurds and the impact of solution concentration on hemp surface and interface zone.
8. The thermal diffusivity of dry samples is affected by many factors, including porosity, content of hemp, degree of compaction, properties of alkali-activated, and amount of crystalline and amorphous products. 3-D imaging analysis using X-ray microscopy

(XRM), such as nano/micro-CT scan, could be used to analyze the components of hempcrete on micro/nanoscale, which will lead to relating the details with thermal properties and a higher understanding of their mechanism effect.

9. Future studies could be conducted into the microstructure of hempcrete and thermal data analysis for sufficient samples because the standard deviation for thermal diffusivity is mostly higher than the conductivity.
10. For future studies, estimating the energy consumption in actual buildings using the suggested walls in this paper and comparing performance with those with traditional walls is recommended.
11. Experimentally evaluate the effect of hollow blocks to store and lose thermal energy and compare the performance to the filled cavities with insulation materials such as polystyrene and foam and phase change materials.

REFERENCES:

Chapter 1:

[1] S. Real, M. G. Gomes, A. Moret Rodrigues, and J. A. Bogas, "Contribution of structural lightweight aggregate concrete to the reduction of thermal bridging effect in buildings," *Constr. Build. Mater.*, vol. 121, pp. 460–470, 2016, doi: 10.1016/j.conbuildmat.2016.06.018.

[2] Natural Resources Canada, "Heating equipment for residential use," *Nrcan*, pp. 1–4, 2022, [Online]. Available: https://www.nrcan.gc.ca/energy-efficiency/products/product-information/heating-equipment-for-residential-use/13740

[3] U. S. E. P. Agency, "Renewable Heating And Cooling," pp. 1–10, 2016, [Online]. Available: https://www.epa.gov/rhc/renewable-space-heating

[4] M. Martínez, N. Huygen, J. Sanders, and S. Atamturktur, "Thermo-fluid dynamic analysis of concrete masonry units via experimental testing and numerical modeling," *J. Build. Eng.*, vol. 19, no. May, pp. 80–90, 2018, doi: 10.1016/j.jobe.2018.04.029.

[5] Council Directive 2010/31/EU of the European Parliament, "Directive 2010/31/EU of the European Parliament and of the Council of 19 May 2010 on the Energy Performance of Buildings," *Optics InfoBase Conference Papers*. 2010. [Online]. Available: https://www.legislation.gov.uk/eudr/2010/31

[6] Canadian Standards Association-CSA, "CSA Standards on concrete masonry units-A165 SERIES-14 (R2019)," 2014. [Online]. Available: https://www.csagroup.org/store/product/A165 SERIES-14/

[7] National Concrete Masonry Association, "ASTM Specifications for Concrete Masonry Units," p. 9, 2012, [Online]. Available: https://ncma.org/resource/astm-specifications-for-concrete-masonry-units/

[8] T. Bergman, A. Lavine, F. Incropera, and D. Dewitt, *Fundamentals of Heat and Mass Transfer*, 7th ed.

[9] P. Shafigh, I. Asadi, and N. B. Mahyuddin, "Concrete as a thermal mass material for building applications - A review," *J. Build. Eng.*, vol. 19, no. April, pp. 14–25, 2018, doi: 10.1016/j.jobe.2018.04.021.

[10] H. Uysal, R. Demirboga, R. Şahin, and R. Gül, "The effects of different cement dosages, slumps, and pumice aggregate ratios on concrete thermal conductivity and density," *Cem. Concr. Res.*, vol. 34, no. 5, pp. 845–848, 2004, doi: 10.1016/j.cemconres.2003.09.018.

[11] H. Zhou and A. L. Brooks, "Thermal and mechanical properties of structural lightweight concrete containing lightweight aggregates and fly-ash cenospheres," *Constr. Build. Mater.*, vol. 198, pp. 512–526, 2019, doi: 10.1016/j.conbuildmat.2018.11.074.

[12] U. Dhakal, U. Berardi, M. Gorgolewski, and R. Richman, “Hygrothermal performance of hempcrete for Ontario (Canada) buildings,” *J. Clean. Prod.*, vol. 142, pp. 3655–3664, 2017, doi: 10.1016/j.jclepro.2016.10.102.

[13] B. C. Act, “Ontario Building Code 2012,” no. 1, pp. 9–10, 2014.

[14] M. A. Khan, “Physical and Microstructural Properties of Insulating Hempcrete Mixes and their Impact as Infill System on the Foundations due to Increase in Dead Load,” no. March, 2020.

[15] N. Stevulova, J. Cigasova, I. Schwarzova, A. Sicakova, and J. Junak, “Sustainable bio-aggregate-based composites containing hemp hurds and alternative binder,” *Buildings*, vol. 8, no. 2, pp. 1–14, 2018, doi: 10.3390/buildings8020025.

[16] N. M. Nurazzi *et al.*, “A review on the mechanical performance of hybrid natural fiber polymer composites for structural applications,” *Polymers (Basel).*, vol. 13, no. 13, 2021, doi: 10.3390/polym13132170.

[17] M. Le Troëdec, C. S. Peyratout, A. Smith, and T. Chotard, “Influence of various chemical treatments on the interactions between hemp fibres and a lime matrix,” *J. Eur. Ceram. Soc.*, vol. 29, no. 10, pp. 1861–1868, 2009, doi: 10.1016/j.jeurceramsoc.2008.11.016.

[18] S. Pantawee, T. Sinsiri, C. Jaturapitakkul, and P. Chindaprasirt, “Utilization of hemp concrete using hemp shiv as coarse aggregate with aluminium sulfate [Al2(SO4)3] and hydrated lime [Ca(OH)2] treatment,” *Constr. Build. Mater.*, vol. 156, pp. 435–442, 2017, doi: 10.1016/j.conbuildmat.2017.08.181.

[19] G. Balčiunas, I. Pundiene, L. Lekunaite-Lukošiune, S. Vejelis, and A. Korjakins, “Impact of hemp shives aggregate mineralization on physical-mechanical properties and structure of composite with cementitious binding material,” *Ind. Crops Prod.*, vol. 77, pp. 724–734, 2015, doi: 10.1016/j.indcrop.2015.09.011.

[20] N. Stevulova *et al.*, “Properties characterization of chemically modified hemp hurds,” *Materials (Basel).*, vol. 7, no. 12, pp. 8131–8150, 2014, doi: 10.3390/ma7128131.

[21] L. Wang, H. Lenormand, H. Zmamou, and N. Leblanc, “Effect of variability of hemp shiv on the setting of lime hemp concrete,” *Ind. Crops Prod.*, vol. 171, no. November, p. 113915, 2021, doi: 10.1016/j.indcrop.2021.113915.

[22] M. M. Kabir, H. Wang, K. T. Lau, and F. Cardona, “Effects of chemical treatments on hemp fibre structure,” *Appl. Surf. Sci.*, vol. 276, pp. 13–23, 2013, doi: 10.1016/j.apsusc.2013.02.086.

[23] R. Walker, “A Study of the Properties of Lime-Hemp Concrete with Pozzolans,” 2013.

[24] Natural Resource Canada, “Energy Fact Book 2022–2023,” 2023.

[25] P. Nejat, F. Jomehzadeh, M. M. Taheri, M. Gohari, and M. Z. Muhd, “A global review of

energy consumption, CO2 emissions and policy in the residential sector (with an overview of the top ten CO2 emitting countries)," *Renew. Sustain. Energy Rev.*, vol. 43, pp. 843–862, 2015, doi: 10.1016/j.rser.2014.11.066.

[26] Natural Resources Canada, "Energy Efficiency Trends in Canada 1990 to 2004," *Energy*, no. March, pp. 1–48, 2006, doi: http://oee.nrcan.gc.ca/publications/statistics/trends11/pdf/trends.pdf.

[27] N. R. Canada, "Net zero energy ready buildings in Canada," pp. 1–7, 2020, [Online]. Available: https://codes4climate.efficiencycanada.org/net-zero-energy-ready-buildings-in-canada/

[28] Y. Abdellatef, M. A. Khan, A. Khan, M. I. Alam, and M. Kavgic, "Mechanical, thermal, and moisture buffering properties of novel insulating hemp-lime composite building materials," *Materials (Basel).*, vol. 13, no. 21, pp. 1–18, 2020, doi: 10.3390/ma13215000.

Chapter 2:

[1] T. Bergman, A. Lavine, F. Incropera, and D. Dewitt, *Fundamentals of Heat and Mass Transfer*, 7th ed.

[2] H. Uysal, R. Demirboga, R. Şahin, and R. Gül, "The effects of different cement dosages, slumps, and pumice aggregate ratios on concrete thermal conductivity and density," *Cem. Concr. Res.*, vol. 34, no. 5, pp. 845–848, 2004, doi: 10.1016/j.cemconres.2003.09.018.

[3] P. Shafigh, I. Asadi, and N. B. Mahyuddin, "Concrete as a thermal mass material for building applications - A review," *J. Build. Eng.*, vol. 19, no. April, pp. 14–25, 2018, doi: 10.1016/j.jobe.2018.04.021.

[4] C. Costa, "Materials for construction and civil engineering: Science, processing, and design," *Springer Int. Publ. Switz. 2015*, pp. 1–902, 2015, doi: 10.1007/978-3-319-08236-3.

[5] R. Siddique and M. I. Khan, *Chapter 4; Metakaolin*. 2011. doi: 10.1007/978-3-642-17866-5.

[6] A. Bicer and F. Kar, "Thermal and mechanical properties of gypsum plaster mixed with expanded polystyrene and tragacanth," *Therm. Sci. Eng. Prog.*, vol. 1, pp. 59–65, 2017, doi: 10.1016/j.tsep.2017.02.008.

[7] B. E. N. Tz, "M E A S U RE M EN T O F TH ER M AL PR O PER TI ES O F G Y PS UM B O A RD A T E L E V A T ED T E M PER A TU RES," pp. 656–665.

[8] C. Republic, C. Republic, and C. Republic, "THERMAL AND HYGRIC PROPERTIES OF GYPSUM : REFERENCE MEASUREMENTS," pp. 52–57.

[9] P. Bekhta and E. Dobrowolska, "Thermal properties of wood-gypsum boards," *Holz als*

Roh - und Werkst., vol. 64, no. 5, pp. 427–428, 2006, doi: 10.1007/s00107-005-0074-8.

[10] K. Amarray, M. Garoum, S. Raefat, N. Laaroussi, and A. Ettahir, "The influence of the expanded clay granules ratio on the thermal conductivity and thermal diffusivity of gypsum plaster-based composites's," *IOP Conf. Ser. Mater. Sci. Eng.*, vol. 446, no. 1, 2018, doi: 10.1088/1757-899X/446/1/012002.

[11] H. Binici and O. Aksogan, "Insulation material production from onion skin and peanut shell fibers, fly ash, pumice, perlite, barite, cement, and gypsum," *Mater. Today Commun.*, vol. 10, no. 112, pp. 14–24, 2017, doi: 10.1016/j.mtcomm.2016.09.004.

[12] Y. Xu and D. D. L. Chung, "Increasing the specific heat of cement paste by admixture surface treatments," *Cem. Concr. Res.*, vol. 29, no. 7, pp. 1117–1121, 1999, doi: 10.1016/S0008-8846(99)00080-0.

[13] A. Reilly *et al.*, "The thermal diffusivity of hemplime, and a direct measurement method," *Constr. Build. Mater.*, vol. 212, pp. 707–715, 2019, doi: 10.1016/j.conbuildmat.2019.03.264.

[14] K. Vance, G. Falzone, I. Pignatelli, M. Bauchy, M. Balonis, and G. Sant, "Direct Carbonation of Ca(OH)2 Using Liquid and Supercritical CO2: Implications for Carbon-Neutral Cementation," *Ind. Eng. Chem. Res.*, vol. 54, no. 36, pp. 8908–8918, 2015, doi: 10.1021/acs.iecr.5b02356.

[15] K. Van Balen and D. Van Gemert, "Modelling lime mortar carbonation," *Mater. Struct.*, vol. 27, no. 7, pp. 393–398, 1994, doi: 10.1007/BF02473442.

[16] A. J. Edwards, "Properties of Hydraulic and Non-Hydraulic Limes for Use in Construction," Napier University, 2005.

[17] Z. Zhao, X. Qu, F. Li, and J. Wei, "Effects of steel slag and silica fume additions on compressive strength and thermal properties of lime-fly ash pastes," *Constr. Build. Mater.*, vol. 183, pp. 439–450, 2018, doi: 10.1016/j.conbuildmat.2018.05.220.

[18] M. Čáchová *et al.*, "Application of ceramic powder as a supplementary cementitious material in lime plasters," *Medziagotyra*, vol. 22, no. 3, pp. 440–444, 2016, doi: 10.5755/j01.ms.22.3.7433.

[19] E. Vejmelková, M. Keppert, Z. Keršner, P. Rovnaníková, and R. Černý, "Mechanical, fracture-mechanical, hydric, thermal, and durability properties of lime-metakaolin plasters for renovation of historical buildings," *Constr. Build. Mater.*, vol. 31, pp. 22–28, 2012, doi: 10.1016/j.conbuildmat.2011.12.084.

[20] M. Madrid, A. Orbe, E. Rojí, and J. Cuadrado, "The effects of by-products incorporated in low-strength concrete for concrete masonry units," *Constr. Build. Mater.*, vol. 153, pp. 117–128, 2017, doi: 10.1016/j.conbuildmat.2017.07.086.

[21] R. C. E. Modolo, L. Senff, J. A. Labrincha, V. M. Ferreira, and L. A. C. Tarelho, “Lime mud from cellulose industry as raw material in cement mortars,” *Mater. Construcción*, vol. 64, no. 316, p. e033, 2014, doi: 10.3989/mc.2014.00214.

[22] H. Ero and H. H. Acar, “The Effect of Dry Sludge Addition Supplied From Pulp Mill on the Compressive Strength of Cement,” no. February, pp. 169–174, 2007.

[23] R. Černý, A. Kunca, V. Tydlitát, J. Drchalová, and P. Rovnaníková, “Effect of pozzolanic admixtures on mechanical, thermal and hygric properties of lime plasters,” *Constr. Build. Mater.*, vol. 20, no. 10, pp. 849–857, 2006, doi: 10.1016/j.conbuildmat.2005.07.002.

[24] M. A. Villaquirán-Caicedo, R. M. de Gutiérrez, S. Sulekar, C. Davis, and J. C. Nino, “Thermal properties of novel binary alkali activateds based on metakaolin and alternative silica sources,” *Appl. Clay Sci.*, vol. 118, pp. 276–282, 2015, doi: 10.1016/j.clay.2015.10.005.

[25] J. R. A. Goncalves, Y. Boluk, and V. Bindiganavile, “Thermal properties of fibre-reinforced alkali-activated concrete in extreme temperatures,” *Mag. Concr. Res.*, vol. 70, no. 18, pp. 954–964, 2017, doi: 10.1680/jmacr.17.00189.

[26] X. Fu and D. D. L. Chung, “Effects of silica fume, latex, methylcellulose, and carbon fibers on the thermal conductivity and specific heat of cement paste,” *Cem. Concr. Res.*, vol. 27, no. 12, pp. 1799–1804, 1997, doi: 10.1016/S0008-8846(97)00174-9.

[27] P. Jittabut, “The Study on Physical and Thermal Properties of Alkali activated Pastes,” *Key Eng. Mater.*, vol. 751, pp. 538–543, 2017, doi: 10.4028/www.scientific.net/kem.751.538.

[28] A. J. Nur, Y. M. Liew, M. M. A. Al Bakri, and C. Y. Heah, “Thermophysical Properties of Metakaolin Alkali activateds Based on Na2SiO3/NaOH Ratio,” *Solid State Phenom.*, vol. 280, pp. 487–493, 2018, doi: 10.4028/www.scientific.net/ssp.280.487.

[29] S. A. Zaidan and M. H. Omar, “The effects of bauxite, metakaolin, and porosity on the thermal properties of prepared Iraqi clays refractory mortars,” *Appl. Phys. A Mater. Sci. Process.*, vol. 124, no. 5, pp. 1–8, 2018, doi: 10.1007/s00339-018-1759-2.

[30] V. D. Kunthe, G. Manavendra, and V. M. Sondur, “Effect of thermal properties on fly ash based concrete,” *Int. Res. J. Eng. Technol.*, vol. 05, no. 12, pp. 396–400, 2018.

[31] H. Zhou and A. L. Brooks, “Thermal and mechanical properties of structural lightweight concrete containing lightweight aggregates and fly-ash cenospheres,” *Constr. Build. Mater.*, vol. 198, pp. 512–526, 2019, doi: 10.1016/j.conbuildmat.2018.11.074.

[32] K. Stephan and A. Laesecke, “The Thermal Conductivity of Fluid Air,” *J. Phys. Chem. Ref. Data*, vol. 14, no. 1, pp. 227–234, 1985, doi: 10.1063/1.555749.

[33] R. Alyousef, O. Benjeddou, C. Soussi, M. A. Khadimallah, and M. Jedidi, “Experimental

Study of New Insulation Lightweight Concrete Block Floor Based on Perlite Aggregate, Natural Sand, and Sand Obtained from Marble Waste," *Adv. Mater. Sci. Eng.*, vol. 2019, pp. 1–14, 2019, doi: 10.1155/2019/8160461.

[34] R. Demirboğa and R. Gül, "The effects of expanded perlite aggregate, silica fume and fly ash on the thermal conductivity of lightweight concrete," *Cem. Concr. Res.*, vol. 33, no. 5, pp. 723–727, 2003, doi: 10.1016/S0008-8846(02)01032-3.

[35] S. Real, M. G. Gomes, A. Moret Rodrigues, and J. A. Bogas, "Contribution of structural lightweight aggregate concrete to the reduction of thermal bridging effect in buildings," *Constr. Build. Mater.*, vol. 121, pp. 460–470, 2016, doi: 10.1016/j.conbuildmat.2016.06.018.

[36] L. H. Nguyen, A. L. Beaucour, S. Ortola, and A. Noumowé, "Experimental study on the thermal properties of lightweight aggregate concretes at different moisture contents and ambient temperatures," *Constr. Build. Mater.*, vol. 151, pp. 720–731, 2017, doi: 10.1016/j.conbuildmat.2017.06.087.

[37] I. Asadi, P. Shafigh, Z. F. Bin Abu Hassan, and N. B. Mahyuddin, "Thermal conductivity of concrete – A review," *J. Build. Eng.*, vol. 20, no. July, pp. 81–93, 2018, doi: 10.1016/j.jobe.2018.07.002.

[38] ACI Committee 122R-02, "Guide to Thermal Properties of Concrete and Masonry Systems," *Concrete*, pp. 1–21, 2002, doi: 10.1080/23251042.2017.1414659.

[39] Y. Xu and D. D. L. Chung, "Effect of sand addition on the specific heat and thermal conductivity of cement," *Cem. Concr. Res.*, vol. 30, no. 1, pp. 59–61, 2000, doi: 10.1016/S0008-8846(99)00206-9.

[40] D. Taoukil, A. El-bouardi, H. Ezbakhe, and T. Ajzoul, "Thermal proprieties of concrete lightened by wood aggregates," *Res. J. Appl. Sci. Eng. Technol.*, vol. 3, no. 2, pp. 113–116, 2011.

[41] D. Taoukil, A. El bouardi, T. Ajzoul, and H. Ezbakhe, "Effect of the incorporation of wood wool on thermo physical proprieties of sand mortars," *KSCE J. Civ. Eng.*, vol. 16, no. 6, pp. 1003–1010, 2012, doi: 10.1007/s12205-012-1470-3.

[42] W. V. Liu, D. B. Apel, and V. S. Bindiganavile, "Thermal properties of lightweight dry-mix shotcrete containing expanded perlite aggregate," *Cem. Concr. Compos.*, vol. 53, pp. 44–51, 2014, doi: 10.1016/j.cemconcomp.2014.06.003.

[43] H. Oktay, R. Yumrutaş, and A. Akpolat, "Mechanical and thermophysical properties of lightweight aggregate concretes," *Constr. Build. Mater.*, vol. 96, pp. 217–225, 2015, doi: 10.1016/j.conbuildmat.2015.08.015.

[44] A. C. I. Journal and T. Paper, "Cryogenic Insulating Concrete - Cement-Based Concrete

with Polystyrene Beads," *ACI J. Proc.*, vol. 83, no. 3, 1986, doi: 10.14359/10446.

[45] L. H. Nguyen, A. L. Beaucour, S. Ortola, and A. Noumowé, "Influence of the volume fraction and the nature of fine lightweight aggregates on the thermal and mechanical properties of structural concrete," *Constr. Build. Mater.*, vol. 51, pp. 121–132, 2014, doi: 10.1016/j.conbuildmat.2013.11.019.

[46] R. Walker and S. Pavía, "Moisture transfer and thermal properties of hemp-lime concretes," *Constr. Build. Mater.*, vol. 64, pp. 270–276, 2014, doi: 10.1016/j.conbuildmat.2014.04.081.

[47] G. A. Daoud Atef, "Effect of Rubber Aggregates on the Thermophysical Properties of Self-Consolidating Concrete," *J. Bioprocess. Biotech.*, vol. 04, no. 03, pp. 1–7, 2014, doi: 10.4172/2155-9821.1000156.

[48] F. Collet, S. Prétot, and C. Lanos, "Hemp-Straw Composites: Thermal and Hygric Performances," *Energy Procedia*, vol. 139, pp. 294–300, 2017, doi: 10.1016/j.egypro.2017.11.211.

[49] P. De Bruijn and P. Johansson, "Moisture fixation and thermal properties of lime-hemp concrete," *Constr. Build. Mater.*, vol. 47, pp. 1235–1242, 2013, doi: 10.1016/j.conbuildmat.2013.06.006.

[50] P. Nováková, "Use of technical hemp in the construction industry," *MATEC Web Conf.*, vol. 146, pp. 1–8, 2018, doi: 10.1051/matecconf/201814603011.

[51] B. Mazhoud, F. Collet, S. Pretot, and J. Chamoin, "Hygric and thermal properties of hemp-lime plasters," *Build. Environ.*, vol. 96, pp. 206–216, 2016, doi: 10.1016/j.buildenv.2015.11.013.

[52] E. Gourlay, P. Glé, S. Marceau, C. Foy, and S. Moscardelli, "Effect of water content on the acoustical and thermal properties of hemp concretes," *Constr. Build. Mater.*, vol. 139, pp. 513–523, 2017, doi: 10.1016/j.conbuildmat.2016.11.018.

Chapter 3:

[1] H. Uysal, R. Demirboga, R. Şahin, and R. Gül, "The effects of different cement dosages, slumps, and pumice aggregate ratios on concrete thermal conductivity and density," *Cem. Concr. Res.*, vol. 34, no. 5, pp. 845–848, 2004, doi: 10.1016/j.cemconres.2003.09.018.

[2] P. Shafigh, I. Asadi, and N. B. Mahyuddin, "Concrete as a thermal mass material for building applications - A review," *J. Build. Eng.*, vol. 19, no. April, pp. 14–25, 2018, doi: 10.1016/j.jobe.2018.04.021.

[3] I. Asadi, P. Shafigh, Z. F. Bin Abu Hassan, and N. B. Mahyuddin, "Thermal conductivity

of concrete – A review," *J. Build. Eng.*, vol. 20, no. July, pp. 81–93, 2018, doi: 10.1016/j.jobe.2018.07.002.

[4] S. Pantawee, T. Sinsiri, C. Jaturapitakkul, and P. Chindaprasirt, "Utilization of hemp concrete using hemp shiv as coarse aggregate with aluminum sulfate [Al2(SO4)3] and hydrated lime [Ca(OH)2] treatment," *Constr. Build. Mater.*, vol. 156, pp. 435–442, 2017, doi: 10.1016/j.conbuildmat.2017.08.181.

[5] B. C. Act, "Ontario Building Code 2012," no. 1, pp. 9–10, 2014.

[6] R. Walker, "A Study of the Properties of Lime-Hemp Concrete with Pozzolans," 2013.

[7] R. Walker, S. Pavia, and R. Mitchell, "Mechanical properties and durability of hemp-lime concretes," *Constr. Build. Mater.*, vol. 61, pp. 340–348, 2014, doi: 10.1016/j.conbuildmat.2014.02.065.

[8] U. Dhakal, U. Berardi, M. Gorgolewski, and R. Richman, "Hygrothermal performance of hempcrete for Ontario (Canada) buildings," *J. Clean. Prod.*, vol. 142, pp. 3655–3664, 2017, doi: 10.1016/j.jclepro.2016.10.102.

[9] P. Brzyski, S. Duda, and A. Raczkowski, "Two-dimensional heat transfer analysis of timber structure walls filled with hemp-lime composite," *MATEC Web Conf.*, vol. 252, p. 05015, 2019, doi: 10.1051/matecconf/201925205015.

[10] ASTM D 854 – 02, "Standard Test Methods for of Soil Specific GravitySolids by Water Pycnometer," *ASTM Stand.*, vol. 24, no. 1, p. 120432, 2018, [Online]. Available: https://doi.org/10.1016/j.conbuildmat.2020.118708%0Ahttps://doi.org/10.1016/j.wasman.2018.02.018%0Ahttps://doi.org/10.1016/j.conbuildmat.2019.03.011%0Ahttp://dx.doi.org/10.1007/s40710-017-0210-6%0Ahttp://dx.doi.org/10.1016/j.phpro.2014.07.011%0Ahttps://do

[11] R. Walker and S. Pavía, "Moisture transfer and thermal properties of hemp-lime concretes," *Constr. Build. Mater.*, vol. 64, pp. 270–276, 2014, doi: 10.1016/j.conbuildmat.2014.04.081.

[12] A. Reilly *et al.*, "The thermal diffusivity of hemplime, and a direct measurement method," *Constr. Build. Mater.*, vol. 212, pp. 707–715, 2019, doi:

10.1016/j.conbuildmat.2019.03.264.

[13] P. Brzyski, M. Gładecki, M. Rumińska, K. Pietrak, M. Kubiś, and P. Łapka, “Influence of hemp shives size on hygro-thermal and mechanical properties of a hemp-lime composite,” *Mater. MDPI*, vol. 13, no. 23, pp. 1–17, 2020, doi: 10.3390/ma13235383.

[14] Y. Abdellatef, M. A. Khan, A. Khan, M. I. Alam, and M. Kavgic, “Mechanical, thermal, and moisture buffering properties of novel insulating hemp-lime composite building materials,” *Materials (Basel).*, vol. 13, no. 21, pp. 1–18, 2020, doi: 10.3390/ma13215000.

[15] P. De Bruijn and P. Johansson, “Moisture fixation and thermal properties of lime-hemp concrete,” *Constr. Build. Mater.*, vol. 47, pp. 1235–1242, 2013, doi: 10.1016/j.conbuildmat.2013.06.006.

[16] E. Gourlay, P. Glé, S. Marceau, C. Foy, and S. Moscardelli, “Effect of water content on the acoustical and thermal properties of hemp concretes,” *Constr. Build. Mater.*, vol. 139, pp. 513–523, 2017, doi: 10.1016/j.conbuildmat.2016.11.018.

[17] B. Mazhoud, F. Collet, S. Pretot, and J. Chamoin, “Hygric and thermal properties of hemp-lime plasters,” *Build. Environ.*, vol. 96, pp. 206–216, 2016, doi: 10.1016/j.buildenv.2015.11.013.

[18] A. Bourdot *et al.*, “Characterization of a hemp-based agro-material: Influence of starch ratio and hemp shive size on physical, mechanical, and hygrothermal properties,” *Energy Build.*, vol. 153, pp. 501–512, 2017, doi: 10.1016/j.enbuild.2017.08.022.

[19] M. A. Khan, “Physical and Microstructural Properties of Insulating Hempcrete Mixes and their Impact as Infill System on the Foundations due to Increase in Dead Load,” no. March, 2020.

[20] T. Jami, S. R. Karade, and L. P. Singh, “A review of the properties of hemp concrete for green building applications,” *J. Clean. Prod.*, vol. 239, p. 117852, 2019, doi: 10.1016/j.jclepro.2019.117852.

[21] V. Živica, M. T. Palou, and M. Križma, “Alkali activated Cements and Their Properties: A Review,” *Build. Res. J.*, vol. 61, no. 2, pp. 85–100, 2015, doi: 10.2478/brj-2014-0007.

[22] A. Forster, “An assessment of the relationship between the water vapour permeability and hydraulicity of lime based mortars with particular reference to building conservation material science An assessment of the relationship between the water vapour permeability and,” Heriot-Watt University, 2015.

[23] B. A. Silva, A. P. Ferreira Pinto, A. Gomes, and A. Candeias, “Effects of natural and accelerated carbonation on the properties of lime-based materials,” *J. CO2 Util.*, vol. 49, no. December 2020, 2021, doi: 10.1016/j.jcou.2021.101552.

[24] R. Walker and S. Pavía, “Effect of Hemp’S Soluble Components on the Physical Properties of Hemp Concrete,” *J. Mater. Sci. Res.*, vol. 3, no. 3, pp. 12–23, 2014, doi: 10.5539/jmsr.v3n3p12.

[25] M. Ganjigatti, B. R. Kashinath, and K. B. Prakash, “Effect of Replacement of Cement by Different Pozzolanic Materials on Heat of Hydration and Setting Time of Concrete,” *Int. J. Environ. Agric. Res.*, vol. 1, no. 4, pp. 25–30, 2015.

[26] P. Brzyski, “The effect of pozzolan addition on the physical and mechanical properties of lime mortar,” *E3S Web Conf.*, vol. 49, pp. 1–8, 2018, doi: 10.1051/e3sconf/20184900009.

[27] V. Nozahic, S. Amziane, G. Torrent, K. Saïdi, and H. De Baynast, “Design of green concrete made of plant-derived aggregates and a pumice-lime binder,” *Cem. Concr. Compos.*, vol. 34, no. 2, pp. 231–241, 2012, doi: 10.1016/j.cemconcomp.2011.09.002.

[28] S. Elfordy, F. Lucas, F. Tancret, Y. Scudeller, and L. Goudet, “Mechanical and thermal properties of lime and hemp concrete (‘hempcrete’) manufactured by a projection process,” *Constr. Build. Mater.*, vol. 22, no. 10, pp. 2116–2123, 2008, doi: 10.1016/j.conbuildmat.2007.07.016.

[29] X. Du, Z. Li, T. Tong, B. Li, and H. Liu, “Isothermal drying process and its effect on compressive strength of concrete in multiscale,” *Appl. Sci.*, vol. 9, no. 19, 2019, doi: 10.3390/app9194015.

[30] H. Savastano and V. Agopyan, “Transition zone studies of vegetable fibre-cement paste composites,” *Cem. Concr. Compos.*, vol. 21, no. 1, pp. 49–57, 1999, doi: 10.1016/S0958-

9465(98)00038-9.

[31] S. H. Kang, Y. H. Kwon, and J. Moon, “Controlling the hydration and carbonation in lime-based materials: Advantage of slow carbonation in CO2 curable construction materials,” *Constr. Build. Mater.*, vol. 249, p. 118749, 2020, doi: 10.1016/j.conbuildmat.2020.118749.

[32] A. Peschard, A. Govin, P. Grosseau, B. Guilhot, and R. Guyonnet, “Effect of polysaccharides on the hydration of cement paste at early ages,” *Cem. Concr. Res.*, vol. 34, no. 11, pp. 2153–2158, 2004, doi: 10.1016/j.cemconres.2004.04.001.

[33] A. Govin, A. Peschard, and R. Guyonnet, “Modification of cement hydration at early ages by natural and heated wood,” *Cem. Concr. Compos.*, vol. 28, no. 1, pp. 12–20, 2006, doi: 10.1016/j.cemconcomp.2005.09.002.

[34] M. Eroglu S., Toprak S., Urgan O, MD, Ozge E. Onur, MD, Arzu Denizbasi, MD, Haldun Akoglu, MD, Cigdem Ozpolat, MD, Ebru Akoglu, *Hemp Industrial Production and Uses*, vol. 33. 2012.

[35] A. Evrard and A. De Herde, “Bioclimatic envelopes made of lime and hemp concrete,” *Proceeding of CISBAT*, vol. 2005, no. November, pp. 1–6, 2005, [Online]. Available: http://dial.academielouvain.be/vital/access/services/Download/boreal:73818/PDF_01

[36] N. M. Nurazzi *et al.*, “A review on mechanical performance of hybrid natural fiber polymer composites for structural applications,” *Polymers (Basel).*, vol. 13, no. 13, 2021, doi: 10.3390/polym13132170.

[37] A. M. Neville, *Properties of Concrete: Fourth and Final Edition*. 1997. [Online]. Available: http://www.amazon.com/Properties-Concrete-Fourth-Final-Edition/dp/0470235276

[38] R. Siddique, M. Singh, S. Mehta, and R. Belarbi, “Utilization of treated saw dust in concrete as partial replacement of natural sand,” *J. Clean. Prod.*, vol. 261, 2020, doi: 10.1016/j.jclepro.2020.121226.

[39] M. Ganeshan and S. Venkataraman, “Interface shear strength evaluation of self compacting alkali activated concrete using push-off test,” *J. King Saud Univ. - Eng. Sci.*, vol. 34, no. 2, pp. 98–107, 2022, doi: 10.1016/j.jksues.2020.08.005.

[40] V. D. Gorgots, “Standard Practice for Selecting Proportions for Normal, Heavyweight, and Mass Concrete (ACI 211.1-91) Donald,” 2002.

[41] D. Taoukil, A. El Bouardi, F. Sick, A. Mimet, H. Ezbakhe, and T. Ajzoul, “Moisture content influence on the thermal conductivity and diffusivity of wood-concrete composite,” *Constr. Build. Mater.*, vol. 48, pp. 104–115, 2013, doi: 10.1016/j.conbuildmat.2013.06.067.

[42] J. Page, M. Sonebi, and S. Amziane, “Design and multi-physical properties of a new hybrid hemp-flax composite material,” *Constr. Build. Mater.*, vol. 139, pp. 502–512, 2017, doi: 10.1016/j.conbuildmat.2016.12.037.

[43] L. Arnaud and E. Gourlay, “Experimental study of parameters influencing mechanical properties of hemp concretes,” *Constr. Build. Mater.*, vol. 28, no. 1, pp. 50–56, 2012, doi: 10.1016/j.conbuildmat.2011.07.052.

[44] M. Sonebi, S. Wana, S. Amziane, and J. Khatib, “Investigation of the Mechanical Performance and Weathering of Hemp Concrete,” *1st Int. Conf. Bio-based Build. Mater.*, vol. 33, no. 2, pp. 416–421, 2015, [Online]. Available: http://pure.qub.ac.uk/portal/en/publications/investigation-of-the-mechanical-performance-and-weathering-of-hemp-concrete(21db920e-07d2-462a-9037-db613a13ed8e).html

[45] ASTM D4832 – 02, “Standard Test Method for Preparation and Testing of Controlled Low Strength Material,” *ASTM Int.*, vol. 04, pp. 1–5, 2002, [Online]. Available: https://compass.astm.org/download/D4832.10849.pdf

[46] F. Collet, J. Chamoin, S. Pretot, and C. Lanos, “Comparison of the hygric behaviour of three hemp concretes,” *Energy Build.*, vol. 62, pp. 294–303, 2013, doi: 10.1016/j.enbuild.2013.03.010.

[47] A. Evrard, “Transient hygrothermal behaviour of Lime-Hemp Materials,” 2008. [Online]. Available: http://edoc.bib.ucl.ac.be:81/ETD-papier/submitted/Evrard_Arnaud.html

[48] F. Collet, M. Bart, L. Serres, and J. Miriel, “Porous structure and water vapour sorption of hemp-based materials,” *Constr. Build. Mater.*, vol. 22, no. 6, pp. 1271–1280, 2008, doi: 10.1016/j.conbuildmat.2007.01.018.

[49] A. J. Nur, Y. M. Liew, M. M. A. Al Bakri, and C. Y. Heah, “Thermophysical Properties of Metakaolin Alkali activateds Based on Na2SiO3/NaOH Ratio,” *Solid State Phenom.*, vol. 280, pp. 487–493, 2018, doi: 10.4028/www.scientific.net/ssp.280.487.

[50] S. Columbu, M. Mulas, F. Mundula, and R. Cioni, “Strategies for helium pycnometry density measurements of welded ignimbritic rocks,” *Meas. J. Int. Meas. Confed.*, vol. 173, no. November 2020, p. 108640, 2021, doi: 10.1016/j.measurement.2020.108640.

[51] F. J. Semel and D. A. Lados, “Porosity analysis of PM materials by helium pycnometry,” *Powder Metall.*, vol. 49, no. 2, pp. 173–182, 2006, doi: 10.1179/174329006X95347.

[52] O. Manual, “TRUE VOLUME AND DENSITY ANALYZER Operating Manual,” 2018.

[53] C. Ceramics and E. Carbon, “PentaPyc 5200e PentaFoam 5200e”.

[54] F. Batool, “Effect of Microstructure on Thermal Conductivity of Cement-Based Foam,” University of Alberta, 2015. doi: 10.2109/jcersj.97.1478.

[55] J. R. A. Goncalves, Y. Boluk, and V. Bindiganavile, “Thermal properties of fibre-reinforced alkali-activated concrete in extreme temperatures,” *Mag. Concr. Res.*, vol. 70, no. 18, pp. 954–964, 2018, doi: 10.1680/jmacr.17.00189.

[56] ISO 22007-2, “Plastics-Determination of thermal conductivity and thermal diffusivity,” 2008.

[57] S. E. Gustafsson, “Transient plane source techniques for thermal conductivity and thermal diffusivity measurements of solid materials,” *Rev. Sci. Instrum.*, vol. 62, no. 3, pp. 797–804, 1991, doi: 10.1063/1.1142087.

[58] H. Disk and T. Constants, “TPS 1500 Hot disk thermal constants analyser,” Gothenburg Sweden. [Online]. Available: www.hotdiskinstruments.com

[59] M. Mamun, F. Batool, and V. Bindiganavile, “Thermo-mechanical properties of fibre reinforced cement-based foam exposed to sulphate,” *Constr. Build. Mater.*, vol. 61, pp. 312–319, 2014, doi: 10.1016/j.conbuildmat.2014.03.006.

[60] J. Shen and Q. Xu, “Effect of moisture content and porosity on compressive strength of

concrete during drying at 105 °C," *Constr. Build. Mater.*, vol. 195, pp. 19–27, 2019, doi: 10.1016/j.conbuildmat.2018.11.046.

[61] S. Pavía, R. Walker, and J. McGinn, "Effect of testing variables on the hydration and compressive strength of lime hemp concrete," *First Int. Conf. Bio-based Build. Mater.*, vol. 33, no. 2, pp. 635–640, 2015.

[62] A. M. Neville, *Properties of concrete*, Fifth Edit. 2008. doi: 10.4135/9781412975704.n88.

[63] V. Munro, K. J. Dick, D. Ph, and P. Eng, "The replacement of silica fume with hemp flour in shotcrete applications".

[64] A. Evrard, A. De Herde, and J. Minet, "Dynamical interactions between heat and mass flows in Lime-Hemp concrete," *Proc. 3rd Int. Build. Phys. Conf. - Res. Build. Phys. Build. Eng.*, no. 2001, pp. 69–76, 2006.

[65] B. Belhadj, M. Bederina, N. Montrelay, J. Houessou, and M. Quéneudec, "Effect of substitution of wood shavings by barley straws on the physico-mechanical properties of lightweight sand concrete," *Constr. Build. Mater.*, vol. 66, pp. 247–258, 2014, doi: 10.1016/j.conbuildmat.2014.05.090.

[66] D. Taoukil, A. El-bouardi, H. Ezbakhe, and T. Ajzoul, "Thermal proprieties of concrete lightened by wood aggregates," *Res. J. Appl. Sci. Eng. Technol.*, vol. 3, no. 2, pp. 113–116, 2011.

[67] F. Collet, "Hygric and thermal properties of bio-aggregate based building materials," *RILEM State-of-the-Art Reports*, vol. 23, pp. 125–147, 2017, doi: 10.1007/978-94-024-1031-0_6.

[68] T. Jami, S. R. Karade, and L. P. Singh, *A review of the properties of hemp concrete for green building applications*, vol. 239. Elsevier Ltd, 2019. doi: 10.1016/j.jclepro.2019.117852.

[69] P. B. de Bruijn, K. H. Jeppsson, K. Sandin, and C. Nilsson, "Mechanical properties of lime-hemp concrete containing shives and fibres," *Biosyst. Eng.*, vol. 103, no. 4, pp. 474–479, 2009, doi: 10.1016/j.biosystemseng.2009.02.005.

[70] F. Murphy, S. Pavia, and R. Walker, “AN ASSESSMENT OF THE PHYSICAL PROPERTIES OF LIME-HEMP CONCRETE,” vol. 2, pp. 431–439, 2010.

Chapter 4:

[1] V. Živica, M. T. Palou, and M. Križma, “Alkali activated Cements and Their Properties: A Review,” *Build. Res. J.*, vol. 61, no. 2, pp. 85–100, 2015, doi: 10.2478/brj-2014-0007.

[2] A. M. Rashad, “Alkali-activated metakaolin: A short guide for civil Engineer-An overview,” *Constr. Build. Mater.*, vol. 41, pp. 751–765, 2013, doi: 10.1016/j.conbuildmat.2012.12.030.

[3] M. A. Villaquirán-Caicedo, R. M. de Gutiérrez, S. Sulekar, C. Davis, and J. C. Nino, “Thermal properties of novel binary alkali activated based on metakaolin and alternative silica sources,” *Appl. Clay Sci.*, vol. 118, pp. 276–282, 2015, doi: 10.1016/j.clay.2015.10.005.

[4] M. A. Villaquirán-Caicedo, R. M. de Gutiérrez, S. Sulekar, C. Davis, and J. C. Nino, “Thermal properties of novel binary alkali activated based on metakaolin and alternative silica sources,” *Appl. Clay Sci.*, vol. 118, pp. 276–282, 2015, doi: 10.1016/j.clay.2015.10.005.

[5] Y. Ding, J. Dai, and C. Shi, “Mechanical Properties of Alkali-Activated Concrete : A State-of-the-Art Review Keywords,” 2016.

[6] J. R. A. Goncalves, Y. Boluk, and V. Bindiganavile, “Thermal properties of fiber-reinforced alkali-activated concrete in extreme temperatures,” *Mag. Concr. Res.*, vol. 70, no. 18, pp. 954–964, 2017, doi: 10.1680/jmacr.17.00189.

[7] X. Fu and D. D. L. Chung, “Effects of silica fume, latex, methylcellulose, and carbon fibers on the thermal conductivity and specific heat of cement paste,” *Cem. Concr. Res.*, vol. 27, no. 12, pp. 1799–1804, 1997, doi: 10.1016/S0008-8846(97)00174-9.

[8] P. Jittabut, “The Study on Physical and Thermal Properties of Alkali activated Pastes,” *Key Eng. Mater.*, vol. 751, pp. 538–543, 2017, doi: 10.4028/www.scientific.net/kem.751.538.

[9] A. J. Nur, Y. M. Liew, M. M. A. Al Bakri, and C. Y. Heah, “Thermophysical Properties of Metakaolin Alkali activateds Based on Na2SiO3/NaOH Ratio,” *Solid State Phenom.*, vol. 280, pp. 487–493, 2018, doi: 10.4028/www.scientific.net/ssp.280.487.

[10] T. Luukkonen, Z. Abdollahnejad, J. Yliniemi, P. Kinnunen, and M. Illikainen, “One-part alkali-activated materials: A review,” *Cem. Concr. Res.*, vol. 103, no. October 2017, pp. 21–34, 2018, doi: 10.1016/j.cemconres.2017.10.001.

[11] B. Rangan and D. Hardjito, “Studies on fly ash-based alkali-activated concrete,” *Proc. 4th World ...*, no. November, 2005, [Online]. Available:

http://www.google.com/books?hl=id&lr=&id=wIFo7L_zO8AC&oi=fnd&pg=PA133&dq=djwantoro&ots=FlZypGbTgV&sig=wTzPfRqrskTYXr8KGbO58Fgwij8

[12] A. Fernández-Jiménez and A. Palomo, "Composition and microstructure of alkali-activated fly ash binder: Effect of the activator," *Cem. Concr. Res.*, vol. 35, no. 10, pp. 1984–1992, 2005, doi: 10.1016/j.cemconres.2005.03.003.

[13] P. Risdanareni, K. Schollbach, J. Wang, and N. De Belie, "The effect of NaOH concentration on the mechanical and physical properties of alkali-activated fly ash-based artificial lightweight aggregate," *Constr. Build. Mater.*, vol. 259, p. 119832, 2020, doi: 10.1016/j.conbuildmat.2020.119832.

[14] M. L. Granizo, M. T. Blanco-Varela, and S. Martínez-Ramírez, "Alkali activation of metakaolins: Parameters affecting mechanical, structural and microstructural properties," *J. Mater. Sci.*, vol. 42, no. 9, pp. 2934–2943, 2007, doi: 10.1007/s10853-006-0565-y.

[15] A. Palomo, M. W. Grutzeck, and M. T. Blanco, "Alkali-activated fly ashes: A cement for the future," *Cem. Concr. Res.*, vol. 29, no. 8, pp. 1323–1329, 1999, doi: 10.1016/S0008-8846(98)00243-9.

[16] H. Bakkali, M. Ammari, and I. Frar, "NaOH alkali-activated class F fly ash: NaOH molarity, Curing conditions, and mass ratio effect," *J. Mater. Environ. Sci.*, vol. 7, no. 2, pp. 397–401, 2016.

[17] D. Jayant, *Mineral admixtures in cement and concrete [3] Ghosh, S. N., Sarkar, S. L., - Google Scholar*. [Online]. Available: https://scholar.google.com.eg/scholar?q=Mineral+admixtures+in+cement+and+concrete+%5B3%5D%09Ghosh%2C+S.+N.%2C+Sarkar%2C+S.+L.%2C+&btnG=&hl=en&as_sdt=0%2C5

[18] ASTM, "Astm C618," 2014. doi: 10.1520/C0618.

[19] P. Duxson, G. C. Lukey, and J. S. J. Van Deventer, "Thermal conductivity of metakaolin alkali activateds used as a first approximation for determining gel interconnectivity," *Ind. Eng. Chem. Res.*, vol. 45, no. 23, pp. 7781–7788, 2006, doi: 10.1021/ie060187o.

[20] B. Zhang, K. J. D. MacKenzie, and I. W. M. Brown, "Crystalline phase formation in metakaolinite alkali activateds activated with NaOH and sodium silicate," *J. Mater. Sci.*, vol. 44, no. 17, pp. 4668–4676, 2009, doi: 10.1007/s10853-009-3715-1.

[21] M. . Granizo and M. T. Blanco, "Alkaline Activation of Metakaolin," *Journal of Thermal Analysis*, vol. 52. pp. 957–965, 1998.

[22] R. Walker, S. Pavia, and R. Mitchell, "Mechanical properties and durability of hemp-lime concrete," *Constr. Build. Mater.*, vol. 61, pp. 340–348, 2014, doi:

10.1016/j.conbuildmat.2014.02.065.

[23] P. De Bruijn and P. Johansson, “Moisture fixation and thermal properties of lime-hemp concrete,” *Constr. Build. Mater.*, vol. 47, pp. 1235–1242, 2013, doi: 10.1016/j.conbuildmat.2013.06.006.

[24] R. Walker and S. Pavía, “Moisture transfer and thermal properties of hemp-lime concrete,” *Constr. Build. Mater.*, vol. 64, pp. 270–276, 2014, doi: 10.1016/j.conbuildmat.2014.04.081.

[25] Y. Abdellatef, M. A. Khan, A. Khan, M. I. Alam, and M. Kavgic, “Mechanical, thermal, and moisture buffering properties of novel insulating hemp-lime composite building materials,” *Materials (Basel).*, vol. 13, no. 21, pp. 1–18, 2020, doi: 10.3390/ma13215000.

[26] ASTM D4832 – 02, “Standard Test Method for Preparation and Testing of Controlled Low Strength Material,” *ASTM Int.*, vol. 04, pp. 1–5, 2002, [Online]. Available: https://compass.astm.org/download/D4832.10849.pdf

[27] ISO 22007, “Determination of thermal conductivity and thermal diffusivity,” *Int. Stand. ISO 22007-12017(E)*, vol. 2017, 2017.

[28] S. Columbu, M. Mulas, F. Mundula, and R. Cioni, “Strategies for helium pycnometer density measurements of welded ignimbritic rocks,” *Meas. J. Int. Meas. Confed.*, vol. 173, no. November 2020, p. 108640, 2021, doi: 10.1016/j.measurement.2020.108640.

[29] F. J. Semel and D. A. Lados, “Porosity analysis of PM materials by helium pycnometry,” *Powder Metall.*, vol. 49, no. 2, pp. 173–182, 2006, doi: 10.1179/174329006X95347.

[30] R. Walker, “A Study of the Properties of Lime-Hemp Concrete with Pozzolans,” 2013.

[31] R. J. M. Pellenq *et al.*, “A realistic molecular model of cement hydrates,” *Proc. Natl. Acad. Sci. U. S. A.*, vol. 106, no. 38, pp. 16102–16107, 2009, doi: 10.1073/pnas.0902180106.

[32] A. S. Al-Tamimi, O. S. Baghabra Al-Amoudi, M. A. Al-Osta, M. R. Ali, and A. Ahmad, “Effect of insulation materials and cavity layout on heat transfer of concrete masonry hollow blocks,” *Constr. Build. Mater.*, vol. 254, p. 119300, 2020, doi: 10.1016/j.conbuildmat.2020.119300.

Chapter 5:

[1] S. Pantawee, T. Sinsiri, C. Jaturapitakkul, and P. Chindaprasirt, “Utilization of hemp concrete using hemp shiv as coarse aggregate with aluminium sulfate [Al2(SO4)3] and hydrated lime [Ca(OH)2] treatment,” *Constr. Build. Mater.*, vol. 156, pp. 435–442, 2017, doi: 10.1016/j.conbuildmat.2017.08.181.

[2] B. C. Act, “Ontario Building Code 2012,” no. 1, pp. 9–10, 2014.

[3] E. Gourlay, P. Glé, S. Marceau, C. Foy, and S. Moscardelli, “Effect of water content on the acoustical and thermal properties of hemp concretes,” *Constr. Build. Mater.*, vol. 139, pp. 513–523, 2017, doi: 10.1016/j.conbuildmat.2016.11.018.

[4] R. Walker and S. Pavía, “Moisture transfer and thermal properties of hemp-lime concretes,” *Constr. Build. Mater.*, vol. 64, pp. 270–276, 2014, doi: 10.1016/j.conbuildmat.2014.04.081.

[5] P. De Bruijn and P. Johansson, “Moisture fixation and thermal properties of lime-hemp concrete,” *Constr. Build. Mater.*, vol. 47, pp. 1235–1242, 2013, doi: 10.1016/j.conbuildmat.2013.06.006.

[6] H. Uysal, R. Demirboga, R. Şahin, and R. Gül, “The effects of different cement dosages, slumps, and pumice aggregate ratios on the thermal conductivity and density of concrete,” *Cem. Concr. Res.*, vol. 34, no. 5, pp. 845–848, 2004, doi: 10.1016/j.cemconres.2003.09.018.

[7] M. Eroglu S., Toprak S., Urgan O, MD, Ozge E. Onur, MD, Arzu Denizbasi, MD, Haldun Akoglu, MD, Cigdem Ozpolat, MD, Ebru Akoglu, *Hemp Industrial Production and Uses*, vol. 33. 2012.

[8] T. Jami, S. R. Karade, and L. P. Singh, “A review of the properties of hemp concrete for green building applications,” *J. Clean. Prod.*, vol. 239, p. 117852, 2019, doi: 10.1016/j.jclepro.2019.117852.

[9] R. Walker, “A Study of the Properties of Lime-Hemp Concrete with Pozzolans,” 2013.

[10] N. Stevulova *et al.*, “Properties characterization of chemically modified hemp hurds,” *Materials (Basel).*, vol. 7, no. 12, pp. 8131–8150, 2014, doi: 10.3390/ma7128131.

[11] U. Benitha Sandrine, V. Isabelle, M. Ton Hoang, and C. Maalouf, “Influence of chemical modification on hemp-starch concrete,” *Constr. Build. Mater.*, vol. 81, pp. 208–215, 2015, doi: 10.1016/j.conbuildmat.2015.02.045.

[12] P. Brzyski, S. Duda, and A. Raczkowski, “Two-dimensional heat transfer analysis of timber structure walls filled with hemp-lime composite,” *MATEC Web Conf.*, vol. 252, p.

05015, 2019, doi: 10.1051/matecconf/201925205015.

[13] ASTM D 854 – 02, “Standard Test Methods for of Soil Specific GravitySolids by Water Pycnometer,” *ASTM Stand.*, vol. 24, no. 1, p. 120432, 2018, [Online]. Available: https://doi.org/10.1016/j.conbuildmat.2020.118708%0Ahttps://doi.org/10.1016/j.wasman.2018.02.018%0Ahttps://doi.org/10.1016/j.conbuildmat.2019.03.011%0Ahttp://dx.doi.org/10.1007/s40710-017-0210-6%0Ahttp://dx.doi.org/10.1016/j.phpro.2014.07.011%0Ahttps://do

[14] Y. Abdellatef, M. A. Khan, A. Khan, M. I. Alam, and M. Kavgic, “Mechanical, thermal, and moisture buffering properties of novel insulating hemp-lime composite building materials,” *Materials (Basel).*, vol. 13, no. 21, pp. 1–18, 2020, doi: 10.3390/ma13215000.

[15] A. Shea, M. Lawrence, and P. Walker, “Hygrothermal performance of an experimental hemp-lime building,” *Constr. Build. Mater.*, vol. 36, pp. 270–275, 2012, doi: 10.1016/j.conbuildmat.2012.04.123.

[16] P. Brzyski, M. Gładecki, M. Rumińska, K. Pietrak, M. Kubiś, and P. Łapka, “Influence of hemp shives size on hygro-thermal and mechanical properties of a hemp-lime composite,” *Mater. MDPI*, vol. 13, no. 23, pp. 1–17, 2020, doi: 10.3390/ma13235383.

[17] S. Elfordy, F. Lucas, F. Tancret, Y. Scudeller, and L. Goudet, “Mechanical and thermal properties of lime and hemp concrete (‘hempcrete’) manufactured by a projection process,” *Constr. Build. Mater.*, vol. 22, no. 10, pp. 2116–2123, 2008, doi: 10.1016/j.conbuildmat.2007.07.016.

[18] M. Yoshida, T. Kimura, N. Kurahashi, and K. Osako, “MECHANICAL AND THERMAL PROPERTIES OF HEMP-LIME COMPOSITES,” *Compos. Theory Pract.*, no. July, pp. 19–24, 2015.

[19] N. Stevulova, J. Cigasova, E. Terpakova, J. Junak, A. Sicakova, and I. Schwarzova, “Properties testing of lightweight composites based on hemp hurds,” *16th Eur. Conf. Compos. Mater.*, no. January, 2014.

[20] N. Stevulova, L. Kidalova, J. Junak, J. Cigasova, and E. Terpakova, “Effect of hemp shive

sizes on mechanical properties of lightweight fibrous composites," *Procedia Eng.*, vol. 42, no. August, pp. 496–500, 2012, doi: 10.1016/j.proeng.2012.07.441.

[21] L. Arnaud and E. Gourlay, "Experimental study of parameters influencing mechanical properties of hemp concretes," *Constr. Build. Mater.*, vol. 28, no. 1, pp. 50–56, 2012, doi: 10.1016/j.conbuildmat.2011.07.052.

[22] P. B. de Bruijn, K. H. Jeppsson, K. Sandin, and C. Nilsson, "Mechanical properties of lime-hemp concrete containing shives and fibres," *Biosyst. Eng.*, vol. 103, no. 4, pp. 474–479, 2009, doi: 10.1016/j.biosystemseng.2009.02.005.

[23] B. Mazhoud, F. Collet, S. Pretot, and J. Chamoin, "Hygric and thermal properties of hemp-lime plasters," *Build. Environ.*, vol. 96, pp. 206–216, 2016, doi: 10.1016/j.buildenv.2015.11.013.

[24] J. Williams, M. Lawrence, and P. Walker, "The influence of constituents on the properties of the bio-aggregate composite hemp-lime," *Constr. Build. Mater.*, vol. 159, pp. 9–17, 2018, doi: 10.1016/j.conbuildmat.2017.10.109.

[25] A. Bourdot *et al.*, "Characterization of a hemp-based agro-material: Influence of starch ratio and hemp shive size on physical, mechanical, and hygrothermal properties," *Energy Build.*, vol. 153, pp. 501–512, 2017, doi: 10.1016/j.enbuild.2017.08.022.

[26] F. Murphy, S. Pavia, and R. Walker, "AN ASSESSMENT OF THE PHYSICAL PROPERTIES OF LIME-HEMP CONCRETE," vol. 2, pp. 431–439, 2010.

[27] M. Sonebi, S. Wana, S. Amziane, and J. Khatib, "Investigation of the Mechanical Performance and Weathering of Hemp Concrete," *1st Int. Conf. Bio-based Build. Mater.*, vol. 33, no. 2, pp. 416–421, 2015, [Online]. Available: http://pure.qub.ac.uk/portal/en/publications/investigation-of-the-mechanical-performance-and-weathering-of-hemp-concrete(21db920e-07d2-462a-9037-db613a13ed8e).html

[28] M. Madrid, A. Orbe, E. Rojí, and J. Cuadrado, "The effects of by-products incorporated in low-strength concrete for concrete masonry units," *Constr. Build. Mater.*, vol. 153, pp. 117–128, 2017, doi: 10.1016/j.conbuildmat.2017.07.086.

[29] A. Bouguerra *et al.*, “Measurement Of Thermal Conductivity, Thermal Diffusivity And Heat Capacity Of Highly Porous Building Materials Using Transient Plane Source Technique,” vol. 28, no. 8, pp. 1065–1078, 2001.

[30] M. A. Khan, “Physical and Microstructural Properties of Insulating Hempcrete Mixes and their Impact as Infill System on the Foundations due to Increase in Dead Load,” no. March, 2020.

[31] D. Taoukil, A. El Bouardi, F. Sick, A. Mimet, H. Ezbakhe, and T. Ajzoul, “Moisture content influence on the thermal conductivity and diffusivity of wood-concrete composite,” *Constr. Build. Mater.*, vol. 48, pp. 104–115, 2013, doi: 10.1016/j.conbuildmat.2013.06.067.

[32] A. Reilly *et al.*, “The thermal diffusivity of hemplime, and a method of direct measurement,” *Constr. Build. Mater.*, vol. 212, pp. 707–715, 2019, doi: 10.1016/j.conbuildmat.2019.03.264.

[33] S. Ghosn, N. Cherkawi, and B. Hamad, “Studies on Hemp and Recycled Aggregate Concrete,” *Int. J. Concr. Struct. Mater.*, vol. 14, no. 1, 2020, doi: 10.1186/s40069-020-00429-6.

[34] U. Moonart and S. Utara, “Effect of surface treatments and filler loading on the properties of hemp fiber/natural rubber composites,” *Cellulose*, vol. 26, no. 12, pp. 7271–7295, 2019, doi: 10.1007/s10570-019-02611-w.

[35] G. Balčiunas, S. Vejelis, S. Vaitkus, and A. Kairyte, “Physical properties and structure of composite made by using hemp hurds and different binding materials,” *Procedia Eng.*, vol. 57, pp. 159–166, 2013, doi: 10.1016/j.proeng.2013.04.023.

[36] G. Balčiunas, I. Pundiene, L. Lekunaite-Lukošiune, S. Vejelis, and A. Korjakins, “Impact of hemp shives aggregate mineralization on physical-mechanical properties and structure of composite with cementitious binding material,” *Ind. Crops Prod.*, vol. 77, pp. 724–734, 2015, doi: 10.1016/j.indcrop.2015.09.011.

[37] S. Liu, L. Ge, S. Gao, L. Zhuang, Z. Zhu, and H. Wang, “Activated carbon derived from

bio-waste hemp hurd and retted hemp hurd for CO2 adsorption," *Compos. Commun.*, vol. 5, no. December, pp. 27–30, 2017, doi: 10.1016/j.coco.2017.06.002.

[38] V. D. Gorgots, "Standard Practice for Selecting Proportions for Normal, Heavyweight, and Mass Concrete (ACI 211.1-91) Donald," 2002.

[39] ASTM D4832 – 02, "Standard Test Method for Preparation and Testing of Controlled Low Strength Material," *ASTM Int.*, vol. 04, pp. 1–5, 2002, [Online]. Available: https://compass.astm.org/download/D4832.10849.pdf

[40] F. Collet, M. Bart, L. Serres, and J. Miriel, "Porous structure and water vapour sorption of hemp-based materials," *Constr. Build. Mater.*, vol. 22, no. 6, pp. 1271–1280, 2008, doi: 10.1016/j.conbuildmat.2007.01.018.

[41] A. Evrard, "Transient hygrothermal behaviour of Lime-Hemp Materials," 2008. [Online]. Available: http://edoc.bib.ucl.ac.be:81/ETD-papier/submitted/Evrard_Arnaud.html

[42] A. Evrard and A. De Herde, "Bioclimatic envelopes made of lime and hemp concrete," *Proceeding of CISBAT*, vol. 2005, no. November, pp. 1–6, 2005, [Online]. Available: http://dial.academielouvain.be/vital/access/services/Download/boreal:73818/PDF_01

[43] A. J. Nur, Y. M. Liew, M. M. A. Al Bakri, and C. Y. Heah, "Thermophysical Properties of Metakaolin Alkali activateds Based on Na2SiO3/NaOH Ratio," *Solid State Phenom.*, vol. 280, pp. 487–493, 2018, doi: 10.4028/www.scientific.net/ssp.280.487.

[44] S. Columbu, M. Mulas, F. Mundula, and R. Cioni, "Strategies for helium pycnometry density measurements of welded ignimbritic rocks," *Meas. J. Int. Meas. Confed.*, vol. 173, no. November 2020, p. 108640, 2021, doi: 10.1016/j.measurement.2020.108640.

[45] F. J. Semel and D. A. Lados, "Porosity analysis of PM materials by helium pycnometry," *Powder Metall.*, vol. 49, no. 2, pp. 173–182, 2006, doi: 10.1179/174329006X95347.

[46] O. Manual, "TRUE VOLUME AND DENSITY ANALYZER Operating Manual," 2018.

[47] C. Ceramics and E. Carbon, "PentaPyc 5200e PentaFoam 5200e".

[48] A. Al-Tamimi, "Thermal Diffusivity of Hemp Concrete: Experimental and Numerical

Studies," University of Alberta, 2023.

[49] ISO 22007-2, "Plastics-Determination of thermal conductivity and thermal diffusivity," 2008.

[50] M. Mamun, F. Batool, and V. Bindiganavile, "Thermo-mechanical properties of fibre reinforced cement-based foam exposed to sulphate," *Constr. Build. Mater.*, vol. 61, pp. 312–319, 2014, doi: 10.1016/j.conbuildmat.2014.03.006.

[51] N. Stevulova, J. Cigasova, I. Schwarzova, A. Sicakova, and J. Junak, "Sustainable bio-aggregate-based composites containing hemp hurds and alternative binder," *Buildings*, vol. 8, no. 2, pp. 1–14, 2018, doi: 10.3390/buildings8020025.

[52] R. Siddique, M. Singh, S. Mehta, and R. Belarbi, "Utilization of treated saw dust in concrete as partial replacement of natural sand," *J. Clean. Prod.*, vol. 261, 2020, doi: 10.1016/j.jclepro.2020.121226.

[53] B. Belhadj, M. Bederina, N. Montrelay, J. Houessou, and M. Quéneudec, "Effect of substitution of wood shavings by barley straws on the physico-mechanical properties of lightweight sand concrete," *Constr. Build. Mater.*, vol. 66, pp. 247–258, 2014, doi: 10.1016/j.conbuildmat.2014.05.090.

Chapter 6:

[1] N. Stevulova, J. Cigasova, I. Schwarzova, A. Sicakova, and J. Junak, "Sustainable bio-aggregate-based composites containing hemp hurds and alternative binder," *Buildings*, vol. 8, no. 2, pp. 1–14, 2018, doi: 10.3390/buildings8020025.

[2] N. M. Nurazzi *et al.*, "A review on mechanical performance of hybrid natural fiber polymer composites for structural applications," *Polymers (Basel).*, vol. 13, no. 13, 2021, doi: 10.3390/polym13132170.

[3] M. Le Troëdec, C. S. Peyratout, A. Smith, and T. Chotard, "Influence of various chemical treatments on the interactions between hemp fibres and a lime matrix," *J. Eur. Ceram. Soc.*, vol. 29, no. 10, pp. 1861–1868, 2009, doi: 10.1016/j.jeurceramsoc.2008.11.016.

[4] S. Pantawee, T. Sinsiri, C. Jaturapitakkul, and P. Chindaprasirt, "Utilization of hemp

concrete using hemp shiv as coarse aggregate with aluminium sulfate [Al2(SO4)3] and hydrated lime [Ca(OH)2] treatment," *Constr. Build. Mater.*, vol. 156, pp. 435–442, 2017, doi: 10.1016/j.conbuildmat.2017.08.181.

[5] G. Balčiunas, I. Pundiene, L. Lekunaite-Lukošiune, S. Vejelis, and A. Korjakins, "Impact of hemp shives aggregate mineralization on physical-mechanical properties and structure of composite with cementitious binding material," *Ind. Crops Prod.*, vol. 77, pp. 724–734, 2015, doi: 10.1016/j.indcrop.2015.09.011.

[6] N. Stevulova *et al.*, "Properties characterization of chemically modified hemp hurds," *Materials (Basel).*, vol. 7, no. 12, pp. 8131–8150, 2014, doi: 10.3390/ma7128131.

[7] L. Wang, H. Lenormand, H. Zmamou, and N. Leblanc, "Effect of variability of hemp shiv on the setting of lime hemp concrete," *Ind. Crops Prod.*, vol. 171, no. November, p. 113915, 2021, doi: 10.1016/j.indcrop.2021.113915.

[8] M. M. Kabir, H. Wang, K. T. Lau, and F. Cardona, "Effects of chemical treatments on hemp fibre structure," *Appl. Surf. Sci.*, vol. 276, pp. 13–23, 2013, doi: 10.1016/j.apsusc.2013.02.086.

[9] R. Walker, "A Study of the Properties of Lime-Hemp Concrete with Pozzolans," 2013.

[10] G. Balčiunas, S. Vejelis, S. Vaitkus, and A. Kairyte, "Physical properties and structure of composite made by using hemp hurds and different binding materials," *Procedia Eng.*, vol. 57, pp. 159–166, 2013, doi: 10.1016/j.proeng.2013.04.023.

[11] U. Benitha Sandrine, V. Isabelle, M. Ton Hoang, and C. Maalouf, "Influence of chemical modification on hemp-starch concrete," *Constr. Build. Mater.*, vol. 81, pp. 208–215, 2015, doi: 10.1016/j.conbuildmat.2015.02.045.

[12] T. Jami, S. R. Karade, and L. P. Singh, "A review of the properties of hemp concrete for green building applications," *J. Clean. Prod.*, vol. 239, p. 117852, 2019, doi: 10.1016/j.jclepro.2019.117852.

[13] M. Eroglu S., Toprak S., Urgan O, MD, Ozge E. Onur, MD, Arzu Denizbasi, MD, Haldun

Akoglu, MD, Cigdem Ozpolat, MD, Ebru Akoglu, *Hemp Industrial Production and Uses*, vol. 33. 2012.

[14] L. Y. Mwaikambo and M. P. Ansell, "Chemical modification of hemp, sisal, jute, and kapok fibers by alkalization," *J. Appl. Polym. Sci.*, vol. 84, no. 12, pp. 2222–2234, 2002, doi: 10.1002/app.10460.

[15] J. Cigasova, N. Stevulova, and J. Junak, "Influence of binder nature on properties of lightweight composites based on hemp hurds," *Int. J. Mod. Manuf. Technol.*, vol. 5, no. 2, pp. 27–31, 2013.

[16] D. Taoukil, A. El Bouardi, F. Sick, A. Mimet, H. Ezbakhe, and T. Ajzoul, "Moisture content influence on the thermal conductivity and diffusivity of wood-concrete composite," *Constr. Build. Mater.*, vol. 48, pp. 104–115, 2013, doi: 10.1016/j.conbuildmat.2013.06.067.

[17] R. Kumar, S. Obrai, and A. Sharma, "Chemical modifications of natural fiber for composite material," *Der Chem. Sin.*, vol. 4, no. 4, pp. 68–72, 2013.

[18] X. Li, L. G. Tabil, and S. Panigrahi, "Chemical treatments of natural fiber for use in natural fiber-reinforced composites: A review," *J. Polym. Environ.*, vol. 15, no. 1, pp. 25–33, 2007, doi: 10.1007/s10924-006-0042-3.

[19] C. Treatment, N. Fibre, S. Hydroxide, C. Fibre, and S. Fibre, "Mercerization Natural fibers and their composites Mechanical performance of natural fibers – based thermosetting composites," 2008.

[20] R. Walker and S. Pavía, "Effect of Hemp'S Soluble Components on the Physical Properties of Hemp Concrete," *J. Mater. Sci. Res.*, vol. 3, no. 3, pp. 12–23, 2014, doi: 10.5539/jmsr.v3n3p12.

[21] N. Stevulova and I. Schwarzova, "Changes in the Properties of Composites Caused by Chemical Treatment of Hemp Hurds," *Int. J. Chem. Nucl. Metall. Mater. Eng.*, vol. 8, no. 5, pp. 409–413, 2014.

[22] N. Stevulova, J. Cigasova, A. Sicakova, and J. Junak, "Lightweight composites based on

rapidly renewable natural resource," *Chem. Eng. Trans.*, vol. 35, no. January, pp. 589–594, 2013, doi: 10.3303/CET1335098.

[23] S. Ghosn, N. Cherkawi, and B. Hamad, "Studies on Hemp and Recycled Aggregate Concrete," *Int. J. Concr. Struct. Mater.*, vol. 14, no. 1, 2020, doi: 10.1186/s40069-020-00429-6.

[24] U. Moonart and S. Utara, "Effect of surface treatments and filler loading on the properties of hemp fiber/natural rubber composites," *Cellulose*, vol. 26, no. 12, pp. 7271–7295, 2019, doi: 10.1007/s10570-019-02611-w.

[25] N. Števulová, E. Terpáková, J. Čigášová, J. Junák, and L. Kidalová, "Chemically treated hemp shives as a suitable organic filler for lightweight composites preparing," *Procedia Eng.*, vol. 42, no. August, pp. 948–954, 2012, doi: 10.1016/j.proeng.2012.07.488.

[26] R. Siddique, M. Singh, S. Mehta, and R. Belarbi, "Utilization of treated saw dust in concrete as partial replacement of natural sand," *J. Clean. Prod.*, vol. 261, 2020, doi: 10.1016/j.jclepro.2020.121226.

[27] A. Bifulco *et al.*, "A new strategy to produce hemp fibers through a waterglass-based ecofriendly process," *Materials (Basel).*, vol. 13, no. 8, pp. 1–11, 2020, doi: 10.3390/MA13081844.

[28] F. Branda *et al.*, "Silica treatments: A fire retardant strategy for hemp fabric/epoxy composites," *Polymers (Basel).*, vol. 8, no. 8, pp. 1–17, 2016, doi: 10.3390/polym8080313.

[29] E. Gourlay, P. Glé, S. Marceau, C. Foy, and S. Moscardelli, "Effect of water content on the acoustical and thermal properties of hemp concretes," *Constr. Build. Mater.*, vol. 139, pp. 513–523, 2017, doi: 10.1016/j.conbuildmat.2016.11.018.

[30] X. Du, Z. Li, T. Tong, B. Li, and H. Liu, "Isothermal drying process and its effect on compressive strength of concrete in multiscale," *Appl. Sci.*, vol. 9, no. 19, 2019, doi: 10.3390/app9194015.

[31] ISO 22007, "Determination of thermal conductivity and thermal diffusivity," *Int. Stand.*

ISO 22007-12017(E), vol. 2017, 2017.

Chapter 7:

[1] Real S, Gomes MG, Moret Rodrigues A, Bogas JA. Structural lightweight aggregate concrete contributes to reducing thermal bridging effect in buildings. Constr Build Mater 2016;121:460–70. https://doi.org/10.1016/j.conbuildmat.2016.06.018.

[2] Natural Resources Canada. Heating equipment for residential use. Nrcan 2022:1–4.

[3] Agency USEP. Renewable Heating And Cooling 2016:1–10.

[4] Martínez M, Huygen N, Sanders J, Atamturktur S. Thermo-fluid dynamic analysis of concrete masonry units via experimental testing and numerical modeling. J Build Eng 2018;19:80–90. https://doi.org/10.1016/j.jobe.2018.04.029.

[5] Council Directive 2010/31/EU of the European Parliament. Directive 2010/31/EU of the European Parliament and of the Council of 19 May 2010 on the Energy Performance of Buildings. Opt InfoBase Conf Pap 2010.

[6] Canadian Standards Association-CSA. CSA Standards on concrete masonry units-A165 SERIES-14 (R2019). vol. 14. 2014.

[7] National Concrete Masonry Association. ASTM Specifications for Concrete Masonry Units 2012:9.

[8] Blanco JM, Frómeta YG, Madrid M, Cuadrado J. Thermal performance assessment of walls made of three types of sustainable concrete blocks using fem and validated through an extensive measurement campaign. Sustain 2021;13:1–18. https://doi.org/10.3390/su13010386.

[9] Al-Awsh WA, Qasem NAA, Al-Amoudi OSB, Al-Osta MA. Experimental and numerical investigation on innovative masonry walls for industrial and residential buildings. Appl Energy 2020;276:115496. https://doi.org/10.1016/j.apenergy.2020.115496.

[10] Hongxia Z, Kang P, Baoquan C, Xuanyi L. Numerical simulation of the thermal theory of sintered coal gangue self-insulation block and wall. MATEC Web Conf 2018;175. https://doi.org/10.1051/matecconf/201817501021.

[11] Kant K, Shukla A, Sharma A. Heat transfer studies of building brick containing phase change materials. Sol Energy 2017;155:1233–42. https://doi.org/10.1016/j.solener.2017.07.072.

[12] Imafidon OJ, Ting DS-K. Energy consumption of a building with phase change material walls – The effect of phase change material properties. J Energy Storage 2022;52:105080. https://doi.org/https://doi.org/10.1016/j.est.2022.105080.

[13] Elmarghany MR, Radwan A, Shouman MA, Khater AA, Salem MS, Abdelrehim O. Year-long energy analysis of building brick filled with phase change materials. J Energy Storage 2022;50:104605. https://doi.org/https://doi.org/10.1016/j.est.2022.104605.

[14] Vega M, Llantoy N, Chafer M, Ushak S, Cabeza LF. Life cycle assessment of the inclusion of phase change materials in lightweight buildings. J Energy Storage 2022;56:105903. https://doi.org/https://doi.org/10.1016/j.est.2022.105903.

[15] Sun X, Zhang Y, Xie K, Medina MA. A parametric study on the thermal response of a building wall with a phase change material (PCM) layer for passive space cooling. J Energy Storage 2022;47:103548. https://doi.org/https://doi.org/10.1016/j.est.2021.103548.

[16] Zhang Y, Sang G, Li P, Du M, Guo T, Cui X, et al. Study the influence of thermo-physical parameters of phase change material panels on the indoor thermal environment of passive solar buildings in Tibet. J Energy Storage 2022;52:105019. https://doi.org/https://doi.org/10.1016/j.est.2022.105019.

[17] Almitani KH, Abu-Hamdeh NH, Alazwari MA, Salilih EM, Almasri RA, Sajadi SM. Role of solar radiation on the phase change material usefulness in the building applications. J Energy Storage 2022;45:103542. https://doi.org/https://doi.org/10.1016/j.est.2021.103542.

[18] Wernery J, Ben-Ishai A, Binder B, Brunner S. Aerobrick - An aerogel-filled insulating brick. Energy Procedia 2017;134:490–8. https://doi.org/10.1016/j.egypro.2017.09.607.

[19] Su H, Wu D, Shen M, Chen W, Wang S. Development and performance test including mechanical and thermal of new tenon composite block masonry walls. Adv Mater Sci Eng 2019;2019. https://doi.org/10.1155/2019/5253946.

[20] Al-Tamimi AS, Baghabra Al-Amoudi OS, Al-Osta MA, Ali MR, Ahmad A. Effect of insulation materials and cavity layout on heat transfer of concrete masonry hollow blocks. Constr Build Mater 2020;254:119300. https://doi.org/10.1016/j.conbuildmat.2020.119300.

[21] Baghabra O, Al-Osta M, Al-Tamimi A. THERMAL INSULATING MASONRY HOLLOW BRICKS. US 10,538,916 B1, 2020.

[22] Haik R, Peled A, Meir IA. Thermal performance of alternative binders lime hemp concrete (LHC) building: comparison with conventional building materials. Build Res Inf 2021;49:763–76. https://doi.org/10.1080/09613218.2021.1889950.

[23] John E, Hale M, Selvam P. Concrete as a thermal energy storage medium for thermocline solar energy storage systems. Sol Energy 2013;96:194–204. https://doi.org/10.1016/j.solener.2013.06.033.

[24] Laing D, Bahl C, Bauer T, Fiss M, Breidenbach N, Hempel M. High-temperature solid-media thermal energy storage for solar thermal power plants. Proc IEEE 2012;100:516–24. https://doi.org/10.1109/JPROC.2011.2154290.

[25] ANSYS. ANSYS Free Student Software Downloads. ANSYS, Inc 2018:1. https://www.ansys.com/academic/free-student-products.

[26] Bergman T, Lavine A, Incropera F, Dewitt D. Fundamentals of Heat and Mass Transfer. 7th ed. n.d.

[27] Reilly A, Kinnane O, Lesage FJ, McGranaghan G, Pavía S, Walker R, et al. The thermal diffusivity of hemplime, and a method of direct measurement. Constr Build Mater 2019;212:707–15. https://doi.org/10.1016/j.conbuildmat.2019.03.264.

[28] Gourlay E, Glé P, Marceau S, Foy C, Moscardelli S. Effect of water content on the acoustical and thermal properties of hemp concretes. Constr Build Mater 2017;139:513–23. https://doi.org/10.1016/j.conbuildmat.2016.11.018.

[29] De Bruijn P, Johansson P. Moisture fixation and thermal properties of lime-hemp concrete. Constr Build Mater 2013;47:1235–42. https://doi.org/10.1016/j.conbuildmat.2013.06.006.

[30] Tran Le AD, Maalouf C, Mai TH, Wurtz E, Collet F. Transient hygrothermal behaviour of a hemp concrete building envelope. Energy Build 2010;42:1797–806. https://doi.org/10.1016/j.enbuild.2010.05.016.

[31] Ahlberg J, Georges E, Norlén M. The potential of hemp buildings in different climates 2014.

[32] Journal ACI, Paper T. Cryogenic Insulating Concrete - Cement-Based Concrete with Polystyrene Beads. ACI J Proc 1986;83. https://doi.org/10.14359/10446.

[33] Ahmad MR, Chen B, Farasat Ali Shah S. Investigate the influence of expanded clay aggregate and silica fume on the properties of lightweight concrete. Constr Build Mater 2019;220:253–66. https://doi.org/10.1016/j.conbuildmat.2019.05.171.

[34] Taoukil D, El-bouardi A, Ezbakhe H, Ajzoul T. Thermal proprieties of concrete lightened by wood aggregates. Res J Appl Sci Eng Technol 2011;3:113–6.

[35] Djoudi A, Khenfer MM, Bali A, Bouziani T. Effect of the addition of date palm fibers on thermal properties of plaster concrete: Experimental study and modeling. J Adhes Sci Technol 2014;28:2100–11. https://doi.org/10.1080/01694243.2014.948363.

[36] Jelidi A, Bouslama S. Use effects of blast furnace slag aggregates in hydraulic concrete. Mater Struct Constr 2015;48:3627–33. https://doi.org/10.1617/s11527-014-0427-z.

[37] Vejmelková E, Keppert M, Keršner Z, Rovnaníková P, Černý R. Mechanical, fracture-mechanical, hydric, thermal, and durability properties of lime-metakaolin plasters for renovation of historical buildings. Constr Build Mater 2012;31:22–8. https://doi.org/10.1016/j.conbuildmat.2011.12.084.

[38] System Material Database, Thermal Conductivity, Specific Heat Capacity and Density. n.d.

[39] Pan J, Zou R, Jin F. Experimental study on specific heat of concrete at high temperatures and its influence on thermal energy storage. Energies 2017;10. https://doi.org/10.3390/en10010033.

[40] Hoivik N, Greiner C, Barragan J, Iniesta AC, Skeie G, Bergan P, et al. Long-term performance results of concrete-based modular thermal energy storage system. J Energy Storage 2019;24:100735. https://doi.org/10.1016/j.est.2019.04.009.

[41] Walker R. A Study of the Properties of Lime-Hemp Concrete with Pozzolans. 2013.

[42] Dhakal U, Berardi U, Gorgolewski M, Richman R. Hygrothermal performance of hempcrete for Ontario (Canada) buildings. J Clean Prod 2017;142:3655–64. https://doi.org/10.1016/j.jclepro.2016.10.102.

Chapter 8:

[1] S. Real, M. G. Gomes, A. Moret Rodrigues, and J. A. Bogas, "Contribution of structural lightweight aggregate concrete to the reduction of thermal bridging effect in buildings," *Constr. Build. Mater.*, vol. 121, pp. 460–470, 2016, doi: 10.1016/j.conbuildmat.2016.06.018.

[2] Natural Resources Canada, "Heating equipment for residential use," *Nrcan*, pp. 1–4, 2022, [Online]. Available: https://www.nrcan.gc.ca/energy-efficiency/products/product-information/heating-equipment-for-residential-use/13740

[3] U. S. E. P. Agency, "Renewable Heating And Cooling," pp. 1–10, 2016, [Online]. Available: https://www.epa.gov/rhc/renewable-space-heating

[4] M. Martínez, N. Huygen, J. Sanders, and S. Atamturktur, "Thermo-fluid dynamic analysis of concrete masonry units via experimental testing and numerical modeling," *J. Build. Eng.*, vol. 19, no. May, pp. 80–90, 2018, doi: 10.1016/j.jobe.2018.04.029.

[5] Council Directive 2010/31/EU of the European Parliament, "Directive 2010/31/EU of the European Parliament and of the Council of 19 May 2010 on the Energy Performance of Buildings," *Optics InfoBase Conference Papers*. 2010. [Online]. Available: https://www.legislation.gov.uk/eudr/2010/31

[6] Canadian Standards Association-CSA, "CSA Standards on concrete masonry units-A165 SERIES-14 (R2019)," 2014. [Online]. Available: https://www.csagroup.org/store/product/A165 SERIES-14/

[7] National Concrete Masonry Association, "ASTM Specifications for Concrete Masonry Units," p. 9, 2012, [Online]. Available: https://ncma.org/resource/astm-specifications-for-concrete-masonry-units/

[8] J. M. Blanco, Y. G. Frómeta, M. Madrid, and J. Cuadrado, "Thermal performance

assessment of walls made of three types of sustainable concrete blocks by means of fem and validated through an extensive measurement campaign," *Sustain.*, vol. 13, no. 1, pp. 1–18, 2021, doi: 10.3390/su13010386.

[9] W. A. Al-Awsh, N. A. A. Qasem, O. S. B. Al-Amoudi, and M. A. Al-Osta, "Experimental and numerical investigation on innovative masonry walls for industrial and residential buildings," *Appl. Energy*, vol. 276, no. July, p. 115496, 2020, doi: 10.1016/j.apenergy.2020.115496.

[10] Z. Hongxia, P. Kang, C. Baoquan, and L. Xuanyi, "Numerical simulation of thermal theory of sintered coal gangue self-insulation block and wall," *MATEC Web Conf.*, vol. 175, 2018, doi: 10.1051/matecconf/201817501021.

[11] J. Wernery, A. Ben-Ishai, B. Binder, and S. Brunner, "Aerobrick - An aerogel-filled insulating brick," *Energy Procedia*, vol. 134, pp. 490–498, 2017, doi: 10.1016/j.egypro.2017.09.607.

[12] H. Su, D. Wu, M. Shen, W. Chen, and S. Wang, "Development and performance test including mechanical and thermal of new tenon composite block masonry walls," *Adv. Mater. Sci. Eng.*, vol. 2019, 2019, doi: 10.1155/2019/5253946.

[13] K. Kant, A. Shukla, and A. Sharma, "Heat transfer studies of building brick containing phase change materials," *Sol. Energy*, vol. 155, pp. 1233–1242, 2017, doi: 10.1016/j.solener.2017.07.072.

[14] A. S. Al-Tamimi, O. S. Baghabra Al-Amoudi, M. A. Al-Osta, M. R. Ali, and A. Ahmad, "Effect of insulation materials and cavity layout on heat transfer of concrete masonry hollow blocks," *Constr. Build. Mater.*, vol. 254, p. 119300, 2020, doi: 10.1016/j.conbuildmat.2020.119300.

[15] O. Baghabra, M. Al-Osta, and A. Al-Tamimi, "THERMAL INSULATING MASONRY HOLLOW BRICKS," US 10,538,916 B1, 2020 [Online]. Available: https://patents.google.com/patent/US10538916B1/en

[16] R. Haik, A. Peled, and I. A. Meir, "Thermal performance of alternative binders lime hemp concrete (LHC) building: comparison with conventional building materials," *Build. Res. Inf.*, vol. 49, no. 7, pp. 763–776, 2021, doi: 10.1080/09613218.2021.1889950.

[17] T. Bergman, A. Lavine, F. Incropera, and D. Dewitt, *Fundamentals of Heat and Mass Transfer*, 7th ed.

[18] A. Reilly *et al.*, "The thermal diffusivity of hemplime, and a method of direct measurement," *Constr. Build. Mater.*, vol. 212, pp. 707–715, 2019, doi: 10.1016/j.conbuildmat.2019.03.264.

[19] E. Gourlay, P. Glé, S. Marceau, C. Foy, and S. Moscardelli, "Effect of water content on the

acoustical and thermal properties of hemp concretes," *Constr. Build. Mater.*, vol. 139, pp. 513–523, 2017, doi: 10.1016/j.conbuildmat.2016.11.018.

[20] P. De Bruijn and P. Johansson, "Moisture fixation and thermal properties of lime-hemp concrete," *Constr. Build. Mater.*, vol. 47, pp. 1235–1242, 2013, doi: 10.1016/j.conbuildmat.2013.06.006.

[21] A. D. Tran Le, C. Maalouf, T. H. Mai, E. Wurtz, and F. Collet, "Transient hygrothermal behaviour of a hemp concrete building envelope," *Energy Build.*, vol. 42, no. 10, pp. 1797–1806, 2010, doi: 10.1016/j.enbuild.2010.05.016.

[22] J. Ahlberg, E. Georges, and M. Norlén, "The potential of hemp buildings in different climates," 2014.

[23] ISO 22007, "Determination of thermal conductivity and thermal diffusivity," *Int. Stand. ISO 22007-12017(E)*, vol. 2017, 2017.

[24] M. Mamun, F. Batool, and V. Bindiganavile, "Thermo-mechanical properties of fibre reinforced cement-based foam exposed to sulphate," *Constr. Build. Mater.*, vol. 61, pp. 312–319, 2014, doi: 10.1016/j.conbuildmat.2014.03.006.

Appendix A:

[1] H. Uysal, R. Demirboga, R. Şahin, and R. Gül, "The effects of different cement dosages, slumps, and pumice aggregate ratios on concrete thermal conductivity and density," *Cem. Concr. Res.*, vol. 34, no. 5, pp. 845–848, 2004, doi: 10.1016/j.cemconres.2003.09.018.

[2] X. Fu and D. D. L. Chung, "Effects of silica fume, latex, methylcellulose, and carbon fibers on the thermal conductivity and specific heat of cement paste," *Cem. Concr. Res.*, vol. 27, no. 12, pp. 1799–1804, 1997, doi: 10.1016/S0008-8846(97)00174-9.

[3] Y. Xu and D. D. L. Chung, "Increasing the specific heat of cement paste by admixture surface treatments," *Cem. Concr. Res.*, vol. 29, no. 7, pp. 1117–1121, 1999, doi: 10.1016/S0008-8846(99)00080-0.

[4] R. Demirboğa, "Influence of mineral admixtures on thermal conductivity and compressive strength of mortar," *Energy Build.*, vol. 35, no. 2, pp. 189–192, 2003, doi: 10.1016/S0378-7788(02)00052-X.

[5] F. Batool, "Effect of Microstructure on Thermal Conductivity of Cement-Based Foam," University of Alberta, 2015. doi: 10.2109/jcersj.97.1478.

[6] C. Costa, "Materials for construction and civil engineering: Science, processing, and design," *Springer Int. Publ. Switz. 2015*, pp. 1–902, 2015, doi: 10.1007/978-3-319-08236-3.

[7] K. Vance, G. Falzone, I. Pignatelli, M. Bauchy, M. Balonis, and G. Sant, “Direct Carbonation of Ca(OH)2 Using Liquid and Supercritical CO2: Implications for Carbon-Neutral Cementation,” *Ind. Eng. Chem. Res.*, vol. 54, no. 36, pp. 8908–8918, 2015, doi: 10.1021/acs.iecr.5b02356.

[8] A. Reilly *et al.*, “The thermal diffusivity of hemplime, and a method of direct measurement,” *Constr. Build. Mater.*, vol. 212, pp. 707–715, 2019, doi: 10.1016/j.conbuildmat.2019.03.264.

[9] P. De Bruijn and P. Johansson, “Moisture fixation and thermal properties of lime-hemp concrete,” *Constr. Build. Mater.*, vol. 47, pp. 1235–1242, 2013, doi: 10.1016/j.conbuildmat.2013.06.006.

[10] R. Walker and S. Pavía, “Moisture transfer and thermal properties of hemp-lime concretes,” *Constr. Build. Mater.*, vol. 64, pp. 270–276, 2014, doi: 10.1016/j.conbuildmat.2014.04.081.

[11] V. D. Kunthe, G. Manavendra, and V. M. Sondur, “Effect of thermal properties on fly ash based concrete,” *Int. Res. J. Eng. Technol.*, vol. 05, no. 12, pp. 396–400, 2018.

[12] Z. Zhao, X. Qu, F. Li, and J. Wei, “Effects of steel slag and silica fume additions on compressive strength and thermal properties of lime-fly ash pastes,” *Constr. Build. Mater.*, vol. 183, pp. 439–450, 2018, doi: 10.1016/j.conbuildmat.2018.05.220.

[13] R. Demirboğa and R. Gül, “The effects of expanded perlite aggregate, silica fume and fly ash on the thermal conductivity of lightweight concrete,” *Cem. Concr. Res.*, vol. 33, no. 5, pp. 723–727, 2003, doi: 10.1016/S0008-8846(02)01032-3.

[14] Y. Xu and D. D. L. Chung, “Effect of sand addition on the specific heat and thermal conductivity of cement,” *Cem. Concr. Res.*, vol. 30, no. 1, pp. 59–61, 2000, doi: 10.1016/S0008-8846(99)00206-9.

[15] Y. Xu and D. D. L. Chung, “Cement of high specific heat and high thermal conductivity, obtained by using silane and silica fume as admixtures,” *Cem. Concr. Res.*, vol. 30, no. 7, pp. 1175–1178, 2000, doi: 10.1016/S0008-8846(00)00296-9.

[16] S. A. Farhan, M. F. Khamidi, M. H. Murni, M. F. Nuruddin, A. Idrus, and A. M. Al Yacouby, “Effect of silica fume and MIRHA on thermal conductivity of cement paste,” *WIT Trans. Built Environ.*, vol. 124, pp. 331–339, 2012, doi: 10.2495/HPSM120291.

[17] M. R. Ahmad, B. Chen, and S. Farasat Ali Shah, “Investigate the influence of expanded clay aggregate and silica fume on the properties of lightweight concrete,” *Constr. Build. Mater.*, vol. 220, pp. 253–266, 2019, doi: 10.1016/j.conbuildmat.2019.05.171.

[18] H. Zhou and A. L. Brooks, “Thermal and mechanical properties of structural lightweight concrete containing lightweight aggregates and fly-ash cenospheres,” *Constr. Build. Mater.*, vol. 198, pp. 512–526, 2019, doi: 10.1016/j.conbuildmat.2018.11.074.

[19] E. Belhadj, C. Diliberto, and A. Lecomte, “Properties of hydraulic paste of basic oxygen furnace slag,” *Cem. Concr. Compos.*, vol. 45, pp. 15–21, 2014, doi: 10.1016/j.cemconcomp.2013.09.016.

[20] P. Setayeshgar, Y. Boluk, and V. Bindiganavile, “Efficacy of forest based ash as a supplementary cementing material for concrete,” *Can. J. Civ. Eng.*, vol. 44, no. 8, pp. 652–660, 2017, doi: 10.1139/cjce-2016-0351.

[21] J. Stolz, Y. Boluk, and V. Bindiganavile, “Wood ash as a supplementary cementing material in foams for thermal and acoustic insulation,” *Constr. Build. Mater.*, vol. 215, pp. 104–113, 2019, doi: 10.1016/j.conbuildmat.2019.04.174.

[22] M. Madrid, A. Orbe, E. Rojí, and J. Cuadrado, “The effects of by-products incorporated in low-strength concrete for concrete masonry units,” *Constr. Build. Mater.*, vol. 153, pp. 117–128, 2017, doi: 10.1016/j.conbuildmat.2017.07.086.

[23] X. Chen, M. K. Zhou, P. L. Cong, and X. Li, “Influence of SO3 Content on the Strength of Cement-Fly Ash Stabilized Crushed-Stones,” *Geosynth. Civ. Environ. Eng.*, pp. 398–402, 2009, doi: 10.1007/978-3-540-69313-0_76.

[24] P. Chindaprasirt, S. Rukzon, and V. Sirivivatnanon, “Resistance to chloride penetration of blended Portland cement mortar containing palm oil fuel ash, rice husk ash and fly ash,” *Constr. Build. Mater.*, vol. 22, no. 5, pp. 932–938, 2008, doi: 10.1016/j.conbuildmat.2006.12.001.

[25] P. Jittabut, “The Study on Physical and Thermal Properties of Alkali activated Pastes,” *Key Eng. Mater.*, vol. 751, pp. 538–543, 2017, doi: 10.4028/www.scientific.net/kem.751.538.

[26] A. A. Raheem, I. A. Akinteye, and S. A. Lasisi, “A Study of Thermal Conductivity of Corn Cob Ash Blended Cement Mortar,” *Constr. Mater. Struct.*, no. December 2011, pp. 261–267, 2014.

[27] A. A. Abioye, F. A. Olutoge, O. M. Ofuyatan, and S. O. Oyebisi, “Effect of corncob ash blended cement on the properties of lateritic interlocking blocks,” *Prog. Ind. Ecol. An Int. J.*, vol. 11, no. 4, p. 373, 2018, doi: 10.1504/pie.2017.10013954.

[28] M. Čáchová *et al.*, “Application of ceramic powder as supplementary cementitious material in lime plasters,” *Medziagotyra*, vol. 22, no. 3, pp. 440–444, 2016, doi: 10.5755/j01.ms.22.3.7433.

[29] D. Jayant, *Mineral admixtures in cement and concrete [3] Ghosh, S. N., Sarkar, S. L., - Google Scholar*. [Online]. Available: https://scholar.google.com.eg/scholar?q=Mineral+admixtures+in+cement+and+concrete+%5B3%5D%09Ghosh%2C+S.+N.%2C+Sarkar%2C+S.+L.%2C+&btnG=&hl=en&as_sdt=0%2C5

[30] ASTM, “Astm C618,” 2014. doi: 10.1520/C0618.

[31] E. Vejmelková, M. Keppert, Z. Keršner, P. Rovnaníková, and R. Černý, “Mechanical, fracture-mechanical, hydric, thermal, and durability properties of lime-metakaolin plasters for renovation of historical buildings,” *Constr. Build. Mater.*, vol. 31, pp. 22–28, 2012, doi: 10.1016/j.conbuildmat.2011.12.084.

[32] S. A. Zaidan and M. H. Omar, “The effects of bauxite, metakaolin, and porosity on the thermal properties of prepared Iraqi clays refractory mortars,” *Appl. Phys. A Mater. Sci. Process.*, vol. 124, no. 5, pp. 1–8, 2018, doi: 10.1007/s00339-018-1759-2.

[33] I. Sumirat, Y. Ando, and S. Shimamura, “Theoretical consideration of the effect of porosity on thermal conductivity of porous materials,” *J. Porous Mater.*, vol. 13, no. 3, pp. 439–443, 2006, doi: 10.1007/s10934-006-8043-0.

[34] D. F. Mahdi, “Preparation of Refractory Mortar from Iraqi Raw Materials,” pp. 37–40, 1813.

[35] J. Shackelford and R. Doremus, *Ceramic and Glass Materials*. 2008. doi: 10.1007/978-0-387-73362-3.

[36] V. Živica, M. T. Palou, and M. Križma, “Alkali activated Cements and Their Properties: A Review,” *Build. Res. J.*, vol. 61, no. 2, pp. 85–100, 2015, doi: 10.2478/brj-2014-0007.

[37] X. Bingyu, “Effect of Heating Rate on the Thermal Properties of High Strength Mortar,” University of Alberta Effect, 2019.

[38] M. Bederina, L. Marmoret, K. Mezreb, M. M. Khenfer, A. Bali, and M. Quéneudec, “Effect of the addition of wood shavings on thermal conductivity of sand concretes: Experimental study and modelling,” *Constr. Build. Mater.*, vol. 21, no. 3, pp. 662–668, 2007, doi: 10.1016/j.conbuildmat.2005.12.008.

[39] G. Jia, Z. Li, P. Liu, and Q. Jing, “Applications of aerogel in cement-based thermal insulation materials: An overview,” *Mag. Concr. Res.*, vol. 70, no. 16, pp. 822–837, 2018, doi: 10.1680/jmacr.17.00234.

[40] C. J. Kobus and J. David Schall, “Thermal properties of a concrete aerogel paste composite,” *ASME Int. Mech. Eng. Congr. Expo. Proc.*, vol. 8A-2018, pp. 1–5, 2018, doi: 10.1115/IMECE2018-88660.

[41] M. F. Khamidi, C. Glover, S. A. Farhan, N. H. A. Puad, and M. F. Nuruddin, “Effect of silica aerogel on the thermal conductivity of cement paste for the construction of concrete buildings in sustainable cities,” *WIT Trans. Built Environ.*, vol. 137, pp. 665–674, 2014, doi: 10.2495/HPSM140601.

[42] H. Garbalińska and J. Strzałkowski, “Thermal and strength properties of lightweight

concretes with variable porosity structures," *J. Mater. Civ. Eng.*, vol. 30, no. 12, pp. 1–9, 2018, doi: 10.1061/(ASCE)MT.1943-5533.0002549.

[43] T. Gao, B. P. Jelle, A. Gustavsen, and S. Jacobsen, "Aerogel-incorporated concrete: An experimental study," *Constr. Build. Mater.*, vol. 52, pp. 130–136, 2014, doi: 10.1016/j.conbuildmat.2013.10.100.

[44] R. Alyousef, O. Benjeddou, C. Soussi, M. A. Khadimallah, and M. Jedidi, "Experimental Study of New Insulation Lightweight Concrete Block Floor Based on Perlite Aggregate, Natural Sand, and Sand Obtained from Marble Waste," *Adv. Mater. Sci. Eng.*, vol. 2019, pp. 1–14, 2019, doi: 10.1155/2019/8160461.

[45] H. Oktay, R. Yumrutaş, and A. Akpolat, "Mechanical and thermophysical properties of lightweight aggregate concretes," *Constr. Build. Mater.*, vol. 96, pp. 217–225, 2015, doi: 10.1016/j.conbuildmat.2015.08.015.

[46] W. V. Liu, D. B. Apel, and V. S. Bindiganavile, "Thermal properties of lightweight dry-mix shotcrete containing expanded perlite aggregate," *Cem. Concr. Compos.*, vol. 53, pp. 44–51, 2014, doi: 10.1016/j.cemconcomp.2014.06.003.

[47] A. C. I. Journal and T. Paper, "Cryogenic Insulating Concrete - Cement-Based Concrete with Polystyrene Beads," *ACI J. Proc.*, vol. 83, no. 3, 1986, doi: 10.14359/10446.

[48] L. H. Nguyen, A. L. Beaucour, S. Ortola, and A. Noumowé, "Experimental study on the thermal properties of lightweight aggregate concretes at different moisture contents and ambient temperatures," *Constr. Build. Mater.*, vol. 151, pp. 720–731, 2017, doi: 10.1016/j.conbuildmat.2017.06.087.

[49] L. H. Nguyen, A. L. Beaucour, S. Ortola, and A. Noumowé, "Influence of the volume fraction and the nature of fine lightweight aggregates on the thermal and mechanical properties of structural concrete," *Constr. Build. Mater.*, vol. 51, pp. 121–132, 2014, doi: 10.1016/j.conbuildmat.2013.11.019.

[50] S. Real, M. G. Gomes, A. Moret Rodrigues, and J. A. Bogas, "Contribution of structural lightweight aggregate concrete to the reduction of thermal bridging effect in buildings," *Constr. Build. Mater.*, vol. 121, pp. 460–470, 2016, doi: 10.1016/j.conbuildmat.2016.06.018.

[51] B. Brown, *Chapter 5 : Aggregates for Concrete*, vol. 32, no. 5. 1998. doi: 10.4324/9780203478981.ch16.

[52] A. L. Marshall, "The thermal properties of concrete," *Build. Sci.*, vol. 7, no. 3, pp. 167–174, 1972, doi: 10.1016/0007-3628(72)90022-9.

[53] D. P. Bentz, M. A. Peltz, A. Durán-Herrera, P. Valdez, and C. A. Juárez, "Thermal properties of high-volume fly ash mortars and concretes," *J. Build. Phys.*, vol. 34, no. 3, pp.

263–275, 2011, doi: 10.1177/1744259110376613.

[54] I. Z. Yildirim and M. Prezzi, “Geotechnical Properties of Fresh and Aged Basic Oxygen Furnace Steel Slag,” *J. Mater. Civ. Eng.*, vol. 27, no. 12, p. 04015046, 2015, doi: 10.1061/(asce)mt.1943-5533.0001310.

[55] A. Jelidi and S. Bouslama, “Use effects of blast furnace slag aggregates in hydraulic concrete,” *Mater. Struct. Constr.*, vol. 48, no. 11, pp. 3627–3633, 2015, doi: 10.1617/s11527-014-0427-z.

[56] A. D. Tran Le, C. Maalouf, T. H. Mai, E. Wurtz, and F. Collet, “Transient hygrothermal behaviour of a hemp concrete building envelope,” *Energy Build.*, vol. 42, no. 10, pp. 1797–1806, 2010, doi: 10.1016/j.enbuild.2010.05.016.

[57] B. Mazhoud, F. Collet, S. Pretot, and J. Chamoin, “Hygric and thermal properties of hemp-lime plasters,” *Build. Environ.*, vol. 96, pp. 206–216, 2016, doi: 10.1016/j.buildenv.2015.11.013.

[58] E. Gourlay, P. Glé, S. Marceau, C. Foy, and S. Moscardelli, “Effect of water content on the acoustical and thermal properties of hemp concretes,” *Constr. Build. Mater.*, vol. 139, pp. 513–523, 2017, doi: 10.1016/j.conbuildmat.2016.11.018.

[59] G. Mohamed and B. Djamila, “Properties of dune sand concrete containing coffee waste,” *MATEC Web Conf.*, vol. 149, p. 01039, 2018, doi: 10.1051/matecconf/201714901039.

[60] E. Serri, M. Z. Suleiman, and M. A. O. Mydin, “The Effects of Oil Palm Shell Aggregate Shape on the Thermal Properties and Density of Concrete,” *Adv. Mater. Res.*, vol. 935, pp. 172–175, 2014, doi: 10.4028/www.scientific.net/amr.935.172.

[61] D. Taoukil, A. El Bouardi, F. Sick, A. Mimet, H. Ezbakhe, and T. Ajzoul, “Moisture content influence on the thermal conductivity and diffusivity of wood-concrete composite,” *Constr. Build. Mater.*, vol. 48, pp. 104–115, 2013, doi: 10.1016/j.conbuildmat.2013.06.067.

[62] D. Taoukil, A. El-bouardi, H. Ezbakhe, and T. Ajzoul, “Thermal proprieties of concrete lightened by wood aggregates,” *Res. J. Appl. Sci. Eng. Technol.*, vol. 3, no. 2, pp. 113–116, 2011.

[63] A. Bouguerra, A. Ledhem, F. Barquin, R. M. Dheilly, and M. Queneudec, “Effect of Microstructure on the Mechanical and Thermal,” *Cem. Concr. Res.*, vol. 28, no. 8, pp. 1179–1190, 1998.

[64] P. Bekhta and E. Dobrowolska, “Thermal properties of wood-gypsum boards,” *Holz als Roh - und Werkst.*, vol. 64, no. 5, pp. 427–428, 2006, doi: 10.1007/s00107-005-0074-8.

[65] D. Taoukil, A. El bouardi, T. Ajzoul, and H. Ezbakhe, “Effect of the incorporation of wood wool on thermo physical proprieties of sand mortars,” *KSCE J. Civ. Eng.*, vol. 16, no. 6, pp.

1003–1010, 2012, doi: 10.1007/s12205-012-1470-3.

[66] L. Qin, X. Gao, and T. Chen, “Recycling of raw rice husk to manufacture magnesium oxysulfate cement based lightweight building materials,” *J. Clean. Prod.*, vol. 191, pp. 220–232, 2018, doi: 10.1016/j.jclepro.2018.04.238.

[67] D. K. Panesar and B. Shindman, “The mechanical, transport and thermal properties of mortar and concrete containing waste cork,” *Cem. Concr. Compos.*, vol. 34, no. 9, pp. 982–992, 2012, doi: 10.1016/j.cemconcomp.2012.06.003.

[68] J. K. Prusty, S. K. Patro, and S. S. Basarkar, “Concrete using agro-waste as fine aggregate for sustainable built environment – A review,” *Int. J. Sustain. Built Environ.*, vol. 5, no. 2, pp. 312–333, 2016, doi: 10.1016/j.ijsbe.2016.06.003.

[69] M. G. Salemane and A. S. Luyt, “Thermal and Mechanical Properties of Polypropylene – Wood Powder Composites,” vol. 1, no. June, pp. 25–32, 2005, doi: 10.1002/app.23521.

[70] J. Wilson, “Thermal Properties Of Building Materials,” *Mater. Compd. Adhes. Substrates, Number 1, Tech. Data, Vol. 14*, pp. 1–2, 2008.

[71] G. A. Daoud Atef, “Effect of Rubber Aggregates on the Thermophysical Properties of Self-Consolidating Concrete,” *J. Bioprocess. Biotech.*, vol. 04, no. 03, pp. 1–7, 2014, doi: 10.4172/2155-9821.1000156.

[72] I. Berkovitch, *Design and Control of Concrete Mixtures*. 1984.

[73] H. Paiva, L. P. Esteves, P. B. Cachim, and V. M. Ferreira, “Rheology and hardened properties of single-coat render mortars with different types of water retaining agents,” *Constr. Build. Mater.*, vol. 23, no. 2, pp. 1141–1146, 2009, doi: 10.1016/j.conbuildmat.2008.06.001.

[74] A. Pierre, A. Perrot, V. Picandet, and Y. Guevel, “Cellulose ethers and cement paste permeability,” *Cem. Concr. Res.*, vol. 72, pp. 117–127, 2015, doi: 10.1016/j.cemconres.2015.02.013.

[75] P. Shafigh, I. Asadi, and N. B. Mahyuddin, “Concrete as a thermal mass material for building applications - A review,” *J. Build. Eng.*, vol. 19, no. April, pp. 14–25, 2018, doi: 10.1016/j.jobe.2018.04.021.

[76] D. L. Bean and T. B. Husbands, *TECHNICAL REPORT REMR-CS-3 LATEX ? uJIV11XTURES t-OR PORTLAND CEMENT CONCRETE AND IViORTAR by Waterways Experiment Station , Corps of Engineers US Army Corps of Engineers*. 1986.

[77] B. Nagy, S. G. Nehme, and D. Szagri, “Thermal properties and modeling of fiber reinforced concretes,” *Energy Procedia*, vol. 78, pp. 2742–2747, 2015, doi: 10.1016/j.egypro.2015.11.616.

[78] M. Mamun, “The Fractal Nature of Cement-Based Systems Under Sustained Elevated Temperatures,” 1386.

[79] H. Awang, A. O. Mydin, and A. F. Roslan, “Effect of additives on mechanical and thermal properties of lightweight foamed concrete,” *Adv. Appl. Sci. Res.*, vol. 3, no. 5, pp. 3326–3338, 2012.

[80] W. Khaliq and V. Kodur, “Thermal and mechanical properties of fiber reinforced high performance self-consolidating concrete at elevated temperatures,” *Cem. Concr. Res.*, vol. 41, no. 11, pp. 1112–1122, 2011, doi: 10.1016/j.cemconres.2011.06.012.

[81] C. K. Y. Leung and M. S. W. Lin, “High Performance Cementitious Materials With Thermal Insulation Property,” vol. 2012, no. June, pp. 236–241, 2012.

[82] M. A. Othuman Mydin, N. A. Rozlan, N. M. Sani, and S. Ganesan, “Analysis of Micro-Morphology, Thermal Conductivity, Thermal Diffusivity and Specific Heat Capacity of Coconut Fibre Reinforced Foamed Concrete,” *MATEC Web Conf.*, vol. 17, p. 01020, 2014, doi: 10.1051/matecconf/20141701020.

[83] A. Djoudi, M. M. Khenfer, A. Bali, and T. Bouziani, “Effect of the addition of date palm fibers on thermal properties of plaster concrete: Experimental study and modeling,” *J. Adhes. Sci. Technol.*, vol. 28, no. 20, pp. 2100–2111, 2014, doi: 10.1080/01694243.2014.948363.

[84] M. A. O. Mydin, M. N. M. Nawi, M. A. C. Munaaim, N. Mohamad, A. A. A. Samad, and I. Johari, “Effect of steel fibre volume fraction on thermal performance of Lightweight Foamed Mortar (LFM) at ambient temperature,” *J. Adv. Res. Fluid Mech. Therm. Sci.*, vol. 47, no. 1, 2018.

[85] L. Qiu *et al.*, “A review of recent advances in thermophysical properties at the nanoscale: From solid state to colloids,” *Phys. Rep.*, vol. 843, pp. 1–81, 2020, doi: 10.1016/j.physrep.2019.12.001.

[86] P. Jittabut, *Effect of Nanosilica on Mechanical and Thermal Properties of Cement Composites for Thermal Energy Storage Materials*, vol. 79. Elsevier B.V., 2015. doi: 10.1016/j.egypro.2015.11.454.

[87] P. Li, H. Wu, Y. Liu, J. Yang, Z. Fang, and B. Lin, “Preparation and optimization of ultra-light and thermal insulative aerogel foam concrete,” *Constr. Build. Mater.*, vol. 205, pp. 529–542, 2019, doi: 10.1016/j.conbuildmat.2019.01.212.

[88] J. Fang, J. Feng, and C. Zhang, “Thermal conductivity of low density carbon aerogels,” *J. Porous Mater.*, vol. 19, no. 5, pp. 551–556, 2012, doi: 10.1007/s10934-011-9504-7.

[89] Y. Xie, S. Xu, Z. Xu, H. Wu, C. Deng, and X. Wang, “Interface-mediated extremely low thermal conductivity of graphene aerogel,” *Carbon N. Y.*, vol. 98, pp. 381–390, 2016, doi:

10.1016/j.carbon.2015.11.033.

[90] R. Černý, A. Kunca, V. Tydlitát, J. Drchalová, and P. Rovnaníková, “Effect of pozzolanic admixtures on mechanical, thermal and hygric properties of lime plasters,” *Constr. Build. Mater.*, vol. 20, no. 10, pp. 849–857, 2006, doi: 10.1016/j.conbuildmat.2005.07.002.

[91] B. Seng, C. Magniont, S. Lorente, and S. Spagnol, “Evaluation of hemp concrete thermal properties,” pp. 984–989, 2016, doi: 10.1109/UIC-ATC-ScalCom-CBDCom-IoP-SmartWorld.2016.144.

[92] B. Haba, B. Agoudjil, A. Boudenne, and K. Benzarti, “Hygric properties and thermal conductivity of a new insulation material for building based on date palm concrete,” *Constr. Build. Mater.*, vol. 154, pp. 963–971, 2017, doi: 10.1016/j.conbuildmat.2017.08.025.

[93] J. R. A. Goncalves, Y. Boluk, and V. Bindiganavile, “Thermal properties of fibre-reinforced alkali-activated concrete in extreme temperatures,” *Mag. Concr. Res.*, vol. 70, no. 18, pp. 954–964, 2017, doi: 10.1680/jmacr.17.00189.

[94] M. T. Tran, X. H. Vu, and E. Ferrier, “Mesoscale experimental investigation of thermomechanical behaviour of the carbon textile reinforced refractory concrete under simultaneous mechanical loading and elevated temperature,” *Constr. Build. Mater.*, vol. 217, pp. 156–171, 2019, doi: 10.1016/j.conbuildmat.2019.05.067.

[95] E. Vejmelková, P. Konvalinka, P. Padevět, and R. Černý, “Thermophysical and Mechanical Properties of Fiber-Reinforced Composite Material Subjected To High Temperatures,” *J. Civ. Eng. Manag.*, vol. 16, no. 3, pp. 395–400, 2010, doi: 10.3846/jcem.2010.45.

[96] R. Černý *et al.*, “Hygrothermal properties of glass fiber reinforced cements subjected to elevated temperature,” *Mater. Struct. Constr.*, vol. 37, no. 273, pp. 597–607, 2004, doi: 10.1617/14019.

[97] I. Introduction, “The T h e r m a l Diffusivity of Ice and W a t e r Between - 4 0 and + 60 ~ C,” vol. 3, pp. 540–543, 1968.

APPENDIX A: FACTORS AFFECTING THERMAL DIFFUSIVITY OF CONCRETE, AS SUPPLEMENTARY FOR CHAPTER 2.

Appendix A.1: Hydraulic binders:

Cement (C):

As shown in Table 2.1, the density and thermal conductivity of concrete increases with increasing cement content [1][2][3][4]. This is attributed chiefly to the decrement in porosity and the increment in CSH gel (i.e., low CH, typically about 20% from quantitative X-ray diffraction [5]). A decrement in the specific heat capacity was indicated with increasing cement content due to mainly pores decrement [2]. Hence, increasing the cement content results in a considerable increment (about 25%) in thermal diffusivity [3][2].

Hydraulic Lime (HLi):

Lime is obtained by calcination of limestone with a significant clay content (6.5-20 %, by mass) [6]. Clay is either as impurities in limestone (Natural Hydraulic Lime NHL= NHL2, NHL3.5, NHL5) or has to be added artificially to the limestone (Hydraulic Lime -HL). Hydraulic lime sets and hardens due to the hydration process of the hydraulic compounds forming CSH, CAH, and AFm (The addition of gypsum is to retard the setting) [6]. The carbonation process occurs with the presence of slaked lime and CO_2 to form calcite ($CaCO_3$) [7][6].

$$Calcination\ Process\ \begin{cases} Clay\ Decomposition\ (Al2O3.SiO2 \rightarrow Al2O3+SiO2) \\ Limestone\ Decarbonation\ (CaCO3 \rightarrow CaO+CO2) \end{cases}$$

$$Carbonation\ process\ \{Ca(OH)_2 + CO_2 \rightarrow CaCO_3\ (Calcite) + H_2O\}$$

Lime binders have a typical density of 1.40 g/cm^3, and thermal conductivity of 0.70 W/m K [8]. NHL (15%) was used with slaked lime (75%) and fly ash (10%) to produce hemp concrete with a thermal diffusivity of 0.249-0.300 mm^2/s [9]. Furthermore, lower values of diffusivity were obtained (about 0.164 mm^2/s) with the usage of cement (10%), NHL (20%), and slaked lime (70%) [10]. Thus, NHL enhances the hydraulicity in the mixtures due to the higher content of slaked lime

(i.e., producing more CSH). In general, only NHL would increase the thermal diffusivity (Similar to cement) due to the higher hydraulicity (i.e., more CSH and less porosity).

Appendix A.2: Hydraulic binders:

Fly Ash (FA):

Fly ash is a pozzolan material with larger particles and amorphous silica content (3 times lower) than silica fume [9]. As shown in Table 2.1, the addition of 30% FA in mortar slightly reduced the density and significantly the conductivity by about 33% due to the amorphous structure, lower density of fly ash, and increasing porosity of matrix (Because of the larger grain size of fly ash) [4]. Similarly, the density and conductivity of concrete with FA reduced by 5 and 12%, respectively, while Cp values increased considerably (about 20%). Thus, the thermal diffusivity decreased by about 30% [11]. As a comparison with SF, the amount of CSH produced from the hydration of SF is higher (due to the higher content of amorphous silica and higher surface area), and the thermal conductivity of SF (about 0.092 W/m K) is relatively lower than FA (about 0.119 W/m K). Thus, the thermal diffusivity of the SF mixture would be somewhat lower than that of the FA mixture [12].

Silica Fume (SF):

Silica fume is a pozzolanic admixture containing about 85-98% amorphous silicon dioxide (i.e., SF has low thermal conductivity) [5]. The thermal conductivity of crystalline silica is about 15 times that of amorphous one [13]. Therefore, adding SF decreases density and thermal conductivity significantly because of the amorphous structure and lower density of SF [5][4]. The specific heat capacity of amorphous structure is higher than crystalline because the porosity is higher. Hence, more energy will be stored at the pores and the interface zones with pores [2][14][3][15][12]. Therefore, adding SF in concrete increased Cp due to the high amorphous silica and CSH content. Silica fume is a very fine material (high surface area). More barriers and interface zones will be formed between SF and the cement matrix, reducing thermal conductivity and increasing specific heat capacity. Adding silica fume (SF) will considerably affect the paste's thermal properties. As the experimental results presented in Table 2.1 and Figure 2.3, the effect of SF addition in paste is the highest, then mortar and concrete is the least. For the paste, the addition of 25% SF reduced the density (due to the lower density of SF) and porosity (due to filling pores with more CSH) by

about 8%, which led to a reduction of 24% in thermal conductivity [16]. This reduction increased with silane-treated SF (due to the network of covalent coupling) or using water-reducing agents (i.e., low water content) by about an other14% [14][2][3]. The Cp increased slightly by less than 10%. Thus, the thermal diffusivity decreased significantly by about 30% with 15% of SF [14][2]. For mortars, the effect of SF addition is reduced due to sand [14][4]. Although the density and thermal conductivity reduction was less than 10% and the Cp increased with the same amount, the diffusivity reduced by about 20% [14]. Further, adding SF with cement lime paste does not improve thermal diffusivity because the density is reduced by about 20% with the same increment on Cp and negligible effect on the k-value [12]. For foamed concrete, SF slightly increased the density, conductivity, and heat capacity and negligibly affected the diffusivity, as indicated in [17][18], which may be due to the formation of more CSH that fills the foam pores. Demirboga and Gul proved experimentally a reduction in thermal conductivity and density with the replacement of cement with silica fume and fly ash, which ascribed to the lower specific gravities of pozzolanas compared to cement [16][13].

Blast Furnace Slag (BFS):

Blast furnace slag is a pozzolan material with a chemical composition similar to FA with a higher lime content. Thus, BFS has a hydraulic and pozzolan reaction due to the high content of CaO and SiO_2 (39.56 and 37.68%, respectively [4]). However, the specific gravity of BFS is 2.86, which is greater than the value of FA (2.40) [4]; hence, the density and thermal conductivity of BFS samples were higher than FA ones [4]. As shown in Table 2.1, the addition of 30% BFS reduced the density (slightly) and noticeably the conductivity (about 14%) [4], which ascribed to the lower density of BFS.

Basic Oxygen Furnace Steel Slag (BOFSS):

Steel slag is a by-product of steel production, produced in extensive contents and rarely utilized [19][12]. BOFSS has a high content of CaO (similar to cement). Still, the cementitious activity of steel slag during the hydration process is much lower than that of FA and SF due to the highly crystalline nature of BOFS (XRD analysis) [19]. Thus, the formation of CSH gel was slowed. As

shown in Table 2.1, BOFSS increased porosity (about 11%) due to low reactivity. Thus, the density negligibly decreased, and thermal conductivity reduced by about 20% [12]. In divergent, the specific heat capacity considerably reduced (about 15%) with increasing the content, ascribed to the crystalline structure of BOFSS; hence, the thermal diffusivity reduced by about 10% [12].

Wood Ash (WA):

The wood ash contains a high content of CaO (63%) and a considerable amount of SO_3 (18%), and the mean particle size is about ten times of Portland cement Type GU [20][21]. The bulk density of wood ash is 0.320 g/cm^3, and different particle sizes and shapes were observed, tiny crystalline particles mixed with larger irregular particles [20]. As shown in Table 2.1, replacing 20% wood ash (with cement) in concrete increased the porosity by 20%; hence, the thermal conductivity was reduced by 20% with a slight reduction in density [22]. WA seems to be relatively low reactive as a binder, which may be ascribed to the crystalline structure of WA. Thus, part of WA acts as a filler more than a binder, reducing compressive strength and forming more pores (less paste to cover the filler surface) [22]. The specific heat capacity increased with increasing WA by about 18%, compared to normal concrete [22], ascribed to increasing porosity. Therefore, the thermal diffusivity reduced significantly by around 30% for normal concrete [22]. Interestingly, the presence of SO_3 in WA can simulate the pozzolan reaction with CH to produce a large ettringite (AFt) content to fill the pores [23]. However, the large particle sizes of WA may disturb the hydration and pozzolan reaction.

Rice Husk Ash (RHA):

Rice husk is an agricultural waste from rice mills used as fuel for generating heat. Rice husk ash contains about 88% amorphous silica, making RHA work as a pozzolan admixture [24][25]. As a result of high silica content, the addition of RHA reduced the thermal conductivity to about 35% [25][16] due to amorphous silica and the new amount of amorphous CSH (i.e., porosity increased). The density decreased with increasing the content of RHA to about 11 and 8% for the contents of 10 and 25%, respectively [25][16] due to the lower density of RHA (relative to cement) and the porosity increment (which may due to larger particle size of RHA). Hence, the thermal

conductivity reduced with increasing the content of RHA due to reducing density and increasing porosity. Thus, specific heat capacity increased slightly (Amorphous structure of RHA) [25]. Consequently, the thermal diffusivity values reduced considerably by about 30% [25].

Corn Cob Ash (CCA):

Corn cob is agricultural crop waste produced widely over the world. CCA is a pozzolan admixture with 66.38% SiO_2 and 11.57% CaO, which could be blended with cement to improve its thermal properties [26]. The thermal conductivity of CCA concrete (with 25% cement replacement) is about 71% lower than concrete with normal cement [26], which is ascribed to the lower density of CCA and high content of amorphous silica [27]. The Cp values are expected to be increased. Hence, the diffusivity would be decreased.

Brick Powder (BP):

The brick powder has a high content of silica and alumina (50 and 20%) [28]. The introduction of BP into slaked lime-based plaster has a considerable reduction in the thermal conductivity and diffusivity (by about 50%) with a slight increment in Cp (about 10%), which is ascribed to the amorphous silica (from BP) [28]. The density and porosity were slightly affected [28].

Metakaolin (MK):

Metakaolin is a pozzolanic admixture mainly composed of silica and alumina, produced by calcinating kaolin [29] and satisfying the ASTM C618 standards [30]. The presence of metakaolin enhanced concrete's strength, durability, and rheological properties [5]. Metakaolin acts like pozzolanic admixtures during hydration, which reacts with CH to produce silica and alumina [5]. As shown in Table 2.1, the addition of MK in lime plaster decreased porosity (> 10%) due to the formation of CSH gel, while the density was slightly reduced due to the lower density of MK relative to slaked lime [31]. Therefore, the thermal conductivity increased (about 10%), and Cp was negligibly affected, leading to a slight increment in thermal diffusivity [31]. Similar findings in Table 2.1 [32], the density of refractory mortar (Type of mortars used as thermal insulation under high temperatures without changing) was slightly reduced with the addition of metakaolin

due to increasing porosity by about 29% for the content of 40% of MK. The formation of pores is ascribed to the change in phases (evaporation of water) during firing (about 1200ºC), leading to the formation of vacancies in the structure [32]. The k-value decreased with decreasing the density (i.e., higher porosity) by about 18%. Further, Cp is hugely reduced by 73% because the porosity is relatively low compared to solid volume, and the heat stored in a solid material is much higher than that in a porous [33][32]. Therefore, the thermal diffusivity increased to 68% compared to mortar without MK.

Kaolin (KL):

As shown in Table 2.1, kaolin was used to produce refractory mortar with powder fire clay bricks (FCB). Kaolin and FCB are mainly composed of silica (>50%) and alumina (>30%) [34]. Adding kaolin increased the density by about 10% with a content of 47% because the density of the added kaolin is much higher than FCB and increased the formation of the Mullite phase (i.e., decreasing porosity) [34]. Mullite is a ceramic material with a crystal structure ($3Al_2O_3.2SiO_2$), which has stability and a refractory nature at high temperatures [35]. The thermal conductivity reduced sharply to about 85% (40% kaolin) because adding kaolin increases the water absorption capacity. This leads to the densification of some regions and the formation of air pores in other regions of the matrix [34]. The specific heat capacity increased slightly with the addition of kaolin [34]. As a result, the calculated thermal diffusivity values are shallow due to the high values of Cp (5.8 to 6.7 J/g K) and super low k-values (0.003 to 0.00052 W/m K).

Bauxite (Bx):

Bauxite binder is produced by firing bauxite rocks at 1200 °C, then crushed and grinded to be used to prepare refractory mortar with kaolin [32], and mainly composed of alumina (60%) and silica (20%) [34]. Kaolin was replaced by bauxite with different dosages, which increased the density by 14% and slightly decreased the porosity due to the production of mullite (Al_4SiO_8) (i.e., denser than kaolin) and glass phase (amorphous) filling the voids [32]. Therefore, the thermal conductivity and specific heat capacity increased by 12 and 30%, respectively Table 2.1. However, adding Bx increased Cp pointedly because the heat stored in a solid material is much higher than

that in the porous [33], as well as the reduction of porosity. As a result, the thermal diffusivity was reduced by increasing the content of Bx by about 40%.

Appendix A.3: Alkali-activated binders:

A new type of cementitious binder produced by a chemical reaction (Alkali activatedisation Reactions) between aluminosilicate materials and alkaline activating agents to form aluminosilicate gel (Alkali activated) with binders properties of setting and hardening to be used as a promising binder alternate for constructions [36]. Pozzolanas such as fly ash and blast furnace slag were considered aluminosilicate materials (rich in alumina and silica) and thus could be used for alkali-activatedisation reactions [36]. The alkaline activating agents commonly include sodium hydroxide and sodium silicate, while sodium carbonate and potassium hydroxide were rarely used [36].

$$Aluminosilicate Aluminosilicate\ Material + Alkaline\ Activating\ Agent\ +\ H_2O \rightarrow \text{Aluminosilicat } (Geopolymer)$$

Appendix A.4: Effect of Argillaceous aggregate

Argillaceous aggregates are fine-grained composites mainly of aluminosilicate and clay minerals such as kaolinite and chlorite. Most argillaceous aggregates have porous and glassy structures, which minimize density and thermal conductivity and maximize heat storage capacity (i.e., reduce thermal diffusivity). Thus, this type of aggregate could be a great candidate for thermal conservation composites. As a logic, the presence of fine particles of argillaceous aggregates would lead to pozzolanic behavior.

Sand (S):

Sand has a large particle size and negligible reactivity with cement compared to cementitious materials. The addition of sand to concrete reduces the heat capacity (about 13%) and increases the thermal conductivity (9%) [14], which is attributed to the crystalline behavior of sand particles (Similar findings by Xie [37]). Further, the large particle size of sand results in a smaller interface area with cement matrix; thereby, the slippage at the interface decreases (i.e., slightly reduced Cp), and the scattering at the interface also decreases (i.e., reducing thermal barrier and increasing slightly k-value). Generally, the interface zone for finer particles such as silica fume is much higher; thereby, the behavior will be reversed (increase Cp and reduce k), improving thermal diffusivity by 18% [14]. The type of sand affects the thermal properties because the chemical composition with high crystalline silica content tends to increase density and thermal conductivity. Dune sand has a tightened particle size distribution and less crystalline silica content than river sand; hence, dune sand's density and thermal conductivity are lower than river sand [38].

Aerogel

Aerogels could be classified either on the surface properties as hydrophilic or hydrophobic aerogels or the production of inorganic, organic or inorganic–organic aerogels [39]. Silica aerogel is the earliest discovered aerogel (inorganic aerogel) and is widely used in research as thermal insulation material [39]. The authors reviewed using different types of aerogel to reduce concrete and mortar thermal conductivity [39]. The results proved a super reduction in thermal conductivity with increasing content of aerogel (0.10-0.60 W/m K) for about 25 studies presented and discussed

[39] (Similar findings by [40]). Aerogel particles are brittle and light, floating and accumulating during mixing with binder. Therefore, the uniformity of the mixture was affected negatively, resulting in a reduction in mechanical and thermal insulation properties [39]. Furthermore, aquaphobic aerogels are hardly mixed with the paste due to their hydrophobic property [39]. The presence of activated silica (amorphous silica) in silica aerogel (as filler/aggregate) may cause an alkali-silica reaction with (OH) available in cement pores alkaline solution. Therefore, cracks may occur due to swelling and interior pressure. Further, Silica aerogel granules have an advantage in this possible application because they are smaller than a grain of sand, which is one concrete component. Because of their small size, there is a better possibility for mixing a relatively homogeneous composite mixture [40]. Khamidi1 et al. proved a super reduction of about 95% in thermal conductivity (about 0.076 W/m K) of cement paste with 20 ml of silica aerogel due to about 25% porosity [41]; thus, the diffusivity absolutely would be significantly reduced. Garbalińska1 et al. used a hydrophobic silica aerogel (mainly composed of SiO_2) with a particle size of 0.40-0.70 mm and a content of 20% of total concrete volume [42]. The results showed that the thermal diffusivity reduced by about 50%, as compared to the control mix (without aerogel), which ascribed to the extreme pores of aerogel (10 and 30 nm) [42] (Similar findings for hydrophobic silica aerogel [43]).

Expanded Perlite Aggregate (EPL):

Perlite is a siliceous volcanic glass (amorphous) with a chemical composition mainly of SiO_2 (70-80%) and Al_2O_3 (12-16%) [44]. The volume of perlite expanded 4-20 times the original volume when heated above 870^{o}C. Due to the high porosity (70-85%) and amorphous structure, perlite has low density (0.39-0.42 g/cm^3) and low thermal conductivity (0.04 W/m K) [44][1]. Therefore, the effect of perlite on thermal properties is encouraging, as proved by many studies. The density of concrete with 50% replacement of EPL decreased to about 52% due to increasing the porosity significantly (about 64%); hence, the thermal conductivity was reduced dramatically by 81% due to the amorphous structure of perlite (Table 2.2) [45]. The specific heat capacity increased considerably by 26%, which may ascribed to the increment of porosity, moisture content (perlite has high water absorption), and high specific heat capacity of perlite (0.837 J/m K) [45]. As a

result, the thermal diffusivity decreased significantly by 75% with the substitution of 50% of EPL [45]. A similar improvement was observed by Liu et al. [46] by introducing perlite in shotcrete with 100% replacement of sand with an increment of about 20% on the specific heat capacity. Thus, the thermal diffusivity reduced by about 58% [46]. The addition of perlite is affected by moisture and cement content because of their high thermal properties [47].

Vermiculite (Vc) Aggregate:

Vermiculite is a micaceous mineral with a laminar structure and extremely high water absorption (about 300% of weight) [47]. Like perlite, Vc expanded when subjected to high temperature or chemical reaction [47]. The addition of vermiculite improves all thermal properties of cementitious composites. The density and thermal conductivity were significantly reduced by about 80% due to the high porosity and insulation of Vc (Table 2.2) [47]. The specific heat capacity increased by 61% [47], which may attributed to the high water absorption (water has high Cp). Hence, the thermal diffusivity decreased with the same amount of Cp.

Expanded Clay Aggregate (ECA)

Expanded clay is a lightweight aggregate formed by enlarging the ecological clay at a high temperature of about 1200^{o}C. The expanded clay has a crystal structure, which contains mainly 59% quartz (SiO_2), aluminate, iron oxide, and smaller amounts of amorphous aluminosilicate (XRD analysis) [17]. The particles of EC are spherical and have a highly porous inner structure and a non-porous outer surface [17]. Combining ECA and stable foam with densities of 0.335 and 0.180 g/cm^3 proved the efficiency of producing lightweight concrete with ECA macro pores (0.1-2 mm) and foam micropores [17]. The solid parts of ECA and ESA have a higher mass of ferrite and alumina than pumice aggregates, which increases the density and thermal conductivity [18]. Adding 50% of ECA for foamed concrete reduced all thermal properties, including density and thermal conductivity, with 37 and 46 % percentages due to increasing porosity by about 47% [17]. The specific heat capacity was reduced considerably by about 24% [17], which may ascribed to the crystalline structure of ECA (i.e., absorb lesser energy). Thus, the thermal diffusivity was reduced markedly by about 20%, which increased by adding silica fume to about 26% [17]. On

the other hand, for concrete without foam, the specific heat capacity has negligible changes with increasing the content of ECA. In contrast, Cp increased by 21% compared to normal-weight concrete (NWC) due to the higher porosity. As compared to NWC, the thermal conductivity reduced impressively by about 70% due to the reduction of density (about 37%) [48]; hence, the removal of diffusivity was promising at 61% [48].

Expanded Shale Aggregate (ESA)

The expanded shale aggregates are similar to ECA and have a crystal structure containing quartz, iron oxide, and aluminate, as indicated in the XRD results [49]. ESA consists of a porous inner structure surrounded by a skeleton, which is relatively denser [48][49]. As expected, the results of all thermal properties improved significantly. The density was reduced by 35%, and the thermal conductivity was almost double compared to normal-weight concrete. In comparison, the specific heat capacity increased by 24% due to the porous structure of ESA [48][49].

Pumice (Pu):

Pumice is a porous, glassy volcanic rock consisting primarily of about 73% SiO2 and 13% alumina [49]. Pumice contains about 25% of non-connected pores [49], and high water absorption reached 80% [47]. Pumice aggregate has a promising thermal effect on concrete like perlite because of its porous and glassy structure [1]. As indicated in Table 2.2, the density and thermal conductivity reduced by about 46 and 80%, respectively, while the Cp increased significantly to 40% [45]. Thereby, the thermal diffusivity decreased dramatically by 75% [45]. Similar behavior was obtained in the same trend with a significant reduction in thermal diffusivity with 100% replacement of Pu [1][48].

Riverlite Aggregate (RLA) (expanded clay Agg.)

As shown in XRD analysis, RLA included both amorphous and crystalline minerals (such as quartz and spinel) [18]. The porosity of fine and coarse RLA is 47 and 58%, respectively [18]. The experimental data in Table 2.2 shows the effect of coarse RLA is higher than fine particles on the thermal properties due to the higher porosity (about 10% higher) and content of coarse particles.

The thermal conductivity and density reduced considerably by about 26 and 42%, respectively, for coarse RLA, with a noticeable increment in Cp of about 16% (i.e., the thermal diffusivity reduced meaningfully by about 47%). The enhancement of thermal properties increased using fine and coarse RLA, reducing thermal diffusivity by about 64%. On the contrary, the improvement reduced the use of fine particles of the LWA with a diffusivity reduction of 27%. The specific heat capacity increased by 18% for the combination particles while slightly increased for fine aggregates (about 4%).

Agrex (Ag), Leca (Le), Lytag (Ly), and Stalite (St) Aggregates:

Using SLWA (Agrex, leca, lytag, and stalite) enhanced the thermal characteristics of concrete. The results revealed a reduction of 19-31%, 39-53% in density and thermal conductivity, and an increment of 36-35% in specific heat capacity, reducing 38-47% in thermal diffusivity compared to NWC [50]. Therefore, SLWA aggregates proved high thermal efficiency for steady (low thermal conductivity) and unsteady (low thermal diffusivity) states. The expanded clay aggregates disclose better thermal insulation than the other aggregates due to their low density and high porosity.

Appendix A.5: Effect of calcareous aggregate

This type of aggregate is alkaline sedimentary rocks rich in calcium carbonate ($CaCO_3$) or lime [51]. The crystalline structure of calcite ($CaCO_3$) increases conductivity and reduces heat capacity; thus, the thermal diffusivity is increased, such as in gravel and CWM. Furthermore, in the presence of fine particles of calcareous aggregates (hydraulic behavior), more amorphous CSH would be produced, which means a slight reduction in diffusivity. On the other hand, some calcareous aggregates have or induce a porous structure (i.e., decreased conductivity and increased heat capacity), affecting thermal diffusivity (i.e., considerable reduction in thermal diffusivity) such as FAC and BFS.

Gravel (Limestone) (G):

The addition of gravel increased all thermal properties of concrete in different ranges (Table 2.2). The highest increment was on thermal conductivity and thermal diffusivity by about 70% and 60%,

while the density and specific heat were increased slightly by 10% and 13%, respectively, compared to cement paste [14] [50]. The increment of gravel thermal properties is due to the high thermal conductivity (3.03 W/m K), density (2.46 g/cm^3), and specific heat capacity (0.846 J/g K) [18] [52]. Further, the higher surface area of gravel decreases the dispersing at the interface zone with the cement matrix, which leads to increased thermal conductivity (i.e., the larger the particles, the higher thermal conductivity). Limestone aggregates showed lower thermal diffusivity than siliceous aggregates due to the lower thermal conductivity [53].

Crushed Waste Marble (CWM):

The marble waste is crushed to obtain the desired particle size and used as a replacement for aggregates in concrete [44]. The chemical composition of CWM shows a high content of calcite ($CaCO_3$ = 93.30%) and quicklime (CaO = 52.28%), which gives the crystalline behavior (i.e., has high density and thermal conductivity) [44]. Therefore, adding CWM decreases the porosity from 56 – 44% with the substitution of 100% of sand; hence, the density, thermal conductivity, and specific heat capacity increased by 9, 68, and 48%, respectively. Further, CWM's higher density and Cp and k-value increased these properties [44]. Therefore, the thermal diffusivity increased significantly by about 33% for 100% of CWM [44].

Fly-Ash Cenospheres (FAC):

Fly-ash cenospheres is a lightweight filler with an average particle size of 81μm and used to replace fine, normal-weight aggregates. The density of FAC is 910 kg/m^3 and induces micro air porous in the cement matrix [18]. Even though FAC contains crystalline components (XRD analysis [18]) such as quartz, calcite, and mullite, the micro size FAC induced micro-cellular structure, which reduced the density and thermal conductivity (both are almost linearly proportioning) [18]. On the contrary, the specific heat capacity of LWAC increased with decreasing the density and porosity due to the higher heat capacity of FAC; hence, the thermal diffusivity was undoubtedly reduced by up to 33% [18].

Steel Slag (SS):

Steel slag is an artificial aggregate produced during the metallurgical process, separating impurities using active slag. Steel slag has a crystalline structure containing portlandite, calcite, and the oxides of iron, manganese, and aluminum, as indicated in XRD analysis [54]. The addition of steel slag in concrete is expected to negatively affect (i.e., increasing thermal diffusivity) the thermal properties due to the crystalline structure.

Blast-Furnace Slag (BFS) Aggregates:

Blast furnace slag is artificial aggregate with two types: crystallized and vitrified (glassy or amorphous) blast furnace slag (CS & VS). The CS is produced by slowly cooling the slag at ambient temperature. In contrast, VS is produced by rapidly cooling the slag with water, and both are composed mainly of silica (SiO_2), lime (CaO), alumina (Al_2O_3), and magnesia (MgO), as indicated in the XRD analysis [55]. The crystallized and vitrified blast furnace slag behaves like lightweight aggregates due to closed pores. The hydraulic behavior of furnace slag (as cement and lime) consumed a lower amount of Portlandite due to the existence of fine particles of CS and VS (i.e., a new amount of CSH formed). Therefore, the thermal conductivity reduced significantly for both CS and VS (about 58%, as compared to sand and limestones), while the Cp value decreased slightly due to the crystalline structure of CS [55]. Thus, the thermal diffusivity reduced by about 50%.

Appendix A.6: Effect of bio-sourced aggregate

The bio aggregates are hydrophilic macromolecules, giving the hemp concrete a hygroscopic property (absorbing and releasing environmental moisture) [56]. In other words, hemp concrete is susceptible to vapor and liquid water compared to normal concrete [56]. Therefore, the water content of hemp concrete reached 10% for relative humidity of 50% (most commonly RH experienced in buildings) and higher than 25% for RH greater than 90%. As a result, hemp concrete's properties must be studied to investigate the effect of water content on thermal and acoustic properties [57]. Furthermore, the porosity of hemp concrete influenced the characteristic behavior and divided into three types [58]:

- Macropores (>1mm) due to the imperfect arrangement of hemp shives.
- Mesopores (0.01- 0.1 mm) within hemp shiv and binder.
- Micropores (> 0.01 μm) within the binder matrix.

Coffee Waste (CW):

The ground of coffee waste mainly consists of Carbone and has low density (0.387 kg/m^3), low thermal conductivity (0.30 W/m K), and high porosity (52%) [59]. The replacement of sand by 20% of ground CW reduced the density and greatly the thermal conductivity by 13 and 48%, respectively, due to the porous structure of CW and the pores related to the poor adhesion between CW and binders (i.e., Thermal conductivity of air (0.024 W/m K) much lower than all the other components of concrete) [59]. The Cp value increased with increasing the content of CW by 34% due to the pores. Hence, the thermal diffusivity reduced significantly by 60% [59].

Oil Palm Shell Aggregate (OPS):

Oil pal shell is crushed and sieved as lightweight aggregate to produce insulation concrete. The specific gravity and k-value of OPS are 1.20 and 0.13 W/m K [60]. The data shows that the addition of 35% OPS of the total volume decreased the density and thermal conductivity by about 25 and 72%, while the values of Cp have no significant changes [60]. The diffusivity values have considerably improved by about 58%, ascribed to the porosity, low specific gravity, and low k-value of OPS [60].

Saw Dust (SD) or Wood Shavings (WS):

Sawdust is small and fine particles of wood produced using carpentering equipment [22]. Many studies introduced sawdust in concrete and proved a reduction in mechanical properties and an enhancement in thermal properties. Therefore, pre-treatments were conducted on sawdust, which improved strength and negatively affected thermal behavior [22]. The porosity increased significantly with the addition of sawdust to about 57% due to the interaction between cement and saw matrix (Table 2.2) [22][38]. Therefore, thermal conductivity and diffusivity reduced significantly by 51 and 54%, respectively. Further, the specific heat increased dramatically by

about 35% due to the high porosity and high specific heat of sawdust [22]. There is a good agreement with the results obtained by the authors for concrete with wood shavings [61][62][63]. Wood coarse particles exert more diffusivity than fine particles by about 30%, ascribed to the higher porosity generated by the looser interaction between coarse wood pieces and gypsum matrix [64].

Wood Wool (WW):

The thermophysical properties of wood wool (light and insulator) gave an advantage to be used in concrete and mortar. The following study was found in the literature for using wood wool in cement mortar. It is apparent in Table 2.2 that the density and thermal conductivity reduced significantly by 16 and 33%, respectively, due to the porosity (ascribed to the interaction between cement and wood matrices). On the contrary, the specific heat capacity increased by 32% due to the Cp of wood and porosity (i.e., absorb high energy). Therefore, the thermal diffusivity decreased significantly by 46% [65]. In the same trend, many studies concluded with the same results [22][62]. In conclusion, bio aggregates have a very high potential to improve the thermophysical properties of concrete.

Rice Husk (RiH)

Similarly, adding rice husk to concrete has the same impact as the bio aggregates. Adding 32% of RiH dramatically decreased the density and thermal conductivity by 63 and 76%, respectively [66]. The specific heat capacity was not measured but expected to be increased and the thermal diffusivity to be decreased.

Cork Aggregates (CoA):

Cork is a light organic substance split from the bark of Cork Oak trees, which produced about 340,000 tons a year overall the world, and only 68000-85000 tons of cork is utilized. Cork is a construction material with cement due to its unique composition and cellular structure, which gives low density and thermal conductivity [67][68]. The presence of high content of cork in concrete retarded the hydration proof of cement [67]. The addition of cork reduced the density and thermal

conductivity by 22 and 30% for substituting 30% of cork [67]. Further, the thermal conductivity is not only controlled by the density but also affected by the size and the gradation of cork [68].

Appendix A.7: Effect of Synthetic aggregate

The usage of some industrial materials as artificial aggregates instead of natural aggregates to enhance specific properties of concrete or due to the lack of natural aggregates. Furthermore, using waste materials for construction protects the environment from pollution and the cost of recycling. The thermal properties of concrete crumb rubber and polystyrene are better than normal concrete due to their thermal insulation properties.

Polystyrene Beads (PSB):

Expanded polystyrene is a white-pored thermoplastic material (foam) consisting mainly of 98% air. EPS has very low thermal conductivity and water absorption; thereby, it has a high potential to enhance the thermal properties of concrete [69]. The porous structure and low k-value (0.03 W/m K) of EPS reduced the density and thermal conductivity of concrete by about 62 % [70][47][14], as illustrated in Table 2.2. Also, the Cp increased appreciably by about 50% due to expanded polystyrene's porosity and high specific heat capacity (1.2 J/g K). The thermal diffusivity decreased by about 50% for an additional 11% of EPS compared to normal mortar [14][47].

Crumb Rubber (CRu):

Tires could be crushed into small particles and sieved and may be treated to be used in concrete as lightweight aggregates. Crumb rubber has a high potential to improve thermal properties because of its low density (0.95 -1.12 g/cm^3), thermal conductivity (0.16-0.243 W/m K), and high specific heat capacity of 1.915 J/g K [71]. Adding 50%, CRu decreased the density and thermal conductivity by about 32 and 70%, respectively, while the specific heat capacity increased by about 18% [45] (Table 2.2). The density of the composition is reduced due to the low specific gravity of the rubber as compared to the other matrix and to the higher air entrainment into the system [71]. The reasons for decreasing the thermal conductivity are the insulating effect of rubber particles and trapped air on the surface of rubber aggregates [71]. Hence, the air content increased to about 42% for the content of 50% of CRu. Therefore, more energy was absorbed, and the thermal diffusivity decreased significantly by about 64% [71].

Appendix A.8: Effect of chemical admixtures

Ingredients added to the concrete mixture to improve cost and fresh and hardened properties of concrete, such as air-entraining agents, water-reducing agents, retarders and accelerators, etc. [72]. The addition of chemical admixtures affects the matrix's hydration production, density, and porosity; thereby, the thermal properties would be significantly affected.

Water Retaining Agents:

Chemical admixtures retain water inside the cement matrix and prevent evaporation for hydration polymer and cellulose water-reducing agents [73]. Therefore, more CSH would be produced, reducing thermal diffusivity [73].

Methylcellulose (Me):

The purpose of cellulose admixtures is to retain the water inside the mixture for hydration and uniformity. Hence, the cement hydration lasts longer to form more CSH [74]. Although the addition of 0.8% Me reduced the porosity by about 11%, the density and thermal conductivity reduced by about 9 and 38%, respectively (Table A.1), which may be attributed to the formation of tiny pores cutting capillary network and reducing capillary action [73][10]. On the other hand, the heat capacity slightly increased due to the bound water in hydrates (Cp for bound water 2.20 J/g K [10]) and the new amount of CSH [75][10] (Similar findings [2]). Therefore, the thermal diffusivity reduced significantly by around 35% [2] (Similar results obtained by the authors [10]).

Latex (La):

Latex is a polymer matrix that covers the hydrated cement grains and the aggregates, forming a barrier to prevent moisture loss (i.e., Enhancing cement hydration and providing a polymeric network) [76]. The impact of a high concentration of latex (25% by weight of cement) addition to cement paste is similar to a low concentration of Methylcellulose (0.8% by weight of cement), even though the amount of latex is much higher. The reason may be attributed to the liquid form of Methylcellulose (i.e., solution distributed uniformly in the mix rather than solid) [2]. As shown in Table A.1, with the addition of 30% latex compared to plain cement paste, density, and air

content reduced slightly by about 11%. In comparison, thermal conductivity decreased significantly by about 46% due to the high insulation of latex [2] and the formation of CSH (i.e., high potential to reduce thermal diffusivity). On the other hand, the specific heat increased very slightly. Consequently, there is a remarkable reduction in thermal diffusivity reached 40%.

Silane (Si):

Silane is a molecular compound used as a coating for admixtures (as silica fume) and carbon fibers to enhance the wettability of these admixtures by water [15], reducing the amount of water-reducing agents. Silane reacts with active groups such as OH^{-} to form a chemical bond. Further, silane reacts with cement during curing [3]. However, the addition of silane (2% by weight of cement) with silica fume (15% by weight of cement) significantly increases the thermal conductivity and heat capacity by 44 and 26% (i.e., increase thermal diffusivity by 21%), as compared to 0% Si [15] (Table A.1), as similarly found in reference [3]. SF generally decreases thermal conductivity and increases heat capacity (i.e., reduces thermal diffusivity). In contrast, silane increases thermal conductivity and heat capacity (i.e., thermal diffusivity) [3]. This increment may be ascribed to silane molecules' covalent reaction that connects the matrix components with covalent coupling [15].

Table A.1: Effect of chemical admixtures on thermal properties of paste, mortar, and concrete

Mix Type	Chemical Admixtures	ρ (g/cm^3)	K (W/m K)	Cp (J/g K)	α (mm^2/s)	Porosity (%)	W/B	Ref
Paste (With C)	**Me** (0.4-0.8%)	1.99-1.81	0.52-0.32	0.703-0.742	0.37-0.24	2.32-2.07	0.45-0.32	[2]
Paste with (C+SF)	**Me** (0.4%)	1.72-1.69	0.36-0.33	0.765-0.771	0.27-0.25	3.14-2.97	0.35	[2]
Paste with (Li+GGBS+MK)	**Me** (0.5%)	0.565-0.531	0.126-0.123	1.25-1.28	0.178-0.181	-	1.55	[10]
Paste (With C)	**La** (20-30%)	1.99-1.76	0.52-0.28	0.703-0.736	0.37-0.22	2.32-2.07	0.45-0.23	[2]
Paste with (C+SF)	**Si** (0.2-2%)	1.98-2.07	0.403-0.719	0.782-1.057	0.260-0.329	-	0.35	[15]

As recommendations for future research, methylcellulose and latex (water retaining agents) could be used to minimize thermal diffusivity, particularly in hemp concrete, because water absorption by hemp aggregates would be minimized (i.e., water is retained for workability and hydration). Silane could be used as a coating for hemp aggregates to enhance the bond with the binder's matrix due to the covalent coupling of silane particles. Further, waterproofing silane may significantly reduce the hygienic behavior of hemp and retain water inside hemp particles (i.e., maximize the heat capacity of the entire composition).

Appendix A.9: Effect of Reinforcement Agents

Many researchers studied concrete's thermal properties, and most learned the effect of aggregates, temperature, and moisture, but few papers investigated the influence of fibers [77]. Fibers bring air into the matrix during mixing and handling concrete; therefore, the porosity increases, reducing density and thermal conductivity. Hence, the heat capacity increases, and the thermal diffusivity decreases [77]. Another study proved that fiber addition increases the total porosity and reduces the tortuosity (like wood ash [21]), which is the pore connectivity in the cementitious matrix [78]. The thermophysical properties of fibers affect the thermal properties of the concrete.

Steel Fibers (StF):

Steel fiber has high density, thermal conductivity (2-3.5 W/m K), and specific heat capacity [18][77]. Therefore, the thermal properties of concrete with steel fibers increased with fiber content. As shown in Table A.2, the density, thermal conductivity, specific heat capacity, and thermal diffusivity increased by 7.5, 20, 9, and 16% compared to identical specimens without StF [18]. The same trend was obtained with smaller increment ratios because of the lower contents of StF [77].

Carbon Fibers (CF):

The addition of carbon fibers reduced the thermal diffusivity by about 16% due to the reduction of thermal conductivity (19%) and density (11%) and the increment of specific heat capacity (8%) [2] (Table A.2). Despite the high thermal conductivity of carbon fibers, the thermal conductivity reduced because the air content significantly increased by 47% [2]. Further, the fiber matrix interface with the cement matrix forms a high degree of slippage that absorbs more energy and increases the heat capacity of the composite.

Polypropylene Fibers (PPF):

The hydrophobic feature of polypropylene fibers enhanced the water retaining in the matrix during mixing, leading to higher porosity. Therefore, the higher content of PP fiber generates a higher pores content and a higher thermal insulation. However, moisture in the pores increased the

thermal conductivity compared to the control specimen [79]. As shown in Table A.2, the addition of PPF in concrete slightly reduces the density, thermal conductivity, and Cp by about 6, 13, and 6% due to the low content of fibers (1 kg/m^3); hence, the thermal diffusivity expected to be reduced by 15% [80], which similarly obtained by [79][81].

Coconut Coir Fiber (CCF):

Adding CCF decreased the thermal conductivity by about 16% and increased the specific heat capacity by about 12%. Hence, the diffusivity considerably reduced by about 26% [82]. As expected, bio fibers enhanced the thermal insulation of concrete.

Date Palm Fiber (DPF):

Similar to CCF, the addition of DPF decreased the density thermal conductivity by 49 and 14%, respectively, due to interior (i.e., Porous structure of fibers) and exterior porosity (i.e., Pores between fibers) [83]. The Cp value increased by 32%, leading to an increment in the thermal diffusivity by 12%.

Table A.2: Effect of reinforcement agents on thermal properties of paste, mortar, and concrete

Mix Type	Reinforcement Agent	ρ (g/cm^3)	K (W/m K)	Cp (J/g K)	α (mm^2/s)	Porosity (%)	W/B	Ref
Concrete (With **C**)	**StF** (116kg/m^3)	2.259-2.387	1.923-2.105	0.883-0.907	0.964-0.972	-	0.27	[18]
	StF (20-35%)	2.378-2.420	2.83-2.86	0.832-0.831	1.430-1.422	7.46-7.47	0.48	[77]
	StF (42kg/m^3)	2.52-2.58	3.30-3.50	0.794-0.775	1.65-1.75	-	0.44	[80]
Foamed Mortar (With **C**)	**StF** (0.2-0.4%)	0.60	0.215-0.248	0.578-0.619	0.480-0.661	-	0.45	[84]
Concrete (With **C**)	**PF** (1-2kg/m^3)	2.378-2.397	2.83-2.76	0.832-0.832	1.430-1.384	7.46-7.14	0.48	[77]
Paste (With **C**)	**CF** (0.5-1%)	1.99-1.66	0.52-0.34	0.703-0.792	0.37-0.26	2.32-3.97	0.45-0.35	[2]
Concrete (With **C**)	**GF** (1kg/m^3)	2.378-2.400	2.83-2.67	0.832-0.832	1.430-1.337	7.46-7.75	0.48	[77]
Concrete with (**C+FA**)	**PPF** (1kg/m^3)	-	3.30-2.80	C_v=2	1.65-1.40	-	0.44	[80]
Foamed mortar (With **C**)	**PPF** (0.2-0.4%)	0.60	0.19-0.16	0.900-0.700	0.35-0.39	69-70	0.45	[79]
Foamed mortar (With **C**)	**CCF** (0.2-0.4%)	1.352-1.364	0.57-0.48	1.004-1.135	0.42-0.31	-	0.45	[82]
Concrete (With **Gy**)	**DPF** (1-2%)	1.89-0.970	0.895-0.764	1.50-2.20	0.316-0.358	-	-	[83]

Appendix A.10: Nanomaterial

Nanomaterials are solid or fluid materials on a nanoscale, and nanotechnology is involved in changing or characterizing the properties of nanomaterials. Solid nanomaterials could be classified according to their shape into four categories: bulk, fiber, film, and powder. At the same time, nanofluids may be classified into metals, metals, non-metal oxides, carbon-based, carbides, and polymers [85]. Nano-porous materials may have a superior effect of thermal diffusivity (if used in concrete) because of their ultra-high porosity and low density, ultra-low thermal conductivity, and excellent gas storage characteristics [85]. Lin Qiu et al. conducted a literature review on the thermal diffusivity of nanomaterials, which showed that silicon nanomaterials showed ultra-low thermal diffusivity (<0.01 mm^2/s) [85]. Further, some polymers, aerogel, and traditional materials showed low values of diffusivity (<0.10 mm^2/s) [85]. Zheng et al. showed that the effective thermal conductivity and thermal diffusivity of the SiO_2 nano-powder increased with temperature; however, both values decreased as the particle diameter was reduced. Jittabut added up to 5% (by weight of cement) nano-silica (Particle sizes of 12, 50, and 150 nm) to cement paste, and the thermal diffusivity reduced slightly (about 10%) [86] (No significant change in Cp). The density and thermal conductivity were decreased by 13 and 25%, respectively, due to the porous structure of nano silica [86]. Nano aerogel is a promising high insulation material due to the porous structure (>95%) leading to a lower value of density (< 0.32 g/cm^3) and thermal conductivity (< 0.036 W/m K) and a higher thermal storage capacity [85]. Nano-porous silica aerogel (94% porosity, particle size 250 μm) was used in foamed concrete with c/aerogel of 17:1 [87]. The results indicated a 50% reduction in density and thermal conductivity compared to the foamed concrete. Thus, the diffusivity is expected to be significantly reduced [87]. Carbon aerogel is recommended for high-temperature applications because of its thermal stability and maintaining mesoporous nanostructure at high temperatures [88]. Further, graphene aerogels are ultralight aerogels (two times heavier than air) and have a thermal diffusivity of 0.01-1.5 mm^2/s [89].

Appendix A.11: External factors affecting thermal diffusivity

Water

The thermal conductivity of concrete varies with changing temperature (because the moisture content is affected by temperature). It increased with increasing moisture content filling the pores (because the thermal conductivity of water is about 25 times that of air) [1]. Further, there is an increment of 5% in thermal conductivity due to a 1% increment in the unit weight of concrete by water absorption [1]. Hence, the transient method is preferred to measure thermal conductivity for moist concrete than the steady state [80]. Since both thermal conductivity and specific heat capacity increase with moisture content, the thermal diffusivity was expected to be decreased [52].

Moisture Content:

The moisture inside concrete is used for hydration or filling the air voids of aggregates and cementitious matrix. The thermal conductivity and specific heat capacity of water are 0.601 W/m K and 4.20 J/g K, while the air values are 0.026 W/m K and 1.005 J/g K (at 20^{o}C) [48] hence the presence of water will much increase density, thermal conductivity and specific heat capacity, thus, the thermal diffusivity may be increased or decreased (Figure A.1) (i.e., Thermal diffusivity with varying moisture content depends on relative variation of thermal conductivity and volumetric heat capacity) [57]. Therefore, the thermal diffusivity increases when the thermal conductivity increases faster than the volumetric heat capacity and vice versa. The phenomena may vary based on w/c ratio, pore structure, aggregate type, and relative humidity. A reduction in thermal diffusivity with increasing moisture content was observed with Lightweight aggregate concrete [48][52] and wood ash-foamed concrete [21]. On the other hand, an increment in thermal diffusivity was observed with lightweight shotcrete [46] and lime plaster [28][31] [90]. For hemp concrete and plaster, the thermal diffusivity increased with increasing moisture content until reaching maximum diffusivity (not max moisture content). The values decreased until they became fully saturated (i.e., Upward parabolic) [57][61][91] (Similar findings for wood gypsum boards [64]).

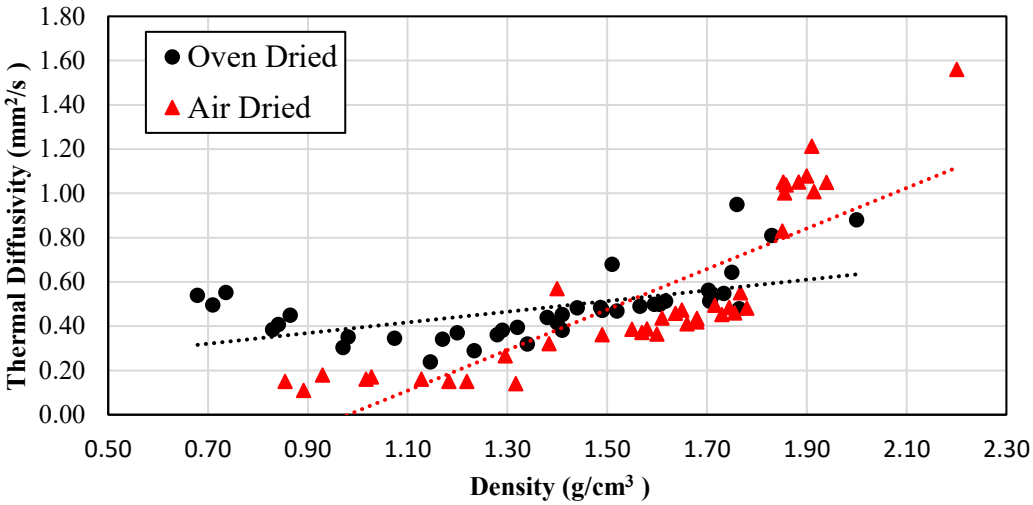

Figure A.1: Effect of moisture content on thermal diffusivity

Relative Humidity (RH):

The surface of concrete absorbs water vapor, depending on the relative humidity and the nature of concrete ingredients (hygroscopic behavior). The moisture content of hemp concrete increased steeply when RH exceeded 60% due to the sorption of hemp (i.e., moist content increased) [56][9][90][92]. The increment of thermal conductivity and specific heat of LWAC at the partial saturation state (50% RH conditioning) is 17 and 5% on average because the thermal conductivity and specific heat of vapor water are higher than dry air [48] (Similar results found by [9]). For hemp lime plaster, the sorption gradually increases with relative humidity and could reach 10% water mass for an RH of 100% [57]. Further, the thermal conductivity and heat capacity increased considerably by 10 and 18% for RH of 15 and 65%, respectively [57] (Similar results obtained for hemp concrete [91]), which ascribed to the hygroscopic behavior of hemp [56]. The thermal diffusivity is negligibly affected by changing relative humidity (for 50%) due to the slight effect on conductivity and heat capacity, as shown in Figure A.2.

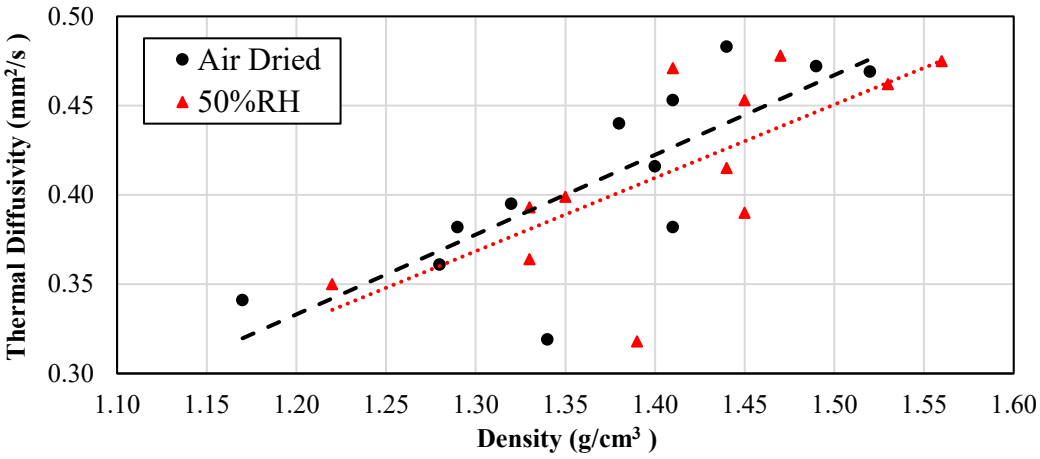

Figure A.2: Effect of relative humidity on thermal diffusivity

Temperature

The values of thermal diffusivity are affected by the temperature. Goncalves et al. tested the thermal conductivity and volumetric heat capacity of plain alkali-activated fly ash concrete (oven-dried samples) with temperatures between -30 and 300ºC. Thus, we could calculate the thermal diffusivity [93]. The results proved the diffusivity decreased with increasing temperature, as shown in Figure A.3, which may be ascribed to stabilizing conductivity and increasing volumetric heat capacity with increasing temperature. Similarly, Marshall found a reduction of 24% in thermal diffusivity with increasing the temperature from 10 to 65ºC due to the same reason [52] (the same trend seen by Tran et al. [94]). The results of Xie for thermal diffusivity of cement mortar followed the same trend with stabilizing heat capacity and decreasing thermal conductivity due to the evaporation of bounded water (i.e., peak evaporation point about 270ºC) [37]. However, Vejmelkova et al. tested glass-fibered paste for thermal diffusivity as a function of temperature [95]. The results proved that the values increased considerably in low-temperature ranges (20-600oC). At the same time, the increment in diffusivity became steep after 600ºC due to the inclusion of convection and radiation into thermal diffusivity results [95] (Same trend for glass fibered cement paste found by Podebradskfi [96]). Similarly, Nguyen et al. found that the thermal diffusivity of concrete

increased with increasing temperatures because thermal conductivity and heat capacity increased due to the presence of water and mineral phases in the XRD of aggregates [48] (Figure A.3). The thermal conductivity of water (as liquid) increased with temperature [97]. At the same time, Cp decreased (i.e., Cp liquid water = 4.18, Cp bounded or vapor water= 2.03 J/g K) [48]. Further, the heat capacity of minerals increased with temperature and could reach 20-30% [48]. However, the behavior of thermal diffusivity with varying temperatures depends on concrete compositions, including aggregate type and the presence of water and air [48]. Since the properties of air and water change with temperature, heat transfer would be affected [48].

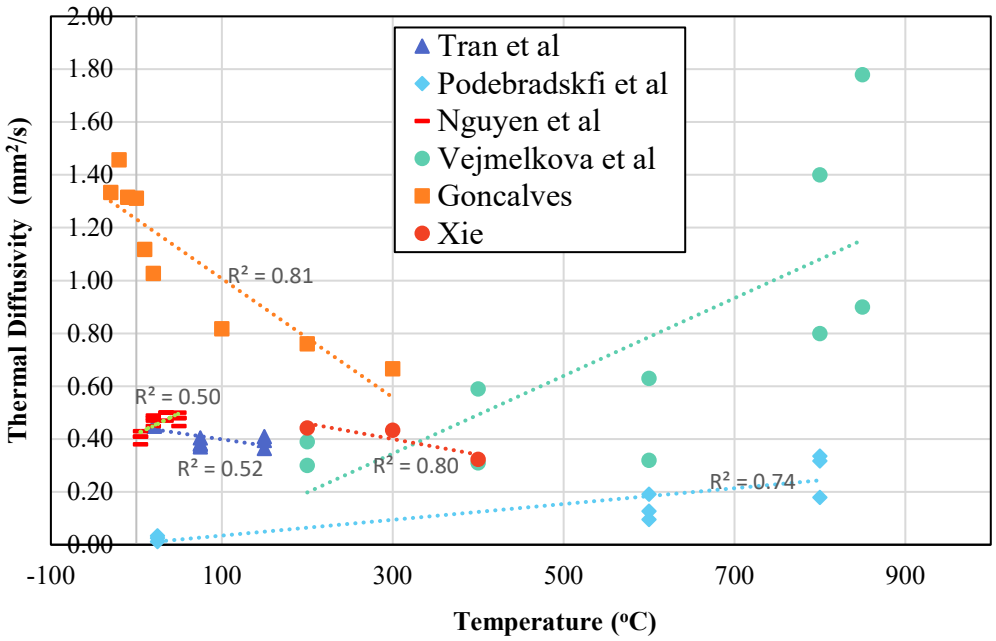

Figure A.3: Effect of temperature on thermal diffusivity